INVESTIGATION OF TOXICITY OF ZINC SELENIUM/ZINC SULPHIDE (ZnSe/ZnS) QUANTUM DOTS AT MOLECULAR LEVEL

A THESIS PRESENTED BY

RESHMA V G

TO

THE SREE CHITRA TIRUNAL INSTITUTE FOR MEDICAL SCIENCES AND TECHNOLOGY, TRIVANDRUM

Thiruvananthapuram

IN PARTIAL FULFILLMENT OF THE REQUIREMENTS

FOR THE AWARD OF

DOCTOR OF PHILOSOPHY

2020

CERTIFICATE

I, **Reshma V G**, hereby certify that I had personally carried out the work depicted in the thesis entitled "**Investigation of toxicity of Zinc Selenium/Zinc sulphide (ZnSe/ZnS) quantum dots at molecular level**". No part of the thesis has been submitted for the award of any other degree or diploma prior to this date.

Place: Thiruvananthapuram

Date: ۱۱.۰۵.۲۰۲۵

Reg. No: 2015/PhD/08

Signature: Reshma.V.G.

Name: Reshma V G.

Dr. P V Mohanan

Toxicology Division

This is to certify that ***Ms. Reshma V G***in the Toxicology Division of this institute has fulfilled the requirements prescribed for the Ph.D. degree of the SreeChitraTirunal Institute for Medical Sciences and Technology, Trivandrum. The thesis entitled *"**Investigation of toxicity of Zinc Selenium/Zinc sulphide (ZnSe/ZnS) quantum dots at molecular level**"* was carried out under my direct supervision. No part of the thesis was submitted for the award of any degree or diploma prior to this date.

*Clearance was obtained from the Institute Animal Ethics Committee (IAEC) for carrying out the study. IAEC approval No: SCT/IAEC-261/FEBRUARY/2018/95.

Signature:

Date: 11/03/2018

Dr. P. V. Mohanan
Scientist & Head, Toxicology Division
Sree Chitra Tirunal Institute for Medical-
Sciences and Technology (Govt. of India),
Biomedical Technology Wing, Poojappura,
Thiruvananthapuram-695 012, Kerala, India.

The thesis entitled

"Investigation of toxicity of Zinc Selenium/Zinc Sulphide (ZnSe/ZnS) quantum dots at molecular level"

Submitted by

Reshma V G

for the degree of
Doctor of philosophy

of

THE SREE CHITRA TIRUNAL INSTITUTE
FOR
MEDICAL SCIENCES AND TECHNOLOGY, TRIVANDRUM
Thiruvananthapuram

Is evaluated and approved by

Name of the guide

Dr. P. V. Mohanan
Scientist & Head, Toxicology Division
Sree Chitra Tirunal Institute for Medical-
Sciences and Technology (Govt. of India),
Biomedical Technology Wing, Poojappura,
Thiruvananthapuram-695 012, Kerala, India.

Name of thesis examiner

21/3/2020

ACKNOWLEDGEMENT

It is a pleasure to thank many people who have motivated and supported me during all those years of my PhD life and made this thesis possible.

I express my gratitude to our Director Prof. Asha Kishore and Dr. H.K. Varma, Head, Biomedical Technology Wing, Sree Chitra Tirunal Institute for Medical Sciences and Technology for providing necessary support and facilities for completing my Ph.D. work.

I sincerely thank our former Directors Prof. K. Radhakrishnan, Prof.Jagan Mohan Tharakan and former Heads of Biomedical Technology Wing Dr. G.S. Bhuvaneshwar, Dr. C.P. Sharma, Shri. O.S. Neelakantan Nair, former Dean Prof. Suresh Nair, Present Dean Dr.Kalliyanakrishnan V., Registrar Dr. George A.V., Deputy Registrar Dr. Santhosh Kumar and former Deputy Registrar Dr.Sundar Jayasingh S. for their academic assistance.

I acknowledge my sincere thanks to the Department of Science and Technology- Innovation in Science Pursuit For Inspired Research (DST-INSPIRE) New Delhi, for the Junior Research Fellowship and Senior Research Fellowship (Award letter No: IF 150363; date: 24June 2015).

I would like to thank my Doctoral Advising Committee members, Dr. H.K. Varma, Dr. Anil Kumar P.R and Dr.Kamalesh K. Gulia in their efforts in reviewing and evaluating my research work.

I thank The Director, NIIST, Trivandrum, and Dr Rajeev kumar Sukumaran, Principle Scientist & head of Microbial process and technology Division and research scholar Meena for extending their research facilities.

I would like to acknowledge my sincere gratitude to all Departments and Divisions Head, especially Dr.Prabha D. Nair (former Associate Dean and HoD, DAB), Dr. T.V. Kumary (former Associate Dean) Dr. H.K. Varma, Dr. A. Maya Nandkumar, Dr. Uma Shankar P.R, Dr.Lisy K. Krishnan, Dr.Rekha M.R., Dr. Manoj Komath for providing their support in completing my work.

I gratefully acknowledge my sincere gratitude to Mr. Sreekanth, Dr. Suresh Babu S., Mr. Willi Paul, Mrs Deepa, Mrs. Susan Mani, Mr. Prem Mohan M, Ms Neethu and Ms Maneesha for their timely support.

Special thanks to the staff and students of Toxicology Division who have made my time here in the lab a memorable one. I am grateful for the friendship and unyielding support offered by Dr.Remya N.S., Ms Prajitha N, Ms Athira S.S, Ms Ashtami Jayakumar, Ms Anju Surendranath, Ms Vandana, Ms Varsha, Mr. Shaji S., Mr. Harikumar G., Mrs. Amrutha Kumari M.S. and Mrs. Lekha. I also thank my

seniors Dr. Biby T Edwin., Dr.Syama S., Dr.Reshma S Cherian, Dr Sruthy S and Ms. Sukanya V.S for the entire support offered during my work.

My heartfelt thanks to all those who have helped me in completing my PhD work by providing valuable information and support, especially all my companion PhD students inside and outside of my campus.

I would like to express my heartfelt gratitude and respect to my PhD supervisor Dr. P.V. Mohanan, for his support in completing my PhD work.

Most importantly my deepest appreciation and gratitude goes to my parents, Mr. Gopi and Mrs. Anitha Gopi, for their unending love, prayers, faith and patience that encouraged me to accomplish my task. I greatly value the love and care that my sister, Greeshma bestowed on me to stay calm and sane through these difficult years. My grandmother and naani with their constant prayers has been the most comforting presence in my life. Most of all I owe my every thanks and gratitude to my father, Gopi V R, for the burdens he took on himself to ensure I could traverse through life with minimal difficulty.

Last but not the least thanks my beloved, warm hearted husband Mr. Vineeth P.N for tolerating me and motivating me to strive towards my goal. I owe my sincerest thanks to him for walking every step of the way with me with no regard for his own hardships. Without his love, encouragement and constant support, I would not have finished this thesis.

My immense gratefulness to the Lord Almighty which has been a guiding force throughout my life.

Reshma V G

TABLE OF CONTENTS

LIST OF FIGURES

LIST OF TABLES

ABBREVIATIONS

µg	Microgram
µl	Microliter
µM	Micromolar
AB/AM	Antibiotic/ Antimycotic
ADME	Adsorption, Distribution, Metabolism, Excretion
AFM	Atomic Force Microscopy
ALP	Alkaline phosphatase
ALT	Alanine transaminase
AO	Acridine orange
AST	Aspartate transaminase
BBB	Blood Brain Barrier
BET	Brunauer-Emmett-Teller
BSA	Bovine serum albumin
CNTs	carbon nanotubes
ºC	Celsius
cm	Centimetre
cmc	Critical micelle concentration
CPCSEA	Committee for the Purpose of Control and Supervision of Experiments on Animals
CPM	Counts per minutes
CVD	chemical vapour deposition
Cyt.B	cytochalasin B
D	dimension
DAPI	4',6-diamidino-2-phenylindole
DCFH-DA	Dichloro-dihydro-fluorescein diacetate
dH2O	Deionised water
DLS	Dynamic light scattering
DMEM	Dulbecco's Modified Eagle Medium
DMSO	Dimethyl Sulphoxide
DNA	Deoxyribonucleic acid
DTPA	Diethylene triamine penta acetic acid
DWNTs	double-walled nano tubes
EDX	Energy Dispersive X-ray
EDTA	Ethylene diamine tetra acetic acid
EtBr	Ethidium bromide
eV	Electron volt
FACS	Fluorescence Activated Cell Sorting
FBS	Foetal Bovine Serum
FSC	Forward scatter
g	Gram
GPx	Glutathione Peroxidise
GR	Glutathione reductase

GSH	Reduced glutathione
GSSG	Oxidized glutathione
h	Hour
H & E	Haematoxylin and Eosin
HCT	Haematocrit
HGB	Haemoglobin
HR-TEM	High Resolution TEM
i.p.	Intraperitoneal
i.v.	Intravenous
IAEC	Institutional Animal Ethics Committee
ICP-OES	Inductively Coupled Plasma Optical Emission Spectroscopy
IL	Interleukin
JC1	5,5′,6,6′-tetrachloro-1,1′,3,3′-tetra Ethyl benzimidazolylcarbocyanineiodide
kg	Kilogram
kV	Kilovolt
LC50	Lethal concentration 50%
LPO	Lipid peroxidation
LPS	Lipopolysaccharides
M	Molar
MCHC	Mean corpuscular hemoglobin concentration
MDA	Malonedialdehyde
mg	Milligram
min	Minutes
ml	Millilitre
mm	Millimetre
mM	Millimolar
MMP	Mitochondrial membrane potential
MRI	Magnetic Resonance imaging
MTT	3-(4, 5-Dimethylthiazol-2-yl)-2, 5-Diphenyltetrazolium Bromide
MWNTs	Multi-walled carbon nanotubes
NADPH	Nicotinamide Adenine Dinucleotide Phosphate (Reduced)
NF-κB	Nuclear Factor –κB
nHAP	nanohydroxyapatite
nm	Nanometre
NO	Nitric Oxide
NOAEL	No Observed Adverse Effect Level
NRU	Neutral red uptake
PBS	Phosphate Buffered Saline
PDI	Polydispersity index
PI	Propidium Iodide
PL	Photoluminescence

PLT	Platelet
PNP	Polymeric nanoparticles
POM	Polarised Optical Microscopy
PS	Phosphatidylserine
QDs	Quantum dots
RBC	Red blood cell
RNA	Ribonucleic acid
RNS	Reactive nitrogen species
ROS	Reactive Oxygen Species
rpm	Revolutions per minutes
s	Second
SD	Standard Deviation
SDS	Sodium Dodecyl Sulphate
SEM	Scanning electron microscopy
SOD	Superoxide dismutase
SSC	Sideward scatter
SWNTs	single-walled nanotubes
TEM	Transmission electron microscopy
TGA	Thermogravimetric analysis
TiO2 NP	Titanium dioxide nanoparticles
TLR	Toll like receptor
UV- Vis	Ultra Violet-visible
V	Volt
v/v	Volume/Volume
w/v	Weight/Volume
WBC	White blood cells
XPS	X-ray photoelectron spectroscopy
XRD	X-Ray powder Diffraction
ZnO NP	Zinc oxide nanoparticle
ZnSe/ZnS QDs	Zinc Selenium/Zinc Suphide quantum dots

SYNOPSIS

"Investigation of toxicity of Zinc Selenium/Zinc Sulphide (ZnSe/ZnS) quantum dots at molecular level".

Semiconductor nanocrystals or Quantum dots (QDs) are the nanotech's miracle molecules whose quantum properties assure a wide range of applications across several medical and non-medical fields. Most widely used traditional QDs contain highly toxic heavy metals like Cadmium and Lead as major elements. Leakage of heavy metals from the core is the main reason of QD toxicity. In the biomedical application scenario, development of Cadmium free, nontoxic water soluble QDs is very essential. The surge for the development of ZnSe/ZnS QDs has originated from the demand of non-toxic and more biocompatible QDs for biomedical applications. However only limited reports are available on intrinsic safety/toxicological aspect of the same. As there is a higher prospect of extensive *in vivo* applications in future, ZnSe/ZnS QDs requires a comprehensive toxicological evaluation.

The aim of the present work is to investigate safety/toxicity of ZnSe/ZnS QDs at molecular level. An effort was made to study the interaction of HepG2 and HEK 293 cells with ZnSe/ZnS QDs. Based on the available reports, current study hypothesized that interaction of ZnSe/ZnS QDs with HepG2 and HEK cells can lead to less toxic effects and it do not cause any toxicological response in mice. In order to address the hypothesis, the study is divided into three objectives.

Major objectives are:

Objective 1: Synthesis and characterization of ZnSe/ZnS QDs

Objective 2: *In vitro* evaluation of ZnSe/ZnS QDs with HepG2 and HEK cell lines.

Objective 3:

- **Part 1:** Acute toxicity, immunotoxicity, haematological, clinical biochemistry oxidative stress and histopathological studies.
- **Part 2:** Elemental analysis, biodistribution and ADME & T (Absorption, Distribution, Metabolism, Excretion and Toxicity) profiling studies.

The thesis comprises of six chapters. The first introductory chapter covers the background and relevance of the study. This chapter briefly elaborates about nanotechnology, nanoparticles, types of nanoparticles, quantum dots, types of quantum dots, toxicology and nanotoxicology.

Second chapter emphasizes on the review of literature. Here the existing literature on quantum dots, synthesis of QDs, structure and characterization, physico-chemical properties, applications, toxicity of QDs- mechanism of toxicity and parameters influencing toxicity are being narrated.

Third chapter details the materials and methodologies adapted to fulfil the objectives. The section introduces the cell lines used for the study (HepG2 and HEK 293 cells) as well as the justification of the selection of cells and ZnSe/ZnS QDs.

Present study has divided into three objectives. The first objective describes the synthesis and characterization of ZnSe/ZnS QDs. It is synthesized by green method and is based on bottom-up aqueous colloidal synthetic (ACS) route. Optical characterization of QDs was carried out by absorption and emission spectroscopy. Fluorescence stability was also studied. The QDs of interest were observed under UV light and fluorescence microscope. Physicochemical characterization was performed using Transmission Electron Microscopy (TEM), Dynamic Light Scattering (DLS), zeta potential analysis, Fourier Transform Infrared Spectroscopy (FTIR), Raman spectra, Inductively Coupled Plasma Optical Emission Spectrometry, X-ray Diffraction (XRD) and Thermal analysis by Thermo Gravimetric Analysis (TGA), Differential Thermal Analysis (DTA) and Derivative Thermo Gravimetry (DTG).

Objective two of this section explains about *in vitro* toxicity studies using HepG2 and HEK293 cell lines. The first phase explains *in vitro* studies using HepG2 cells. The cells were exposed to different concentrations of ZnSe/ZnS QDs for 6 and 24 h. The cytotoxicity of HepG2 cells were analysed using MTT, neutral red uptake (NRU) and trypan blue exclusion assays. Cytotoxicity of ZnSe/ZnS QDs also confirmed by the LDH assay. Particle uptake by the cells and morphological changes were studied using confocal and phase contrast microscopy respectively. Morphological changes were also studied by Giemsa staining. Cytoskeltal integrity and nuclear condensation results

in cells due to the QDs treatment and was studied by Rhodamine phalloidin and acridine orange staining. Mitochondrial membrane potential (MMP) and lysosomal stability was studied using JC-1 and acridine orange (AO) dyes respectively. Generation of reactive oxygen species (ROS) in the presence of ZnSe/ZnS QDs was studied using fluorescence probe Dichlorofluorescien diacetate (DCFHDA). Griess reagent assay was used to estimate the generation of nitrile radical. Glutathione (GSH) level in cells treated with different concentration of ZnSe/ZnS QDs was estimated for the analysis of oxidative stress. Cell cycle pattern changes were studied by flowcytometry analysis of propidium iodide (PI) stained cells. DNA fragmentation was studied by DNA ladder assay. Flow cytometry analysis of Calcein AM/PI staining was used to study cell death. Caspase 3/7 activation assay was carried out to study about the mechanism behind the cell death induced by the ZnSe/ZnS QDs. Second phase of this section describes the *in vitro* toxicity studies using HEK cell lines. Time and dose dependent toxicity of ZnSe/ZnS QDs studied by MTT, NRU, Trypan blue exclusion and LDH assay. QDs uptake by HEK cells studied by confocal and flow cytometry analysis. Cell phenotype was assessed by phase contrast microscopy and coomassie brilliant blue staining. MMP and lysosomal stability was studied using JC-1 and AO staining respectively. ROS and nitrile radical production analysis were carried out by the DCFHDA and Griess reagent. Oxidative stress and DNA fragmentation studies were carried out by the estimation of GSH content and DNA ladder assay. Calcein AM –PI, Annexin V/PI and caspase 3/7 activation assays were used to study apoptosis.

The third objective of this study explains *in vivo* toxicity study of ZnSe/ZnS QDs using the Swiss albino mice. This objective has two parts. Part 1 deals with the acute toxicity, immunotoxicity, hematology, clinical biochemistry, oxidative stress and histopathological studies. Part 2 pertained on elemental analysis, biodistribution, ADME & T (Absorption, Distribution, Metabolism, Excretion and Toxicity) profiling studies.

Animals were randomly divided into 7 groups of three animals each on the basis of route of exposure and time of observation. Mice were exposed to a single dose of 10 mg/ml via both intraperitoneal (i.p.) and intravenous (i.v.) injection. They were

observed on 3rd, 7th and 14th day of experiment. Animals were sacrificed at the end of 3rd, 7th and 14th days of exposure of ZnSe/ZnS QDs. Before sacrifice, body weight was recorded and blood was collected from all the animals for haematological and clinical biochemistry analyses. Urine was also collected for analysis. Gross pathology was observed during sacrifice. Subsequently, organ weight was recorded and organs such as liver, kidney, brain and spleen were collected and subjected to histopathology and elemental analysis. Small portion of the liver and brain was subjected to oxidative stress analysis. Splenocyte proliferation assay was carried out by isolating spleen from the treated mice. Blood Brain Barrier (BBB) integrity after the QDs treatment can be analysed by measuring brain volume. Isolated tissues (liver, kidney, spleen and brain), blood, urine and faeces were used to study biodistribution and toxicokinetics by ICP-OES. On account of ICP-OES data, Absorption, Distribution, Metabolism, Excretion and Toxicity (ADME & T) profiling studies were carried out.

The fourth and fifth chapter details the results and discussion respectively. Both of these chapters are divided into three sections each. The first section describes the synthesis and characterization of ZnSe/ZnS QDs. Blue fluorescent ZnSe/ZnS QDs were synthesised by a facile aqueous phase route. Optical characteristics of the QDs were observed by fluorescence and absorption spectra. ZnSe/ZnS QDs has absorbance at 340 nm and fluorescence emission at 416 nm. Synthesized ZnSe/ZnS QDs exhibited fluorescence stability for four months. From the TEM image, average diameter of particles is found to be approximately 5-6 nm. DLS analysis revealed that the hydrodynamic size and zeta potential is 33 nm and -33.5 ± 5.91 respectively. ZnSe/ZnS QDs show combined FTIR spectra bands at 3265.49 cm^{-1}, 3175 cm^{-1}, 2989.66 cm^{-1}, 1546.91 cm^{-1}, 1390.68 cm^{-1} compared to spectra of ZnSe, GSH and MPA. Raman spectra of ZnSe/ZnS QDs showed representative peaks of both LO and 2 LO phonon modes of ZnSe and ZnS. It was estimated that 1 g of ZnSe/ZnS QDs contains Zinc (Zn), Selenium (Se) and Sulphur (S) by weight 379.58, 0.763and 378.53 mg respectively. XRD pattern of ZnSe/ZnS QDs showed diffraction angles located between the cubic ZnSe and ZnS. Thermal analysis gives an idea about decomposition of ZnSe/ZnS QDs occurs at 300º C at the rate of 167.417 µg/min.

Second section explains the interaction of ZnSe/ZnS QDs on HepG2 and HEK cell lines. ZnSe/ZnS QDs was effectively internalized by both HepG2 and HEK cells and was found to distribute throughout the cytoplasm. ZnSe/ZnS QDs were not observed in nucleus. HepG2 cells remain intact without any morphological distortion; whereas HEK cells underwent slight morphological changes at higher concentrations. *In vitro* exposure of ZnSe/ZnS QDs in HepG2 cells caused cytotoxicity, mechanical damage, cytoskeletal rearrangement and ROS mediated apoptosis with slight effect in loss of MMP, lysosomal destabilization and increase in caspase 3/7 activation at high concentration (100µg/ ml) of 24 h exposure. DNA ladder was not formed as a result of ZnSe/ZnS QDs interaction with HepG2 cells. Apoptotic cell death occurs in HepG2 cells. ZnSe/ZnS QDs exposed to kidney cells resulted in mitochondrial hypopolarisation, lysosomal destabilization and ROS generation only at 100µg/ ml of 24 h exposure. DNA laddering was not observed in HEK cells. Absence of DNA fragments observed in DNA ladder assay confirmed that ZnSe/ZnS QDs are not directly or indirectly inducing DNA damage. Necrosis was confirmed to occur in HEK cells; which presents the underlying cue for cell death.

Third section consists of two parts. First part explains acute toxicity (10 mg/kg body weight) study of ZnSe/ZnS QDs in Swiss Albino mice with single exposure via both intraperitoneal and intravenous injection. Clinical or behavioural changes were not observed on acute exposure of ZnSe/ZnS QDs. Any loss of body and organ weight did not induce by single exposure of 10 mg/kg ZnSe/ZnS QDs. No changes in haematological and clinical chemistry parameters were noted after acute exposure of ZnSe/ZnS QDs. ZnSe/ZnS QDs induced oxidative stress only in liver; not in brain. Histological examination did not show any severe symptoms of toxicity in kidney, spleen and brain, however moderate pathological changes were observed in the liver. Exposure to ZnSe/ZnS QDs initiates immune response by increasing the spleenocytes proliferation at 3rd day of post exposure which became normal at the end of 14th day. Second part explains about ADME & T (Absorption, Distribution, Metabolism, Excretion and Toxicity) profiling studies on the basis of ICP-OES data. Biodistribution study by ICP-OES showed ZnSe/ZnS QDs distributed in liver, kidney, spleen and brain. ZnSe/ZnS QDs was not fully cleared from blood at the end of observation

period (14th day). ADME indicated that the route of excretion of ZnSe/ZnS QDs is by faecal matter and urine.

In the final chapter, results are summarized and concluded that blue fluorescence coloured ZnSe/ZnS QDs with the size of 5-6 nm was successfully green synthesized with absorption at 340 nm and emission at 416 nm. These QDs have fluorescence stability for four months. Various physicochemical characterization techniques ensured different properties of ZnSe/ZnS QDs. All these characterization results authenticate ZnSe/ZnS QDs. The preliminary toxicity screening using HepG2 and HEK cells as *in vitro* models suggests that ZnSe/ZnS QDs can be used for various biomedical application at a concentration less than 100µg/ ml. ZnSe/ZnS QDs failed to induce any toxic effects in both HepG2 and HEK cells except at a concentration of 100 µg/ ml during 24h exposure. A single administration of ZnSe/ZnS QDs (10 mg/ml) did not induce any acute toxicity in haematological and clinical chemistry parameters. Nevertheless they induce oxidative stress and moderate pathological changes in liver. Immunotoxicity evaluation showed that splenocyte proliferation occurs at 3rd day and the same was recovered to the normal range on subsequent days. Bio distribution study by ICP-OES showed ZnSe/ZnS QDs were distributed in liver, kidney, spleen and brain. Most of the ZnSe/ZnS QDs are excreted through faeces and urine. As far as the futuristic clinical applications are concerned, long term toxicity evaluations are recommended to ensure the non-toxic and biocompatible nature of ZnSe/ZnS QDs.

CHAPTER 1: INTRODUCTION

1 INTRODUCTION

Nanoparticles are mainspring of nanoscience and nanotechnology. Nanoscience and technology is an extensive and interdisciplinary area of research with vast possibilities and has been extensively growing worldwide from the past few years. The term '*nano'* originated from the Greek word '*nanos'* which means 'dwarf' (Hagens, 2007). Because of this reason very small object usually comes to the mind whenever think about nanoscience or nanotechnology. This branch deals with the particles having at least one spatial dimension in the size range of 1 to 100 nm (Laurent *et al*., 2008). Fifty years ago, the concept of nanotechnology was introduced by Nobel Laureate Richard P. Feynman. In 1959, the famous statement 'there's plenty of room at the bottom' spoken by him at the American Physical Society inspired a field of endeavour now called 'nanotechnology', a term coined by Professor Noro Taniguchi of the Tokyo University of Science in 1974. Richard Feyman also gave the idea of a reduction in print font size that might permit the Encyclopedia Britannica to fit on the head of a pin. He also proposed that it would be possible to arrange the atoms the way want wanted (Patil *et al*., 2008).

Nanoparticles are defined as a set of substances where at least one dimension is less than approximately 100 nanometers (Srivatsan, 2012). One nanometer is one billionth of a meter or 10^{-9} of a meter. The logarithmical scale showing the size of nanoparticles compared with various biological and non-biological objects are referenced in figure 1.1. For size reference, the haemoglobin molecule is 5 nm, most viruses are 10-100 nm and a human cell 10000-20000 nm (Figure. 1.1).

Some nanoparticles occur naturally and some others are designed purposefully and already been applied in many commercial products and processes. The nanoparticles can be found in cosmetics, stain-resistant clothing, electronics, sporting goods, tires and in many other daily used personal care products (Wei and Yan, 2016). Ramos *et al.,* (2017) observed potent application of nanoparticles in biomedicine, such as imaging, diagnosis, drug delivery *etc., etc.,* This is mainly because of their unique optical, magnetic, electrical, chemical and thermal properties which are not seen in their conventional, bulk counterparts.

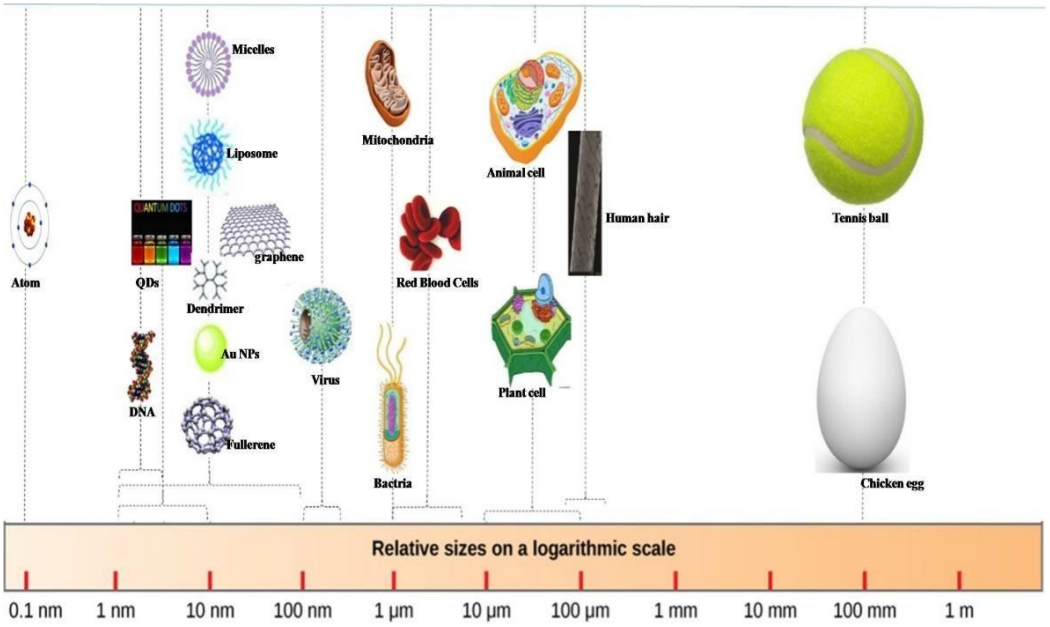

Figure 1.1: Logarithmical scale showing the size of nanoparticles compared with various biological and non-biological objects.

There are two main reasons responsible for these unique properties of nanoparticles which include their increased relative surface area and quantum effects. Small sized nanoparticles have larger surface area to volume ratio than their conventional forms, which can lead to greater chemical reactivity. Another stringent feature is the quantum confinement of energy. Reduced imperfections imply another counter part of nanoparticles in comparison with corresponding bulk materials. Considering the unique photo-physical properties of these nanoparticles, it can be used for variety of application in various fields such as biomedicine, drug designing, cosmetics, electronics, food industry and environmental remediation to enhance the performance of renewable energy harvesting, automotive catalytic converters in mechanical industry *etc.*, (Ealias and Saravanakumar, 2017).

There are two methods widely used for the synthesis of nanoparticles. The first one is bottom up method and second one is top down method (Figure 1.2). In bottom up method, nanostructures are built upon by atom-by-atom or molecule-by-molecule or cluster-by cluster assemblies from the bottom phase. These include Sol-Gel process, chemical vapour deposition, chemical reduction methods *etc.*,

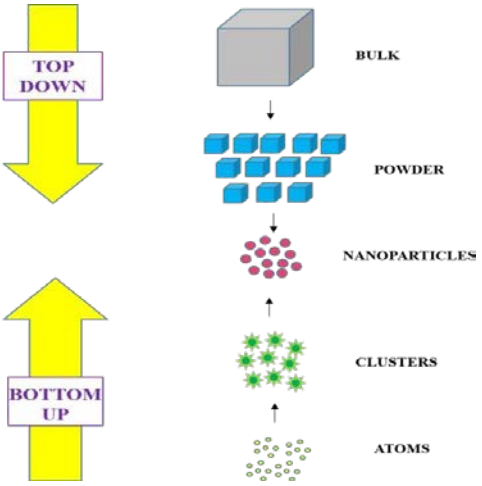

Figure 1.2: Bottom up and top down approaches in nanoparticle synthesis.

In the top-down method, the process involves making nanostructures starting with larger molecules and breaking down to nanosize e.g. lithography, epitaxial, ball milling *etc.*, (Anu and Saravanakumar, 2017). Bottom-up method plays a very important role in preparing nanoparticles having very small size. Whereas top-down process cannot deal with the very minute objects. The bottom-up method generally produces nanostructures with fewer defects as compared to the nanostructures produced by the top-down method. Reduction in Gibbs free energy is the main driving force behind the bottom-up method. Consequently, the particles formed are close to their equilibrium state. In case of top-down techniques, significant crystallographic defects can be introduced to the nanoparticles formed and these defects can affect the surface properties like reduced conductivity, excessive heat production *etc*., Nanoparticles are also synthesised via biological routes; from algae, yeast, fungi, bacteria and plants. In this green and environmental friendly biosynthesis method, bacteria, fungi, plant extracts *etc.*, are used along with the precursors to produce nanoparticles instead of conventional chemical route for bio-reduction and capping purposes (Rajput, 2015).

Characterization refers to the study of particle features like its size, shape, charge, morphology, composition, structure and various other properties such as physical, electrical, magnetic *etc*., Properties of nanoparticles significantly change with their physico-chemical characteristics. Therefore, it is very essential to characterize the nanoparticles for elucidating its wide variety of applications (Mourdikoudis *et al*., 2018). Nanoparticle toxicity sturdily depends on their physical and chemical properties such as the size, shape, electric charge, crystallinity, stability, surface chemistry, aggregation and chemical composition of the core and shell (Sukhanova *et al*., 2018).

The properties of nanoparticles can very well affect its physical stability and *in vivo* distribution so that physico-chemical characterisation is a mandatory requirement before it is subjected for biomedical applications. Different characterisation tools and techniques have been employed for the analysis of various physicochemical properties of nanoparticles. Advanced microscopic techniques such as Scanning Electron Microscopy (SEM), Transmission Electron Microscopy (TEM), Atomic Force Microscopy (AFM) and Polarised Optical Microscopy (POM) are most important for morphological characterisations. Structural characterisation can be done using X-ray Powder Diffraction (XRD), X-ray Photoelectron Spectroscopy (XPS), Energy Dispersive X-ray (EDX), Raman spectroscopy, Fourier-Transform Infra-Red spectroscopy (FTIR), Brunauer-Emmett-Teller (BET) and Zeta size analyser. Ultra Violet-visible (UV-Vis) spectroscopy, Photoluminescence (PL) spectroscopy and null ellipsometer are well recognized optical instruments which can be used to study the optical properties of nanoparticles (Mourdikoudis *et al*., 2018).

1.1 TYPES OF NANOPARTICLES

Nanoparticles are classified on the basis of their source and dimensionality. It is also divided into various categories depending on their composition (Figure 1.3) (Hett, 2004).

1.1.1 BASED ON THEIR SOURCE

Nanoparticles are classified as natural or synthetic on the basis of their source of origin. Natural nanoparticles are found in the body of organisms, insects, plants, animals and humans. They are also produced as a result of photochemical reactions, volcanic eruptions, forest fires, dust storms, cosmic dust and ocean water evaporation (Jeevanandam *et al*., 2018). Synthetic nanoparticles are a new category of nanoparticles that may prompt hostile environmental and human health effects. Simple combustion during cooking, fuel combustion and coal for power generation, smoke from vehicles or airplane engines, chemical manufacturing, ore refining and welding are some of the anthropogenic activities that lead to nanoparticle formation. Carbon, ZnO, TiO_2 and hydroxyapatite nanoparticles are present in sporting goods, cosmetics and toothpaste.

1.1.2 BASED ON THEIR DIMENSION

Pokropivny and Skorokhod made a new system of classification for nanoparticles such as 0D, 1D, 2D and 3Ds. This classification is based on the electron

movement along the dimensions in the nanoparticles. In the case of zero dimensions, electrons are entrapped in a dimensionless space (e.g. Quantum Dots). Electrons and holes are completely confined in QDs. In the case of one dimensional nanoparticles, electrons can move along the x-axis, which is less than 100 nm. Thin monolayer films used in biological sensors, magneto-optical devices and information storage systems are examples of 1D particles. Similarly, two and three dimensional nanoparticles have electron movement along the x, y axis and x, y, z axis respectively. Carbon nanotubes are 2D particles whereas dendrimers and Fullerenes belongs to 3D classification (Pokropivny and Skorokhod, 2007).

1.1.3 BASED ON THE COMPOSITION OF NANOPARTICLES

1.1.3.1 CARBON BASED NANOPARTICLES

Fullerenes and carbon nanotubes (CNTs) are two major groups of carbon based nanoparticles. Carbon nanofibers, carbon black, carbon onions and graphene are also included under the category of carbon-based nanoparticles. Fullerenes are made up of globular hollow cage. Their high strength, electrical conductivity, structure, versatility and electron affinity make them as an attractive candidate of commercial interest. C60 and C70 are the renowned fullerenes with a diameter of 7.114 and 7.648 nm, respectively (Cha *et al*., 2013).

CNTs are elongated, tubular structured, carbon based nanoparticles having a diameter of 1-2 nm. These are third allotropic crystalline form of carbon sheets structurally similar to graphite sheet rolling upon itself. The rolled sheets can be single, double or many walled and therefore they named as single-walled (SWNTs), double-walled (DWNTs) or multi-walled carbon nanotubes (MWNTs) respectively. CNTs are widely used in pristine form as a support medium for different inorganic and organic catalysts and nanocomposites. It is also used for many commercial applications such as fillers and efficient gas adsorbents for environmental remediation due to their exceptional physical, chemical and mechanical characteristics. Fabrication of these carbon based nanoparticles are possible by versatile methods of synthesis such as arc discharge, laser ablation and chemical vapour deposition (CVD) (Jeevanandam *et al*., 2018).

1.1.3.2 ORGANIC NANOPARTICLES

These groups of particles made typically from organic matter, apart from

carbon based and inorganic based nanoparticles. The exploitation of weak non- covalent interactions for the self-assembly and design of molecules helps to transform the organic nanoparticles into desired structures such as polymeric nanoparticles, liposomes, micelles and dendrimers. Polymeric nanoparticles (PNP) are normally organic based particles and most of them are Nano spheres or Nano capsular in shape. Nano spheres are matrix particles whose overall mass is generally solid and the other molecules are adsorbed at the outer boundary of the spherical surface. Micelles and liposomes have a hollow core, also known as Nano capsules. In the case of the Nano capsular structure, the solid mass is encapsulated within the particle completely (Geckeler and Rao, 2011). Liposomes are vesicles composed of a phospholipid bilayer surrounding a hollow core into which drugs or other molecules can be loaded for delivery to tumours or other disease sites. Both hydrophobic and hydrophilic drugs and molecules can be efficiently carried by these liposomes (McMillan *et al*., 2011). Micelles are formed as aggregates of surfactant molecules when the surfactant concentration exceeds the critical micelle concentration (CMC) in water. In case of normal micelles, the hydrophobic hydrocarbon chains of the surfactants are oriented towards the interior of the micelle and hydrophilic groups of the surfactants are in contact with the surrounding aqueous medium. Higher than the CMC, the physical state of the surfactant molecules changes considerably and the additional surfactant exists as micelles or aggregates (Husseini and Pitt, 2008).

1.1.3.3 COMPOSITE BASED NANOPARTICLES

Nanocomposites are multiphase nanoparticles in which at least one of the phases shows dimensions in the nanometer range that can either combine with other nanoparticles or with larger or bulk-type materials (e.g., hybrid nanofibers) or even with more complicated structures such as a metal organic frame works. The composites may be any combinations of metal-based, carbon-based or organic-based nanoparticles with any form of ceramic, metal or polymer bulk materials. Incorporation of Nano hydroxyapatite (nHAP) within a chitosan (CS)/silk fibroin (SF) Nano fibrous membrane scaffold (NMS) was proved to be an excellent tool for bone tissue engineering (Lai *et al*., 2015). Both graphene and CNTs based nanocomposite hydrogels are evaluated for applications such as conductive tapes, actuators, tissue engineering scaffolds, biosensors, biomedical devices and drug delivery systems (Goenka *et al*., 2014). Designing of therapeutic devices for drug delivery and tissue

engineering applications was found possible by using poly (N-isopropyl acrylamide) (PNI-PAAm) based nanoparticles/ hydrogels (Gaharwar *et al*., 2014).

1.1.3.4 INORGANIC NANOPARTICLES

These include metal and metal oxide nanoparticles, semiconductors, silicon and ceramics. Metal nanoparticles are purely made of submicron scale entities of pure metals (e.g., gold, platinum, silver, titanium, zinc, cerium, iron and thallium) or their metal precursors (e.g., oxides, hydroxides, sulphides, phosphates, fluorides and chlorides). Currently metallic nanoparticle evolved as a good agent for drug delivery and biosensors. Diverse metals have been explored for the synthesis of metallic nanoparticles. Among them silver and gold nanoparticles are of prime importance for biomedical applications. Variable ligands such as peptide, sugars, protein and DNA have been linked to nanoparticles as a part of surface functionalization and it is easily possible because of their large surface area (Kim *et al*., 2018).

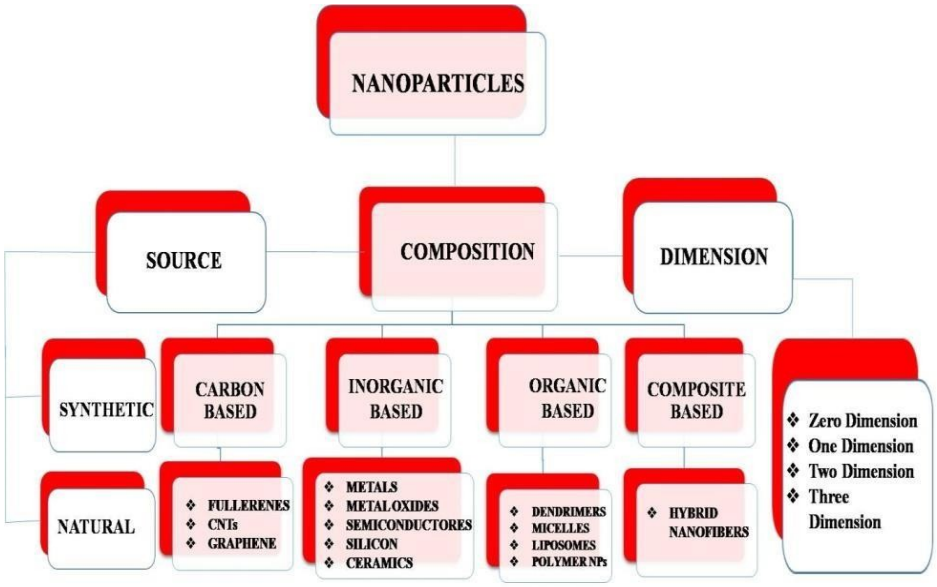

Figure 1.3: Classification of nanoparticles: based on the source, dimension and composition.

The metal elements are capable of forming a large diversity of oxide compounds such as Al_2O_3, MgO, ZrO_2, CeO_2, TiO_2, ZnO, Fe_2O_3 and SnO. Metal oxides have attracted considerable interest in many fields like sensors, microelectronic circuits, piezoelectric devices, coatings for the passivation of surfaces againstcorrosion, fuel cells, catalysts (Falcaro *et al*., 2016), therapeutics, bio sensing and bio- imaging (Andreescu et al., 2012).

Titania is the material of interest in medical implants. It provides an exceptional biocompatible surface for cell attachment and proliferation. Ceria based nanoparticles have recently received a great deal of attention because of their auto-catalytic, redox and antioxidant properties. ZnO nanoparticles are widely used for wound dressings and coating of various medical devices to prevent biofilm formation. Magnetic nature of Fe_3O_4 makes it suitable for a broad range of application such as hyperthermia, magnetic resonance imaging contrast agent or drug delivery (Corr, 2012). Silicon dioxide nanoparticles (silica nanoparticles), used for biological applications on account of their excellent biocompatibility, facile synthetic route, low toxicity, thermal stability and large-scale synthetic availability (Kim *et al*., 2014). Ceramic nanoparticles are predominantly made up of carbides, oxides, phosphates and carbonates of metals and metalloids such as titanium, calcium, silicon *etc*., These nanoparticles have been successfully used as drug delivery agent against a number of diseases, such as glaucoma, bacterial infections and tumour. It is also considered to be an excellent carrier for genes, drugs, proteins and imaging agents. These applications are mainly due to a number of favourable properties of ceramic nanoparticles such as high heat resistance and chemical inertness (Thomas *et al*., 2015).

Semiconductor nanoparticles are also known as Quantum dots (QDs) with a size of 1–10 nm and possess distinct characteristics between metals and non-metals. QDs have wide band gaps and therefore showed significant amendment in their properties with band gap tuning. QDs are very important materials in photo optics, photo catalysis and electronic devices and are found exceptionally efficient in water splitting applications (Valizadeh *et al*., 2012). Main applications of QDs are theranostics tool for *in vitro* and *in vivo* detection, analysis of biomolecules, DNA hybridization, immunoassays, diagnostic tools (Magnetic Resonance Imaging), development of non- viral vectors for gene therapy, time graded fluorescence imaging of tissue, labelling of cells, therapeutic tools for cancer treatment, transport vehicles for DNA and protein (Bailey *et al*., 2004).

1.2 QUANTUM DOTS

Quantum dots (QDs) are nanometer sized semiconductor crystals, generally fall within 2–10 nm size range and possess size tunable optical and electrical

properties. Currently 'nanotechnology' focuses on developing new generation Quantum dots for multitasking purposes like biomedical diagnostics, photo catalysts, photo detector devices, light emitting diodes *etc*., QDs are zero dimensional nanoparticles in which the electrons and holes are completely confined. This is also known as artificial atom as a consequence of its quantum properties (Drbohlavova *et al*., 2009). Sharp and narrow luminescent emission peaks are observed for isolated atoms. However, nanoparticles composed of approximately 100-10000 atoms exhibits distinct narrow optical line spectra. Due to this reason, QDs are often described as artificial atoms (Alivisatos, 1996). Semiconductor nanocrystals are composed of groups II - IV (CdSe, CdS and CdTe), IV -VI (PbS, PbSe, PbTe, SnTe) and III-V (InP, InAs) elements of periodic table (Ji *et al*., 2014). The QDs (2-10nm size) are completely different from the bulk material of the same kind, because of the 'quantum confinement' effect. If the radii of QDs are on the Bohr-exciton radius, then the quantum dots are said to be in weak confinement regime and the radii less than the Bohr-exciton radius, then the quantum dots are said to be in strong confinement regime. Strong confinement of excitons of QDs, is the main reason for their exceptional photo physical properties. These properties include size/composition tunable light emission, broad absorption spectra and size tunable narrow emission spectra, enormous absorption extinction coefficients, high fluorescent quantum yields, photochemical robustness, resistance to photo bleach effect, reduction in fluorescence intermittency, large stokes shift *etc.*, (Mohanan and Reshma, 2019). Basic structure of core-shell type QDs consist of a semiconductor core encrusted by a shell. The shell is often made of a larger band gap semiconductor which improves the optical properties of QDs and prevents leaching of metal ions from the core. Surface of the shell can be further modified by various proteins, peptides, antibodies and receptors depending on their solubility criteria and respective applications. Core-shell QDs research intended for biological applications has four basic steps and is mentioned below:

- core synthesis
- shell growth
- aqueous solubilisation
- bio molecular conjugation.

The QDs are used in *in vitro* and *in vivo* imaging, drug/gene delivery, photodynamic therapy (PDT), pathogen and toxin detections *etc*., Toxicity is a major

obstacle while considering QDs for various biomedical applications. Most of the QDs used in various biomedical applications contain major heavy metals like cadmium and lead. Leakages of these heavy metal ions are responsible for the toxicity. Hence researchers started to concentrate on the synthesis of less toxic, heavy metal free QDs. QDs doped with transition elements are the new trendy attractive approach for reducing cytotoxicity (Maysinger and Winnik, 2013). Significant challenges still exist and need to be validated before their clinical applications.

1.3 TYPES OF QUANTUM DOTS

Murray *et al.,* successfully synthesised colloidal CdX (X = S/Se/Te) QDs with size tunable band edge absorption and emissions (Murray *et al*., 1993). Because of their excellent optical and electrochemical properties, CdX is the most explored QDs. Cadmium ions present in these QDs become a great barrier towards its biological applications. In pursuance of improving the stability as well as photoluminescence (PL) quantum yield and biocompatibility of these core nanocrystals, a layer of high band gap semiconductor was introduced to enclose the core nanocrystals to form core- shell structure. This shell structure prevents leaching of metal ions from the core along with the improvement of photoluminescence. CdSe/CdS and CdSe/ZnS are the most extensively studied QDs during the early days. Subsequently additional 'core-shell' QDs was developed, such as CdTe/CdS, CdSe/ZnSe, CdTe/ZnS. Further 'core-shell- shell' QDs were also developed (e.g.: CdTe/CdS/ZnS). Heavy metals present in the traditional nanocrystals hampers their biomedical application, which demand for more biocompatible heavy metal free QDs.

1.3.1 BASED ON THEIR COMPOSITION

1.3.1.1 HEAVY METAL CONTAINING QDs

These are the traditional QDs which contain heavy metals like cadmium and lead, as the main elements of their composition. CdS, CdSe, CdTe, CdS/ZnS, CdSe/ZnS, CdSeTe/ZnS, PbS are few examples of QDs. It is well known that leaked heavy metal ions are responsible for the toxicity. Exposure to even very low levels of Lead and Cadmium ions are known to cause cancer, cardiovascular diseases, damage to kidneys, liver and central nervous system. Neurological, reproductive and developmental disorders are becoming more serious problems associated with adults as

well as children (Carrillo and Vázquez, 2014).

1.3.1.2 HEAVY METALS FREE QDS

Fabrication of heavy metal free QDs like carbon dots (C-dots), graphene, Silicon, Ag_2Se, Ag_2S, InP, ZnSe/ZnS and $CuInS_2$/ZnS are flourished in accordance with the demand for non-toxic and more biocompatible QDs for biological applications (Xu *et al*., 2016).

1.3.1.3 DOPED QDS

Enhancement of optical properties of QDs can be achieved by a process known as doping. In this process, impurities known as dopants added to disturb the band structures by local quantum states that lie within the band gaps. Dopants have the capacity to auto-ionize, devoid of any thermal activation due to quantum confinement. This is an important facet when QDs are used for a variety of technological applications especially magnetic, optoelectronic and biological applications. There are several transition elements such as Mn, Cr, Fe, Cu, Co and Ag as well as other elements such as P, Li, Na and B were doped in QDs depending on the applications (Bera *et al*., 2010).

1.3.1.4 ALLOYED QDS

By keeping the constant size of QDs, the band gap can be engineered by alloying the core structure and modifying the optical properties. QDs alloyed with multiple semiconductors shows mixed or intermediate optoelectronic properties, e.g. CdHgTe QDs (Bailey *et al*., 2004).

1.3.2 BASED ON BAND ALIGNMENT

QDs again classified into two on the basis of band alignment and are type-I and type-II. In self-assembled QDs, the band alignment of the interfaces is one of the key parameters that determines both electron and hole spatial distribution inside or around the dots. This charge distribution fallout in a completely distinct behavior for QD emission. On the basis of band alignment or lay out, QDs are divided into two types. In type-I QDs, photo created electrons and holes are both confined in the QD layer. In type-II structures, either the electron or the hole is confined in the dot and the other carrier remains in neighboring QDs due to the coulomb attraction between the e-h pair

(Iikawa *et al*., 2004). Type-I have contravariant band layout whereas QDs of type-II have covariant band layout (figure1.4). Type I and II can be distinguished on the basis of characteristic structure of PL spectrum. In the presence of moderate magnetic field, highly sensitive type-II dots shows multi peak PL spectrum. Therefore, type 2 QDs show complex spectrum compared to Type 1 single peak PL spectrum (Tytus *et al*., 2008).

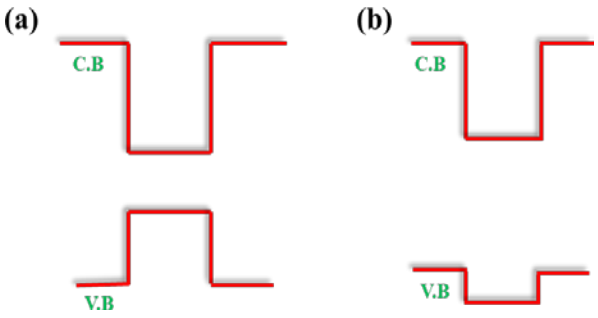

Figure 1.4: Band lay out for (a) Type I QD & (b) Type II QD. C. B: Conduction band, V. B: Valance band.

1.4 TOXICOLOGY

Toxicology is the basic science of poison that deals with study of how chemicals impede with the normal function of a biological system. Poison is any chemical which is toxic and can cause serious health hazards when used by any means either intentionally or un-intentionally. Classical Paracelsus (1493-1541) theory seeded the concept of toxicology, where it explains about linear relationship between the doses vs. toxicity. According to this concept, 'All materials are poisons; there is none which is not a poison. The precise dose discriminates a poison and a cure', or the dose makes the poison. The study of toxicology offers safety to humans and environment from toxic effects of toxicants. This study will eventually guide toward the development of newer, innovative and more selective drug therapies to treat different ailments (Sullivan *et al*., 2005).

1.5 NANOTOXICOLOGY

Nano toxicology is a branch of bio nanoscience to address the adverse effects caused by nanoparticles (Buzea *et al*., 2007). The risks related with nanoparticles depend on their exposure and hazard potential. Environmental and occupational

exposure in combination with other toxic agents can cause injurious effect to the human health (Gwinn and Vallyathan, 2006). Occupational exposure is caused by regular involvement of the person with nanoparticles. Nano toxicology is mandatory pre-requisite for the commercialization of many nanotechnology products. An assessment of their potential toxicity is highly critical in this situation. Currently, evaluation of nanoparticle toxicity is based on various *in vitro* methods established for hazard characterization of chemicals. Screening techniques commonly used for evaluation of toxicity of macro-scale substances may not be appropriate for nanoparticles. Characterization of nanoparticle hazard have to be adapted or modified with regard to their Nano specific properties (Oberdorster *et al*., 2005). It is difficult to design Nano toxicological studies using classical/traditional toxicology methods, because the nanoparticles do not show a linear relationship between dose and toxicity. Moreover, one of the major challenges encountered in Nano toxicology is the lack of internationally validated/ harmonized guidelines/standards.

CHAPTER 2: REVIEW OF LITERATURE

2. REVIEW OF LITERATURE

2.1 QUANTUM DOTS

Human beings are living in nanotechnology era where a functional system can be engineered at molecular level. Nanotechnology is an emerging area that has achieved prominence in every field of life from sunscreen to an excellent electronic chip. The progress in nanoparticle synthesis and nanotechnology research has demonstrated a strong driving force in all fields of engineering, healthcare and science. Quantum Dots (QDs) are one of the foremost groups of nanoparticles widely exploited for various industrial and biomedical applications. The concept of QDs was first developed by Alexey Ekimovat (1981) and Brus (1985) in solid (glass crystals) and liquid state respectively. The term 'Quantum Dots' was coined by Mark Reed in 1988, that implies a miniature and discrete unit of any physical property (Reed *et al*., 1988). This name was derived from the fact that the optical properties of nanocrystals (NC) i.e. 'dots' are dictated by quantum mechanics (Matea *et al*., 2017). QDs are known as new generation nanometer sized semiconductor inorganic crystals. Technically they are defined as 'small crystals containing a variable number of electrons that occupy well-defined, discrete quantum states and have electronic properties intermediate between bulk and discrete fundamental particle'. QD have the same arrangement of atoms as in the respective bulk material but many more surface atoms are present on the surface due to 3-dimensional truncation (Khalid and Kontis, 2008). Physical, chemical and electronic properties change spectacularly at this level due to *quantum effects* resulting from *quantum confinement*. These QDs display physicochemical properties, such as high fluorescence stability, broad absorption spectra, narrow and symmetric emission spectra, high and broad energy absorption cross sections. Their emission colors depend on their size, chemical composition and surface chemistry. Therefore, QDs can be tuned from the ultraviolet to the infrared region via visible wavelengths. These properties make them suitable for various applications in solid- state lighting and color display, photo detectors, photovoltaic and quantum computing. In biomedical field, they are used for *in vitro* and *in vivo* imaging, drug/gene delivery, photodynamic therapy (PDT) and theranostics (Bonilla *et al*., 2016). Their long- standing effect on cell viability is becoming vital as QDs are progressively used for various biomedical applications. Cadmium (Cd) based chalcogenide

like CdTe, CdSe and CdS nanocrystals are regarded as a promising materials for this field. But Cd^{2+} present in the QDs leaches out into the tissues causing toxicity. Thus researchers working in the QDs are now much concentrating on the green synthetic approach (Bonilla and Kouznetsov, 2016a).

2.2 SYNTHESIS OF QUANTUM DOTS

There are mainly two approaches in QDs synthesis (Figure 2.1);

- batch synthetic method
- scaled up synthetic method

2.2.1 BATCH SYNTHETIC METHOD

The methods of synthesis are broadly divided into three types (Valizadeh *et al.*, 2012);

- bottom-up method
- top-down method and
- Other methods.

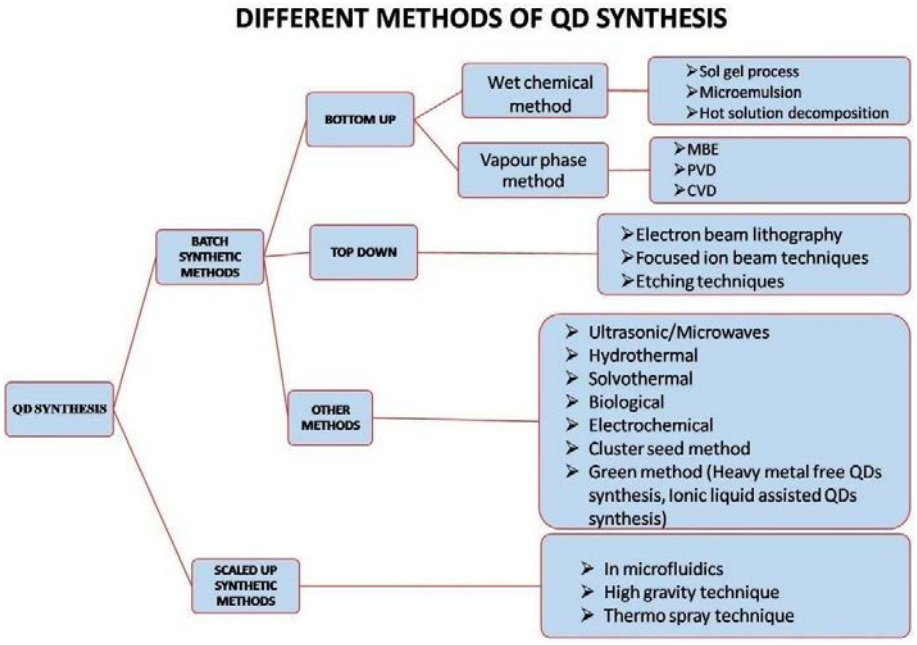

Figure 2.1: Different methods of QD synthesis.

2.2.1.1 BOTTOM-UP METHOD

This approach comprises colloidal chemistry techniques that implicate the reactions between solvents, stabilizing agents and molecular precursors producing colloidal semiconductor nanocrystals. By this approach, QDs will arrange by self-assembly in the solution following a chemical reduction (Bera *et al*., 2010). Easy to synthesis with minimum equipment and low costs material are the peculiar features of bottom-up method, when compared to top-down synthetic method. Wet chemical and vapor phase methods are the two sub divisions of bottom-up method (Wang and Xia., 2004).

2.2.1.1.1 **WET-CHEMICAL METHOD**

This method mainly follows the conservative precipitation method with varying control of parameters. The precipitation process regularly involves both nucleation and limited growth of nanoparticles. Homogeneous, heterogeneous or secondary nucleation types are existing (Burda *et al*., 2005). Homogeneous nucleation occurs when solute atoms or molecules combine and reach a critical size without the assistance of a pre-existing solid interface. Generally, wet-chemical method includes the following.

2.2.1.1.2 SOL-GEL PROCESS

Nanoparticles including QDs are synthesized by this technique for many years. A sol is the nanoparticles dispersed in a solvent by *Brownian* motion. It is prepared using a metal precursor generally nitrates, acetates or alkoxidesin an acidic or basic medium. This process mainly includes three steps; hydrolysis, condensation and growth. In short, the metal precursor hydrolyzes in the medium and condenses to form a sol, followed by polymerization to form a network of gel. II-VI & IV-VI type QDs, like CdS, ZnO, PbS are synthesized by this process (Bera *et al*., 2010). The process is effortless, commercial and apt for scale-up. The main disadvantages of the sol-gel process comprise a broad size distribution and a high amount of defects (Sashchiuk *et al*., 2002). Therefore, this synthesis technique is used scarcely.

2.2.1.1.3 MICRO EMULSION PROCESS

Micro emulsion process is well-opted method for synthesizing QDs at room

temperature. The process can be grouped as normal micro emulsions (oil-in-water) and reverse micro emulsions (water-in-oil). QDs synthesized by the reverse micelle process uses two immiscible liquids. They are polar and non-polar, which are mixed and stirred to form emulsion. Micelles terminated by hydrophilic and hydrophobic groups on opposite ends are formed with the help of many surfactants like cetyl trimethyl-ammonium bromide (CTAB), aerosol OT (AOT), triton-X or sodium dodecyl sulphate (SDS). These micelles can act as thermodynamically stable 'nanoreactors'. II-VI core and core/shell QDs, such as CdS, CdS: Mn/ZnS (Yang *et al*., 2005), ZnS/CdSe, CdSe/ZnSe (Mallouk e*t al*., 1992), ZnSe (Karanikolos *et al.*, 2004) and IV-VI QDs (Ogawa *et al*., 1997) are prepared by reverse micelle technique. Easy control of the QDs size by changing the molar ratio of water to surfactant and ease of dispersion of the QDs are some of the advantages of this process. Low yield and integration of impurities and defects are some of the noted disadvantages.

2.2.1.1.4 ORGANOMETALLIC SYNTHESIS

This method is the most famous method for QD synthesis. Organometallic synthesis of QDs was developed in early 1990s by Steigerwald and Brus. The organometallic system mainly consists of three components: precursors, organic surfactants and solvents. In some cases, surfactants also serve as solvents (Alivisatos and Yin, 2005). By altering the concentration of precursors and time of crystal growth, size of metal chalcogenide based QDs can be tuned. Ionic sources of the component materials are essential for this type of synthesis. Pyrolysis of organometallic compound into a hot coordinating solvent is an essential step of this synthetic method. After dissolving in the solvent, they decompose into reactive species known as monomers followed by nanocrystal nucleation and growth. High reaction temperature (>150-350°C) is essential for the synthetic method and this condition will help to improve the photoluminescence and removes crystalline defects (Cingarapu *et al*., 2012). Organometallic methods are not ideal for synthesis due to the use of toxic, unstable chemicals and high reaction temperatures (Jiao *et al*., 2012).

2.2.1.1.5 COLLOIDAL SYNTHETIC PROCESS

The classic work of LaMer and Dinegar from 1940-1950 proposed a mechanism for synthesis of colloidal nanocrystals. In this process, there are three stage colloidal formation models and are depicted in the figure 2.2;

1) Monomer accumulation, *i.e.* the precursors chemically converts into active atomic or molecular species called monomers when the reaction medium is warm adequately.
2) Homogeneous nucleation occurs after decomposition of precursors at a high-temperature and reacts to form a super saturation of monomers.
3) Diffusion controlled growth (i.e., Ostwald ripening) (Pan *et al*., 2015).

The three stages are depicted in Figure 2.2.

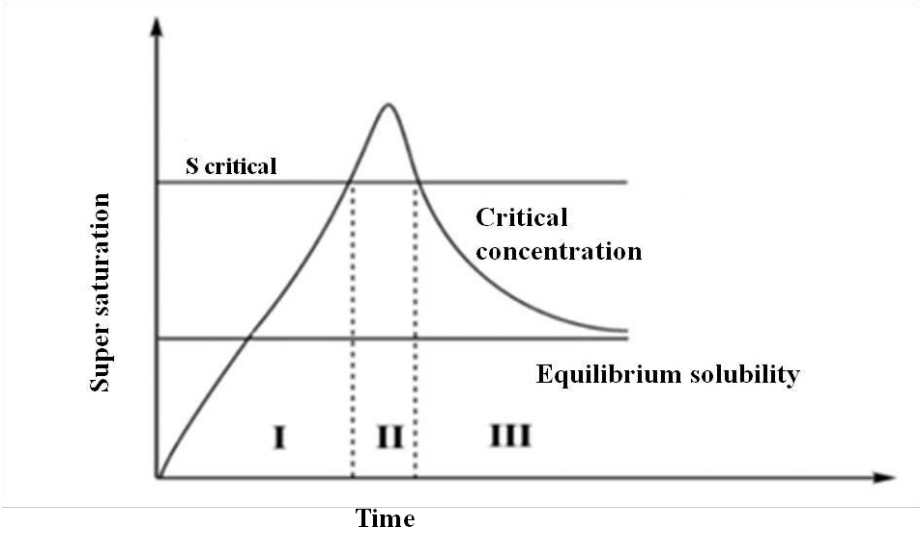

Figure 2.2: Three-stage colloidal formation model (LaMer's model): (I) monomer accumulation; (II) homogeneous nucleation; and (III) diffusion-controlled growth (i.e., Ostwald ripening) adapted from (Pan *et al*., 2015).

Normally there are two methods used for nanocrystal synthesis;

- hot injection method and
- non-injection methods.

In 1993, Murray group reported hot injection method for the first time (Murray *et*

al., 1993). They synthesized monodispersed cadmium chalcogenide QDs by special method of LaMer's three stage crystal formation model which excludes stage I. The non-injection method was initially introduced by Cao *et al.,* in 2004 which include all the stages of LaMer's model. The non-injection method is the simplest and convenient method due to the less demanding experimental processes. A high reaction temperature and a long reaction time are essential for a typical non-injection process, since non-metal solids generally used as precursors need to be dissolved to initiate the nucleation (Yang *et al*., 2005).

2.2.1.1.6 AQUEOUS COLLOIDAL SYNTHESIS

In this method, almost similar route is applicable for all the nanocrystals. In brief, metal salt is dissolved in water in the presence of the thiol as stabilizing agent. It is necessary to purge inert gas to the original solution before the chalcogen source is injected. The common thiols used are 2-mercaptoethanol, 1-thioglycerol, thioglycolic acid (TGA), thiolactic acid, 1-mercapto-2-propanol and 1, 2-dimercapto-3-propanol. Various parameters such as molar concentration of reactants, pH of the mixture, reaction temperature and heating time affects the QDs synthesis through aqueous route. pH influences aggregation of QDs which in turn give rise to reduction in fluorescence. At higher temperature, growth rate of QDs increases which will curtail the creation of surface defects and thus improve the fluorescence properties of the QDs. Heating time also has direct influence on the QDs growth. Longer heating time will result in large sized higher wavelength emitting QDs formation. Advantages of aqueous colloidal synthesis over organometallic method are;

- Use environmental friendly and biocompatible solvents
- Inert atmosphere is not strictly necessary
- can scale up easily
- Possibility for functionalization of QDs, with capping agent which is capable of covalent or electrostatic linking (Bonilla and Kouznetsov, 2016).

2.2.1.1.7 VAPOR-PHASE METHODS

In this method, QDs formation begins with layer formation by atom-by-atom growth. As a result, QDs self-assemble on a substrate short of any designing. Three mode of layer growth can be observed according to the interfacial energies and lattice mismatch.

2.2.1.2 TOP-DOWN SYNTHESIS PROCESSES

This includes process by which a bulk semiconductor is thinned to form the QDs using physical or chemical techniques. These methods include ion implantation, electron beam lithography and X-ray lithography. Electron beam lithography, reactive- ion and wet chemical etching are commonly used for getting 30 nm ranged QDs. Focused ion or laser beams have also been used to formulate 2-10 nm sized QDs. These processes involve costly equipment and production of large quantity of material waste. It is not reasonable for large scale QDs production since it is time consuming and expensive (Drbohlavova *et al*., 2009). Structural defectiveness by patterning and integration of impurities into the QDs are also major drawbacks of this method.

2.2.1.3 OTHER SYNTHESIS PROCESSES

Mixture of precursors in water is exposed to sonic waves or microwaves which will provide energy to dissociate the precursor and water molecules resulting in the growth of QDs. Size range of 1-5 nm QDs are synthesized by passing ultrasound waves. In another case, acetate precursors of metal ions were dispersed in a solution and seleno- urea was added and sonicated for an hour under argon atmosphere. The temperature of the solution is maintained at 80 ºC throughout the time required to produce QDs (Zhu *et al*., 2000). Hydrothermal process is also another type of QDs synthesis method. Here, crystallization of inorganic salts occurs from aqueous solution and this process is regulated by pressure and temperature. Size and shape of QDs can be regulated by changing the factors like temperature, pressure, aging, reaction time and reactants (Karmakar *et al*., 2015). Solvo-thermal synthetic method is similar to the hydrothermal process. Only difference is in case of precursor solution which is usually non-aqueous in solvo-thermal method. Du *et al.*, synthesized ultra-minute $CuInSe_2$ QDs by solvo- thermal method (Du *et al*., 2014).

2.2.2 SCALED UP SYNTHESIS METHOD

Synthesis of QDs is controlled by parameters like temperature, precursor injection rate and stirring rate. All these are critical factors for the quality of final product. Continuous reactor is an alternative to batch reactor. In the former, reactors are continuously fed and the products are obtained continuously. Consistent quality products are obtained from this system since parameters are well regulated.

Microfluidics is typical continuous reactors which are integrated with heaters and fluid control elements. Synthesis of QDs in microfluidics offers much higher levels of reaction process control than those attained in conventional batch-type reactors. Surface functionalized CdTe and CdSe QDs are synthesized in the same manner as the organometallic method of batch system. However, the temperature is the only factor that varies in microfluidics system and size of the QDs can be controlled by simply regulating the reaction time (Lignos *et al*., 2014). High gravity reactors such as rotating packed bed (RPB) and spinning disc processor (SDP) are designed for the QDs synthesis. But its application level data are yet to be updated (Hartlieb *et al*., 2007), (Chen *et al*., 2000). Thermospray synthetic approach is very promising for the synthesis of ligand coated QDs since it will prevent the aggregation of QDs, so that well dispersed QDs are obtained (Amirav *et al*., 2005).

2.3 STRUCTURE AND CHARACTERIZATION

2.3.1 STRUCTURE OF QDs

QDs are fabricated from semiconducting materials and are represented by atomic clusters or nanocrystallites. QDs regularly consist of few hundreds to a few millions of atoms but only a lesser number of electrons (≤100) are free (Matagne *et al*., 2000). Typical QDs size range between 2-20 nm, but as stated by some literature their diameter must be strictly below 10 nm (Ferancová and Labuda, 2008). Structurally QDs comprise of a semiconductor core, encrusted by a shell and a ligand capping facilitating improved solubility in aqueous buffers (Ghasemi *et al*.,) (Figure. 2.3).

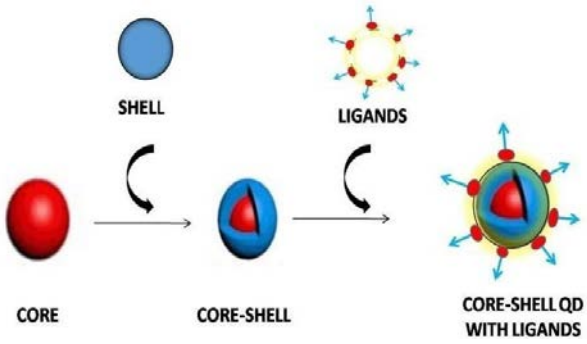

Figure 2.3: Schematic illustration of basic structure of QDs.

Inorganic core is liable for its important semiconducting character and optical properties. The organic surfactants used during the QDs synthesis eventually forms ligands on the surface of core. One of the main problems is that all the surface atoms are unbound to ligands and reside as bare. These dangling bonds are traps on the surface. Energy loss happen when an electron or hole gets stuck on the trap, as a result they cannot fluorescence. In 1996 Hines and Guyot-Sionnest solved this problem by their smart idea. QDs core surface was passivated by another inorganic shell before capping of core with ligands. Shell has wider band gap than the core material. This idea helped to improve the optical properties of QDs as well as suppresses the surface defects by binding up all the surface dangling bonds thereby eliminating trap sites. This modification also helps to avoid photo bleaching, loss of quantum yield (QY) and blinking of QDs. Nature of Ligands also known as capping agents leads main role in biomedical application of QDs. The application of QDs in biology is possible only if it is soluble in water. Alcohols, carboxylic acids, primary amines, thiols and long chain organophosphorates are common ligands employed in various QDs synthesis. Ligand exchange and encapsulation are two methods mainly used for making the water soluble QDs. QDs synthesized in organic solvents are generally hydrophobic ligands like TOPO and TOP. In ligand exchange method, hydrophobic ligand is replaced by thiol based hydrophilic ligands. Encapsulation of QDs with silica, PEG and phospholipids are also make them water soluble (Yu *et al*., 2006). These ligands help in bio conjugation with carbohydrates, peptides, virus, DNA fragments and natural products via hydrophobic interactions or electrostatic and covalent coupling (Chaniotakis and Frasco, 2010). Ligands play a decisive role in colloidal stability, particle size distribution, solubility, particle morphology, prevents uncontrolled growth and agglomeration (Green *et al*., 2010.

Materials are divided into three well known categories such as conductors (metals), semiconductors and insulators based on electron conductivity. Conductivity of solid materials is determined by the difference in energy level between the valance and conduction bands. Valance band (VB) is the highest electronic energy level occupied by electrons at room temperature whereas conduction band is the lowest electronic energy level that is not occupied by electrons. An electron in the valance band gains energy either by absorption of a photon or by thermal means and enters the conduction band, resulting in a positively charged hole in the valance band. The energy difference between valance and conduction bands called band gap energy, determines the energy that must be gained by an electron to enter the conduction band and is expressed in electron volt (eV).

In bulk semiconductors, the valance and conduction bands are parted by a band gap which is intermediate between those of conductors and insulators. Upon light exposure, light is absorbed and electron gets excited from the valance band to the conduction band causing a vacant hole (H+) in VB. Fluorescence is emitted when electrons coming back to VB. Within the small time scale of the light absorption, electrons and holes recognize one another and move around in bulk material. As in the Bohr model of atom, electron orbits the hole at some average distance and holds them together by columbic attraction. Electron-hole pair is termed as ‘exciton’. The distance between electron- hole pair is known as exciton Bohr radius. When three dimensions of bulk semiconductor material are truncated to nanometer scale, particles become smaller than the Bohr radius. This will bring about confinement of energy due to the squeezing of electron hole pairs. Briefly, the quantum confinement effect is detected when the size of the particle is too minor to be comparable to the wavelength of the electron. The term ‘quantum’ reflects the atomic territory of particles and ‘confinement’ means to restrain the motion of randomly moving electron to specific energy levels (discreteness). So as the size of a particle decrease up to a nano scale, confinement of dimension makes the energy levels discrete and this will in turn widen the band gap and ultimately increases the band gap energy. The band gap and wavelength are inversely related to each other. Smaller the QDs synthesized, more squeezing of electron hole pairs occurs leading to higher energy level and shorter wavelength (blue), while larger QDs emits red color. Degree of quantum confinement can be confirmed by the ratio of radius of QDs to bulk exciton Bohr radius (Figure 2.4)

'Particle-in-Box Model', is the most widely used model to predict quantum confinement. It was first developed by Efros and Efros in 1982 and later modified by Brus (Brus & Steigerwald, 1983). The importance of Brus model is mentioned below;

- NC is spherical with a radius 'R'.
- interior of the NC is a uniform medium (i.e. there are no point charges or occupied spaces other than excited electron and hole) and
- the potential energy outside the NC is infinite.

Thus the electron and hole are always found within the NC, i.e. the surface of NC defines the wall of the box (Rosenthal *et al*., 2011). In brief, this model assumes a particle in a potentially well with an infinite potential barrier at the particle boundary.

The QDs are confined in 0D, 1D or 2D (dimension) depending on their charge carriers. On the basis of this quantization effects, the semiconductor structures can be broadly divided into three groups (Alivisatos and Yin, 2004). Confinement in one direction forms two-dimensional (2D) structures that have been termed quantum films or quantum wells. Carrier confinement in two directions creates one-dimensional (1D) quantum wires and confinement in three dimensions creates already mentioned quantum dots, where the electrons are mostly localized; these structures are said to be zero-dimensional (0D).

2.3.2 PHYSICO-CHEMICAL PROPERTIES OF QUANTUM DOTS

QDs exhibit unique optical properties as a result of confinement of electron hole pairs (excitons) within the grain boundary of the nanocrystals. The photo-physical properties include size and composition tunable light emission, broad absorption spectra and narrow emission spectra. It also has enormous absorption extinction coefficients, photochemical robustness, high fluorescent quantum yields, resistance to photo bleach effect, large stokes shift, reduction in fluorescence intermittency. These unique photo-physical properties of QDs make them apt for wide range of biomedical applications such as gene therapy, imaging and drug delivery. The physico-chemical properties of quantum dots are discussed below;

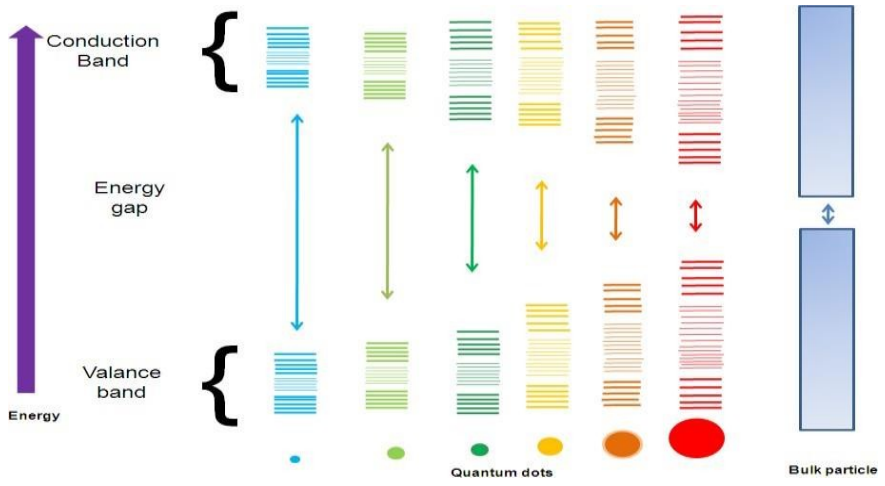

Figure 2.4: Schematic representation of size tunable optical properties of QDs illustrating increase in emission wavelength with increasing QD size (adapted from Mohanan & Reshma., 2018)

2.3.2.1 LIGHT EMISSION

Size and composition determine the colour and emission wavelength of QDs. It can emit light at wavelengths ranging from (400-4000) the ultraviolet (UV) to the infrared (IR) (Jamieson *et al*., 2007) by adjusting their size. Degree of confinement increases as size of QDs decreases, which will lead to formation of an exciton of higher energy thereby increasing the band gap energy. Emission will be towards shorter wavelength (blue region) because of high band gap energy. Energy is inversely proportional to wavelength of light. Different emissions are produced depending on the elements associated with QDs. Emission wavelength range of Cadmium sulfide (CdS) comes under UV blue region of the spectra while cadmium selenium (CdSe) comes under visible region. The cadmium tellurium (CdTe) comes under far red/near infrared region (NIR).

2.3.2.2 BROAD ABSORPTION SPECTRA AND NARROW EMISSION SPECTRA

QDs have broad excitation spectra, which permit excitation by a wide range of wavelengths. QDs require energy to move an electron from the ground state to the excited state. Emission spectra is obtained when an atom or molecule undergo a transition from excited higher energy level to lower energy ground level with an emission of photon energy (hυ). This property is very useful for exciting multiple QDs by a single wavelength of UV or visible light. This implies emitting multiple

wavelength fluorescence light in order to discriminate between tissues or other molecules using different colors. One single source of light can excite all the different size QDs present in the sample that can simplify the instrumentation. Different wavelengths of the emission light can be easily identified and separated from each other because their emission wavelength is narrow (Gao *et al*., 2005).

2.3.2.3 ABSORPTION EXTINCTION COEFFICIENTS

This is a measurement of strength of a chemical species to absorb light at a given wavelength. Light intensities are severely attenuated by scattering and absorption. Massive absorption extinction coefficients make them brighter probes in *in vivo* conditions under limited photon (Mohanan and Reshma, 2019).

2.3.2.4 FLUORESCENT QUANTUM YIELDS

Quantum yield (QY) is an intrinsic property of a fluorescent material defined as ratio of photons absorbed to photons emitted via fluorescence. Lumina fluorescence spectrometer is used for QY measurement (Chaniotakis and Frasco, 2010).

2.3.2.5 PHOTO-CHEMICAL STABILITY

Photochemical stability of QDs has continuously been admired as one of the most important characteristics of QDs. This is the most desirable property of the super-resolution microscopy. The stability increases the number of potential uses of QDs. This exceptional resistance towards photochemical degradation is mainly due to the inorganic nature of QDs (Hanaki *et al*., 2003).

2.3.2.6 PHOTO BLEACHING

Photo bleaching is a phenomenon by which luminescent material decays irreversibly due to light induced excitation leading to the decrease of fluorescence intensity. Dyes and fluorescent proteins photo bleach simply after a relatively low number of photon absorption/emission cycles. But QDs have open to exhibit constant fluorescence intensity for up to thousands times more cycles than the dyes and another fluorescent protein (Gao et al., 2005)

2.3.2.7 STOKES SHIFT

Stokes shift is named after the Irish physicist George G stokes. It is the difference in frequency or wavelength units between positions of band maxima of

absorption and emission spectra of the same electronic transition. There is a large stokes shift, concerning about the absorption and emission spectrum of QDs. It often considered as an agreeable property since it allows for complete separation of wavelengths for excitation and detection. Thus avoids the most crosstalk (Rizvi et al., 2010).

2.3.2.8 FLUORESCENCE INTERMITTENCY

Like all other fluorescent emitters, QDs are also having an interesting property known as blinking or fluorescence intermittency. Blinking is an intriguing phenomenon, especially occurs during continuous excitation of the molecule. The underlying mechanism of this property is mainly caused by the presence of the dangling bonds or unpaired valence electrons. This is the property by which core of QDs charged through an 'Auger ionization' event by trapping excited electrons or holes at the surface. This will modify the photo physical performance of QDs. This also cause the QDs to fluctuate between emissive and non-emissive states, that often remain off for a short period compared to that of fluorophores. Passivation of QDs core with thick crystalline shells leads to reduced fluorescence intermittency (Rosenthal *et al*., 2011).

2.3.3 CHARACTERIZATION

Characterization of nanoparticles is a branch of Nano metrology and is very essential in Nano toxicology studies, to assess occupational health hazards, and control of manufacturing process. Physico-chemical parameters influence the nanoparticles properties when compared with the corresponding bulk material. Hence it is very crucial to characterize the nanoparticles for wide variety of applications. Extensive range of techniques is available to measure these properties, including microscopy, spectroscopy and particle counters. Optical characterization of QDs is usually offered by UV-VIS, fluorescence spectrophotometer and photoluminescence spectroscopy. Both the techniques are non-destructive, fast and contactless methods. UV-Visible spectrophotometer is used to measure the absorbance and transmittance. Absorbance is measured on the basis of Beer Lambert law.

2.3.3.1 SCANNING ELECTRON MICROSCOPE (SEM)

SEM provide high resolution images of the surface of QDs. Working principle of SEM is same as the light microscope, only difference is measuring electrons

scattered from the surface instead of photons. So SEM is capable of magnifying images up to 200,000 times and sensitivity up to 1 nm (Heera and Shanmugam 2015).

2.3.3.2 TRANSMISSION ELECTRON MICROSCOPE (TEM)

Electron microscope offer very powerful tools to explore nanometer scaled structures in solids, especially by using High Resolution Transmission Electron Microscope (HRTEM), conventional Transmission Electron Microscope (TEM) and Scanning Electron Microscope (SEM). A wide variety of imaging methods such as Scanning Tunnelling Microscopy (STM), Atomic Force Microscopy (AFM), Scanning Transmission Electron Microscopy (STEM), Energy Filtered Electron Microscopy (EFTEM), *etc*., are used to investigate growth, the self-assembling and the physical properties of QDs. Among these HRTEM and TEM imaging techniques are suitable methods to characterize directly the shape and size of the nanometer scaled structures and related defects. HRTEM help to get the cross-sectional image and TEM for getting plan view by electron diffraction contrast imaging (DC) with bright field (BF) and dark field (DF) modes. Electron microscope imaging is the only direct method of structure investigation with a sufficient resolution for capped QDs without destructing the dots. TEM analysis may directly confirm whether QDs composition is smooth or in homogeneous distribution. The dot height may be proportional to the deposited materials (Scheerschmidt and Werner, 2002). Gaan *et al.,* (2010) was used Scanning Tunnelling Spectroscopy to monitor the quantum size effects on the electronic structure of QDs in correlation with their morphologies.

2.3.3.3 ATOMIC FORCE MICROSCOPE (AFM)

Topological feature of QDs can be studied by AFM. This is a scanning probe microscopic technique applicable for both conductive and insulating samples. AFM measures the force between the tip and the sample surface by using a pyramid shaped probe that is 3-6 μm in length with a tip diameter of ~25 nm.

2.3.3.4 DYNAMIC LIGHT SCATTERING (DLS)

DLS is a frequently used technique for the hydrodynamic particle size analysis. This is comparatively fast technique which is applicable in the liquid phase. It is based on the dynamic change in the scattering of coherent monochromatic laser light due to

the diffusion of small particles in the solution. In case of QDs, it is very clear that core size distribution is hardly accessible through this mechanism because of the fact that the ligand shell is no longer negligible (Marczak *et al*., 2010)

2.3.3.5 X-RAY PHOTO ELECTRON SPECTROMETER (XPS)

XPS also known as ESCA (Electron Spectroscopy of Chemical Analysis) used to estimate elemental composition on the surface of material up to 10 nm. XPS spectra consist of kinetic energy (KE) measurement and the electrons number escaping from the surface of the material. Binding energy of the electrons to the surface atom is calculated from the KE. Binding energy of the electrons reveals the oxidation state of the specific element present on the surface.

2.3.3.6 FOURIER TRANSFORM INFRARED SPECTROMETER (FTIR)

FTIR is one of the main analytical techniques when limited amount of sample is available. The sample integrity can be preserved due to its nondestructive nature. The FTIR record infrared spectra in the mid infrared region (MIR) within the range of 400-4500 cm^{-1}. Infrared (IR) absorption of the functional groups may vary over a wide range because of the complex interaction of atoms within the molecule. It has been found that many functional groups give characteristic IR absorption at specific narrow frequency range (Radu *et al., 2012*).

2.3.3.7 X-RAY DIFFRACTION (XRD).

Crystal structure and phase of the QDs can be analysed by the conventional XRD technique. This can also be considered as a method to analyze the size and purity of the QDs by measuring the distance between atomic planes. The broad XRD peaks imply tiny size of QDs. Powder XRD is a non-destructive technique (Sun *et al*., 2012).

2.3.3.8 RAMAN SPECTROSCOPY

Raman spectroscopy gives fingerprint of a chemical based on the vibrational information and is specific for the chemical bonds present in it. Laser light interact with phonons results in shifting of laser photons energy. Shift in energy will provide information about phonon modes in the system. It gives idea about crystallographic orientation of the sample.

2.4 APPLICATIONS OF QDS

Studies on colloidal QDs were reported that last two decades have noticed a massive transition in the use of QDs for various non biomedical or biomedical applications (Figure 2.5). International semiconductor device community initially focused on the self-assembly of QDs during growth on a two dimensional semiconductor surface and over the last ten years more concentrated on their applications (Sun *et al*., 2012).

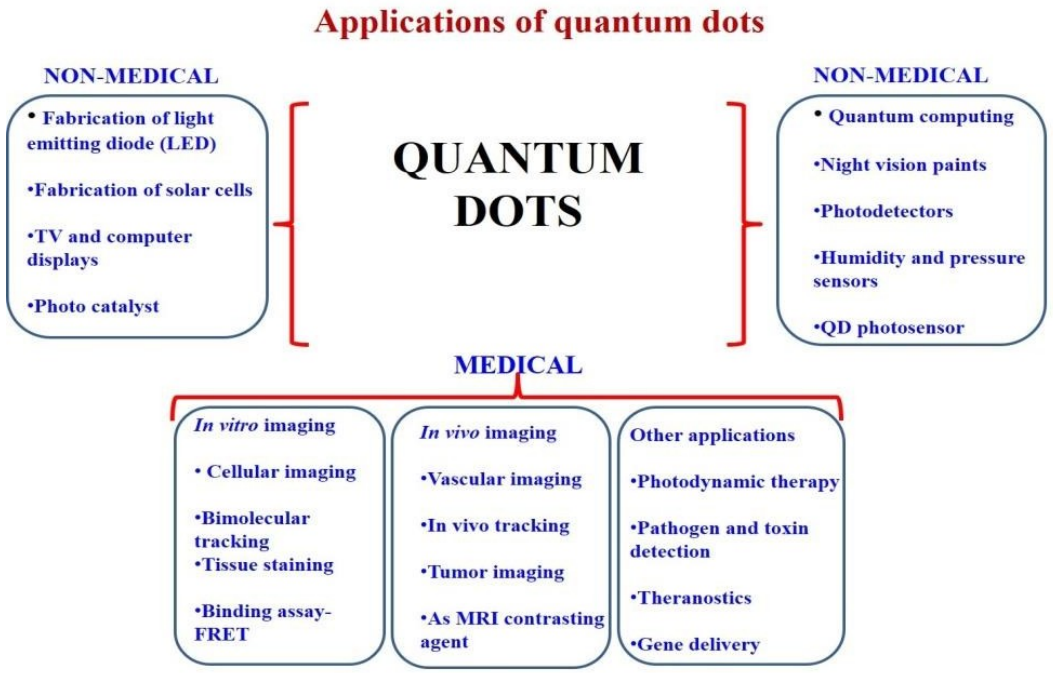

Figure 2.5: Various applications of QDs in biomedical and non-biomedical fields.

2.4.1 NON BIOMEDICAL APPLICATIONS

2.4.1.1 QDs IN FABRICATION OF SOLAR CELL DEVICE (PHOTOVOLTAICS)

Ample and fresh solar energy warrant immediate attention due to the increased demand of energy for human activities. Every day, approximately 9 X 10^{22} J of energy reaches the earth from sun and about 9 x 10^{18} J of energy consumed by humankind (Bera *et al*., 2010). Difference in carrier mobilities is a major factor leading to the

superior efficiency of inorganic devices compared to organic or hybrid devices. Mainly four consecutive processes are take place in a solar cells and are;

1. absorption of light and exciton formation
2. exciton diffusion
3. charge separation and
4. charge transportation.

Conversion efficiency decreases when excitons form away from the electrode or carrier transport layer to recombine so that it could result in a short exciton lifetime and poor mobility. Organic semiconductors hold relatively high absorption coefficients and inorganic semiconductor act as an excited state electron donor. The combination of organic and inorganic materials is used in solar cells for getting high efficient solar cells. Reported inorganic/organic hybrid solar cells are PbS, TiO_2, ZnO, CdSe, PbSe, $CuInS_2$ and $CuInSe_2$. Merits of QDs application in solar cells are;

- Same QD capable of absorbing the entire sunlight (U.V - visible - IR)
- Significant reduction in hot carrier relaxation dynamics.
- A single photon is capable of generating multiple exciton i.e. QY $\geq$ 100%
- Compared to polymers, QDs are resistant to UV radiation, moisture and oxygen
- Excellent heterojunction with hole conductors are achievable
- Flexible substrate
- Fabrication of QDs based on lower cost solution processes.

Solar cells with QDs can be generally classified in three categories;

(1) P-I-N solar cell with a QDs array,

(2) sensitized QDs and

(3) dispersed QDs (Semonin *et al*., 2012).

The delocalized quantized 3D mini band states could be expected to slow down the carrier cooling and allow the transport and gathering of hot carriers at the respective p and n contacts to produce a higher photo potential. Enhancement of photocurrent occurs in the QDs arrays as a result of ionization. When the number of layers' approaches infinity, the efficiency approaches a theoretical thermodynamic limit of

86%. Yet hot electron transport-collection and impact ionization cannot happen simultaneously; they are mutually exclusive.

2.4.1.2 QD BASED LIGHT EMITTING DIODES

QDs light and white light emitting diodes have very important roles in producing displays for electronic devices. The narrow emission width at half maximum, appropriate size and composition as well as tunable light emission makes them suitable for LED devices. The quantum dots could replace or supplement phosphors used in white LEDs or the color filters in displays, mainly for increasing red emission. It is also possible that QDs could be added to colored LEDs to tune or otherwise refine the emitted colour spectrum. A blue LED normally made from InGaN is found to be typically paired with a yellow emitting phosphor like cerium doped yttrium aluminum garnet, or Ce: YAG. The combination of the blue light from the LED with the emitted yellow light from the phosphor is perceived as white light. Advantages of QD-LED over the traditional displays are;

- emit light in highly specific Gaussian distributions
- they can render colors very precisely and
- utilize very less power (Demir *et al*., 2011).

2.4.1.3 PHOTO DETECTORS

QDs can be applied in photo detectors for both the visible and infrared lights. Photo detectors for infrared light discover applications in night vision cameras, biomedical imaging and atmospheric spectroscopy for gas detection, quality control and product inspection. The visible light photo detectors are used in image sensors for converting the incoming light into electronic signals. QDs can also be used in surveillance, industrial inspection, machine vision, spectroscopy and fluorescent biomedical imaging. The merits of using quantum dots

are the easiness of integration with silicon electronics or with flexible organic substrates. Quantum dot photo detectors (QDPs) can be produced from traditional single crystalline semiconductors or solution processed. Solution processed QDPs are ideal for the integration of several substrates and for use in integrated circuits. Moreover, quantum dots can also be deposited on prefabricated electrodes on a substrate by simple methods such as ink-jet printing, low-temperature evaporation and solution casting. The tunability of optical absorption and emission spectra through the quantum size effect is an another important benefit offered by QDs. Typical fabrication involves deposition of electrode on a glass or ceramic substrate by evaporation and then the colloidal QDs or mixture of QDs in polymers are spin-coated on the substrate to form a solid QD film or QD polymer composite between electrodes. CdSe and InP based QDs useful for UV-Vis region and PbS QDs are useful for photo detectors in the IR region of the electromagnetic spectrum (Konstantatos and Sargent, 2010).

2.4.1.4 QUANTUM COMPUTING

QDs have sprouted the way for powerful 'supercomputers' known as quantum computers. Quantum computers operate and store information using quantum bits or'qubits', which can exist in two states. This remarkable phenomenon facilitates speed of information processing and memory capacity when compared to conventional computers (Imamoglu *et al.*, 2003).

2.4.1.5 NIGHT VISION PAINTS

QDs can be used in infrared emissive paints because they can be tailored to emit in the IR region. This will help in night time patrol and search operations of criminal and terrorist activities. Such IR fluorescent paints applied on the door, railing, road patches will get intensified and reflect light absorbed which is invisible to the naked eye. By using night vision goggles, patrol persons can see any disturbance in the painted area from a distance of 100 meters which is invisible to the criminals and they may not be aware about it. Such paints can last up to six months (Bastiaans *et al.*, 2014).

2.4.2 BIOMEDICAL APPLICATIONS

In 1970s and early 1980s, the importance of semiconductor structures in the field of computer and electronic applications got flourished. During this period, it was well reported that the photo physical properties can be changed by tuning the size and composition of QDs. Based on this, the QDs have been widely used for multiple applications as mentioned in the above. Literatures indicated that these nanometer sized structures have significant applications in biological, biochemical, biomedical areas and healthcare areas (Bera *et al*., 2010). Exceptional fluorescent properties of QDs makes them significant fluorescent labelling candidate in the biochemical and biomedical research area. Development of photoluminescence QDs (PLQDs) for molecular diagnosis of diseases at an early stage is a new invention in this area. This invention is the effort of many researchers including chemists, biologists, physicists, engineers and medical doctors. Bruchez *et al*. and Chan& Nie in 1998 first published articles in science on the application of PLQDs as fluorescent contrast agents for biological labelling and imaging.

Several organic dyes have been used as molecular probes for imaging during last few years. More fluorescent stability is required for imaging. As years passes, organic dyes became unable to fulfill the expectations. Hence QDs rapidly filled the drawbacks of traditional organic dyes on several counts. Unique optical properties of QDs make them as a suitable candidate for *in vitro* and *in vivo* imaging (Matea *et al*., 2017). Fluorescence properties of QDs and organic dyes are given in Table 2.1.

Properties	Dyes	Quantum dots	References
Size	0.5nm, molecule	1-10nm, colloid	He and Ma, 2014
Absorption spectra	Discrete narrow bands (35-100 nm)	Broad and steadily increasing towards U.V wavelength region	Bera *et al*., 2010
Emission spectra	Asymmetric tailing to long wavelength side.	Symmetric	Stier *et al*., 1999
Molar absorption Coefficient	maximum at long wavelength 2.5×10^4-2.5×10^5 M^{-1} cm^{-1}	Higher at the first band absorption 10^5 -10^6 M^{-1} cm^{-1}	He and Ma, 2014
Fluorescence lifetime	Mono exponential decay (1-10ns)	Multi exponential decay (10-100ns)	Shukla *et al* .2014
Spectral multiplexing	Not ideal due to the spectral	Ideal for multicolor experiments	Drbohlavova *et al*.,

	overlap		2009
Quantum yield	Visible (0.5-1.0) NIR (0.05-0.25)	Visible (0.1-0.8) NIR (0.2-0.7)	Yaghini *et al.*,2009
Photo stability	Usually poor	Excellent resistance to photo bleaching	Bajwa *et al.*, 2016
Solubility or dispersibility	Regulated by substitution pattern	Regulated via surface chemistry (ligands)	Yaghini *et al.*,2011
Toxicity	very low to high toxicity depends on the dye	Heavy metals containing QDs are toxic (Little known yet)	Matea *et al.*,2017

Table 2.1: Comparison between photo physical properties of dyes and Quantum dots

2.4.2.1 IN VITRO IMAGING

The term '*In vitro*' literally means 'in glass' which refers to the research involving experimental manipulation 'in glass'. This is done by giving conditions of living cells and renovates what is happen in *in vivo. In vitro* fluorescence imaging mainly includes cellular imaging, bio molecular tracking in cell and tissue staining (Wang *et al*., 2010). Wu and coworkers reported that QDs linked to streptavidin and IgG could be used to label different types of targets (breast cancer marker Her2, microtubule/actin fibers and nuclear antigens) at different sub-cellular locations (extracellular, intracellular and inside the nucleus) and with different types of specimens (live cells, cultured fixed cells and tissue sections). All labelling signals are target specific, bright and considerably photo stable (Chen *et al*., 2008).

Many studies have demonstrated that QD biotags can be widely used for the sub-cellular labelling. Histone protein abundantly found in the HepG2 cells nuclei and is labelled by different size of CdTe QDs (4nm, 4.5nm and 5nm) stabilized by glutathione. The results showed that after one hour of incubation, the nano sized QDs (4 nm) could quickly penetrate the cellular matrix, bind to the dense areas of nucleoli and stained green in colour. The 4.5 nm sized QDs could stain orange in colour after 24h. In contrast, 5 nm sized QDs could only achieve entrance into the cytoplasm after 24h of incubation and stained red in colour. QDs accessibility to different targets within the fixed cellular matrix is affected by the size dependent diffusion processes (Jin *et al*., 2008).

Intra/extra cellular imaging and bio molecular detection has high practical clinical significance. A tumour marker gets over expressed on the surface of cancer cells/tissues. These are typical biomarkers and detection of their presence and quantification is promising for the early detection, categorization and cancer therapy.

Lee *et al*., evaluated potential *in vitro* analysis of two cancer bio-markers, integrin αvβ3 and nucleolin by using the RGD (arginine-glycine-aspartic acid) peptide and aptamer (AS1411). The peptide and aptamer were conjugated on the carboxyl- terminated surfaces of QDs. The developed biomarkers allow multiplex imaging of cancer cells and provide access to excellent cancer-targeting techniques. Confocal microscopy revealed the subcellular localization of two different targets simultaneously and their intracellular distribution (Lee *et al*., 2015). Novel research of Tagit *et al.*, revealed that the tracking of biomolecules movement inside the cells. Vp1 is the chief capsid protein of simian virus 40 (SV40) and can experience molecular self-assembly with QDs. This form of QDs containing virus-like particles (VLPs) termed as SVLP-QDs. SVLP-QDs allow the behaviors of VLPs to be visualized in living cells with the intention of tracing the infection, movement and localization of viruses in living cells (Tagit *et al*., 2017).

Staining of tissue by QDs conjugate is another interesting area of *in vitro* applications. But it is limited to labelling of fixed sections. In 2008, Rosenthal *et al.*, performed QDs labelling of nicotinic receptors (nAChRs) at neuromuscular junctions (NMJs) in mature *ex vivo* mouse diaphragm (Rosenthal *et al*., 2011). The neuroreceptors were targeted with α-bungarotoxin (α-BTX) conjugate and biotinylated α-BTX (bio-α-BTX). The researchers used streptavidin-QD655 to visualize the bound bio-α-BTX in the whole mount tissue. They implemented time-dependence experiments with unfixed mouse diaphragms. Results elucidated that bio-α-BTX binds quickly in fresh *ex vivo* tissue and essentially full labelling was achieved within 10 min. These data suggest that the nAChR remains viable over a period of time when maintained in an *ex vivo* environment.

QDs based fluorescence bio sensing is based on the mechanism of QD mediated Forster Resonance Energy Transfer (FRET). FRET involves the transfer of fluorescence energy from a donor particle to an acceptor particle whenever the donor- acceptor distance is smaller than a critical radius known as the Forster radius. This result in decreased donor's emission, excited state lifetime and rise in the acceptor's emission intensity. FRET is widely used in various immunoassays, monitoring protein interactions, measuring protein conformational changes and assaying enzyme activity. Currently, DNA microarrays are demonstrated by using DNA-functionalized QDs as signaling probes (Bruchez *et al*., 1998).

2.4.2.2 IN VIVO IMAGING

In vivo imaging is typically an experimentation using whole living organism. *In vivo* QDs imaging faces challenges due to the complexity of multicellular organisms. Main imaging applications of QDs include vascular imaging, bio- distribution, tracking and tumour imaging. Properties required for these imaging techniques involve spatial and temporal resolution, non-ionizing excitation energy, tissue penetration depth, detection threshold and biocompatibility. Fluorescence imaging uses less hazardous non ionizing radiations when compared to other imaging techniques like PET and MRI. Imaging of deep tissue can be achieved using QDs by adjusting their size and composition. Emission wavelengths of QDs can be tuned throughout the NIR window and this spectral range gives relatively low absorption coefficients of water and haemoglobin (Matea *et al*., 2017).

Vascular imaging is one of the most successful applications of QDs imaging. In mammals, there are two major circulatory systems namely cardiovascular and lymphatic system. Green light emitting QDs have been used to image skin capillaries and adipose tissues in mice, following intravenous injection (Smith *et al*., 2008). Kim *et al.,* imaged the coronary vasculature of rat heart by using near-infrared QDs. He first achieved mapping axillary sentinel lymph node (SLN) of mouse and femoral SLN of pig using NIR-QDs (Kim *et al*., 2004).

Sandros *et al*., reported a new bio probe, InGaP/ZnS QDs covalently bound to chitosan. The newly developed fluorescent probe addresses the challenge of getting high biologically stable probe for deep-tissue imaging. Long term bio imaging, highly sensitive multiplex *in vitro* assays and *in vivo* cell trafficking studies are possible with chitosan-InGaP/ZnS QDs. QDs are administered into the body through intravenous/intraperitoneal injection for imaging. Once injected the QDs directly interact with the blood cells, components of plasma and vascular endothelium. There are several studies focused on the bio distribution and clearance of QDs. It was found that a detailed quantitative analysis of the kinetics, metabolism and clearance is essential for confirming the suitability of QDs for biomedical applications (Sandros *et al*., 2007).

2.4.2.3 GENE DELIVERY

QDs found to be a promising candidate for gene therapy. RNA interference

(RNAi) is a favorable technique with great opportunity to fight against cancer. Achievement of this technique mainly depends on efficient delivery of therapeutic agents into targets. siRNAs have short half-life since they have negative charge and cannot cross the cell membrane. It also easily gets degraded by RNase (Whitehead *et al*., 2009). Fluorescent quantum dots (QDs) have been investigated as a potential carrier for loading of gene on account of their large surface area and stable chemical properties (Mansoori *et al*., 2014). Negative charge of the nucleic acids is suppressed by the positively charged polymers or liposomes. Imaging of siRNA transfection has been successfully performed by polymer/liposome conjugates of QDs.

2.4.2.4 PHOTODYNAMIC THERAPY (PDT)

QDs have an outstanding role in photodynamic therapy. It is an emerging technique for cancer treatment as well as age-related muscular degeneration. This depends on the production of reactive oxygen species (ROS). Photo activated QDs are not efficient for ROS production. QDs conjugated with photosensitizers can generate ROS readily via Forster Resonance Energy Transfer (FRET). It involves combination of three components namely a photosensitizer, light source and tissue oxygen (atomic oxygen), which cause destruction of tissue. Atomic oxygen generated by the QDs as a result of laser radiation is largely taken up by cancer cells than normal cells (Samia *et al*., 2006). Conventional photosensitizing organic dyes are also capable of cytotoxic ROS production. But unique photo physical properties of QDs make them attractive photosensitizers for PDT. CdSe alone do not produce enough quantity of reactive singlet oxygen (Hsieh *et al*., 2006). So these QDs are used in PDT with a known silicon phthalocyanine PDT photosensitizer. This study supports the role of QDs to sensitize the PDT agent via a fluorescence resonance energy transfer (FRET) mechanism or interact directly with molecular oxygen via a triplet energy-transfer process (TET). Both mechanisms will lead to reactive singlet oxygen production which plays an important role in cancer treatment (Samia *et al*., 2006) (Figure 2.6). Steponkiene *et al.*, established that QDs bound non covalently with second generation photosensitizer chlorin e6 and can be potentially used for the efficient photodynamic therapy of cancer cells (Steponkiene *et al*., 2014).

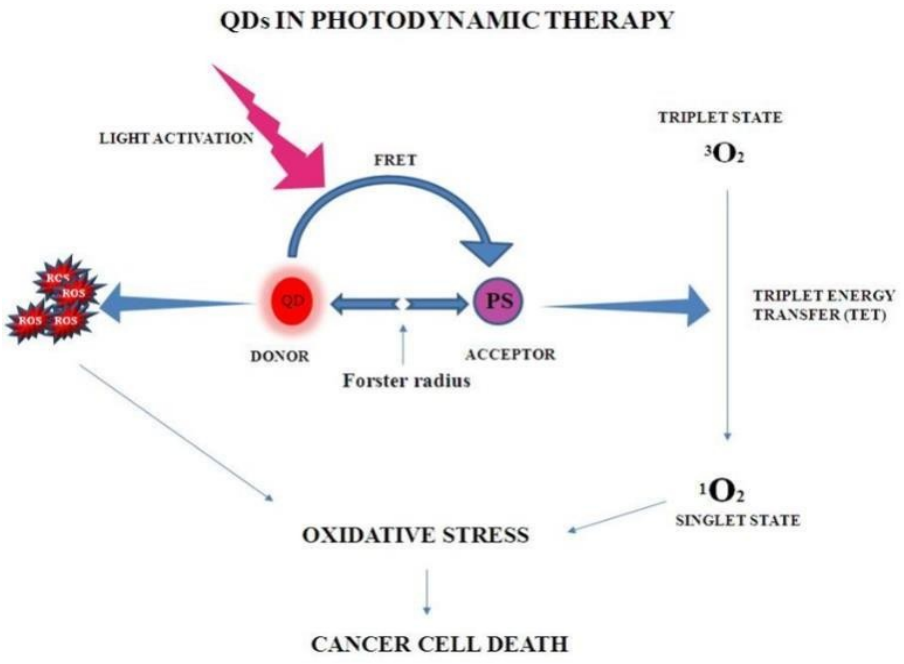

Figure 2.6: Role of QDs to sensitize the PDT agent via fluorescence resonance energy transfer (FRET) mechanism or direct interaction with molecular oxygen via a triplet energy-transfer process (TET) (Mohanan & Reshma, 2018).

2.4.2.5 QDs IN THERAPEUTICS AND DIAGNOSTICS (THERANOSTICS)

The term 'theranostics' is defined to be the combination of diagnostics and therapeutics. Theranostics helps to integrate instantaneous evaluation of drug delivery. Cell specific targeting as well as subsequent uptake is obligatory for a successful diagnostic and therapeutic process. It is possible to monitor the pathway, targeted cells/organ uptake and therapeutic efficiency of the applied drugs in treatment of diseases like cancer, inflammation and pulmonary diseases by applying QDs. QDs do awfully well in imaging applications. QDs also serve as particulate delivery vehicles if the biocompatibility apprehension can be managed. Small size is the unique property of QDs and as size of the QDs decreases, surface area increases which offer an ideal 'platform' to confer several similar or different functionalities. This physical property can be exploited to combine diagnostics and therapy to so-called theranostics. QDs used as theranostic agent (Figure 2.7) are considered as Nano scaffolds to incorporate multiple functional modalities, such as a targeting ligand (protein, peptide or antibody) and therapeutic agent. Cell penetrating ligand attached to QDs gets exposed upon target cell interaction. This interaction allows the multifunctional QDs to enter the cell. Subsequent intracellular release of the drug from drug loaded vesicle occurs as a result

of triggering of stimuli sensitive antennae in response to local stimuli like temperature, pH or enzyme (Walkey, 2014).

For an ideal theranostics process, the following requirements are indispensable.

- It should possess prolonged blood circulation time by evading from the clearance of reticuloendothelial system (RES)
- It should gather in pathological zone (must be cell specific)
- It should penetrate the cells without much damage
- It should supply drug efficiently
- Real-time monitoring of the treatment with the assistance of diagnostic agent (imaging, optical or magnetic) (Figure 2.8).

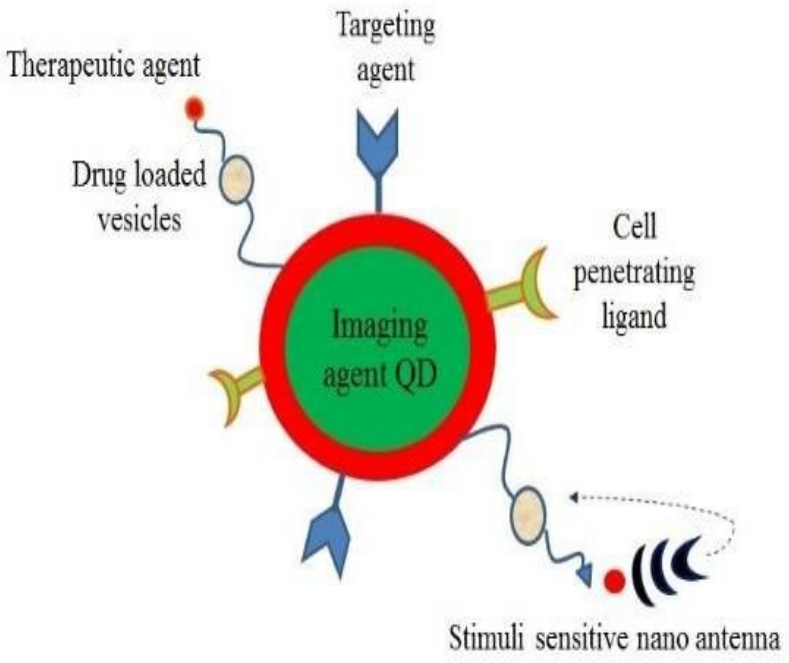

Figure 2.7: QDs as theranostics agent (adapted from Reshma& Mohanan., 2018).

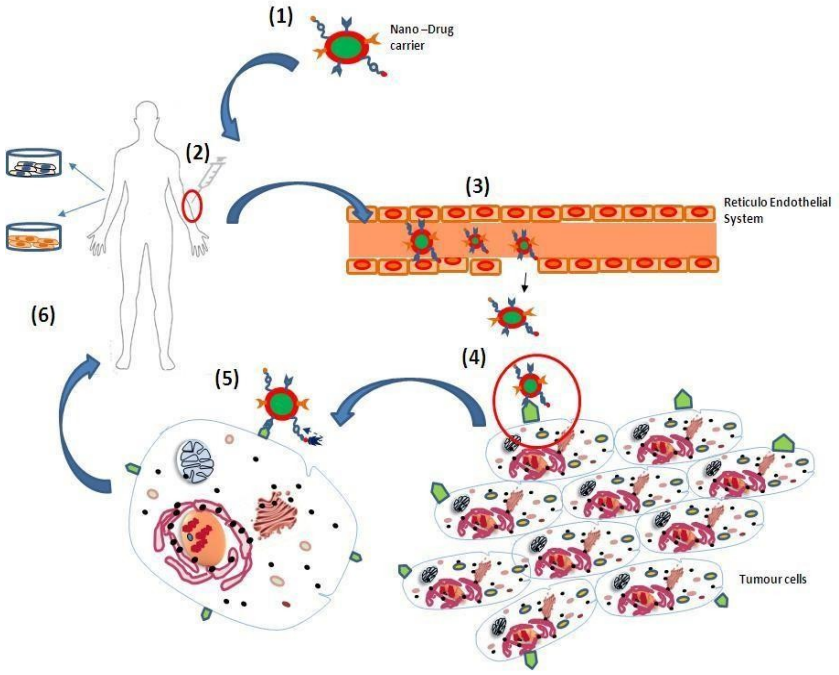

Figure 2.8: Schematic representations of requirements of an ideal theranostic process in human body (adapted from Mohanan & Reshma., 2018).

2.4.2.6 FLUOROMETRIC SENSING OF METABOLITES IN BIOLOGICAL FLUIDS

It is very important to quantitatively categorize the metabolites present in the blood or other biological samples (Cheng *et al*., 2012 and Fernie *et al*.,2004). The existing methods for metabolite identification often suffer from low specificity/sensitivity, high sample consumption, lengthy procedures, or necessity for sophisticated equipment and high skills. QDs are used for the flourimetric measurement of multiple metabolites in blood, which are convenient, sensitive, low cost and require only a little amount of sample (Want *et al*., 2006 and Qiu *et al*., 2009). Li *et al* developed tyramine functionalized graphene QDs which are capable of detecting a spectrum of metabolites present in the blood and other bio fluids (Li *et al*., 2016).

2.4.2.7 SURFACE ENHANCED RAMAN SPECTROSCOPY

Surface Enhanced Raman Spectroscopy (SERS) is a technique for molecular detection and characterization. This technique depends on the enhanced Raman scattering of molecules that are adsorbed on or near SERS active surfaces, such as nanostructured gold or silver. QDs based SERS can be used in medical field in two ways. Firstly, measures the unique fingerprint spectra of pure analytes on QDs in single molecule based SERS. On the other, SERS spectra are acquired from a

collection of nanoparticles where QDs are covered by a monolayer of analyte. *In vivo* tumour targeting and detection is possible by QDs based SERS (Bera *et al*., 2010).

2.5 TOXICITY OF QUANTUM DOTS

The QDs are likely to enter into the physiological system by means of ingestion, inhalation or intravenous applications. Toxicity is the main hindrance for biological application of these particles and must be safe and nontoxic. There are several studies carried out so far on the toxic effect of QDs and mechanism of action. *In vitro* and *in vivo* results are not comparable to each other because of the ambiguous behaviours of both QDs and cells in these two conditions. *In vitro* studies provide good model for understanding the potential toxic actions of QDs. *In vivo* studies are capable of providing details of both the biological and chemical fates of QDs within an intact biological system. Safety assessment of QDs is possible only by pharmacokinetics study. ADME constitutes the most important base in bio safety evaluation. The confirmation of *in vitro* information by comparing with *in vivo* studies is critical. Cadmium based QDs (CdSe and CdTe) are the most extensively studied semiconductor materials leaching of Cd from the core of QDs into the cellular environment which resultant damage of organelles are the main reason for the toxicity. In addition to Cd toxic profile of other heavy metals such as Pb, In and Hg are also demonstrated by several research groups under prolonged period of time (Chaniotakis and Frasco 2010, Qiu *et al*., 2009 and Want et al., 2006).

2.5.1 HEPATOTOXICITY

The end use application determines the route of exposure of QDs and it possible via ingestion, inhalation or intravenous routes. Despite of the route of exposure, they can enter the blood circulation and reach to the secondary tissue like liver. The liver is the metabolic centre of the body. It has an imperative role in metabolic homeostasis, as it is responsible for synthesis, storage, metabolism, redistribution of fats, vitamins and carbohydrates. It also produces an array of serum proteins and large numbers of enzymes as well as cytokines. The liver collects blood carrying toxicants and accumulates materials at much greater levels compared to other organs. This makes liver as a major target organ of toxicants. Hence hepatotoxicity is considered as one of the major toxicities induced by drugs or any other chemicals. Even though liver has the capacity of regeneration, it is susceptible to toxicity induced

by drugs or any other potential chemicals (O'Brien *et al*., 2006). Derfus *et al.,* confirmed that CdSe core QDs provoked acute toxicity in primary hepatocytes. The primary target organ affected by Cd exposure will be liver. About 25% of exposed cadmium gets accumulated in liver. Toxicity induced by cadmium is caused by its binding to sulfhydryl groups leading to mitochondrial protein dysfunction. Cadmium binding causes thiol group inactivation causing oxidative stress. Low concentration of Cd can be detoxified by metallothionein proteins in cytoplasm. But as the concentration of Cd increases, the quantity of metallothionein proteins becomes inadequate to detoxify Cd. The quantity of metallothionein protein in isolated hepatocytes is same as that of liver. Therefore, primary hepatocytes turn out to be perfect model for hepatotoxicity studies (Derfus *et al*., 2004).

Various studies established that different types of QDs decreased the survival rate of HepG2 cells in a time and dose dependent manner. They will cause a significant increase in the apoptosis and necrosis rates. Nguyena *et al*., proved that CdTe QDs decreases HepG2 cell survival rate by significantly increasing the level of apoptosis related proteins Bax, Fas, cytochrome c and caspase 8. This elevation is followed by a significant decrease in anti-apoptotic protein Bcl-2. Ultimately this sequence of alteration would induce apoptosis (Nguyen *et al*., 2013).

A substantial number of studies have confirmed the distribution and toxicity of QDs *in vivo*. Haque *et al.,* also confirmed that CdSe/CdS QDs mainly distributes in the liver and spleen by repeated intraperitoneal injection in mice (Haque *et al*., 2013). The toxicity against the liver cannot be ignored because liver is one of the main sites of accumulation and metabolism of the QDs. ADME of AgSe QDs, surface stabilized with polyethylene glycol (QD-PEG), 2-aminoethanethiol (QD-MEA) and mercaptopropionic acid (QD-MPA) were studied by the Tang *et al*., in 2013. Three QDs were accumulated mainly in the liver and spleen after intravenous injection into the mice. Accumulated QDs were significantly converted to Ag and Se within 7 days. At the 28^{th} day QD-MEA showed some edema and necrosis while other two modified QDs did not cause any effect. Mu *et al.,* (2017) demonstrated that black phosphorous QDs have no long term toxicity.

2.5.2 MECHANISM OF TOXICITY

Significance of QDs for *in vivo* applications remains controversial. Even though many studies showed successful results, anticipated problems were also noted.

Currently available data is only based on the short term animal experiments. Many studies have been reported on QDs toxicity and related mechanism of action. In some cases, capping materials of QDs may be immunogenic and results in complex harmful immune reactions. In most of the cases, heavy metals present in the core may be toxic to host. Most of the QDs were found to be cytotoxic in both *in vitro* and *in vivo* only after the degradation of the surface coating (Hoshino *et al*., 2004).

Reported mechanisms behind the cytotoxicity are;

- Degradation of Cd based QDs and consequent release of free Cd ions (Cd^{2+})
- Reactive Oxygen Species (ROS) and oxidative stress and
- Elevation of intracellular Ca^{2+} levels.

2.5.2.1 Degradation of Cd based QDs and consequent release of free Cd ions (Cd^{2+})

The toxicity induced by Cd containing QDs is attributed by Release of Cd^{2+} ions. QDs are usually degraded by acidic organelles such as lysosomes on cellular uptake. The released Cd^{2+} ions conjugate with thiol groups present in proteins resulting in protein dysfunction (Mo *et al*., 2017). According to the findings of Peng *et al*., QDs could result in increase of metallothionein (MT) gene expression in both the HepG2 cells and zebra fish liver cells (Peng *et al*., 2013). Similar results on MT up regulation on Cd containing QDs treatment as a stress response were also reported (Klaassen *et al*., 2009). Alternations in antioxidant enzymes by ROS production is another way of Cd^{2+} ion induced toxicity. Similarly, elevated ROS production ultimately lead to the cellular oxidative stress (Hussain *et al*., 1987).

The most important site of ROS production in the mitochondria is Complex I and Complex III. Any impairment in the electron transfer through these Complexes will induce enhanced superoxide radical formation (Hussain *et al.,* 1987*)*. Three types of ROS production is reported in QDs treated cells;

1. The decline in the antioxidant system leading to ROS production (Hussain *et al*., 1987).
2. Interruption of complex III electron transport chain of mitochondria cause ROS accumulation (Adam and Chinopoulos 2006).
3. QD cellular biodegradation (Wang *et al*., 2004).

Above ways of ROS production eventually leads to mitochondrial defects notably mitochondrial swelling, outer membrane damage, loss of cytochrome c, deficiency in mitochondrial function, mitochondrial biogenesis and mitochondrial compensatory alterations like giant/micro-mitochondria formation, mitochondrial hyperplasia and eventual mitochondrial degeneration (Lin *et al*., 2008).

2.5.2.2 REACTIVE OXYGEN SPECIES (ROS) AND OXIDATIVE STRESS

ROS production is the major contributing factor for nanoparticle toxicity. ROS with short half-life donate/accept electrons so as to achieve stability. $\cdot O_2^-$, $\cdot OH$, $H_2O_2$are major ROS involved in interaction with macromolecules such as DNA and lipoproteins leading to structural and functional defects. In biological system, antioxidants are responsible for controlling the amount of ROS. Antioxidants terminate free radical chain reaction by reacting with free radicals present and thereby safe guard the important macromolecules. Nguyen *et al*., (2013) reported that ROS elevation and change in antioxidant levels caused by CdTe QDs treatment leading to apoptosis. These QDs cause structural and morphological alternations in mitochondria leading to disruption of electron respiratory chain, respiration collapse causing oxidative stress.

2.5.2.3 ELEVATION OF INTRACELLULAR Ca^{2+} LEVELS

Ca^{2+} is one of the most striking second messengers in eukaryotic cells (Richter *et al*., 2016). Ca^{2+} can activate different protein kinases involved in many biological processes such as cell differentiation, proliferation and apoptosis. Elevated levels of Ca^{2+} weakened mitochondrial membrane permeability, leading to the release of cytochrome c and induced apoptosis (Paesano *et al*., 2016; Richter *et al*., 2016). Reports suggested that QDs cause elevated intracellular Ca^{2+} levels in HepG2 cells (Lu et al., 2016; Nguyen et al., 2015; Paesano et al., 2016). CdTe QDs led to a 7.4-fold increase in Ca^{2+} levels and was mediated via ROS. Meanwhile high levels of Ca2+ concentrations further increased ROS and aggravated oxidative stress (Nguyen et al., 2015).

2.5.2.4 OTHER POTENTIAL MECHANISMS

Apart from the above mechanisms, QDs induce autophagy and stress on endoplasmic reticulum (ER) (Paesano *et al*., 2016; Richter *et al*., 2016). ER stress is

critical to cell survival, and disturbance of its function triggers cellular apoptosis. ER stress is performed mainly by three stress sensors;

1. protein kinase R like ER kinase
2. intron kinase 1 and
3. transcription activator 6 (Iurlaro and Munoz, 2016).

Autophagy is an essential physiological phenomenon in eukaryotic cells. It plays an important role in maintaining cell homeostasis. It clears damaged organelles and destroys long term protein to promote the cell survival rate under the condition of nutritional deficiencies, hypoxia or other harmful factors. Excessive autophagy leads to cell death (Tanida *et al*, 2011). Fan *et al*., (2018) discovered that CdTe/CdS QDs elicit hepatotoxicity through lysosome dependent autophagy activation and ROS production. QDs induced liver toxicity by stimulating ER stress and autophagy along with other mechanisms. An overview of QDs toxicity is presented in the Figure 2.9.

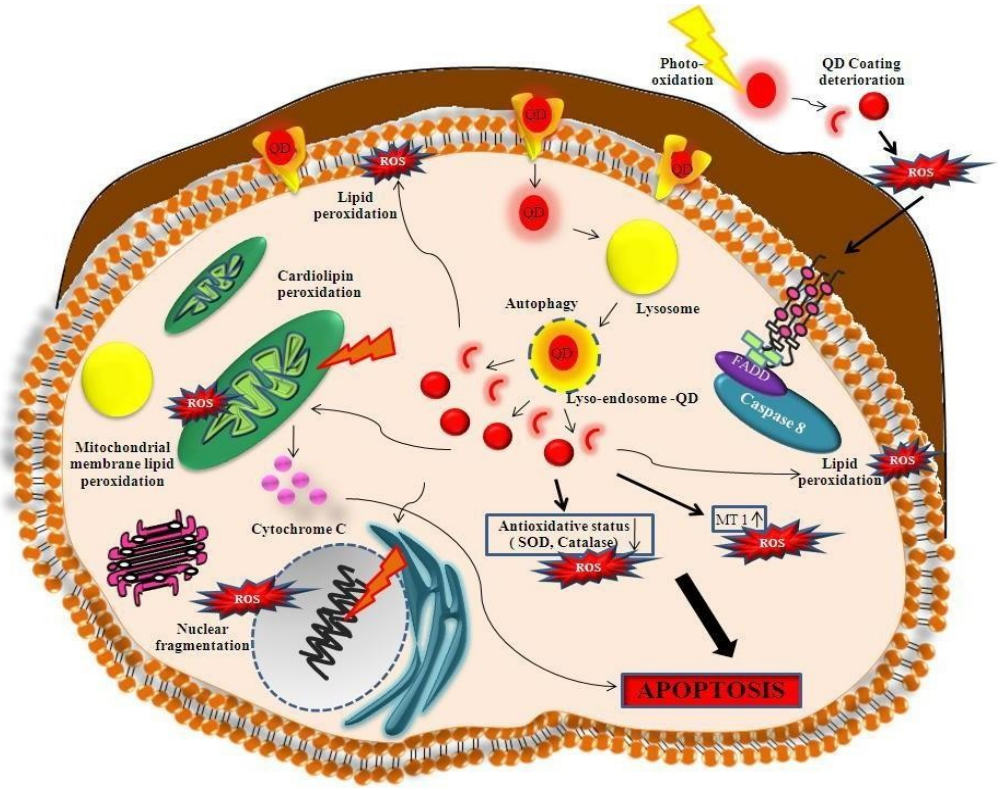

Figure 2.9: Schematic representation of toxicity induced by QDs in live cell highlighting mechanisms of apoptosis. Also shows morphological changes and ROS production (adapted from Reshma & Mohanan, 2018).

2.6 PARAMETERS INFLUENCING TOXICITY

QDs synthesized have unique photo physical properties which in turn verify its potential toxicity. Like all other nanoparticles, cytotoxicity of QDs will influence its unique photo physical properties. Photo physical properties of QDs includes its size, shape, charge, surface functionalization, concentration, redox activity, mechanical stability, aggregation, U.V light activation, mode of interaction with cells, inflammation and pH of the medium. Cytotoxicity elicited by QDs is not a function of its single property but a combination of parameters.

2.6.1 SIZE

Nanoparticle size and surface area largely determines the unique mechanism of nanoparticles interaction with biological system. Nanoparticles especially QDs are characterized by large surface area due to small size impart high catalytic and reaction capacity. Size of QDs is comparable with the size of protein globules (2-10 nm), thickness of cell membranes (10 nm) and diameter of DNA helix (2 nm), which allows them to easily enter cells and cell organelles. Zhang *et al.*, (2015) established the concept that nanoparticles smaller than 5 nm usually overcome cell barriers non- specifically via mechanisms like translocation. Larger particles pass into the cells by phagocytosis, macro pinocytosis and specific and nonspecific transport mechanisms. *In vivo* experiments showed that, their size smaller than 10 nm, the QDs are rapidly distributed among all organs and tissues upon intravenous administration. Particles with hydrodynamic size smaller than 5.5 nm are rapidly and efficiently eliminated from the mice through renal clearance. An acceptable biocompatibility can be achieved by designing QDs by considering the size limit (Choi *et al*, 2007). Nanoparticles with a diameter larger than 6 nm cannot be excreted by the kidneys. It gets accumulate in specific organs such as the liver and spleen, until clearance by the mononuclear phagocyte system happens (Chen *et al*., 2008). Most nanoparticles that accumulate in liver and spleen cause serious side effects. For example, cadmium selenide (CdSe) QDs remain in the tissue for up to eight months and cause hepatotoxicity (Zheng *et al*., 2007).

2.6.2 SHAPE

The characteristic shapes of NPs are spheres, cylinders, ellipsoids, cubes, sheets and rods. NPs toxicity strongly depends on their shape. QDs are 'dots' *i.e*. spherical in shape as their name implies. Spherical NPs are more prone to endocytosis than nanofibers and nanotubes (Champion *et al.,* 2006). QDs have attracted broad attention as a result of their wide optical tunability and efficacy for bio labelling, whereas elongated structures cannot use. Elongated structure have been shown to emit linearly polarized light with a wide energy separation between the absorption and emission maxima (Stokes shift) causing reduction in light reabsorption for light emitting applications (Scher *et al.,* 2003).

2.6.3 COMPOSITION

The use of a metal or metalloid as the core element is one of the main characteristics of QDs. Metals such as arsenic (As), cadmium (Cd), tellurium (Te), lead (Pb), copper (Cu), selenium (Se) and zinc (Zn) are known to be used either singly or in combination. Some of these metals, especially As, Cd, Te, Pb and Cu are toxic to biological systems. Fading of the outer coating by processes such as oxidation, photolysis or low pH, either outside or within the biological system might expose the inner metallic core to the biological environment. This can constitute a toxic risk to the cells and tissues. Influence of composition of the inner core (Cd, Se, Te, Pb) on the toxicity has been well explored. Upon cellular uptake, highly toxic core metals (Cd, Se, Te, Pb) become exposed to cellular environment. Among these core metals, Cd has received most attention in case of imparting QD toxicity. Leakage of Cd ions from the core is one of the offenders for the cytotoxicity of Cd QDs. Cadmium is a class A element whose application is not tolerated under current environmental policy (Wang *et al*., 2012). Similarly, Pb and Hg can also be considered under this class. Hence, heavy metal free QDs like carbon dots (C-dots), silicon QDs (Si QDs), graphene QDs (GQDs), Ag_2Se, Ag_2S, InP, ZnSe/ZnS, CuInS2/ZnS QDs were introduced (Lu *et al*., 2019)

2.6.4 SURFACE CHARGE

Bio-nano interaction is very much affected by the surface charge of the nanoparticles. Surface charge can be modified by coating nanoparticle with differently charged polymers. Folic acid or PEG (polyethylene glycol) is frequently used for improving intracellular uptake and specific cellular targeting. Positively charged nanoparticles are more toxic than negatively and neutrally charged particles. This is because of the electrostatic attraction between the negatively charged cell membrane glycoproteins and positively charged NPs. Also they can strongly bind to negatively charged DNA causing damage. As a result, a prolonged G0/G1 phase often could happen in the cell cycle. Negatively charged NPs have no effect on the cell cycle. It is also demonstrated that CdSe/ZnCdS QDs with a DL-cysteine coating generated a hydrodynamic diameter of six nanometer nanoparticle. The use of a cysteine coating had an effective neutral charge, which paid to the lack of aggregation or protein binding in serum. This lack of affinity ensured that these QDs could be used without concern of unintentional or random interactions (Liu *et al.,* 2011).

2.6.5 SURFACE FUNCTIONALIZATION

Lovric *et al*. (2005) found that CdTe QDs coated with cysteamine and mercaptopropionic acid (MPA) were cytotoxic to rat pheochromocytoma cell (PC12) cultures at concentrations of 10 μg/mL whereas, uncoated CdTe QDs were cytotoxic at concentration of even 1 μg/ml. Ballou *et al.,* demonstrated that surface coating of QDs influences their deposition in various organs like liver, spleen and bone marrow of BALBc mice. In this experiment they used Poly acrylic acid, mPEG-750, mPEG-5000 and COOH-PEG-3400 surface coated QDs. Among these QDs, mPEG-5000 QDs were found to have the longest circulation time in addition to reduced nonspecific accumulation (Ballou *et al*., 2004). Cho *et al.,* explored the effect of different surface coating using four cadmium QDs (MPA-, Cys- or NAC coated CdTe QDs and cysteamine coated CdSe/ZnS QDs on human breast cancer (MCF-7) cells (Choi *et al.*, 2007).

2.6.6 UV LIGHT ACTIVATION

UV illumination used for the QDs localization causes increase of QDs toxicity. UV irradiation energy promotes the dissolution of semiconductor particles in a process called photolysis (Su *et al*., 2009). QDs with stable capping ligand is found to be non-toxic to the cells and animals (Ballou *et al*., 2004)

2.6.7 SHELL OF QDS

Most of the QDs consist of a shell structure around the core. Application of shell on the surface of QDs is not only necessary for changing their optical properties but also helpful for increasing the solubility in water and for improving the biocompatibility. Thus the shell decreases the toxicity of QDs by preventing the leaching of core material. This influences the QDs pharmacokinetics, changing the patterns of QDs distribution and accumulation in the body (Bonilla and Kouznetsov, 2016). The oxidative degradation of the CdSe core due to exposure to air was significantly reduced by the ZnS shell resulting in lower cytotoxicity (Derfus *et al*., 2004). Many reports confirmed the effectiveness of the ZnS shell in reducing the cytotoxicity of CdSe quantum dots (Chan *et al*, 2006; Kirchner *et al*, 2005).

CHAPTER 3: MATERIALS AND METHODS

3. MATERIALS AND METHODS

3.1 CHEMICALS

Zinc acetate dihydrate (Zn $(OAc)_2$. $2H_2O$), Diethylene Triamine Penta Acetic acid (DTPA) and pyrogallol were purchased from Central Drug House (P) Ltd, India. Selenium powder, sodium borohydride, 3-mercaptopropionic acid (MPA), sodium borohydrate were purchased from Sisco Research Laboratory, India. 3-(4,5-Dimethylthiazol-2-yl)-2,5-diphenyltetrazolium bromide (MTT), trypan blue, histopaque, griess reagent, sodium hydroxide, L-glutathione (GSH) and neutral red dye, sodium dodecyl sulphate (SDS), thiobarbituric acid, tris base were purchased from Sigma Chemicals Co. Ltd. (St. Louis, MO, USA). High glucose (HG) - Dulbecco's Modified Eagles Medium (DMEM), fetal bovine serum (FBS), phosphate buffered saline (Ca^{2+}, Mg^{2+}free PBS), trypsin EDTA, antibiotic and antimycotic solution were purchased from Gibco, Grand Island, NY, USA. Rhodamine Phalloidine and 2,7-dichlorofluoresceindiacetate (DCFH-DA) were purchased from Molecular probes, Invitrogen, Carlsbad, CA, USA. Acridine orange (AO) and diluent for DNA extraction, Haematoxylin, eosin, Propidium iodide, ethidium bromide was purchased from Hi-media Pvt. Ltd. India. SensoLyte® Homogeneous AMC Caspase-3/7 Assay Kit was procured from Ana Spec, USA. Calcien AM, JC-1 Dye (Mitochondrial Membrane Potential Probe) and apoptotic DNA ladder kit was purchased from Thermo Fisher Scientific, USA. Coomassie brilliant blue and Folin's reagent were bought from Merck, India. 3H-tritiated thymidine was obtained from American Radiolabelled Chemicals Inc, USA. Reagents for biochemistry and urine analysis were purchased from Erba mannhiem, Germany. Reagents for haematological analysis were procured from Horiba, Japan.

3.2 EQUIPMENTS

Transmission Electron Microscope (TEM): JEOL JEM-2100 LaB6 (JEOL, USA). Dynamic Light Scattering (DLS) and Zeta potential: Malvern Zetasizer Nano ZS (USA) supplied with DTSNano V4.2 software. Fourier Transform Infrared Spectroscopy (FTIR): IR tracer 100 Shimadzu instrument, Singapore. Raman spectra: WITec alpha300 (Germany). Inductively Coupled Plasma Optical Emission Spectroscopy (ICP-OES), Optima 5300 DV ICP-OES spectrometer (Perkin Elmer, USA), Fluorescent microscope (Axio Scope A1 Carl Zeiss, Germany), Phase Contrast Microscope (Nikon), Haematology analyser: Horiba Vet ABC (Japan). Biochemistry analyser: Erba Mannheim XL300 (Germany). Urine analysis: Uro-dipchek 300 (Erba Mannheim, Germany). Microtome Leica RM 2125 RT, Germany. Tissues homogenizer: Polytron P 3100 homogenizer, Switzerland). Scintillation Counter (Hidex, Finland). Laminar air flow (Mark Air particulars, India). CO_2 incubator (Sanyo, Japan). Flow cytometry (BD FACS Aria III, Biosciences, US). UV Visible Spectrophotometer (UV 1601, Shimadzu, Japan, Lamda 25, PerkinElmer, Singapore). RF-5301 spectrofluorimeter (Shimadzu Corp. Japan). Incubator shaker (New Brunswick Scientific, USA), Biophotometer (Eppendorf, Germany), Steam sterilizer (Nat Steel, India). Monochromator based multimode microplate reader (BioTeck Instruments, USA). Nikon Eclipse E600 microscope (Nikon Corporation, Tokyo, Japan). Microplate reader (Says Expert plus, Austria). Refrigerated centrifuge (Eppendorf, USA).

3.3 ANIMAL HUSBANDARY AND WELFARE

Swiss Albino mice were brought from the Division of Laboratory Animal Sciences, Biomedical Technology Wing, Sree Chitra Tirunal Institute for Medical Sciences and Technology (Govt. of India), Trivandrum. Healthy Swiss Albino mice weighing 17-23 g were selected for *in vivo* bio nano interaction studies.

Mice were maintained in a 12h light and dark cycle with constant temperature of 22 ± 2°C and relative humidity of 30-70%. Mice were provided with standard pellet diet and water *ad libitum*. Individual animals were identified by marking with picric acid. Additionally, each animal cage was labelled for name, experiment number, number of animal, date of commencement and end of experimental period. All the

animals were acclimatized for a period of 5 days before beginning the experiments. The animals were routinely monitored for health by cage side observation. All the animals were handled humanely, without causing any pain or distress and with due care for their welfare. The care and management of the animals were carried out in compliance with the regulations of Committee for the Purpose of Control and Supervision of Experiments on Animals (CPCSEA).

3.4 ANIMAL ETHICS

All the experiments were carried out after getting the approval from the Institute Animal Ethics Committee (IAEC). Animal experiments conformed to the guidelines of IAEC regulations which are approved by the CPCSEA, Govt. of India. IAEC approval No: SCT/IAEC-261/FEBRUARY/2018/95.

3. 5 INTRODUCTION OF CELL LINES USED

3.5.1 HepG2

Human liver carcinoma (HepG2) cell line was derived from the liver tissue of a 15 year old Caucasian male who had a well differentiated hepatocellular carcinoma. Hepatocellular carcinoma is the fifth most common cancer worldwide. HepG2 cells are adherent, epithelial cells, growing as monolayer as well as small aggregates. HepG2 cells secrete many plasma proteins such as fibrinogen, transferrin, albumin and plasminogen. HepG2 cells are also referred to hepatoblastoma cell line (Lopez *et al*., 2009). The cell lines were collected from National Centre for Cell Science (NCCS), Pune, India.

3.5.2 HEK 293

HEK293 is a cell line derived from human embryonic kidney cells transfected by an adenovirus grown in tissue culture. They are also known as HEK cells. The source of the cells was a healthy aborted foetus. HEK cells are adherent, epithelial in morphology but they do not show similar growth. Due to the presence of some mRNA and gene products of neuronal cells, it can raise some concern about their use in some experiments. However, these cells are very useful for drug toxicity studies (Srivastava *et al*., 2018). The cell lines were collected from National Centre for Cell Science (NCCS), Pune, India.

3.6 JUSTIFICATION FOR THE SELECTION OF LIVER AND KIDNEY CELL LINES

The liver is the metabolic centre of the body. It has a crucial role in metabolic homeostasis as it is responsible for the storage, synthesis, metabolism and redistribution of carbohydrates, fats and vitamins. It also produces large numbers of serum proteins and an array of enzymes and cytokines. The liver receives and accumulates materials at much higher volumes compared to other organs. Similarly, kidneys are responsible for the clearance of NPs from the blood.

Liver cell lines are the best choice for toxicological and pharmacological studies for the detection of toxic chemicals and evaluating their mechanism of toxicity. Liver toxicity implies chemical derived damage leading to several acute and chronic liver diseases. Drug induced liver injury is a major clinical problem (Griffin and Klayman, 1973) and is the most recurrent reason for the withdrawal of drug from the market. Primary cultured human hepatocytes are the 'gold standard' for hepatotoxicity studies because primary cells can better reflect the real situation of the body. However, they are phenotypically unstable, very difficult for isolation, limited life span and the high variability are drawbacks of their routine use in drug biotransformation and hepatotoxicity assessment.

Hepatic cell lines are extensively used for assessment of liver toxicity because they display similar phenotypic and genotypic characteristics of normal liver cells with functional enzymes responsible for phase I and phase II metabolism of xenobiotics (Sassa *et al*., 1987; Scheers *et al*., 2001) and also they are easy to maintain. Many hepatics *in vitro* models are widely used in understanding the toxicity levels. Liver cell lines HepG2, Hep3B, HBG and HepaRG are commonly found immortalized liver derived cell lines used for *in vitro* assessment of liver toxicity (Guguen *et al*., 2010). HepG2 cell lines are the widely used human hepatocellular carcinoma. These cells are highly differentiated and display many of the genotypic features of normal liver cells (Harries *et al.,* 2001). Consequently, HepG2 cells can be used to screen the cytotoxicity potential of new chemical entities at the lead generation phase (Gerets *et al*. 2009). Schoonen and Westerink (2007) showed that HepG2 cells have low levels of cytochromes (CYPs) but normal levels of phase II enzymes with the exception of UDP glucuronosyl transferases and have been successfully used in toxicity studies. Furthermore, on the basis of whole genome expression of HepG2 cells, it was possible

to discriminate between genotoxic and non genotoxic carcinogens. This entails that HepG2 cells, even with known limitations, still represent a promising *in vitro* model for toxic genomics (Jennen *et al*., 2010).

The kidneys are dynamic organs and signify the major control system upholding body homeostasis, i.e., water and electrolyte balance. So far it is not known whether treatment with ZnSe/ZnS QDs may affect the internal organs of a human body or not. Kidney plays a major role in the filtration of body fluids and the excretion of waste products. Inappropriate exposure of QDs may affect delicate renal cell structure and function. To scrutinise this possibility, the well characterized human embryonic kidney (HEK293) cell line was chosen as a test system, given the extensive use of these cells to assess the cytotoxic effects of chemicals (Almeer *et al*., 2018). Because of these reasons, the HepG2 and HEK 293 cells were used in this study.

3.7 JUSTIFICATION OF SELECTION OF ZnSe/ZnS QDs

Most of the QDs related research has been carried out on Cd based QDs (e.g.: CdSe, CdS). This is because of their wider applications in medicine and biology. They exhibit good photo stability and high quantum yield. Moreover, they can easily be tuned in terms of colour and shows zero scattering. Main reason for the popularity of Cd based QDs is their ease of synthesis using readily available precursors and direct solution phase synthesis methods. Protocols for preparing and using these QDs have

been standardized to a certain extent. They are also available commercially in formats optimized for specific biological assays and applications. The emerging applications of these QDs are in diagnostics and surgeries accompany a parallel increase in terms of toxicity concerns mostly because of the presence of Cd (Rzigalinski *et al*., 2009; Xu *et al*., 2016; Zhang *et al*., 2015). Two major approaches have been put forward to overcome this situation: either to encapsulate the QDs with biocompatible polymers to prevent breakdown of their core material or to synthesise Cd free QDs performing better than the existing Cd containing QDs. The QDs research community has started to use these Cd free QDs for biological applications and evaluated their potential in numerous *in vitro* and *in vivo* models such as cultured cells, tissues and small animals.

Nanostructured ZnSe/ZnS are Cadmium free water dispersible QDs, have size dependent emission in the near UV/blue range of the spectrum (370-460) which is narrower compared to CdSe QDs: 470-650 (Li *et al*., 2015). They consist of atoms

from the II - VI group of periodic table. Core/shell structure of ZnSe/ZnS QDs consist of the wider band gap material ZnS depositing around the narrower band gap material ZnSe and forms a type-I core/shell structure. ZnS shell improves the stability and surface passivation.

It can potentially be exploited in fabrication of optoelectronic devices, blue light emitting diodes (LEDs) (Hines, 1998), solar cells (Jung *et al*., 2012) and as promising low toxic metal candidate for bio labelling (Stefaan *et al*., 2014). ZnSe based nanostructures are increasingly being used for fluorescent labelling, biological assays, imaging of tissues/cells and *in vivo* investigations (Sureshkumar *et al*., 2016). Martynenko *et al* (2015) found that Cd free ZnSe/ZnS QDs can serve as a successful delivery agent and photosensitizer of chlorin e6 in photo dynamic therapy (PDT) against the Erlich Acsite Carcinoma cell culture. In 2014, Soenen S J *et al.,* put forward the possibility of application of ZnSe/ZnS QDs in cellular imaging by evaluating their potential *in vitro* toxicity. Shu *et al* (2014) established that ZnSe/ZnS QDs are perfect candidates for nanoscale drug delivery system (DDS). ZnSe considered as the ideal candidate with UV-blue-emitting for biomedical imaging. This is mainly because of their low toxicity compared with other wide band gap QDs such as CdSe and CdS QDs (Zhao *et al*., 2014).

However, further efforts are essential to improve the performance of Cd free QDs in biomedical applications and to optimize them for specific applications. Doping of these ZnSe/ZnS QDs with other metals improved their fluorescence and therefore used in many applications. Mn doped ZnSe/ZnS quantum dots conjugated with nano hydroxyapatite are being used for cell imaging (Zhou *et al*., 2014) and Mn: ZnSe/ZnS/ZnMnS sandwiched QDs are used for multimodal imaging and theranostic applications (Wang *et al*., 2016). Possible application levels of ZnSe/ZnS and doped ZnSe/ZnS QDs were established by many research groups. However, toxicity evaluation of these QDs is not actively carried out. Beside the applications of ZnSe/ZnS QDs in biomedical fields, they exhibit higher potential to be applied in other scenarios like lighting applications.

The usages of QDs have increased profoundly since the exploitation of heavy metals (Pb, Cd and Hg) in lighting equipment have regulated in the European Union under the Restriction of Hazardous Substances Directive (RoHS) 2011/65/EU. According to the regulation, the level of Cd must not increase beyond 100 ppm. Rare earth activated inorganic phosphorus is a viable alternate in this circumstance. But the

fact is that rare earth metals are considered as critical materials because of the higher cost and scarcity. Blue light emitting ZnSe/ZnS QDs are being widely considered as the most suitable candidate for lighting applications. After all, these are attractive alternatives to Cd-based QDs due to their nontoxic behaviour. Otherwise it is more likely to cause occupational hazards to workers, engineers and also clinicians. In addition to that, commercial products must meet safety standards and comply with regulations. Based on this finding, an effort was made to synthesise heavy metal free, nontoxic QDs such as ZnSe/ZnS QDs. Therefore, it is mandatory to evaluate the safety/ toxicity of ZnSe/ZnS QDs is a validated to be safe QDs for clinical applications.

3.8 OBJECTIVES OF THE STUDY

Aim of the present study is to investigate safety/toxicity of ZnSe/ZnS QDs at molecular level. The objectives of the present studies are;

Objective 1: Synthesis and characterization of ZnSe/ZnS QDs

Objective 2: *In vitro* evaluation of ZnSe/ZnS QDs with HepG2 and HEK cell lines.

Objective 3:

- **Part 1:** Acute toxicity, immunotoxicity, haematological, clinical biochemistry oxidative stress and histopathological studies.
- **Part 2:** Elemental analysis, bio distribution and ADME & T (Absorption, Distribution, Metabolism, Excretion and Toxicity) profiling studies.

SUMMARY OF THE PHD WORK

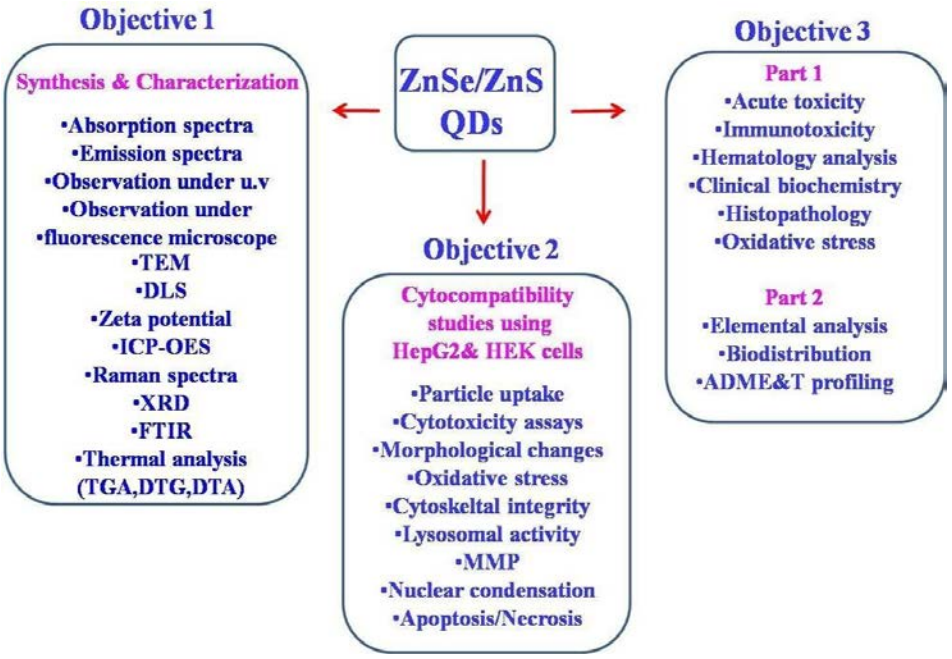

Figure 3.1: Summary of the PhD work

OBJECTIVE 1:

SYNTHESIS AND CHARACTERIZATION OF QDs

3.9 SYNTHESIS OF ZnSe/ZnS QDs

A facile 'green' synthesis method for water dispersible ZnSe/ZnS QDs was adapted from Chang *et al*., in 2013. ZnSe/ZnS QDs were synthesized by the reaction of zinc acetate dihydrate ($Zn(OAc)_2.2H_2O$) and sodium hydrogen selenide (NaHSe). Firstly, 45.8 mg Zinc acetate dihydrate was dissolved in 50 ml deionized water. To this, 92.2 mg L-glutathione (L-GSH) is added and dissolved by stirring. By adding 1 M NaOH drop by drop the pH was adjusted to 10.5. Nitrogen gas pumped for 30 min. Sodium hydrogen selenide (NaHSe) was prepared by adding 15.6 mg Selenium (Se) powder to 1 ml ice cold deionized water and deaerated by nitrogen bubbling for 5 min. 14.8 mg $NaBH_4$ was added and dissolved by vigorous stirring under nitrogen atmosphere in ice bath for 10 min. Then colour of the solution was changed from dark to transparent, colourless solution. This preparation of Sodium hydrogen selenium (NaHSe) was according to the synthesis method reported by Daniel *et al*.,

2015. $4NaBH_4 + 2Se + 7H_2O \; 2 \longrightarrow NaHSe + Na_2B_4O_7 + 14\, H_2$ [Formation of Sodium hydrogen selenium (NaHSe)].

500 µl of sodium hydrogen selenide solution was added to first mixture through a syringe under stirring and nitrogen bubbling, heated to 100 °C. Mixture was refluxed at 100 °C for 60 min. 87µl (106 mg) MPA and 55 mg Zinc acetate dihydrate was added to the above solution. Again pH adjusted to 9.5 by adding 1 M NaOH. Reaction mixture was heated to 100 °C under nitrogen atmosphere for 60 min and the mixture refluxed at 100 °C for 60 min. After that, reaction mixture was allowed to cool down to room temperature. QDs were purified by using excess of absolute ethanol followed by centrifugation to remove unconjugated ligands. Pellets obtained were subjected to drying for overnight at 60 °C (Figure 3.2).

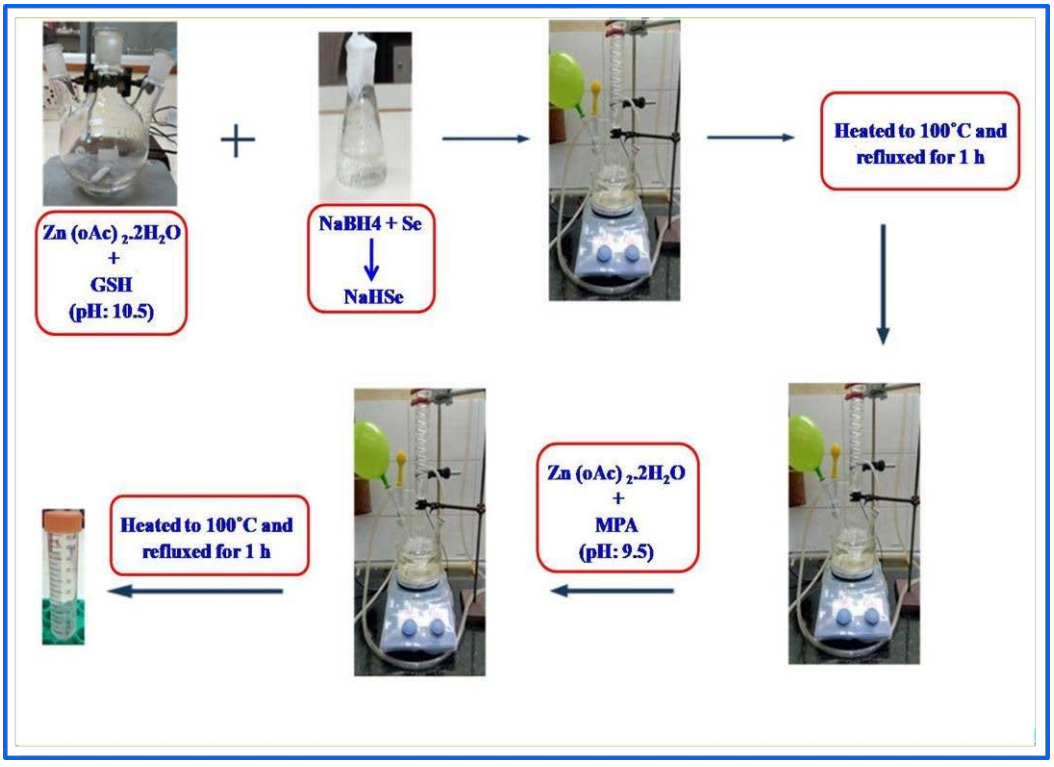

Figure 3.2: Schematic representation of ZnSe/ZnS QDs synthesis.

3.10 CHARACTERIZATION OF ZnSe/ZnS QDs

3.10.1 OPTICAL CHARACTERIZATION

Optical absorption and emission spectroscopy was carried out for the synthesized QDs. UV-Vis absorption spectra were recorded by using spectrophotometer (Shimadzu, Japan). Flourimetric spectra were collected from spectrofluorimeter- Jasco fp 8200 s (Shimadzu Corp. Japan) equipped with a xenon lamp. Quartz cuvette of 1.0 cm optical path length was used in both the experiments.

3.10.1.1 OBSERVATION UNDER U.V LIGHT

Pellet obtained after the synthesis of ZnSe/ZnS QDs was dissolved in water and observed under both visible (normal light) and UV light by a hand held UV lamp of long/short wavelength. These QDs were also compared with water and titanium dioxide nanoparticle *etc.* under the above conditions.

3.10.1.2 OBSERVATION UNDER FLUORESCENCE MICROSCOPE

The synthesis of ZnSe/ZnS QDs was dried overnight and observed under different filters of fluorescent microscope (Axio Scope A1 Carl Zeiss, Germany).

3.10.2 PHYSICO-CHEMICAL CHARACTERIZATION

The synthesized ZnSe/ZnS QDs were characterized for their morphology, size, structure, surface charge, colloidal stability and purity using the following techniques.

3.10.2.1 TRANSMISSION ELECTRON MICROSCOPY (TEM)

TEM is a lively characterization tool for directly imaging QDs to obtain quantitative measures of particle size, size distribution and morphology. QDs were imaged on a TEM -JEOL JEM-2100 LaB6 (JEOL, USA) with 100 kV resolution. Dried QDs (1 mg/ml) were dispersed in ethanol and deposited on 300-mesh carbon film coated copper grid of TEM. The grid was allowed to dry by solvent evaporation.

3.10.2.2 DYNAMIC LIGHT SCATTERING (DLS)

1 mg/ ml of ZnSe/ZnS QDs were dissolved in water and transferred into a cuvette. Hydrodynamic diameter and dispersity of QDs in solution (poly dispersity index (PDI) were measured by DLS. This was carried out using Malvern Zetasizer

Nano ZS (UK).

3.10.2.3 ZETA POTENTIAL

Zeta potential or surface charge of the QDs (1 mg/ ml of ZnSe/ZnS QDs were dissolved in water and transferred into a cuvette) was assessed using a Zetasizer Nano ZS (Malvern, 52 USA) instrument supplied by DTS Nano V4.2 software.

3.10.2.4 FOURIER TRANSFORM INFRARED SPECTROSCOPY (FTIR)

FTIR was also performed using IR tracer 100 Shimadzu instrument. Infrared spectra were recorded 45 scans from the region of 4000-400 cm^{-1} by a resolution of 4. Interactions of various functional groups and chemical bonds present in ZnSe core of QDs and the changes which took place during the process of shell formation were analysed by this method. A spatula of dried and powdered ZnSe/ZnS QDs were placed at the site of examination and analysed.

3.10.2.5 RAMAN SPECTRA

Raman spectroscopy was carried out to determine the electrical and structural properties of the ZnSe/ZnS QDs. Raman spectra was recorded with WITec alpha300 (Germany). Dried and powdered ZnSe/ZnS QDs was subjected to examine with Raman spectroscopy.

3.10.2.6 INDUCTIVELY COUPLED PLASMA OPTICAL EMISSION SPECTROMETRY (ICP-OES)

A known quantity of 0.0844 g dry ZnSe/ZnS QDs sample was digested in hydrochloric/hydrofluoric (HCL/HF) acid mixture and then diluted to a known volume in 30% HCL acid and analyzed as per the work procedure of ICP-OES. The concentration of the element in the solution was determined from the calibration plot obtained by analyzing standard solutions. The results were recorded and processed using Win Lab 32 software.

3.10.2.7 X-RAY POWDER DIFFRACTION (XRD)

XRD was carried out to assess crystalline characteristics of ZnSe/ZnS QDs. This was recorded in a broad range of Bragg angle 2θ ($10^{o} \leq 2\theta \leq 70^{o}$ using a Philip's x'pert pro diffractometer, Ni filtered Cu-Kα (λ= 1.54 Å) at 45kV and 40mA. Dried and powdered ZnSe/ZnS QDs was placed at the examination site of the equipment and analysed.

3.10.2.8 THERMAL ANALYSIS

Thermo gravimetric Analysis (TGA), Differential Thermal Analysis (DTA) and Derivative Thermo Gravimetry (DTG) were carried out to analyze the thermal stability of ZnSe/ZnS QDs. TGA assesses the weight loss of a material as a function of temperature under controlled atmosphere. Release or absorption of heat by ZnSe/ZnS QDs assessed by DTA. Temperature of maximum decomposition of ZnSe/ZnS QDs was given by DTG curve. ZnSe/ZnS QDs analyzed at a temperature range of 100-1000 ºC in Pyris Diamond simultaneous DTA-TGA equipment.

OBJECTIVE 2:

IN VITRO EVALUATION OF ZnSe/ZnS QDS WITH HEPG2 AND HEK CELL LINES

3.11 COLLECTION OF CELL LINES

HepG2 and HEK 293 cell lines were collected from National Centre for Cell Science (NCCS), Pune, India.

3.12 CELL CULTURE AND PASSAGING

Both cell lines were cultured in high glucose DMEM medium containing 10% FBS and incubated at 37 °C with 5% CO_2. Cell lines were maintained in T25 flask

containing DMEM with 10% heat-inactivated FBS (fetal bovine serum), 1% penicillin/streptomycin. The medium was changed in every 3 days. The cultures up to 20 passages with 70-80% confluency were used for the experiments. Following seeding densities were used for all the *in vitro* experiments, unless otherwise stated. An initial seeding density of $1x10^4$cells/well and $5x10^4$cells/well were used in 96 and 4 well plates respectively. An initial seeding density of $1x10^6$cells/well was used in 6 well and single (35mm dishes) well plates. The cells were allowed to attach overnight before QDs exposure.

3.13 IN VITRO TOXICITY STUDIES USING HepG2 CELL LINE

3.13.1 CELL CULTURE AND ZnSe/ZnS QDs TREATMENT

HepG2 cell lines were cultured in high glucose DMEM medium containing 10% FBS and 1% antibiotic/antimycotic (AB/AM) solution, incubated at 37 °C with 5% CO_2. Cells were seeded in appropriate seeding density depends on the plate and kept overnight in 5% CO_2 incubator at 37 °C. The ZnSe/ZnS QDs stock solutions (1mg/ml) were vortexed for 3 min before each experiment to ensure uniform distribution and exposure in the cell culture dishes. Different concentrations (12.5, 25, 50 and 100 µg/ml) of ZnSe/ZnS QDs were exposed to the HepG2 cell lines at different time periods (6 and 24h).

3.13.2 ASSESSMENT OF CELL VIABILITY BY MTT ASSAY

Assessment of cell viability evaluated as a function of mitochondrial activity by 3(4,5-Dimethylthiazol-2-yl)-2,5-Diphenyltetrazolium Bromide (MTT) assay. In brief, 1×10^4 cells were seeded into each well of a 96 well plate. Cells were treated with different concentrations (12.5, 25, 50 and 100 µg/ml) of ZnSe/ZnS QDs at 6 and 24h, followed by 3 h treatment with MTT (50 µg/well). The formazan crystals formed by the intracellular reduction of tetrazolium salt was dissolved by adding 100 µl of DMSO in each well and incubated in dark for 15 min. Absorbance was measured at 540 nm using a multiwell plate reader (Bio-Tek Instruments Inc, USA). Viability rate (%) was calculated from the relative absorbance at 540 nm with respect to the

percentage of control. The percentage of cell viability was calculated as % cell activity A_{con}-A_{neg} , where A_{exp} is the amount of experimental group absorbance, A_{neg} is the amount of blank group absorbance and A_{con} is the amount of control group absorbance.

3.13.3 INTERFERENCE OF PARTICLE WITH MTT

Direct interaction of many QDs with MTT interferes with assay result. The particle interference on MTT result was studied by incubating ZnSe/ZnS QDs of different concentrations (12.5, 25, 50 and 100 µg/ml) with 100µl, 0.05mg/ml MTT for 3 h followed by 100µl DMSO. The absorbance was measured at 540 nm using multiwell plate reader (Bio-Tek Instruments Inc, USA).

3.13.4 CYTOTOXICITY ASSOCIATED WITH PARTICLE DISSOLUTION

Effect of QDs dissolution in medium for exerting toxicity can be assessed by MTT. 12.5, 25, 50 and 100 µg/ml of ZnSe/ZnS QDs were incubated with DMEM supplemented with 10% FBS for 3 days (72 h). Supernatant was taken after the solution was centrifuged at 10000 rpm for 10 min. The cells seeded at an initial density of $1x10^4$cells/well were exposed to the supernatant for 24h and MTT assay was carried out as per section 3.13.2. The results were compared with MTT data obtained from the direct exposure of ZnSe/ZnS QDs with HepG2 cells.

3.13.5 ASSESSMENT OF LYSOSOMAL ACTIVITY BY NEUTRAL RED UPTAKE (NRU) ASSAY

NRU assay measures cell viability based on the uptake of vital dye by live cells. This simple and precise method was originally developed by Boren Freund and Puerner (1985). Cells were seeded in a 96 well plate with density of 1×10^4 cells/well. After 6 and 24h incubation (37 °C), the cells were washed with PBS and treated with different concentration of ZnSe/ZnS QDs (12.5, 25, 50 and 100 µg/ml). Sodium lauryl sulphate (0.02 µg/ml) was used as a positive control. After treatment, 10 µl of 1% neutral red reagent was added in each well and incubated for 3 h at 37°C with 5% CO2. At the end of incubation period, dye was removed and the wells were washed with PBS. The dye entrapped inside the cell was solubilized using the acid alcohol desorbing agent (1% glacial acetic acid and 50% ethanol: V/V) and the plates were kept under dark for 30 min. Absorbance was read spectrophotometrically at 540 nm in micro plate reader.

3.13.6 PARTICLE UPTAKE BY CONFOCAL MICROSCOPY

HepG2 cells were cultured on cover slips placed in 6 well plates and incubated for 24h for achieving 85% of cell confluency. They were treated with 25 µg/ml of ZnSe/ZnS QDs for 4 h and stained as per the procedure described in the section 3.13.12.

3.13.7 PARTICLE UPTAKE IN PRESENCE OF INHIBITOR

Cytochalasin B (Cyt. B) exposed cells were analysed for determining the endocytic pathway of ZnSe/ZnS QDs. Cyt. B is a specific inhibitor of clathrin-dependent endocytic pathway by inducing depolymerization of actin filaments (Hussain *et al.*, 1987). Here, the cells seeded at an initial density of $1x10^4$ cells/well were allowed to attach overnight. The cells were pre- incubated with 2 µM Cyt. B for 4 h. Consequently, cells exposed to different concentrations of ZnSe/ZnS QDs (12.5, 25, 50, 100 µg/ml) for 24h. NRU assay was carried out as described in section 3.13.5.

3.13.8 CELL COUNT BY TRYPAN BLUE EXCLUSION ASSAY

Number of viable cells present in a cell suspension was determined by trypan blue exclusion assay. Trypan blue is a vital azo dye, which is impermeable to cells with intact membrane. In presence of trypan blue dead cells stain blue whereas live cells remain colourless. In brief, cells were seeded in a 6 well plate at a density of 1×10^6 cells/well and incubated overnight in CO_2 incubator. The cells were exposed to ZnSe/ZnS QDs of different concentrations (12.5, 25, 50 and 100 µg/ml) for 6 and 24h. Cells harvested by centrifugation at 1500 rpm for 5 min and resuspended in 100 µl PBS. Cell counting was performed by mixing cell suspension with equal proportion of trypan blue and observed under phase contrast microscope (Axiovert 40 CFL, Zeiss, Germany) using Neubauer cell counting chamber. Four large squares at the corner were counted and number of cells (n) per ml were calculated using formula; n = (total number of cells counted ÷ total number of squares counted) x dilution factor x 10^4.

3.13.9 ASSESSMENT OF CYTOPLASMIC ENZYME RELEASE BY LDH ASSAY

Cytotoxicity of QDs is also evaluated by measuring the level of lactate dehydrogenase (LDH) enzyme released from HepG2 cells. LaDue and Wroblewski (1955) reported the release of lactate dehydrogenase, the cytoplasmic enzyme into the

culture medium. Briefly, HepG2 cells were treated with 12.5, 25, 50 and 100 µg/ml of ZnSe/ZnS QDs for 6 and 24 h. The culture supernatants were transferred to clean flat-bottom plate for enzymatic analysis. The activity of LDH in the supernatants was determined using LDH detection kit (as per the manufacturer's instructions). All samples were assayed in triplicates for LDH content using a microplate spectrophotometer (Bio-Tek Instruments Inc., USA) at 450 nm. The released amount of LDH is expressed as lactate dehydrogenase activity (IU/L) in culture medium.

3.13.10 CELLULAR PHENOTYPE BY PHASE CONTRAST MICROSCOPY

Cells were seeded in six well plates at an initial seeding density of $1x10^6$ cells/well. The morphology of HepG2 cells after 6 and 24 h exposure of ZnSe/ZnS QDs was evaluated under phase contrast microscope (Axiovert 40 CFL, Zeiss) fitted with camera (Axiocam ICm1, Zeiss).

3.13.11 MORPHOLOGY ANALYSIS BY GIEMSA STAINING

The cellular morphology of HepG2 was studied using giemsa staining. The cells were seeded on a cover glass placed in a six well plate at an initial density of 1×10^6 cells per well. After overnight incubation, cells were treated with different concentrations (12.5, 25, 50 and 100 µg/ml) of ZnSe/ZnS QDs in DMEM for 6 and 24h. Cells were washed with ice cold PBS and fixed using 4 % formaldehyde for 15 min. The cells were then stained with 10 % giemsa solution for 5 min. After washing with PBS, slides were observed under compound microscope.

3.13.12 ASSESSMENT OF CHANGES TO CYTOSKELETAL INTEGRITY AND NUCLEAR STRUCTURE

Effect of ZnSe/ZnS QDs on cytoskeletal structure of HepG2 cells were studied by Rhodamine-Phalloidine staining. This stain is specifically bind with a kind of cytoskeletal filament: F actin filament. A six well plate was seeded with an initial cell density of 1×10^6 cells/well. Cells were then treated with different concentrations of ZnSe/ZnS QDs (12.5, 25, 50 and 100 µg/ml) for 24h. Media was removed, cells were rinsed with PBS and fixed by 4% formaldehyde for 15 min at room temperature.

Excess aldehyde was quenched with 0.1 M glycine for 5 min. Fixed cells were then permeabilized using 0.1 % Triton X-100 at room temperature for 1 min. The actin filaments were stained using Rhodamine-Phalloidine stain (1:50) and the nuclei was counterstained with acridine orange (5 µg/ml) for 1 min. Cells were washed (3 times) with PBS and observed under confocal microscope (Olympus FV3000, Japan).

3.13.13 MITOCHONDRIAL MEMBRANE POTENTIAL (MMP) BY JC-1

Change in MMP was analysed by JC1 probe (5, 5′, 6, 6′tetrachloro-1, 1′, 3, 3′-tetraethylbenzimi-dazolylcarbocyanine iodide). JC-1 is a cationic, lipophilic dye that accumulates in the mitochondria in a potential dependent manner. The dye exists as a monomer inside the cytoplasm giving green fluorescence. The dye aggregates to form polymer of red fluorescence inside energized mitochondria with high membrane potential. In brief, the cells were seeded at an initial seeding density of $1x10^6$ cells/well and incubated overnight. After 24h exposure to 12.5, 25, 50 and 100 µg/ml of ZnSe/ZnS QDs, the cells were washed twice in PBS and were incubated for 30 min at 37 °C with 1 µM JC-1 dye. The cells after washing were observed under fluorescence microscope (Axio Scope.A1, Carl Zeiss, Germany) using green and red filter.

3.13.14 ASSESSMENT OF LYSOSOMAL INTEGRITY BY ACRIDINE ORANGE (AO) STAINING

Lysosomal integrity and formation of acidic vesicular organelles (AVOs) inside the HepG2 cells were assessed by AO staining. Cells at an initial density of $1×10^6$ /well were seeded on a cover glass in 6 well plates and allowed to attach overnight at 37 °C. The cells were exposed to different concentrations (12.5, 25, 50 and 100 µg/ml) of ZnSe/ZnS QDs of for 24 h. At the end of treatment period, the cells were incubated with acridine orange (2 µg/ml in citrate phosphate buffer) for 15 min at 37 °C. Cells were washed with PBS and observed under fluorescence microscope using green and red filter (Axio Scope.A1, Carl Zeiss, Germany).

3.13.15 FREE RADICAL FORMATION

3.13.15.1 ASSESSMENT OF REACTIVE OXYGEN SPECIES FORMATION BY DCFHDA

DCFH-DA is a flourimetric probe passively enters the cell and detecting the amount of intracellular ROS by DCFH-DA (Dichloro dihydro fluorescein diacetate). A highly fluorescent compound dichlorofluorescein (DCF) is formed from DCFH-DA as a result of reaction with ROS inside the cell. Cells were seeded at a density of 1×10^4 cells/well and cultured for 24h. After incubation with different concentration of ZnSe/ZnS QDs (12.5, 25, 50, and 100 µg/ml) was exposed to cells for 6 and 24 h. 0.09% hydrogen peroxide (H_2O_2) was used as a positive control. After treatment, the cells were washed with PBS and incubated with 100 µl of DCFH-DA (1 µM) for 45 min in dark. The excess DCFH-DA was removed and replaced with 200 µl PBS. Fluorescence was measured using micro plate reader (Plate Chameleon TM V, Hidex, Finland) with excitation and emission at wavelength of 450 and 535 nm respectively.

3.13.15.2 INFLUENCE OF CATALASE ACTIVITY ON ROS PRODUCTION

Effect of ZnSe/ZnS QDs on catalase activity of HepG2 cells on ZnSe/ZnS QDs induced ROS was assessed using a catalase inhibitor sodium azide (NaN_3). Cells seeded at initial density of $1x10^4$ were allowed to attach overnight. The cells were pre- incubated with 0.1µM NaN_3 for 1 h. Medium was replaced with fresh medium containing 12.5, 25, 50 and 100 µg/ml ZnSe/ZnS QDs. ROS production was estimated in presence of DCFH-DA as described in section 3.13.15.1. The results were compared with that of cells exposed to QDs in the absence of catalase inhibitor.

3.13.15.3 ASSESSMENT OF NITRILE RADICAL FORMATION BY GRIESS REAGENT

Griess reagent is used for the analysis of nitric oxide production in HepG2 cells. In brief, cells were seeded at a density of $1x10^4$ cells/well in a 96 well plate and incubated overnight. Cells were then exposed to 12.5, 25, 50, and 100 µg/ml of ZnSe/ZnS QDs for 6 and 24 h. 50 µl of supernatant was mixed with 50 µl of Griess reagent and incubated at room temperature for 10 min. The absorbance was read at 540 nm using a multiwell plate reader (Bio-Tek, Winooski, USA). The concentration was calculated from the sodium nitrate (0.5, 2.5, 5 and 7.5 µg/ml) standard graph.

3.13.16 ASSESSMENT OF OXIDATIVE STRESS INDUCED BY QDs

Cells at a final density of 6×10^6 in a 25 cm^2 culture flask were exposed to different concentrations of ZnSe/ZnS QDs for 24 h. After exposure, the cells were scraped off and washed with ice cold 1X phosphate buffered solution. The harvested cell pellets were lysed in cell lysis buffer (20 mM Tris-HCl with pH 7.5, 150 mM NaCl and 1 mM Na_2EDTA, 1% Triton, 2.5 mM sodium pyrophosphate). The cells were centrifuged at 15000 g for 10 min at 4 °C. The cell extract (supernatant) was maintained on ice until examined for oxidative stress biomarkers. Protein content was measured using Lowry's method (Lowry *et al*., 1951) with bovine serum albumin as standard.

3.13.16.1 PROTEIN ESTIMATION

Cell lysis was carried out as described in section 3.13.16.1. Total protein in the lysate was assessed by Lowry's method (Lowry *et al*. 1951). This method has sensitivity between 0.01-1 mg/ml. This assay is based on the reaction between copper ions produced by the oxidation of peptide bonds with Folin-Ciocalteu reagent. `

The experimental procedure is carried out as described in Table 3.1. Reading was taken at 660 nm using Lambda 25, UV/Vis spectrophotometer, Perkin Elmer, USA. The protein concentration is calculated from the standard graph (bovine serum albumin as standard)

Reagent	Blank	Test
Distilled water	1ml	0.9ml
Tissue homogenate	-	0.1ml
Solution C	5ml	5ml
Incubate at room temperature for 10min.		
Folin-Ciocalteu reagent	0.5ml	0.5ml
Incubate at dark for 30min		

Table 3.1: Protein estimation by Lowry's method

3.13.16.2 GLUTATHIONE LEVELS

The glutathione level was quantified using Ellman's reagent by the method introduced by Moron *et al*., (1979). The assay mixture contained 4 ml of 0.2 M phosphate buffer and 0.5 ml of cell extract (Table 3.2) and 0.5 ml of 2 mM DTNB (5,5-dithio-bis-(2-nitrobenzoic acid). The reaction was monitored at 412 nm using Lambda 25, UV/Vis spectrophotometer, Perkin lmer, USA. The amount of glutathione was expressed in terms of nmol glutathione/mg protein.

Reagents	**Blank**	**Sample**
0.2M phosphate buffer (pH-8)	4ml	4ml
Tissue homogenate	-	0.5ml
2mM DTNB	0.5ml	0.5ml
Distilled water	0.5ml	-

Table 3.2: Reaction mixture for determination of GSH level.

3.13.17 CELL CYCLE ANALYSIS BY FLOW CYTOMETRY

Influence of QDs in changing the cell cycle patterns were analysed by staining with Propidium Iodide (PI). In brief, the cells seeded at an initial density of $1x10^6$cells/well were exposed to ZnSe/ZnS QDs (12.5, 25, 50, and 100µg/ml) for 24h. Harvested cells were washed with PBS by direct pipetting. The pellets were fixed by adding 1 ml cold 80 % ethanol (kept at -20 °C) by vortexing to avoid cell aggregation. This was kept at -20 °C for at least 2 h (the cells may be kept at this condition for few days). The cells were washed by centrifugation (2000 rpm for 5 min) and resuspended in 300 µl PBS containing 80 µg/ml PI and 200 µg/ml RNase. After 1 h incubation at 37 °C, the solution was made up to 1 ml by adding 700 µl PBS and analysed using flow cytometry (DAKO GALAXY, Germany) with 630 nm long pass filter.

3.13.18 DNA LADDER ASSAY

Inter-nucleosomal DNA fragmentation is one of the hallmarks of apoptosis and was carried out by activated nuclease. $3x10^6$ cells were cultured in T25 flasks at 37 ºC for overnight. The cells were subsequently treated with 12.5, 25, 50 and 100 µg/ml of ZnSe/ZnS QDs for 24 h. DNA ladder assay was performed as per the manufacturer's instructions using Quick Apoptotic DNA ladder detection kit. At the end of exposure period the cells were harvested and washed with PBS. Further the cells were lysed by adding 35 µl of TE lysis buffer and 5 µl Enzyme A and incubated for 10 min in a water bath at 37 °C. Enzyme B solution was added and incubated at 50 °C for 30 min. Ammonium acetate solution and absolute ethanol were added and DNA was allowed to precipitate at -20 °C. This mixture was centrifuged at 12000 rpm for 10 min and the supernatant was discarded. The pellet was air dried for 10 min and resuspended in 30 µl DNA suspension buffer. DNA was loaded on to 1.2 % agarose gel containing 0.5 µg/ml ethidium bromide in 1X TBE (Tris/Borate/EDTA) running buffer and run at 5 V/cm for 1-2 h. DNA bands were visualized using transilluminator (Bio Imaging system, Syngene, UK).

3.13.19 LIVE DEAD ASSAY BY CALCEIN AM - PI

Flow cytometry analysis of calcein AM and PI stained cells was carried out by Live/Dead assay. Acetoxymethylester of calcein is highly lipophilic and is permeable to the cell membrane. Calcein AM itself is not a fluorescent molecule. Calcein-AM split into calcein by the enzyme esterase present inside the cells which, emits strong green fluorescence. This probe is also ideal for evaluating cell adhesion, chemotaxis and multidrug resistance. Calcein AM stains only viable cells. PI is an impermeable dye which enters cell through damaged cell membrane and specifically stains dead cells. In this assay, the cells seeded at an initial density of $1x10^6$/well. The cells were treated with 12.5, 25, 50 and 100 µg/ml of ZnSe/ZnS QDs for 6 and 24 h. The untreated cells were harvested by trypsinization and washed with PBS. The suspended cells were treated with calcein AM (1 µg/ml) for 45 min. After centrifugation, these cells were resuspended in 500 µl PBS containing 0.25 µl of PI and kept for 5 min in dark. These cells were subjected to flow cytometric analysis.

3.13.20 CASPASE 3/7 ACTIVATION ASSAY

Caspases are the cysteine aspartate protease which plays a central role in the execution phase of cell apoptosis. Caspase 3 and 7 are two executioner caspases that act downstream of caspase dependent apoptosis signal cascade. Multiple structural and regulatory proteins, which are critical for cell survival and maintenance, were destructed by activated caspase 3 and caspase 7 (Boyce *et al*., 2004; Crawford & Wells, 2011). Ana spec SensoLyte® Homogeneous AMC caspase 3/7 assay kit was used for the assessment of Caspase 3/7 activation in response to ZnSe/ZnS QDs exposure. HepG2 cells seeded at initial density of $1x10^4$cells /well in a 96 well plates were exposed to different concentration of ZnSe/ZnS QDs (12.5, 25, 50 and 100 µg/ml). Caspase 3/7 substrate was added subsequently to the plates and incubated for 60 min on a plate shaker. The reading was taken at an excitation/emission wavelength (354/442 nm) using fluorescent plate reader (Tecan Infinite M200, Switzerland). The caspase activity was expressed in relative fluorescent unit (RFU).

3.14 IN VITRO TOXICITY STUDIES USING HEK293 CELL LINE

3.14.1 CELL CULTURE AND QD TREATMENT

HEK cells were cultured in high glucose DMEM medium containing 10% FBS and 1% antibiotic/antimycotic (AB/AM) solution, incubated at 37 °C with 5% CO_2 (section 10.1). Cells were seeded in appropriate seeding density depends on the plate and kept overnight in 5% CO_2 incubator at 37 °C. The ZnSe/ZnS QDs stock solutions (1 mg/ml) were vortexed for 3 min before each experiment to ensure uniform distribution. The cells were exposed to 12.5, 25, 50 and 100 µg/ml ZnSe/ZnS QDs for different time durations (6 and 24 h).

3.14.2 MTT ASSAY

Cells seeded at an initial density of $1x10^4$/well were exposed to 12.5, 25, 50 and 100µg/ml of ZnSe/ZnS QDs for 6 and 24 h. The dose response in HEK was studied using MTT assay as detailed in section 3.13.2.

3.14.3 PARTICLE DISSOLUTION AND RELATED TOXICITY

Toxicity related to the QDs dissolved in DMEM medium was studied as per the procedure in the section 3.13.3. The cells seeded at an initial density of $1x10^4$ cells/well were exposed to the supernatant for 24 h and MTT assay was carried out as per section 3.13.2. The results were compared with MTT data obtained from the direct exposure of ZnSe/ZnS QDs with HEK cells.

3.14.4 NEUTRAL RED UPTAKE ASSAY (NRU)

HEK Cells seeded at an initial density of $1x10^4$/well were exposed to 12.5, 25, 50 and 100 µg/ml of ZnSe/ZnS QDs for 6 and 24 h. The NRU assay was carried out as described in section 3.13.5.

3.14.5 TRYPAN BLUE EXCLUSION ASSAY

HEK cells were seeded in a six well plate at a density of 1×10^6 cells/well and incubated overnight in CO_2 incubator. The cells were exposed to ZnSe/ZnS QDs of different concentration (12.5, 25, 50 and 100 µg/ml) for 6 and 24 h. Trypan blue assay was carried out as described in section 3.13.8.

3.14.6 PARTICLE UPTAKE BY CONFOCAL MICROSCOPY

HEK cells were cultured on coverslips placed in 6 well plates and incubated for 24 h for achieving 85 % of cell confluency. Then the cells were treated with 25 µg/ml of ZnSe/ZnS QDs for 4 h and stained as per the procedure described in the section 3.13.12.

3.14.7 PARTICLE UPTAKE (ZnSe/ZnS QDs) IN HEK CELLS BY FLOW CYTOMETRY

In this experiment, HEK cells were seeded in 6 well plates at an initial density of 1×10^5 cells/well and kept overnight for incubation. Cells were then exposed to 12.5 and 100µg/ml concentrations of ZnSe/ZnS QDs for 4 h. Cells were harvested and centrifuged at 1200 rpm. The pellet was resuspended in 500 µl PBS and analysed using flow cytometry.

3.14.8 UPTAKE INHIBITION BY CYTOCHALASIN B

Cellular uptake of QDs in the presence of inhibitor Cyt. B is studied for getting idea about the endocytic pathway by which particle is entered into the cells. The cells seeded at an initial density of $1x10^4$ cells/well were allowed to attach overnight. The detailed procedure is explained as in section 3.13.7.

3.14.9 LDH ASSAY

HEK cells were seeded at a density of 1×10^4 cells/well, treated with 12.5, 25, 50 and 100 µg/ml of ZnSe/ZnS QDs for 6 and 24 h. LDH assay was carried out as described in section 3.13.9.

3.14.10 PHENOTYPIC OBSERVATION BY PHASE CONTRAST MICROSCOPY

Cells were seeded in six well plates at an initial seeding density of $1x10^6$ cells/well. The morphology observed after 6 and 24 h of ZnSe/ZnS QDs exposure under phase contrast microscope (Axiovert 40 CFL, Zeiss) fitted with camera (Axiocam ICm1, Zeiss).

3.14.11 COOMASSIE BRILLIANT BLUE STAINING FOR MORPHOLOGY ANALYSYS

The cellular morphology of HEK was studied using Coomassie brilliant blue staining. The cells were seeded on a cover slip placed in a six well plate at an initial density of 1×10^6 cells/well. After overnight incubation, cells were treated with different concentrations (12.5, 25, 50 and 100 µg/ml) of ZnSe/ZnS QDs in DMEM for 6 and 24 h. Cells were washed with ice cold PBS and fixed using 4% formaldehyde for 15 min. The cells were stained with Coomassie solution for 10 min. After washing with PBS, slides were observed under compound microscope.

3.14.12 MMP BY JC-1

The cells were seeded at an initial seeding density of $1x10^6$cells/well and overnight incubation. After 24 h exposure to 12.5, 25, 50 and 100 µg/ml of ZnSe/ZnS QDs. The change in mitochondrial membrane potential evaluated by using JC-1 probe as described in the section 3.13.13.

3.14.13 LYSOSOMAL INTEGRITY BY AO STAINING

Cells at an initial density of 1×10^6 per well were seeded on a cover glass in a 6 well plates and allowed to attach overnight at 37 °C. The cells were exposed to ZnSe/ZnS QDs of concentration 12.5, 25, 50 and 100 µg/ml for 24 h. Lysosomal integrity assessed by acridine orange staining as described in the section 3.13.14.

3.14.14 FREE RADICAL FORMATION

3.14.14.1 DETECTION OF ROS PRODUCTION

Cells were seeded at a density of 1×10^4 cells/well and cultured for 24 h. After incubation, different concentration of QDs (12.5, 25, 50 and 100 µg/ml) was exposed to cells for different time period such as 6 and 24h. 0.09% hydrogen peroxide (H_2O_2) was used as a positive control. ROS produced in HEK cells as a result of QDs treatment was explained in the section 3.13.15.1.

3.14.14.2 INFLUENCE OF CATALASE ON ROS PRODUCTION

Cells seeded at initial density of $1x10^4$ were allowed to attach overnight. Influence of catalase activity in HEK cells on challenge with ZnSe/ZnS QDs induced

ROS was assessed by a catalase inhibitor sodium azide (NaN_3) as described in the section 3.13.15.2.

3.14.14.3 NITRIC OXIDE PRODUCTION BY GRIESS REAGENT

Cells were seeded at a density of $1x10^4$ cells/well in 96 well plates and incubated overnight. Cells were then exposed to 12.5, 25, 50 and 100 µg/ml of ZnSe/ZnS QDs for 6 and 24 h. Nitric oxide production in HEK cells was detected as mentioned in the section 3.13.15.3.

3.14.15 ASSESSMENT OF OXIDATIVE STRESS

Cells at a final density of approximately 6×10^6 in a 25 cm^2 culture flask were exposed to different concentrations of ZnSe/ZnS QDs for 24 h. After exposure the cells were harvested and lysed as described in section 3.13.16.

3.14.15.1 PROTEIN ESTIMATION

Total protein in the lysate was assessed by Lowry's method (Lowry *et al*. 1951). The experimental procedure is carried out as described in Table 3.1.

3.14.15.2 ESTIMATION OF GSH CONTENT

The glutathione level was quantified using Ellman's reagent by the method introduced by Moron *et al*., (1979) as described in the section 3.13.16.2.

3.14.16 DNA LADDER ASSAY

$3x10^6$ cells were cultured in T25 flasks for overnight. The cells were subsequently treated with 12.5, 25, 50 and 100 µg/ml of ZnSe/ZnS QDs for 24 h. DNA ladder assay was performed as per the manufacturer's instructions using Quick Apoptotic DNA ladder detection kit. Gel preparation and other procedures are same as in the section 3.13.18.

3.14.17 LIVE DEAD ASSAY BY CALCIEN AM-PI

In this assay, the cells seeded at an initial density of $1x10^6$/well. Cells were treated with 12.5, 25, 50 and 100 µg/ml of ZnSe/ZnS QDs for 6 and 24 h. Treated and untreated cells were harvested by trypsinization and washed with PBS. Calcien AM-PI staining was carried out as per in section 3.13.19 and subjected to flow cytometric

analysis.

3.14.18 APOPTOSIS BY ANNEXIN-PI FACS

The QDs induced apoptosis/necrosis on HEK cells were analysed by Annexin/PI kit (Alexa Fluor® 488 Annexin V/Dead Cell Apoptosis Kit, Thermo Fisher scientific, USA). Annexin V binds to the phosphatidyl serine residue present in the outer lipid bilayer membrane of cells undergoing apoptosis. Whereas PI stains dead cells. HEK cells were incubated with ZnSe/ZnS QDs (12.5, 25, 50 and 100 µg/ml) for 24 h and the cell were the stained with annexin V and PI. In brief the treated cells were trypsinized and resuspended in annexin binding buffer (50 µl). These cells were stained with Annexin V (5 µl) for 15 min and propidium iodide (1 µl) for 5 min and incubated before FACS analysis. The analysis was carried out using BD- FACSARIA, BD Biosciences, USA.

3.14.19 CASPASE 3/7 ACTIVATION ASSAY

Human embryonic kidney (HEK) cells seeded at initial density of $1x10^4$ cells /well in 96 well plates were exposed to different concentration of ZnSe/ZnS QDs (12.5, 25, 50 and 100 µg/ml). Caspase 3/7 activation assay was carried out as described in the section 12.20.

OBJECTIVES 3

Toxicity studies were carried out in Swiss albino mice. A schematic representation of the work plan is given in the figure 3.3.

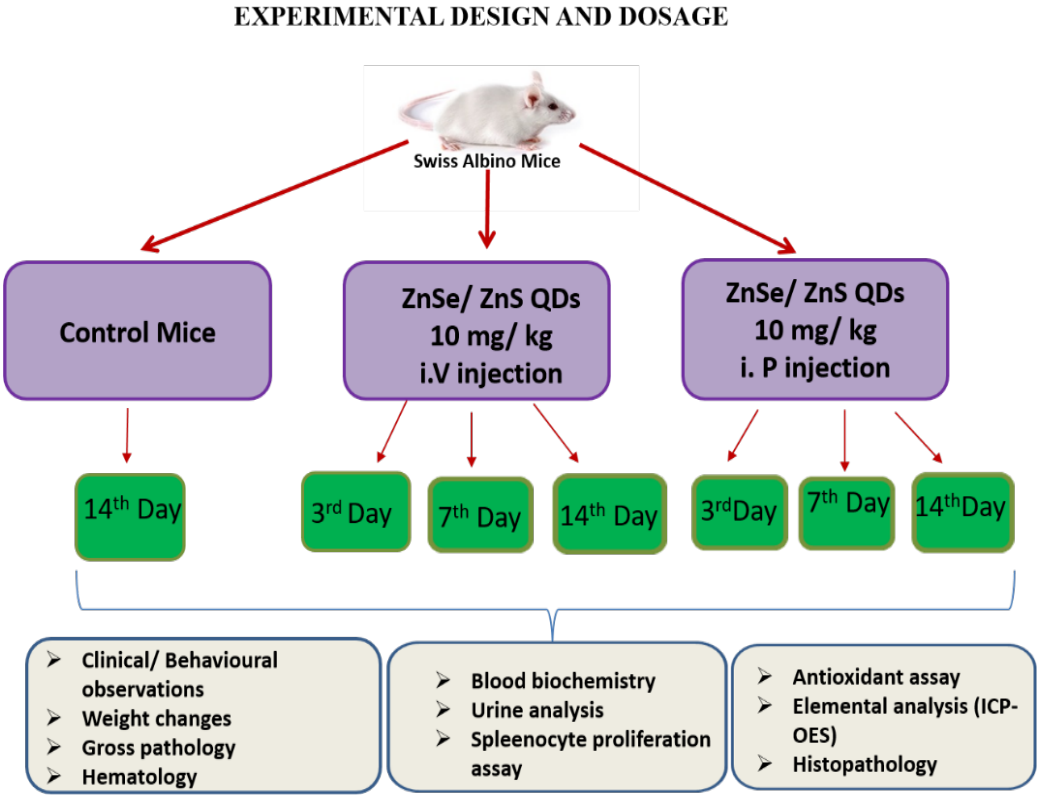

Figure 3.3: Schematic representation of biodistribution and ADME& T profiling.

3.15 EXPERIMENTAL DESIGN AND DOSAGE

Healthy Swiss Albino mice weighing 17-23 g were used for the study. Animals were randomly divided into 7 groups of three animals each, based on route of exposure and the time of observation. The details of the experimental design are given in the Table 3.3. Groups 1 animals served as control received only physiological saline by intravenous injection (50 ml/kg. Animals in the group 2 to 7 received single dose (10 mg/kg body weight) of ZnSe/ZnS QDs in physiological saline [group 2-4 intravenous (i.v) and group 5-7 intraperitoneal (i.p)] (Figure 3.4.a and b). Animals in the control group (group 1) were sacrificed at the end of 14 days. Three animals each from group 2-7 were sacrificed at the end of 3, 7 and 14 days of exposure of ZnSe/ZnS QDs. Before sacrifice (3, 7 and 14 days), body weight was noted and blood was collected from all the animals for haematological and clinical biochemistry analysis. Urine was also collected for analysis. Gross pathology was observed during sacrifice.

Subsequently, organ weight was noted and organs such as liver, kidney, brain and spleen were collected and subjected to histopathology and elemental analysis. A portion of the liver and brain was subjected to oxidative stress analysis and spleen was used for splenocyte proliferation assay. Blood Brain Barrier (BBB) integrity after the QDs treatment can be analyzed by measuring brain volume.

Dose	**Route of exposure**	**Number of animals**		
		3rd day	**7thday**	**14thday**
Control (50 ml/ kg body weight of saline)	Intravenous (i.v.)	-	-	3
	Intraperitoneal (i.p)	-	-	3
ZnSe/ZnSQDs (10mg/kg body weight of saline)	Intravenous (i.v.)	3	3	3
	Intraperitoneal (i.p.)	3	3	3

Table 3.3: Experimental design and dosing in Swiss Albino mice.

Figure 3.4: Intravenous (i.v.) injection (tail vein) in Swiss Albino mice.

PART I: ACUTE TOXICITY, IMMUNOTOXICITY, HAEMATOLOGICAL, CLINICAL BIOCHEMISTRY OXIDATIVE STRESS AND HISTOPATHOLOGICAL STUDIES.

3.16 CLINICAL SIGNS OF EXPERIMENTAL ANIMALS

Home cage observation of animals was carried out regularly (twice a day till the end of experiment) to check for morbidity, mortality and clinical signs after exposure of ZnSe/ZnS QDs. Cage-side observations like change in skin, fur, eyes and mucous, change in behaviour patterns like staggering, spinning, hunched body poster, lethargy, lack of grooming, salivation and piloerection were noted.

3.17 BODY WEIGHT GAIN OF ANIMALS

Body weight of all the animals were monitored and recorded on a regular basis throughout the experimental period (3, 7 and 14 days).

3.18 URINE, FAECAL MATTER AND BLOOD SAMPLES COLLECTION

Urine of the animal was collected at the end of observation period for urine analysis. Blood samples were collected from the orbital sinus/ plexus of each mouse into non-vacuum blood collection tubes (at the end of observation period) for haematological and clinical biochemistry evaluations. Also urine and faecal matter was subjected to elemental analysis.

3.19 URINE ANALYSIS

Urine examined for protein, nitrite, blood, glucose, leukocytes, urobilinogen, ketones bilirubin, specific gravity and pH using urine analyser, Uro-dipchek 300 (Erba Mannheim, Germany).

3.20 HAEMATOLOGY ANALYSIS

Blood was collected from each animals (n=3) and collected in heparinised tubes. The white blood corpuscels (WBC), red blood corpuscels (RBC), hematocrit (HCT), hemoglobin (HGB), Mean Corpuscular Volume (MCV), Mean Corpuscular Hemoglobin (MCH), Mean Corpuscular Hemoglobin Concentration (MCHC) and Platelet (PLT) count were carried out using Horiba Vet abc, Japan instrument.

3.21 CLINICAL BIOCHEMISTRY

Serum biochemistry analysis supports for the assessment of liver and kidney function. Blood from each mice (n=3) was collected in plain tubes and allowed to clot. Serum was separated from the clotted blood by centrifuging the tubes at 3500 rpm for 15 min. The serum samples were analysed for protein, creatinine, albumin, cholesterol, bilirubin, gamma glutamyl transferase (GGT), alkaline phosphatase (ALP), alanine transaminase (SGPT), aspartate aminotransferase (SGOT). These analyses were carried out using biochemical analyser, Erba Mannheim XL300 (Germany).

3.22 GROSS PATHOLOGY

At the end of observation period, all the animals were sacrificed by cervical dislocation. Viscera open and gross pathological examinations were carried out. The animal's body were examined for any visible changes like lumps, lesions, colour changes or damages in the body surface, organs or tissues.

3.23 ORGAN WEIGHT

Organs including liver, kidney spleen and brain were collected from the euthanized mice and wet weight of the organs was recorded.

3.24 HISTOPATHOLOGY

Histopathological analysis was carried out in liver, kidney, spleen and brain collected from each treatment group. The tissue samples for histopathology were washed in saline and collected in 10% neutral buffered formaldehyde immediately after collection to prevent tissue degradation.

3.24.1 TISSUE PROCESSING

Tissue samples were cut into small pieces in order to fit into tissue cassettes. The tissue samples were processed to dehydrate using isopropanol, cleared in xylene and steadily infiltrated in paraffin wax to make thin sectioning possible (as shown in Table 3.4).

Solutions	Duration
Isopropanol I	1 h
Isopropanol II	1 h
Xylene I	45 min
Xylene II	45 min
Xylene III	45 min
Paraffin wax I	1 h
Paraffin wax II	1 h

Table 3.4: Sample processing for Histopathology

3.24.2 EMBEDDING

The tissue samples were taken out of the cassettes using pre-warmed forceps and were embedded into paraffin blocks. Each tissue sample was placed onto the moulds and filled with warm paraffin in such a manner that the cutting surface would comprise a cross section of the tissue. The mould containing the tissue sample was allowed to cool before removing the paraffin blocks from them.

3.24.3 SECTIONING AND SLIDE PREPARATION

Paraffin blocks were sectioned using microtome fitted with disposable metal knifes (Leica RM 2125 RT, Germany). The blocks were trimmed up to the tissue surface exposed. The surface of the tissue was cooled with an ice cube to avoid cracks in the paraffin sections. 5 µm thick sections were cut by adjusting the distance between the block and the knife. The tissue sections were floated on to warm water to expand the sections by removing the wrinkles. The sections were then picked onto cleaned glass slides pre-coated with Meyer's egg albumin.

3.24.4 STAINING OF SLIDES USING HEMATOXYLIN AND EOSIN (H&E) STAIN

H & E stain is referred as the routine staining, used for the morphological examination of any tissue specimen. Hematoxylin is a basic dye that stains the acidic components of the cell (the nucleus) whereas eosin is the acidic dye that stains the basic components of the cell (cytoplasm). The cell differentiation is attained by treating the tissues with the acid and alkali solutions. The counterstaining is executed by using eosin solution which imparts the pink color to the cytoplasm. Detailed procedure is shown in the table 3.5: The stained slides were mounted using DPX to make the samples scratch proof and to provide better optical clarity for observation of slides under microscope.

Steps	Duration
Slides with sections were kept in 50°C oven	1 h
Immersed in Xylene I	10 min
Immersed in Xylene II	10 min
Absolute alcohol	5 min
70% alcohol	5 min
Distilled water	5 min
Harris Hematoxylin	8 min
Tap water	5 min
Acid alcohol	1-2 dips
Tap water	5 min
Scott's tap water	4 min
Tap water	5 min
1% Eosin	4 min
70% ethanol	2 dips
Tap water	1 dip
70% alcohol	2 min
Absolute alcohol	5 min
Xylene I	10 min
Xylene II	10 min
Slides were air dried and mounted with cover glasses using DPX mountant	

Table 3.5: Procedure for Hematoxylin and Eosin staining of tissue sections

3.25 ANTIOXIDANT ASSAY

A portion of liver and brain collected from the toxicity study (section no 3.15) were subjected to estimate the antioxidant levels as mentioned below.

3.25.1 SAMPLE PREPARATION

Liver and brain were collected at the end of 3, 7 and 14 days after exposure of ZnSe/ZnS QDs in mice. The organs were washed in saline and transferred to a container kept on ice. 10% tissue homogenate was prepared in 0.1 M phosphate buffer of pH 7.4 by keeping the samples on ice. The tissue was homogenised at 1000 rpm using tissue homogeniser, Polytron P 3100 (Switzerland). The supernatant of the homogenate was collected after centrifugation at 3500 rpm for 10 min at 4 °C. The supernatant was kept on ice for further use.

3.25.2 TOTAL PROTEIN ESTIMATION

Total protein in the tissue homogenate was estimated by Lowry's method. This method based on the reaction between copper ions produced by the oxidation of peptide bonds with Folin-Ciocalteu reagent. This method is sensitive down to a range of 10 µg/ml. Incubation time and pH is very crucial for getting the reproducible data. The experimental procedure is as described in the Table 3.3. Solution C described in the table was prepared by mixing 50 ml solution of sodium carbonate (1 g in 50 ml distilled water) and 1 ml solution of sodium potassium tartarate (10 mg) and 5 mg copper sulphate. Reading was taken at 660 nm using Lambda 25, UV/Vis spectrophotometer, Perkin Elmer, USA. The protein concentration is calculated from the bovine serum albumin (BSA) standard graph.

3.25.3 LIPID PEROXIDATION (LPO)

Oxidative damage happens to the lipids assessed by the malonedialdehyde (MDA) level, which is the by-product of lipid peroxidation (LPO). It was evaluated following the protocol of Ohkawa *et al*., (1979). Detailed experimental procedure given in the table: 3.6. Final pink coloured solution formed as a result of reaction between thiobarbituric acid and MDA was subjected to spectrophotometer analysis (Lambda 25, UV/Vis spectrophotometer, Perkin Elmer, USA) at 532 nm.

Reagents	**Blank**	**Test**
0.8% TBA	1.5ml	1.5ml
8.1% SDS	0.2ml	0.2ml
20% acetic acid	1.5ml	1.5ml
Tissue homogenate	-	0.2ml
Distilled water	1.0ml	0.8ml
Incubate in water bath at 90° C for 1h		
Distilled water	1ml	1ml
Centrifuge at 3500 rpm for 10 min		

Table 3.6: Reaction mixture for LPO assay

3.25.4 REDUCED GLUTATHIONE (GSH)

Moron *et al*., (1979) developed a method for detecting the GSH level in the cells. Yellow coloured product formed as a result of reaction between GSH and DTNB [5, 5'-dithiobis-(2-nitrobenzoic acid)] detected spectrophotometrically at 412 nm using Lambda 25, UV/Vis spectrophotometer, Perkin Elmer, USA. Detailed experimental procedure given in the table 3.2.

3.25.5 GLUTATHIONE PEROXIDASE (GPX)

Rotruck *et al*., (1973) developed a method for the detection of GPx. GPx is an enzyme family that catalyzes the oxidation of GSH to oxidized form (GSSG) in presence of H_2O_2 and water is the by-product i.e. $2GSH + H_2O_2 \rightarrow GS\text{-}SG + 2H_2O$. Spectrophotometer (Lambda 25, UV/Vis spectrophotometer, Perkin Elmer, USA) is used for the reading at 412 nm. Each step of the procedure is given in the table 3.7.

Reagent	Blank	Test
0.1M phosphate buffer (pH -7)	-	0.4ml
Sodium azide	-	0.1ml
EDTA	-	0.1ml
Tissue homogenate	-	0.1ml
Hydrogen peroxide	-	0.1ml
Distilled water	1ml	1ml
4mM GSH	-	0.2ml
Incubate at 37°C for 0, 90 and 180s for each group of test		
10% TCA	-	0.5ml
Centrifuge at 3500rpm for 5min at 4°C. Collect the supernatant.		
Supernatant	-	1ml
0.3M phosphate solution	4ml	4ml
0.6mM DTNB	0.5ml	0.5ml

Table 3.7: Procedure for GPx activity estimation

3.25.6 GLUTATHIONE REDUCTASE (GR)

In the presence of NADPH, GSSH convert back to GSH by GR. The method developed by Langdon and Mize (1962). The reaction contents are given in Table 3.8. The reading was taken at 0, 1, 2 and 3 min at a wavelength of 340 nm (Lambda 25, UV/Vis spectrophotometer, Perkin Elmer, USA).

Reagents	**Blank**	**Test**
0.1M phosphate buffer (pH-7.6)	2.1ml	2ml
0.5mM EDTA	0.5ml	0.5ml
20mM oxidized glutathione	0.15ml	0.15ml
Incubate at 37°C for 10 min		
2mM NADPH	0.15ml	0.15ml
Tissue homogenate	-	0.1ml

Table 3.8: Procedure for GR activity estimation

3.25.7 SUPEROXIDE DISMUTASE (SOD)

SOD assay was carried out in liver and brain homogenate using modified pyrogallol auto oxidation method developed by Marklund and Marklund 1974. Reading was taken at 420 nm (Lambda 25, UV/Vis spectrophotometer, Perkin Elmer, USA) immediately after the addition of pyrogallol at 0, 1, 2 and 3 min. detailed procedure is given in the table 3.9.

Reagent	Blank	Standard	Test
0.1M Tris buffer (pH -8.2)	3.1ml	2.6ml	2.5ml
1mM EDTA	0.1ml	0.1ml	0.1ml
1mM DTPA	0.5ml	0.5ml	0.5ml
Tissue homogenate	-	-	0.1ml
Pyrogallol	-	0.5ml	0.5ml

Table 3.9: Procedure for SOD activity estimation

3.26 IMMUNOTOXICITY BY SPLENOCYTE PROLIFERATION ASSAY

Immunotoxicity of ZnSe/ZnS QDs assessed by the splenocyte proliferation assay. The splenocytes of animals isolated after each observation period. Spleen was transferred to cold PBS containing antibiotic/antimicotics and was placed on a metallic cell strainer kept over 10 mm petridish under sterile condition. Spleen was mashed by softly teasing it over the metallic cell strainer. The single cell suspension was layered carefully over histopaque and centrifuged at 1500 rpm for 40 min. The cells present in the resulting buffy coat were isolated and washed three times with PBS. The cells were cultured at an initial density of $2x10^5$ cells/well in DMEM medium supplemented with 10 % FBS. After 48 h, 0.5 μCi of tritiated thymidine was added to each well and incubated for 24h. Cells were fixed using 5 % trichloroacetic acid and lysed with SDS/NaOH lysis buffer. The radioactivity was measured by scintillation counter (Hidex, Finland) after adding scintillation fluid. The values were expressed as mean ± SD of counts per minute (CPM).

3.27 BLOOD BRAIN BARRIER (BBB) INTEGRITY

Break down of blood brain barrier will lead to an influx of water into the brain as a result water content increases. The protocol devised by Yang *et al*., (2015) was followed to estimate the brain water content. Mice were exposed to ZnSe/ZnS QDs at a dose of 10 mg/ kg body weight. At the end of 3, 7 and 14 days, brain was collected carefully and wet weight was noted. The dry weight of the brain was measured after

drying at 110°C for 24 h. The brain water content was calculated as: Percentage water content = (wet weight-dry weight)/wet weight x 100 %.

PART 2: ELEMENTAL ANALYSIS, BIODISTRIBUTION AND ADME & T (ABSORPTION, DISTRIBUTION, METABOLISM, EXCRETION AND TOXICITY) PROFILING STUDIES.

3.28 BIODISTRIBUTION BYELEMENTAL ANALYSIS

Elemental analysis was done by Inductively Coupled Plasma Optical Emission Spectroscopy (ICP-OES). Blood, urine, faeces, liver, kidney, spleen and brain of the animals treated (section: 3.15) with ZnSe/ZnS QDs were used for elemental analysis. ICP-OES construct the excitation emission property of electrons and plasma excites the atoms and ions. When an atom or ion is excited, its electrons jump from a lower to higher energy level. Upon relaxation of these electrons to their initial 'ground' state, energy is emitted in the form of photons. The emitted photons possess wavelengths that are characteristic of their respective elements. The intensity of the energy emitted at a particular wavelength is directly proportional to the amount of elements per sample analysed. Hence both qualitative and quantitative estimation of an element is possible by determining the wavelength and intensity at which energy is emitted.

3.28.1 SAMPLE PROCESSING

Blood, urine, faeces, liver, kidney, spleen and brain collected from the mice was freeze dried. 500 mg of the tissues samples (1 ml of blood and urine sample) were serially treated with 2 ml of 50% HNO3 three times, 1 ml of 100 % HNO_3 two times, 1 ml of HCl/HNO_3 (1:1 ratio), followed by $HClO_4/HNO_3$ (1.5: 1 ratio) in a heated sand bath. The acid digestion was continued up to the samples completely digested. This process warranted removal of carbonaceous matter to get metals present in the sample. The resulting residue was rinsed with ultrapure water (resistivity- 18.3 MΩ.cm) into a 15ml volumetric flask. The analysis was carried out using ICP-OES Optima 5300 DV ICP-OES spectrometer (Perkin Elmer, USA) [The solution can be stored at 4°C for analysis].

3.28.2 DETECTION OF ELEMENTS

The elemental analysis was carried out from the digested samples was analysed by ICP-OES, Optima 5300 DV ICP-OES spectrometer (Perkin Elmer, USA). The zinc is detected at the wavelength of 206.2 nm. Selenium and sulphur were detected at wavelengths of 196.026 nm and 181.975 nm respectively. The results were compared with control samples for the assessment of the QDs distribution.

3.29 STATISTICAL ANALYSIS

The results were expressed in mean ± SD and data were analysed by Student's t-test. In all the cases, $p < 0.05$ (*), $P < 0.01$(**) and $P < 0.001$ (***) was considered statistically significant compared to control.

CHAPTER 4: RESULTS

4. RESULTS

OBJECTIVE 1

SYNTHESIS AND CHARCTERIZATIONOF QDs

4.1 SYNTHESIS OF ZnSe/ZnS QDs

Blue fluorescent ZnSe/ZnS QDs were synthesised by a facile aqueous phase route. In this process Zinc acetate dihydrate ($Zn(OAc)_2.2H_2O$) was used as source of Zn^{2+}. Zn $(OAc)_2.2\ H_2O$ and GSH was stirred under nitrogen atmosphere after adjusting pH to 10.5 by using1M NaOH. Sodium hydrogen selenide (NaHSe) produced as a result of reduction of Selenium powder by using reducing agent $NaBH_4$ acted as the selenium source. NaHSe was added to the Zn source and heated to 100 ºC under vigorous stirring and N_2gas bubbling. GSH capped ZnSe core was synthesised by this step. To the crude ZnSe solution, additional Zn precursor (Zn $(OAc)_2.2\ H_2O$) and thiol ligand 3-mercapto propionic acid (3-MPA) was added at room temperature and pH was adjusted to 9.5. Reaction mixture reheated to 100 ºC for the synthesis of ZnS capping over the ZnSe core. ZnSe/ZnS QDs were modified with carboxylic groups on the surface by the addition of 3-MPA. Reaction was terminated by allowing the reaction mixture to cool down to room temperature and a white transparent solution was obtained. These samples were purified by centrifugation by adding equal amount of absolute alcohol. A white precipitate obtained after centrifugation was subjected to overnight drying for getting white powder of ZnSe/ZnS QDs. Chemical reactions taking place during the synthetic process is given below (Figure 4.1).

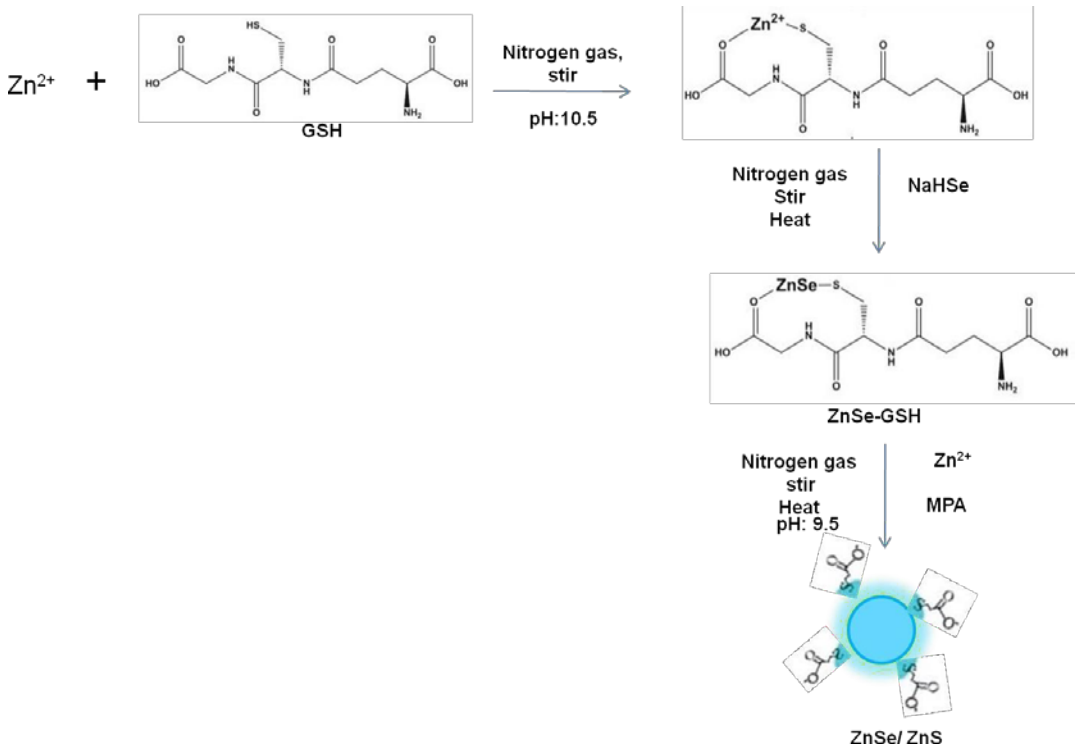

Figure 4.1. Schematic representation of chemical reaction during ZnSe/ZnS QDs synthesis.

Zinc acetate dihydrate (Zn $(OAc)_2$. $2H_2O$) (155.8 mg), GSH (92.2 mg), (3- MPA) (106 mg), Selenium powder (15.6 mg), Sodium borohydride (14.8 mg) were used for the ZnSe/ZnS QDs. The total yield of ZnSe/ZnS QDs was 3mg/50 ml.

4.2 CHARACTERIZATION OF ZnSe/ZnS QDS

The optical, physic-chemical characterisations of the synthesised ZnSe/ZnS QDs were carried out using different techniques as detailed below.

4.2.1 OPTICAL CHARACTERIZATION

Optical characteristics of the QDs were observed by fluorescence and absorption spectra. From the absorption spectra, it can be seen that QDs have a wider range of absorption. The absorption peak of QDs was found to be at 340 nm (Figure 4.2a). ZnSe/ZnS QDs have broad excitation spectra and symmetric narrow emission peak at 416 nm (Figure 4.2b). The full width at half-maximum (FWHM) is 30 nm.

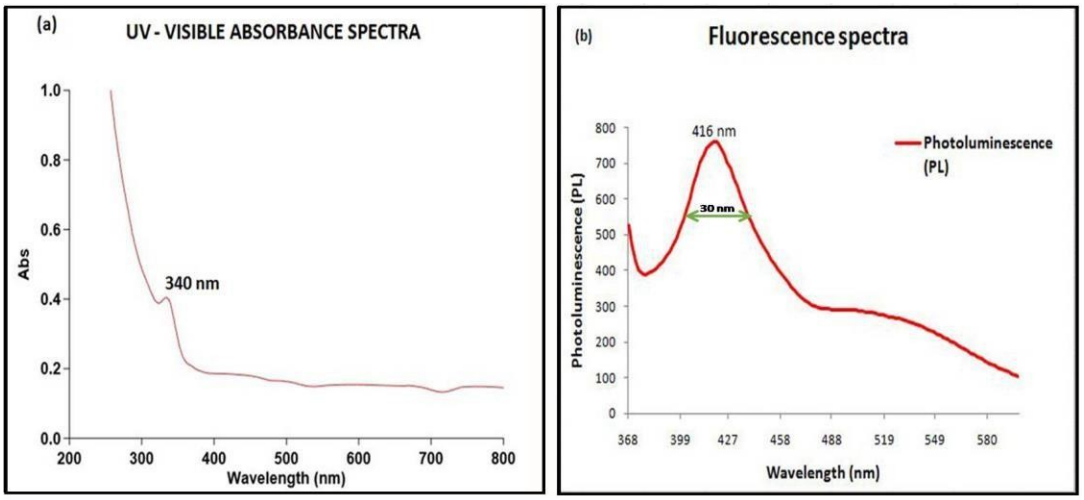

Figure 4.2 a. Absorbance spectra (left), b. fluorescence spectra (right) of ZnSe/ZnS QDs.

4.2.1.1 OBSERVATION UNDER U.V LIGHT

The pellet obtained after the centrifugation was dissolved in water. The solution of ZnSe/ZnS QDs was fully soluble in water and found to be clear and transparent under visible light. But illuminates greenish blue fluorescence under ultraviolet light without any post preparative treatment. ZnSe/ZnS QDs (pellets obtained after centrifugation) observed under UV light and compared with supernatant after centrifugation, TiO_2 NPs, water and alcohol to see the fluorescence. ZnSe/ZnS QDs (pellets) show bright greenish blue fluorescence while all others gave no fluorescence (figure 4.3a, b).

4.2.1.2 OBSERVATION UNDER FLUORESCENCE MICROSCOPE

QDs were observed under different filters of fluorescence microscope. Under blue filter, particle showed blue fluorescence and background (glass slide) was seen as black. Particle was found as black and background was green when used green filter. While no fluorescence was observed under red filter. The size distribution of the ZnSe/ZnS QDs is confirmed by the fluorescence image. This QDs shows partial

monodispersity and some aggregation (figure 4.4 a, b, c).

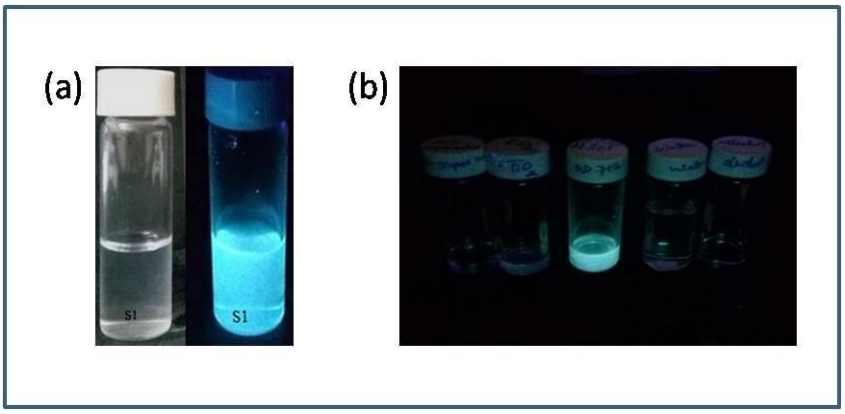

Figure 4.3 a. Observation of ZnSe/ZnS QDs under visible and UV light, b. Observation of supernatant of the solution, TiO_2 NPs, ZnSe/ZnS QDs, water and alcohol under UV light.

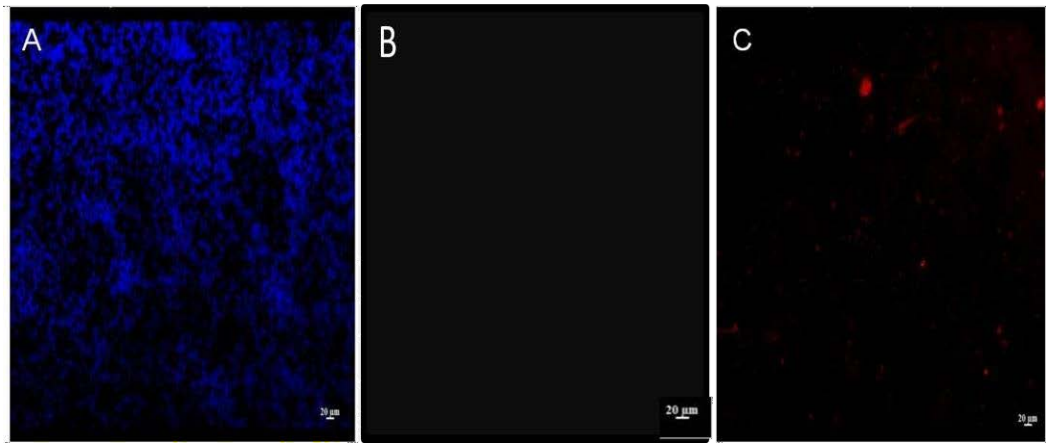

Figure 4.4: Observation of ZnSe/ZnS QDs under blue (a), green (b), red (c) filters of fluorescent microscope. Scale: 20µm, magnification 10X.

4.2.2 PHYSICO-CHEMICAL CHARACTERIZATION

4.2.2.1 TRANSMISSION ELECTRON MICROSCOPY (TEM)

TEM micrograph of the synthesized ZnSe/ZnS QDs is presented in Figure. 4.5a. The TEM micrograph suggests that the particles are almost monodispersed. Some aggregates are also seen. The average diameter of particles is approximately 5-6 nm.

4.2.2.2 DYNAMIC LIGHT SCATTERING (DLS)

Hydrodynamic size (Z-average) of ZnSe/ZnS QDs was found to be 33 nm with a poly dispersity index (PDI) of 0.288 (Figure 4.5b).

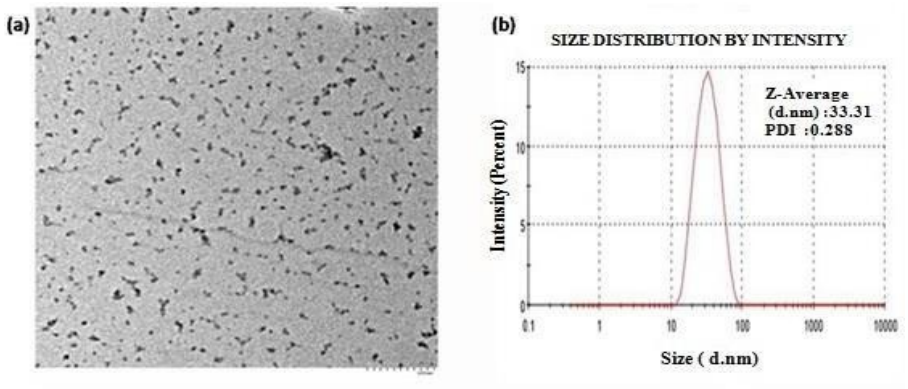

Figure 4.5 a.TEM image and b. Hydrodynamic (DLS) size of ZnSe/ZnS QDs.

4.2.2.3 ZETA POTENTIAL

The surface charge of ZnSe/ZnS QDs was measured by zeta potential and found to be -33.5 ± 5.91 (Figure 4.6).

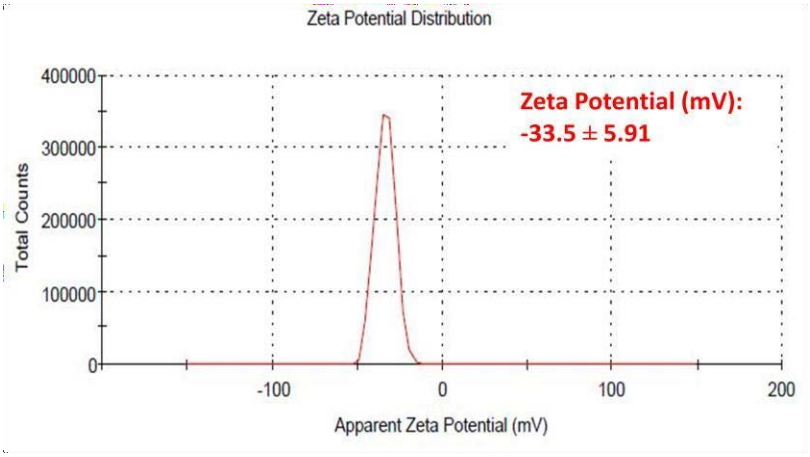

Figure 4.6. Zeta potential of ZnSe/ZnS QDs.

4.2.2.4 FOURIER TRANSFORM INFRARED SPECTROSCOPY (FTIR)

Chemical groups present on the surface of ZnSe/ZnS QDs was investigated by the FTIR spectroscopy (Figure 4.7). FTIR spectra of ZnSe shows characteristic bands at 3397 cm^{-1}, 2985 cm^{-1}, 1573 cm^{-1}, 1400 cm^{-1} corresponding to the stretching vibration of O-H, -CH_2-, C=O and C-O-C bonds respectively. GSH act as a stabilizing

agent in ZnSe core synthesis. Functional group present in GSH are $–NH_2$ (3124 cm^{-1}), -COOH (1713 cm^{-1}) and –SH (2523 cm^{-1}) and have strong propensity to coordinate with inorganic ions and metals. ZnSe/ZnS QDs shows spectra bands at 3395 cm^{-1}, 2985 cm^{-1}, 1573.66 cm^{-1}, 1400 cm^{-1}, 1390.68 cm^{-1} corresponding to the stretching vibration of O-H, $-CH_2-$, C=O, C-O-C bonds respectively. MPA is the stabilizing agent in the ZnSe/ZnS core- shell formation. It consists of C=O stretching of carboxylic group, -S-H- of thiol group and –C-H- stretching of methylene group at the band position of 1654 $cm^{-1,}$ 2580 cm^{-1}, 2938 cm^{-1} respectively.

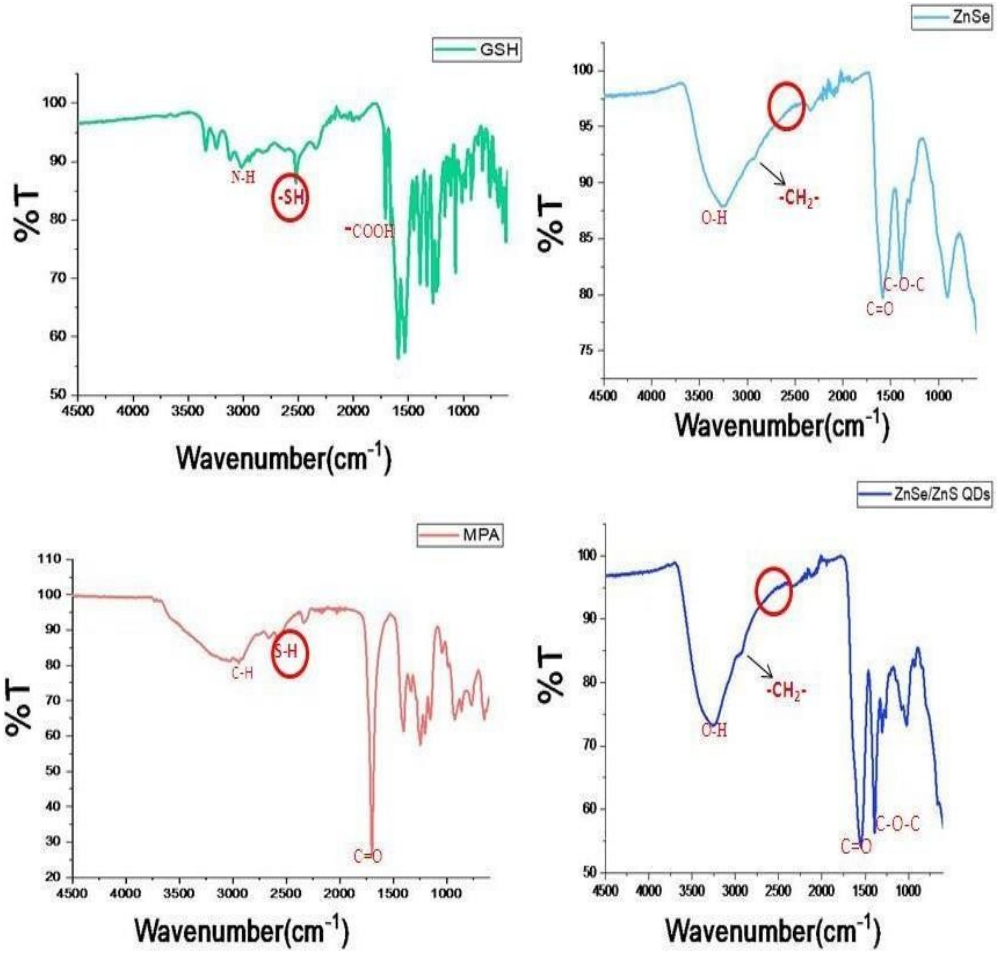

Figure 4.7. FTIR spectra of GSH, ZnSe core, MPA and ZnSe/ZnS QDs.

4.2.2.5 RAMAN SPECTRA

Raman spectra of ZnSe/ZnS QDs showed representative peaks at 240.74, 459.332, 494.5 corresponding to the LO and 2LO phonon modes of ZnSe. The peaks at 308.23 and 551.38 cm^{-1}which corresponds to the longitudinal optical (LO) and 2LO phonon modes of ZnS (Figure 4.8).

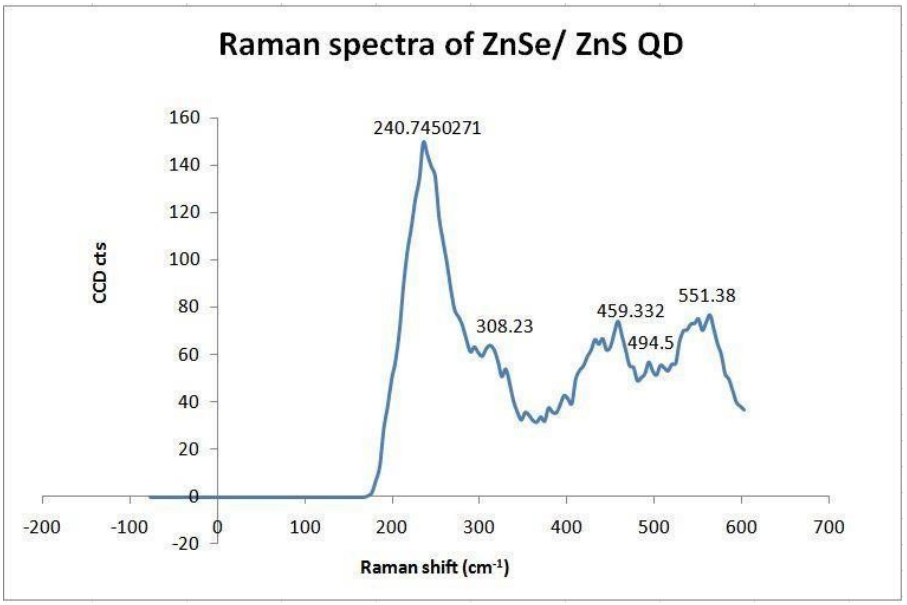

Fig 4.8: Raman spectra of ZnSe/ZnS QDs.

4.2.2.6 INDUCTIVELY COUPLED PLASMA OPTICAL EMISSION SPECTROMETRY (ICP-OES)

Quantitative elemental composition of ZnSe/ZnS QDs was determined by ICP-OES. It was estimated that one g of ZnSe/ZnS QDs contains Zinc (Zn) and Sulphur (S) by weight 379.58 and 378.53 mg respectively. Selenium (Se) was estimated to be very less (0.763 mg) when compared to Zn and S.

Sample	Sample weight(g)	Total amount in (mg/g)		
		S	Se	Zn
ZnSe/ZnS QDs	0.0844	378.53	0.763	379.85

Table 4.1: Elemental composition of ZnSe/ZnS QDs by ICP-OES.

4.2.2.7 X-RAY POWDER DIFFRACTION (XRD)

XRD spectrum (Figure 4.9) of ZnSe/ZnS QDs showed that sample maintained the general pattern of the cubic lattice (111), (220), (311) shown in table 4.2. Average length of (side) ZnSe/ZnS QDs crystal (a) is found to be 5. 701A0.The diffraction peaks are located between cubic ZnSe and ZnS phase (JCPDS NO: 80-0020) that are in good agreement with the characteristic cubic crystal structure of ZnSe/ZnS QDs.

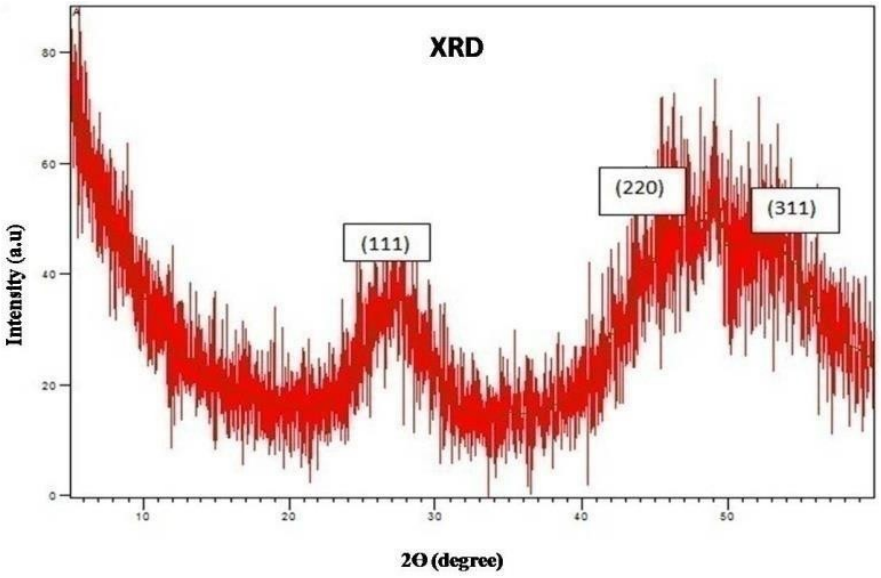

Figure 4.9: XRD pattern of ZnSe/ZnS QDs

Peak no.	2θ	$Sin^2θ$	$1×sin^2θ/sin^2θ$ min	$2×sin^2θ/sin^2θ_{min}$	$3×sin^2θ/sin^2θ_{min}$	$h^2+k^2+l^2$	hkl	a (A^0)
1	26.666	0.05316	1.00	2.00	3.00	3	111	5.785
2	45.399	0.1489	2.8	5.6	8.4	8	220	5.644
3	53.504	0.2024	3.8	7.8869	11.4	11	311	5.676

Table 4.2: Identification of planes of ZnSe/ZnS QDs by XRD.

$$\sin^2\theta = \frac{\lambda^2}{4a^2}\left(h^2 + k^2 + l^2\right)$$

(Whereh,k, l: miller indices, λ : wavelength, a:average length of side of crystal)

Average length (side) of ZnSe/ZnS QDs crystal (a) = 5.701

4.2.2.8 THERMAL ANALYSIS

4.2.2.8.1 THERMO GRAVIMETRIC ANALYSIS (TGA):

Thermal stability of ZnSe/ZnS QDs wasstudied by the thermo gravimetric analysis. Thermo grams of ZnSe/ZnS QDs (Figure 4.10) indicate weight loss as a function of temperature (heating rate as 10°C/min) under nitrogen atmosphere. The weight loss is found to be 12.92 % before reaching melting point: 300 ºC) and gradually increased.16.65% weight reduction was observed in ZnSe/ZnS QDs between 600°C and 700°C, mainly because of the surface adsorbed water molecules and atmospheric carbonates. A steady weight loss of 0.67 % occurs within the 700 -1000 ºC.

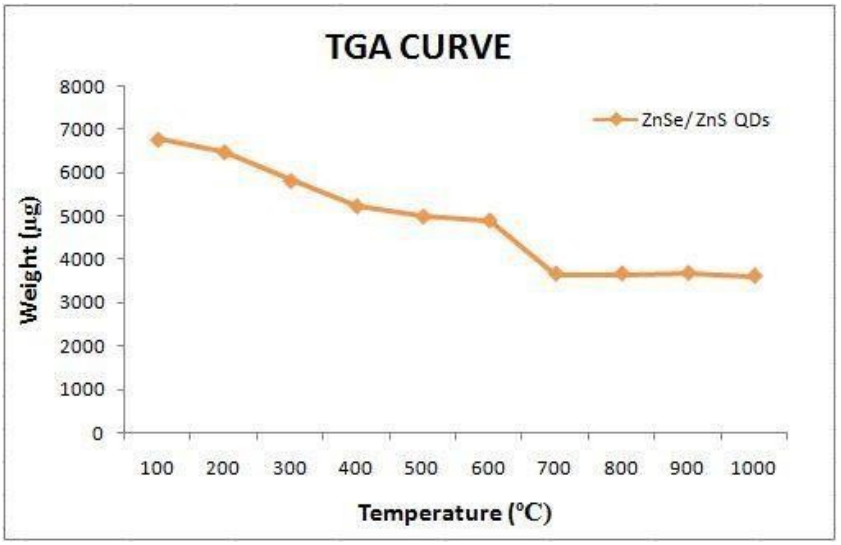

Figure 4.10: TGA curve of ZnSe/ZnS QDs.

4.2.2.8.2 DIFFERENTIAL THERMAL ANALYSIS (DTA):

DTA curve provide information about the transformation of ZnSe/ZnS QDs. Transformation is the process of releases/absorption of heat which is associated with chemical and physical changes in QDs as they are heated /cooled. 300º C is found to be the melting temperature of ZnSe/ZnS QDs (exothermic reaction). The endothermic reaction occurs from the 400-1000 ºC (Figure 4.11).

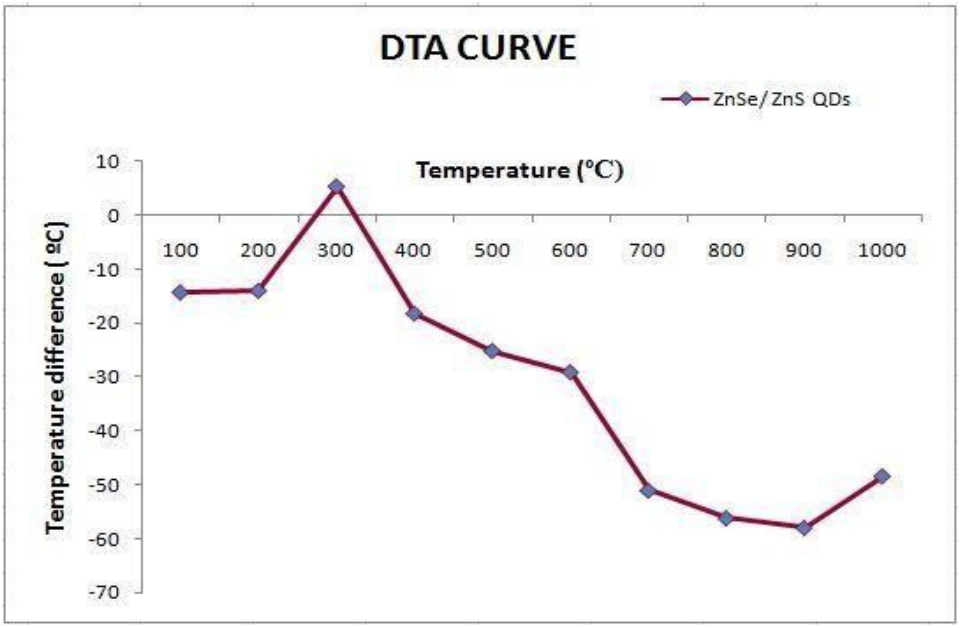

Figure 4.11. DTA curve of ZnSe/ZnS QDs.

4.2.2.8.3 DERIVATIVE THERMOGRAVIMETRY (DTG):

DTG curve is the first derivative of TG curve. From DTG curve, it wasfound that maximum decomposition of ZnSe/ZnS QDs occur at 300 ºC at the rate of 167.417 µg/ min (Figure 4.12).

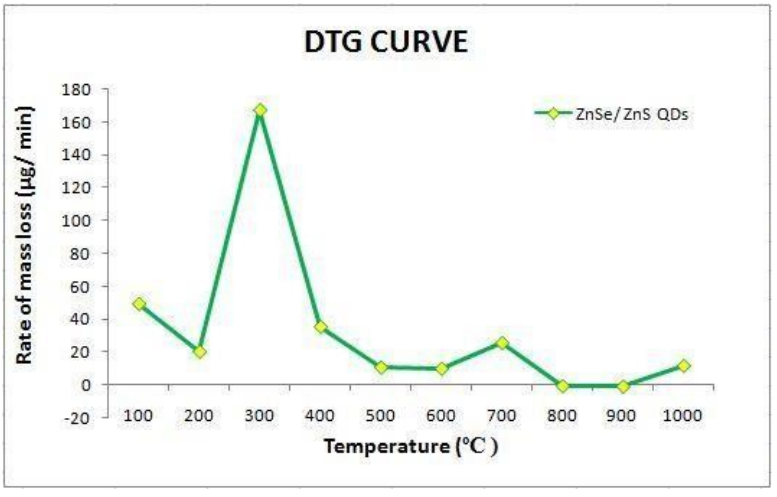

Figure 4.12: DTG curve of ZnSe/ZnS QDs.

OBJECTIVE 2

IN VITRO EVALUATION OF ZnSe/ZnS QDS WITH HEPG2 AND HEK CELL LINES.

4.5. *IN VITRO* TOXICITY STUDIES USING HEPG2 CELL LINE.

4.5.1 ASSESSMENT OF CELL VIABILITY BY MTT ASSAY

A dose dependent decrease in mitochondrial activity was observed in HepG2 cells incubated with ZnSe/ZnS QDs for 6 and 24 h. Decrease in mitochondrial activity was observed in 12.5µg/ml (97.29±0.08), 25µg/ml (92.16±0.15), 50 µg/ml (90.28±0.127) and 100µg/ml (83.82±0.062) when compared to control (6h). Similarly the activity was found to decrease in 12.5µg/ml (88.22±0.115), 25 µg/ml (86.62±0.192), 50 µg/ml (80.31±0.088) and 100µg/ml (65.55±0.062) when compared to control at 24h (Figure 4.13).

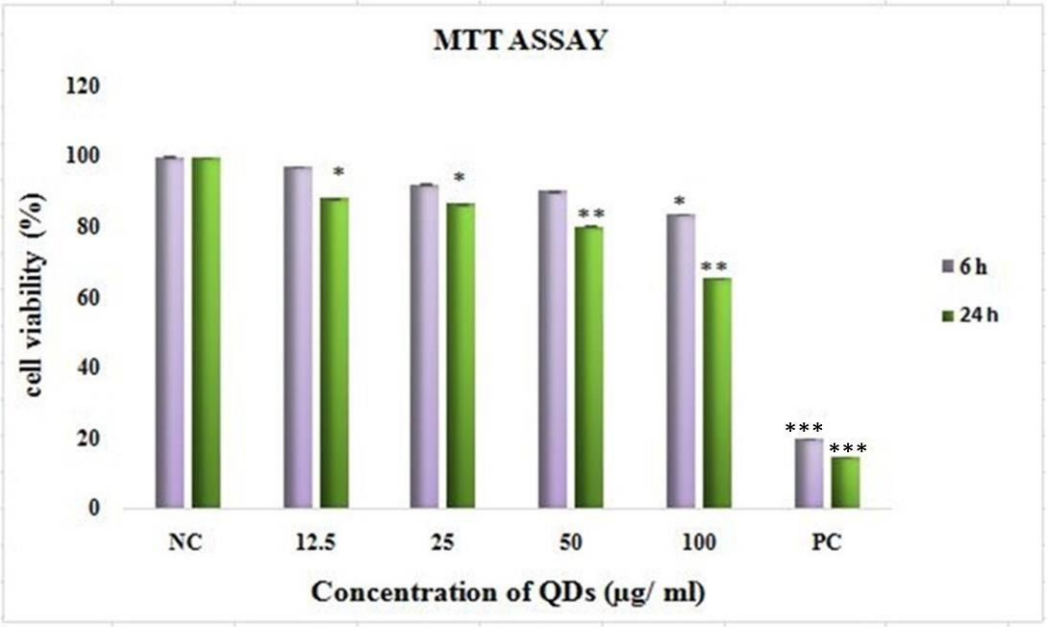

Figure 4.13. MTT assay on HepG2 cells exposed to ZnSe/ZnS QDs for 6 and 24h. The values are expressed in percentage with respect to control. Phenol treated cells were used as positive control. The data represent mean ± SD of three independent experiments. Asterisk above columns denotes statistically significant difference, when compared to the control (*p< 0.05, P< 0.01and **p<0.001).

4.5.2 INTERFERENCE OF PARTICLE WITH MTT

Different concentration of ZnSe/ZnS QDs does not interfere with MTTat an absorbance of 540nm. Figure 4.14 shows similar absorbance values in both control and ZnSe/ZnS QDs.

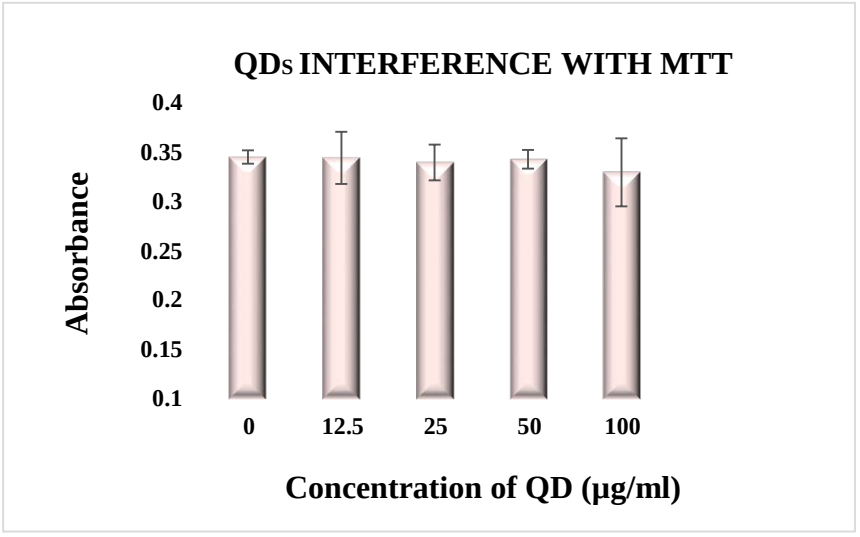

Figure 4.14. MTT assay on cell culture medium incubated with ZnSe/ZnS QDs for 4h. The data represent mean ± SD of three independent experiments.

4.5.3 CYTOTOXICITY ASSOCIATED WITH PARTICLE DISSOLUTION

Figure 4.15 suggested no change in mitochondrial activity when HepG2 cells were exposed to supernatant of ZnSe/ZnS QDs. On the other hand, a statistically significant decrease in mitochondrial activity was observed when ZnSe/ZnS QDsexposed directly to HepG2 cells. The percentage mitochondrial activity observed in supernatant of 100 µg/ml ZnSe/ZnS QDs was 93.09±1.28, whereas 55.55±0.062 percentage activity was observed in direct QDs exposure.

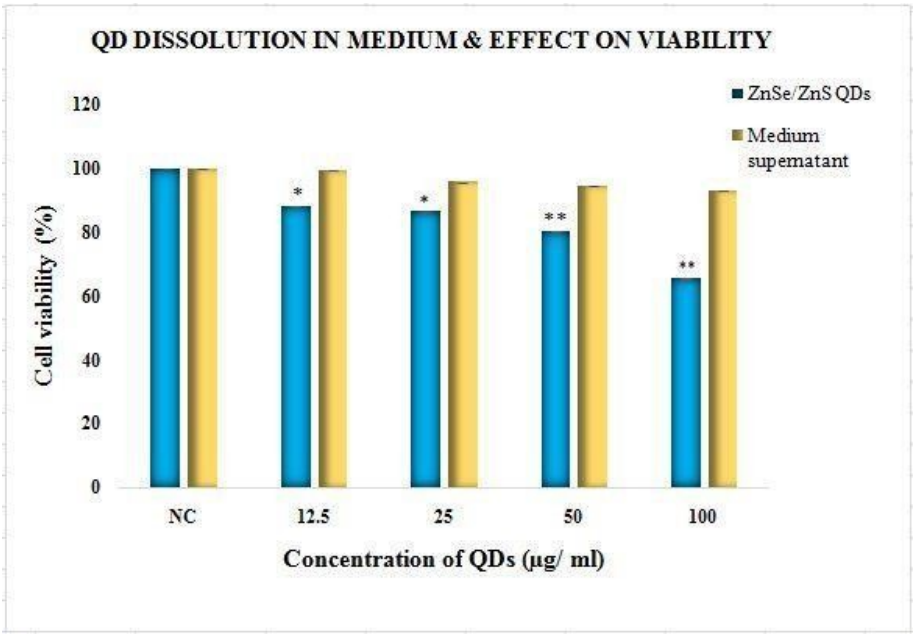

Figure 4.15. MTT assay on HepG2 cells exposed to both ZnSe/ZnS QDs and medium supernatant for 24h. The values are expressed in percentage with respect to control. The data represent mean ± SD of three independent experiments. Asterisk denotes statistically significant difference (*$p<0.05$, and**$p< 0.01$).

4.5.4 ASSESSMENT OF LYSOSOMAL ACTIVITY BY NEUTRAL RED UPTAKE (NRU) ASSAY

In this assay, cell viability was measured in terms of lysosomal activity. Figure 4.16 shows a gradual reduction in cell viability. A statistically significant reduction in the percentage of lysosomal activity was found to be 75.04 ±0.24 at 50µg/ml and 69.83 ±0.10 at100 µg/ml when ZnSe/ZnS QDs exposed (24 h) to HepG2 cells.Whereas no lysosomal activity was observed at 6 h when exposed up to 100µg/ml of ZnSe/ZnS QDs.

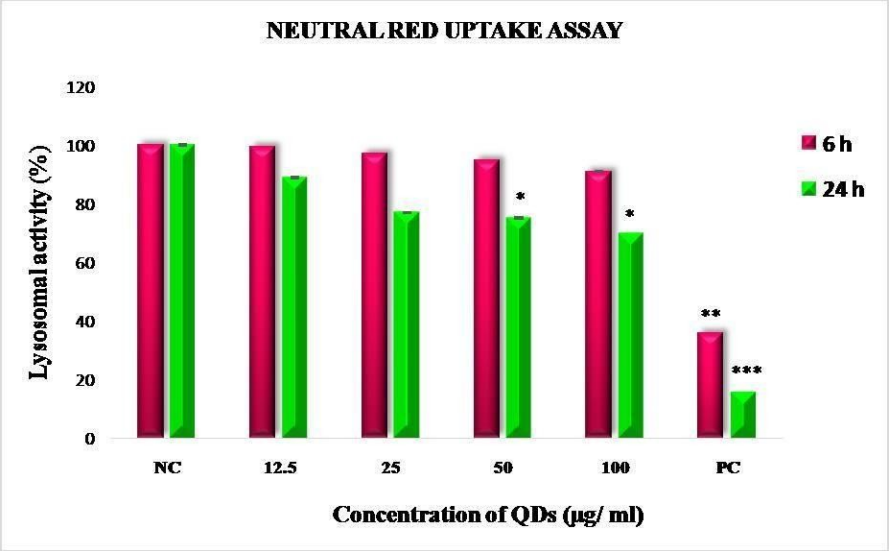

Figure 4.16. Neutral red uptake on HepG2 cells exposed to ZnSe/ZnS QDs at 6 and 24h. The values are expressed in percentage with respect to control. The data represent mean ± SD of three independent experiments. Asterisk denotes statistically significant difference (*p<0.05,**p< 0.01 and ***p<0.001).

4.5.5 PARTICLE UPTAKE BY CONFOCAL MICROSCOPY

Confocal microscopic imaging of HepG2 cells treated with ZnSe/ZnS QDs for 4h confirmed the presence of QDs uptake by the cells. Blue fluorescent spots depict QDs distributed inside the cell. Rhodamine phalloidine stained F-actin filaments (red) inside the cell and acridine orange stained nucleus (green) in fixed cell gave good contrast for the analysis of intracellular uptake of QDs (Figure 4.17).

4.5.6 PARTICLE UPTAKE IN PRESENCE OF INHIBITOR

Particle uptake was confirmed by blocking the uptake by an inhibitor cytochalasin B (Cyt.B). The ZnSe/ZnS QDs mediated toxicity was inhibited by Cyt.B. A statistically significant difference in viability was observed in 100 µg/ml ZnSe/ZnS QDs treated cells. The cell viability dropped significantly from 91.81±0.02 (with Cyt.B) to 69.83± 0.10 (without Cyt.B) at this concentration (Figure 4.18).

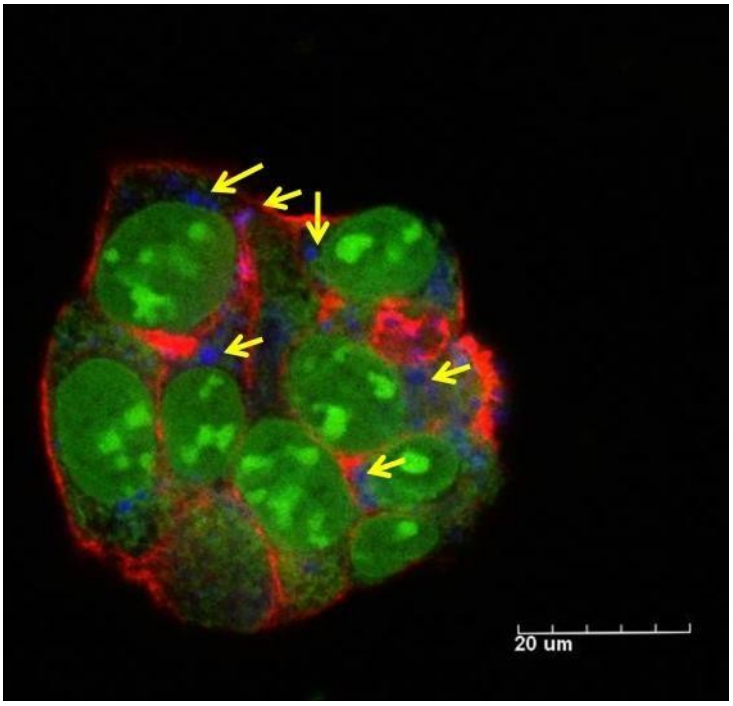

Figure 4.17. Confocal microscopic imaging of HepG2 cells. Cells stained with ZnSe/ZnS QDs, Rhodamine phalloidine and acridine orange. Green, red and blue indicate the fluorescence from the nucleus, F-actin and ZnSe/ZnS QDs respectively. Scale bar: 20µm.

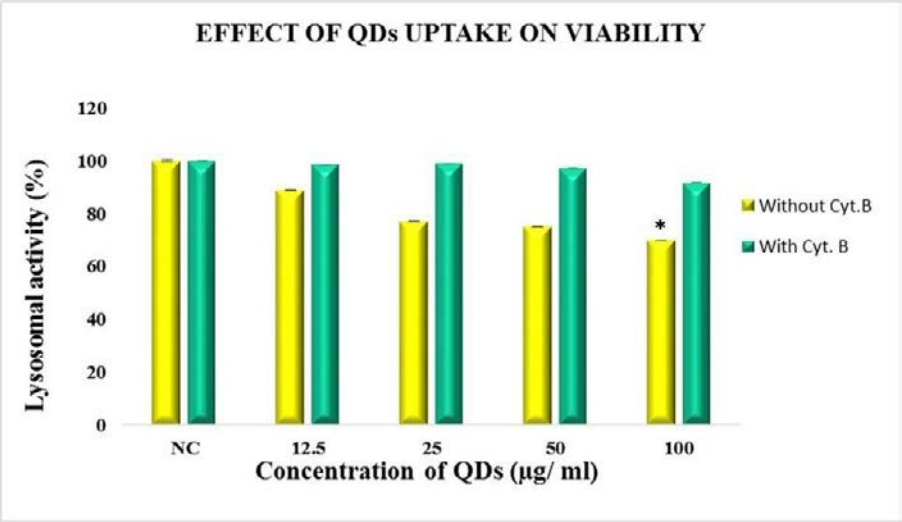

Figure 4.18. Particle uptake in presence and absence of cytochalasin B exposed (6 h) to ZnSe/ZnS QDs in HepG2 cells. The values are expressed in percentage with respect to control. The data represent mean ± SD of three independent experiments. Asterisk denotes statistically significant difference (*$p<0.05$).

4.5.7 CELL COUNT BY TRYPAN BLUE EXCLUSION ASSAY

Time and dose dependent changes in cell count were observed in trepan blue exclusion assay. Slight change in dead cell count was observed at 6 h of ZnSe/ZnS QDs exposure. While significant increase in number of dead cells was found at 12.5, 25, 50 and 100 µg/ml ZnSe/ZnS QDs exposed samples at 24 h. There was a dose dependent increase in dead cells up to 100 µg/ml.

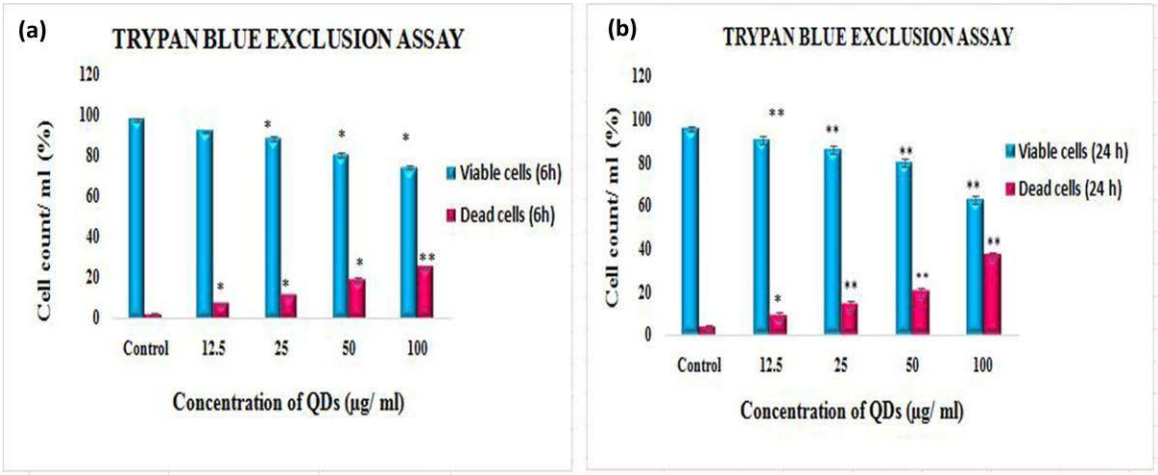

Figure 4.19. Trypan blue exclusion assay on HepG2 cells exposed to ZnSe/ZnS QDs for (a) 6h and (b) 24h. The data represent mean ± SD of three independent experiments. Asterisk denotes statistically significant difference in total cell count, compared to the control group (*$p<0.05$ and **$p<0.01$).

4.5.8 ASSESSMENT OF CYTOPLASMIC ENZYME RELEASE BY LDH ASSAY

This assay was carried out to detect the LDH release on exposure of ZnSe/ZnS QDs to HepG2 cells. It was found that a significant amount of LDH was released when the concentration of QDs increased. The result is portrayed in figure 4.20.

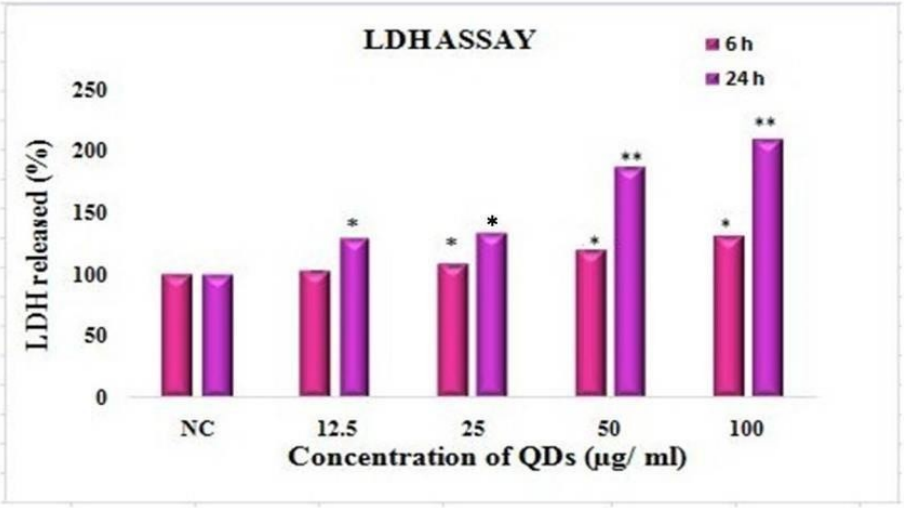

Figure 4.20. LDH release when exposed to ZnSe/ZnS QDs oh HepG2 cells. The data represent mean ± SD of three independent experiments. Asterisk denotes statistically significant difference in total cell count, compared to the control group (*$p<0.05$ and **$p<0.01$).

4.5.9 CELLULAR PHENOTYPE BY PHASE CONTRAST MICROSCOPY

The morphology of cells exposed to ZnSe/ZnS QDs was observed under phase contrast microscope. There were no evident morphological changes seen in the HepG2 cells, however the cell density decreased as concentration increased.

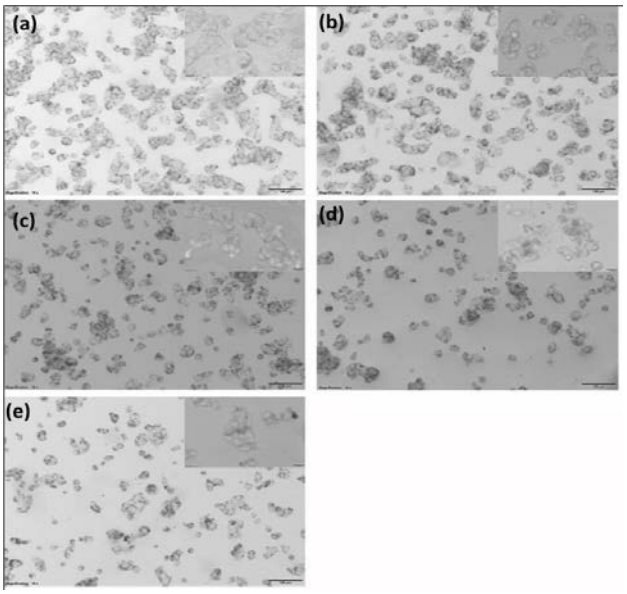

Figure 4.21. Cellular morphology by phase contrast microscopy: (a) HepG2 cells alone, (b) 12.5 µg/ ml, (c) 25 µg/ ml, (d) 50 µg/ ml, (e) 100 µg/ ml of ZnSe/ZnS QDs. Scale bar represents 100µm. Magnification: 10X.

4.5.10 MORPHOLOGY ANALYSIS BY GIEMSA STAINING

Morphological changes of ZnSe/ZnS QDs exposed HepG2 cells were revealed by Giemsa staining. Evident morphological changes were not found even at high concentrations. But cell density was markedly decreased at higher concentrations in 100 µg/ml.

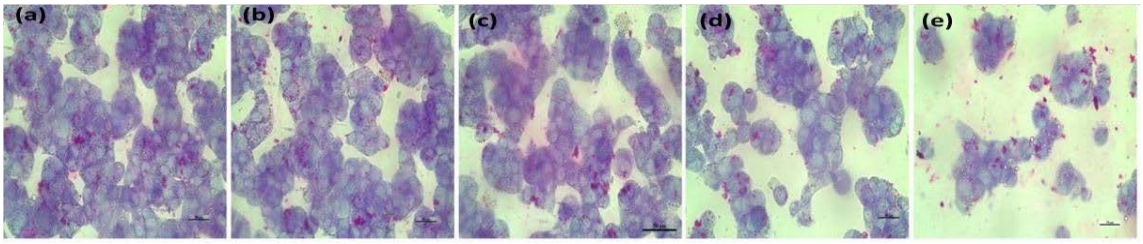

Figure 4.22. Cellular morphology of HepG2 cells exposed to ZnSe/ZnS QDs using Giemsa staining. Untreated cells are used as control. (a) HepG2 cells alone, (b) 12.5 µg/ ml, (c) 25 µg/ ml, (d) 50 µg/ ml, (e) 100 µg/ ml of ZnSe/ZnS QDs. The scale bar represents 50µm. magnification 40X.

4.5.11 ASSESSMENT OF CHANGES TO CYTOSKELETAL INTEGRITY AND NUCLEAR STRUCTURE

Structural changes in cytoskeleton were analysed using Rhodamine phalloidine and nuclear condensation by acridine orange. No cytoskeletal rearrangement was observed in cells treated up to 100 µg/ml at 6 h. cytoskeletal retraction, round morphology and nuclear condensation in HepG2 cells was observed when treated with 100 µg/ml of ZnSe/ZnS QDs (24 h) (Figure 4.23 a, b).

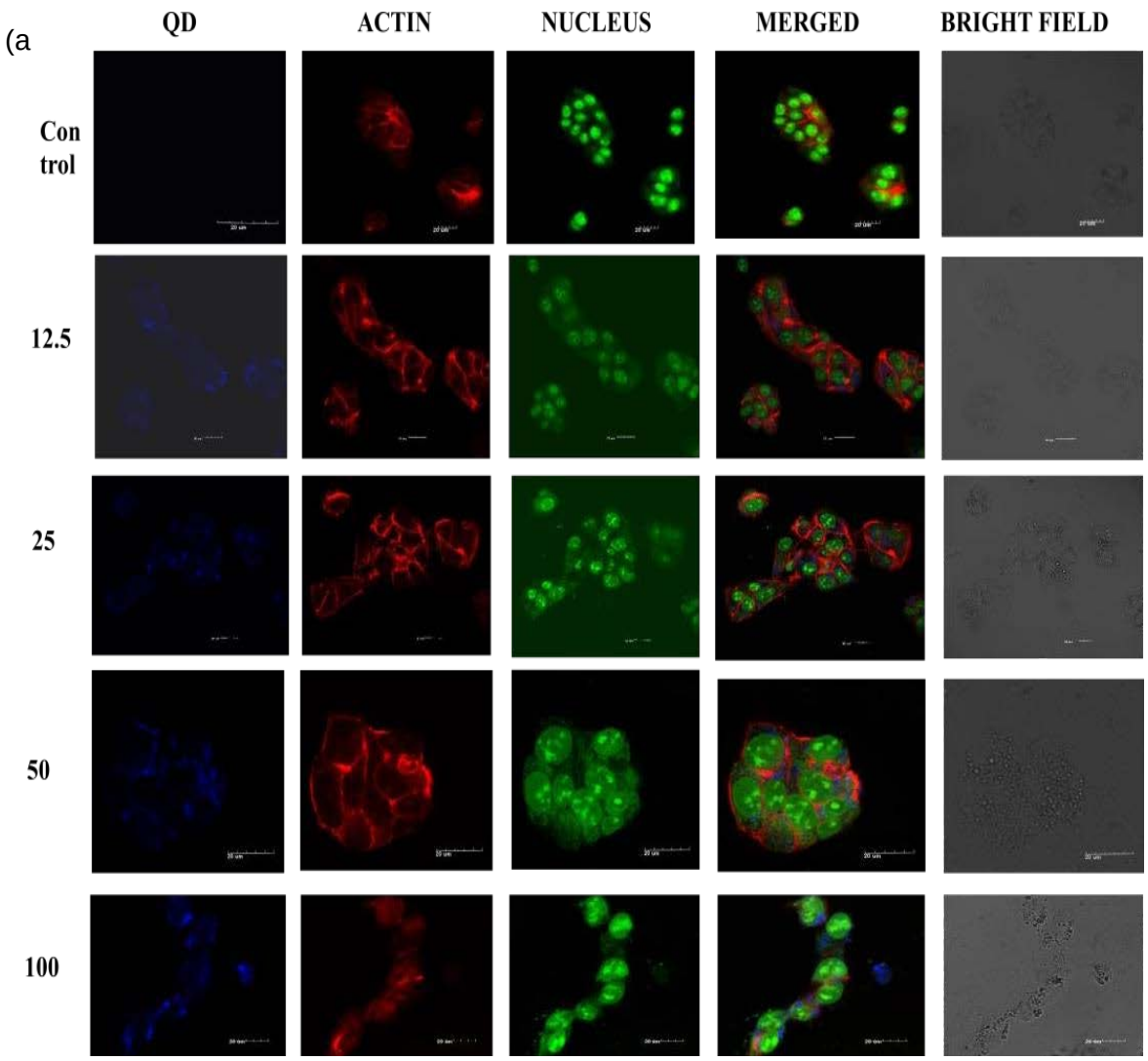

Figure 4.23a. Cytoskeletal arrangement of HepG2 cells exposed to ZnSe/ZnS QDs For 6h using Rhodamine phalloidin staining and nuclear condensation by acridine orange stain. Untreated cells are used as control. The scale bar represents 20µm. Magnification 40X.

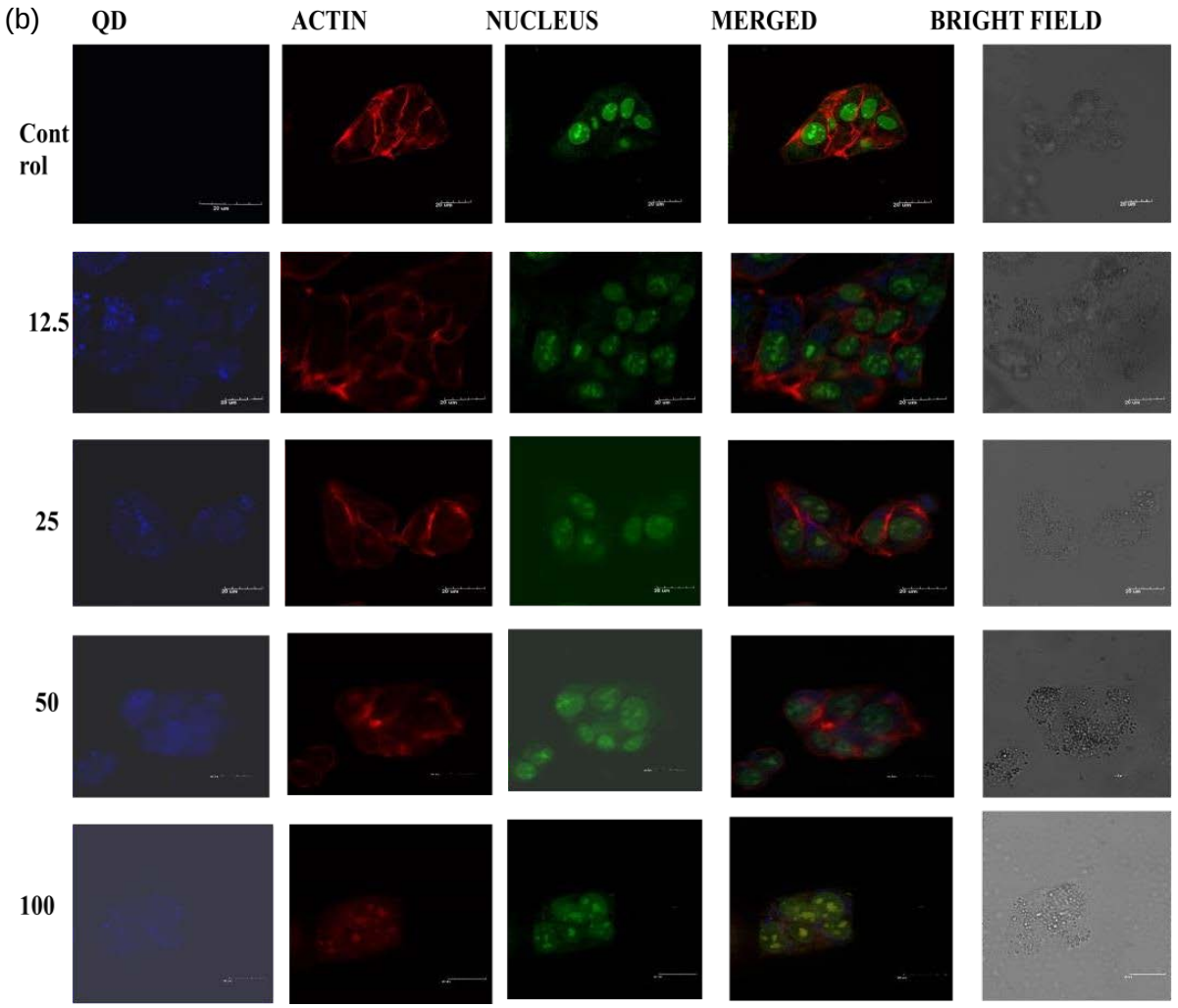

Figure 4.23b. Cytoskeletal arrangement of HepG2 cells exposed to ZnSe/ZnS QDs at 24h using Rhodamine phalloidin staining and nuclear condensation by acridine orange stain. Untreated cells are used as control. The scale bar represents 20µm. Magnification 40X.

4.5.12 MITOCHONDRIAL MEMBRANE POTENTIAL (MMP) BY JC1

JC-1 probe was used for MMP detection. Figure 4.24 showed loss of membrane potential in HepG2 cells exposed to different concentrations of ZnSe/ZnS QDs. The untreated control cells exhibited highest level of the red fluorescence, representative of healthy and active mitochondria. Cells treated with 12.5 µg/ml of ZnSe/ZnS QDs showed red fluorescence comparable to that of control. Green fluorescence was more predominant in cells treated with 50 and 100 µg/ml ZnSe/ZnS QDs signifying loss of MMP.

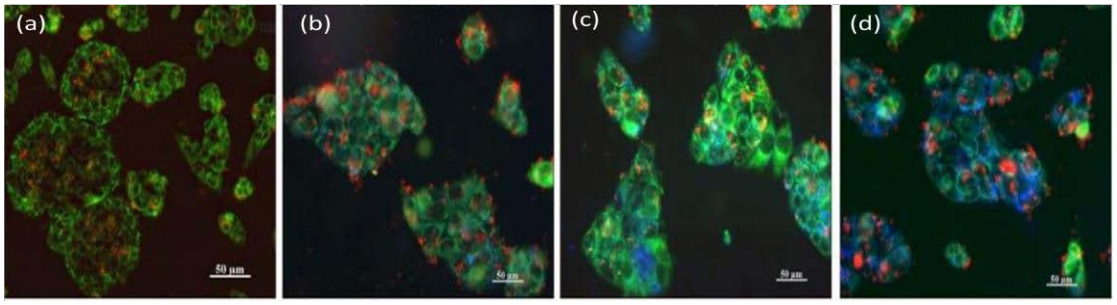

Figure 4.24. Mitochondrial membrane potential of HepG2 cells exposed to ZnSe/ZnS QDs at 24 h. (a) Control, (b) 12.5 µg/ml, (c) 25 µg/ml, (d) 100 µg/ml. Untreated cells are used as control. The red signal represents J aggregates in active mitochondria and green signal represents the diffused monomers in the cytoplasm. Scale bar represents 50 µm. Magnification 20X.

4.5.13 ASSESSMENT OF LYSOSOMAL INTEGRITY BY ACRIDINE ORANGE (AO) STAINING

QDs induced lysosomal membrane damage was monitored by AO staining. AO relocation was assessed by normalizing with untreated control cells. No significant changes in AO relocation was observed in ZnSe/ZnS QDs treated cells when compared to control cell (Figure 4.25). The results suggest that the ZnSe/ZnS QDs exposure induced lysosomal integrity at the highest concentration (100 µg/ml).

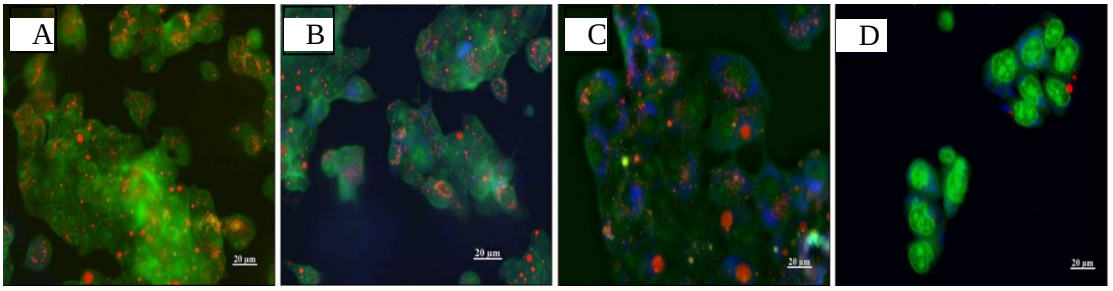

Figure 4.25. Fluorescence images of acid vesicle formation induced by ZnSe/ZnS QDs in HepG2 cells. (A) Acridine orange stained control cells after 24 h, (B) cells treated with ZnSe/ZnS QDs at a concentration of 12.5 µg/ml, (C) 50 µg/ml, (D) 100 µg/ml at 24 h. Scale bar represents 20µm.

4.5.14 FREE RADICAL FORMATION

4.5.14.1 ASSESSMENT OF REACTIVE OXYGEN SPECIES FORMATION BY DCFHDA

Intracellular ROS production is one of the initial responses of nanoparticle toxicity and was measured by DCFHDA. The results are expressed in relative fluorescence intensity (RFU) (Figure 4.26). None of the ZnSe/ZnS QDs treated group exhibited statistically significant increase in ROS formation (12.5 µg/ml: 102.15±28.01, 25 µg/ml: 102.54±16.7, 50 µg/ml: 105.44±23, 100 µg/ml: 106.81±30.2) at 6 h. The ROS formation after 24 h exposure was (12.5 µg/ml: 99.32±24.24, 25 µg/ml: 106.15±28.2, 50 µg/ml:118.23± 13.19, 100 µg/ml: 129.09 ±42.93).

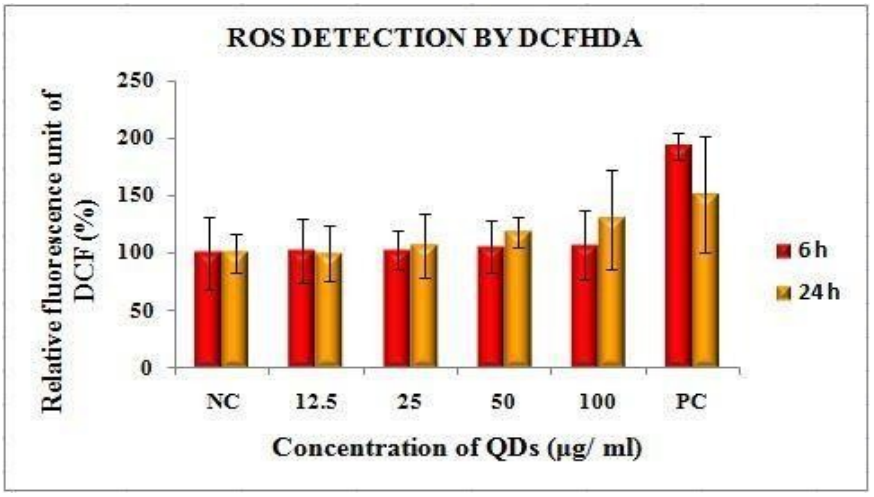

Figure 4.26. ROS production in HepG2 cells exposed to ZnSe/ZnS QDs at 6 and 24 h using DCFH-DA. H_2O_2 treated cells are used as positive control. The values are expressed in percentage fluorescence with respect to control. The data represent mean ± SD of three independent experiments.

4.5.14.2 INFLUENCE OF CATALASE ACTIVITY ON ROS PRODUCTION

Catalase is an enzyme present inside the cells which converts hydrogen peroxides into water and oxygen. The activity of catalase neutralise H_2O_2 generated in hepatocytes. Figure 4.26 a shows effect of catalase activity on ROS production in HepG2 cells exposed to ZnSe/ZnS QDs at 6h and figure 4.27b shows effect of 24h exposure. HepG2 cells exhibited high ROS production compared to control cells only at concentrations of 50 and 100 µg/ml (24 h) (Figure 4.27 b) when pre-treated with catalase inhibitor (NaN_3). In all other case, ROS production is almost same in both conditions (with and without NaN_3).

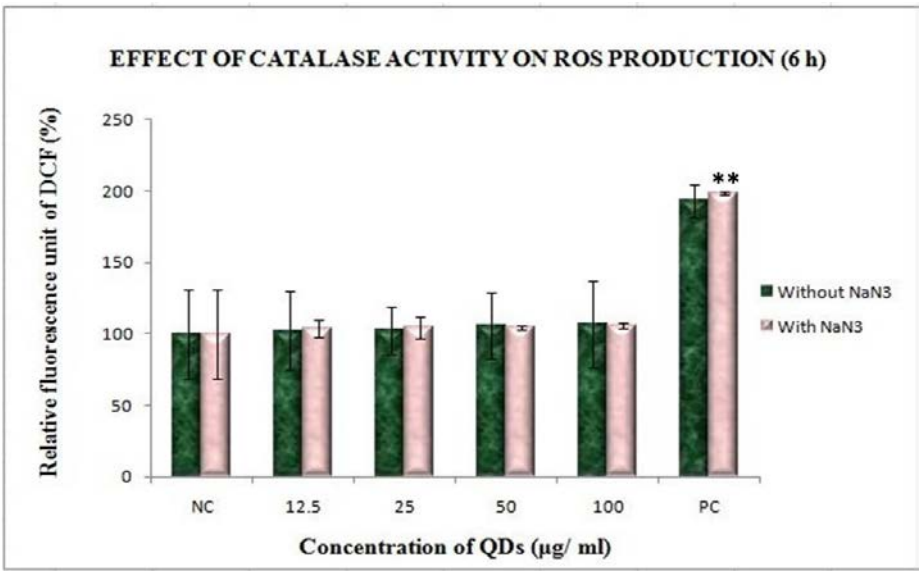

Figure 4.27a. Effect of catalase activity on ROS production in HepG2 cells exposed to ZnSe/ZnS QDs at 6h. The values are expressed in percentage fluorescence with respect to control. The data represent mean ± SD of three independent experiments (**p<0.01).

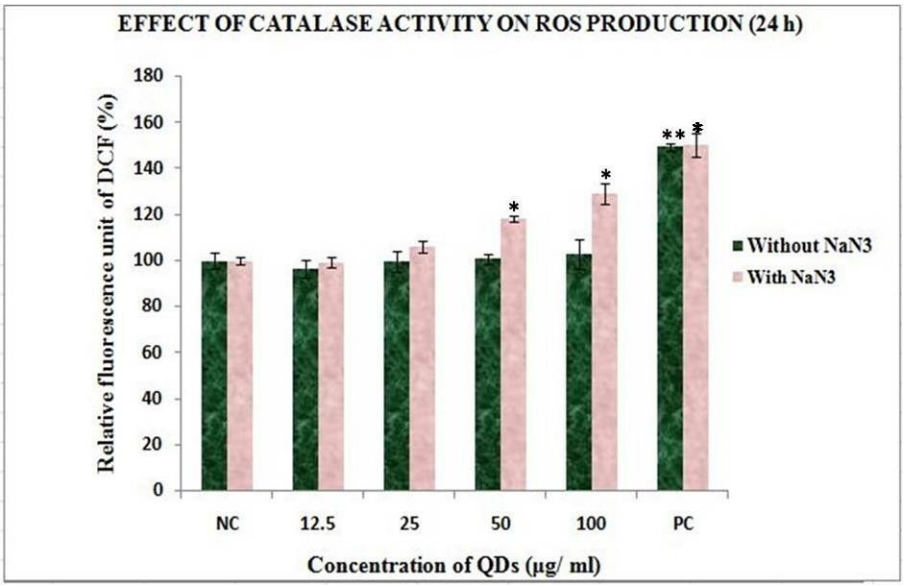

Figure 4.27b. Effect of catalase activity on ROS production in HepG2 cells exposed to ZnSe/ZnS QDs at 24 h. The values are expressed in percentage fluorescence with respect to control. The data represent mean ± SD of three independent experiments (*P<0.05, **p<0.01).

4.5.14.3 ASSESSMENT OF NITRILE RADICAL FORMATION BY GRIESS REAGENT

RNS production in HepG2 cells on exposure to ZnSe/ZnS QDs was analysed using Griess reagent assay. Only the LPS treated positive control cells exhibited a statistically significant increase in RNS production with respect to negative control (cells alone). However, ZnSe/ZnS QDs did not induce RNS production in HepG2 cells. The values were almost similar in both negative and treated groups (Figure 4.28 (a) and (b) represents nitrite production standard graph).

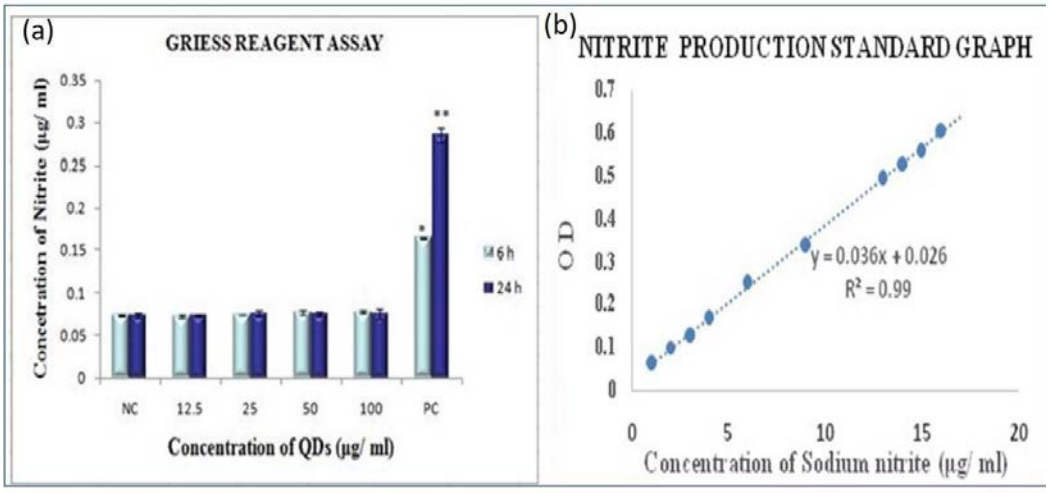

Figure 4.28 (a). RNS production by Griess reagent assay showing nitrite production in HepG2 cells exposed to ZnSe/ZnS QDs for 6 and 24 h. LPS treated samples were used as positive control. (b) Nitrite production standard graph. The data represent mean ± SD of three independent experiments. Asterisk denotes statistically significant difference (*p<0.05, **P<001).

4.5.15 ASSESSMENT OF OXIDATIVE STRESS INDUCED BY QDs

4.5.15.1 PROTEIN ESTIMATION

Protein in HepG2 cells estimated by Lowry's method. Control cells containing 0.951±.001 mg protein. Compared to control cells, ZnSe/ZnS QDs treated cells contains 0.896± 0.002 (12.5 µg/ml), 0.871±.01(25 µg/ml), 0.823±0.02 (50 µg/ml) and 0.710±0.001(100 µg/ml).

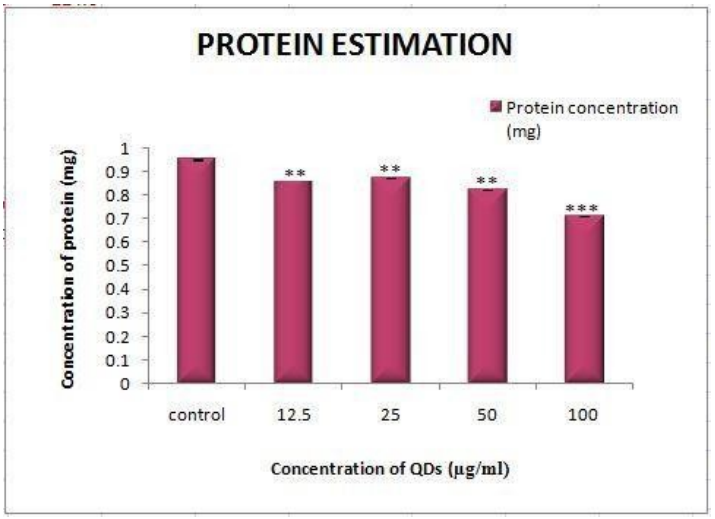

Figure 4.29: Protein level in HepG2 cells after ZnSe/ZnS QDs exposure at 24h.

4.5.15.2 GLUTATHIONE LEVELS

GSH level in HepG2 cells significantly increased with increased concentration of QDs when compared to control at 24 h. Figure 4.30 showed that GSH level in cells with QDs concentrations of 12.5, 25, 50 and 100 µg/ ml were 1.826±0.017, 1.722± 0.183, 1.844 ± 0.147, 1.403 ± 0.123 respectively.

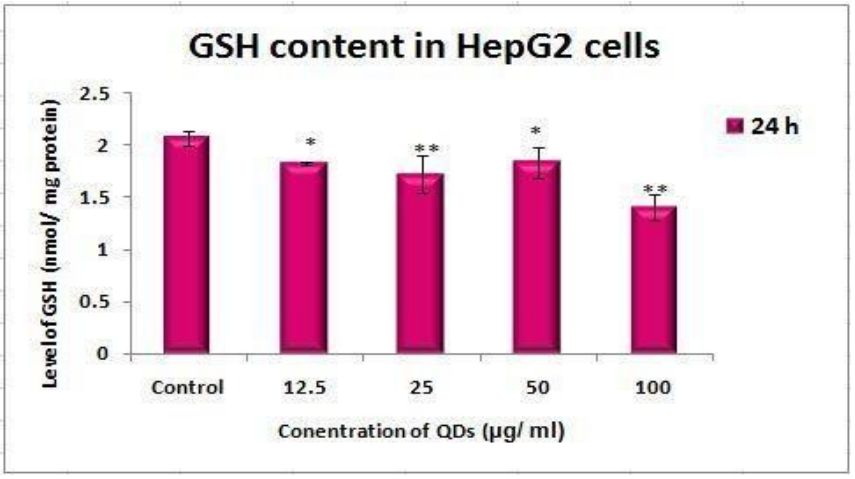

Figure 4.30. GSH level in HepG2 cells after ZnSe/ZnS QDs exposure at 24 h.

4.5.16 CELL CYCLE ANALYSIS BY FLOW CYTOMETRY

The ZnSe/ZnS QDs exposed HepG2 cells were stained with PI and was analysed by FACS. No sub G1 population was observed for the control group. There was no dose dependent increase in subG1 population in the treated group when compared to control. Other cell cycle phases like G0-G1, S and G2-M were comparable in both treatment and control groups. The cell cycle patterns are indicated in Figure 4.31.

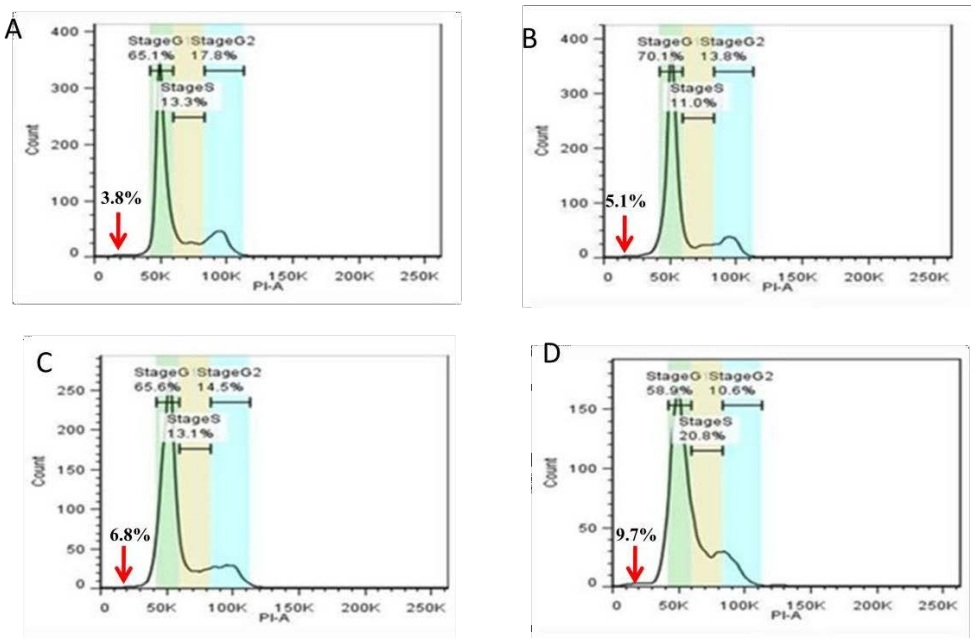

Figure 4.31. Cell cycle analysis of HepG2 cells exposed to ZnSe/ZnS QDs at 24 h. The data represented in PI fluorescence intensity. All the cellular debris has been gated out to represent the data. n=3.

4.5.17 DNA LADDER ASSAY

DNA ladder or smear patterns formation was not evident in any of the treated groups. Both control and treatment samples exhibited a thick band of unfragmented DNA of more than 10,000bp size with no laddering (Figure 4.32).

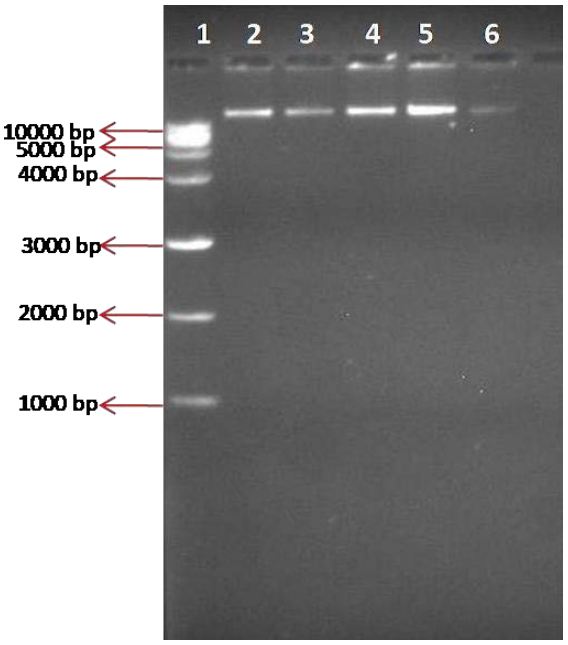

Figure 4.32. DNA ladder assay. Lane 1: Marker DNA, lane 2: Control, Lane 3: 12.5 µg/ml ZnSe/ZnS QDs, Lane 4: 25 µg/ml ZnSe/ZnS QDs, Lane 5: 50 µg/ml ZnSe/ZnS QDs, Lane 6: 100 µg/ml ZnSe/ZnS QDs. Base pairs (bp) of DNA markers are indicated on the left side of figure.

4.5.18 LIVE DEAD ASSAY BY CALCEIN AM-PI

Live dead assay of HepG2 cells upon QDs treatment was carried out by flow cytometry analysis using calcein AM-PI staining. However, the cells treated with 12.5, 25, 50 and 100 µg/ml of ZnSe/ZnS QDs at 24 h showed 91.21, 88.96, 84.30 and 50.80 % viable cells (Figure. 4.33: a-d). Figure 4.33 (e) shows graphical representation of flow cytometric analysis.

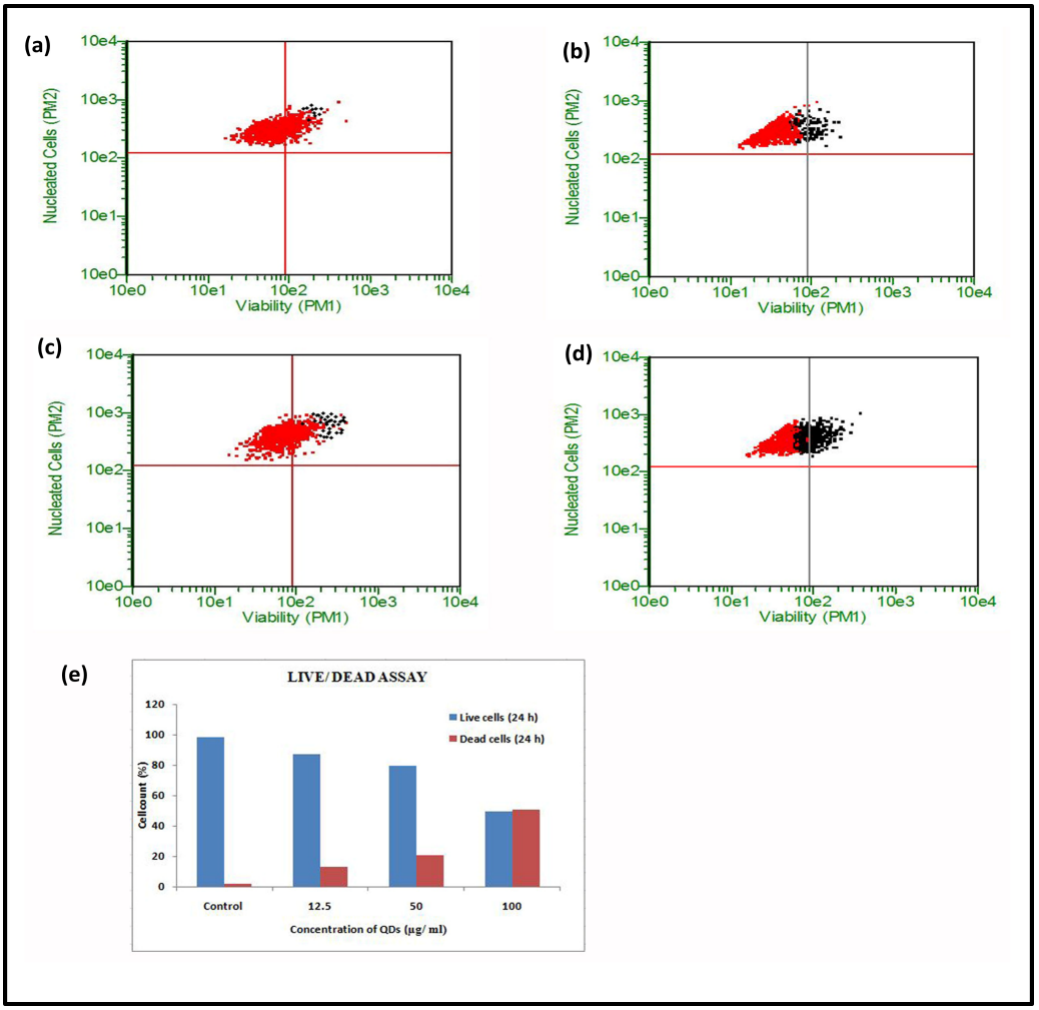

Figure 4.33 ZnSe/ZnS QDs induced death in HepG2 cells: a-c Flow cytometric analysis of Calcein AM stained cells. Black dots represent apoptotic cells and red dots represent viable cells. (a) untreated cells, (b) 12.5 µg/ml, (c) 50 µg/ml, (d) 100µg/ml ZnSe/ZnS QDs treated cells after 24h. (e) Graph representing percentage of viable and dead cells at different concentrations of ZnSe/ZnS QDs (12.5, 50 and 100µg/ml) after 24h.

4.5.19 CASPASE 3/7 ACTIVATION ASSAY

Caspase 3/7 activation assay was carried out to evaluate the apoptosis. Significant increase in caspase activity observed at 50 and 100 µg/ml concentration at 6 and 24h treatment when compared to the control (Figure 4.34).

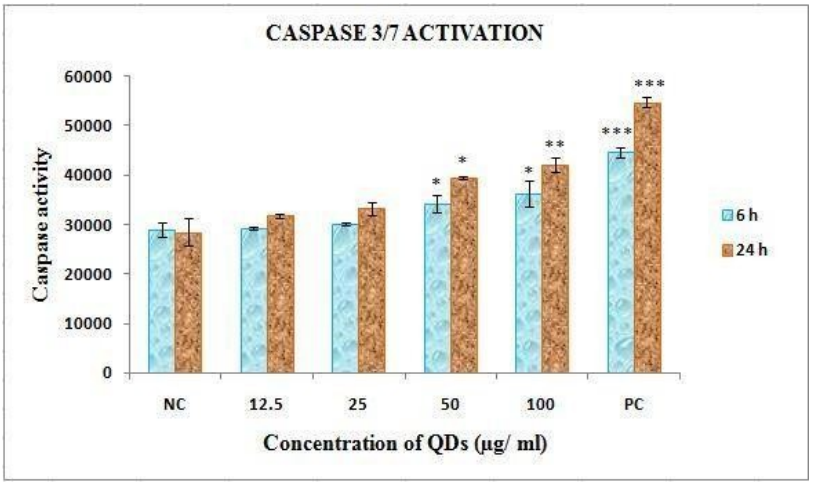

Figure 4.34. Comparison of caspase 3/7 activation in HepG2 cells exposed to ZnSe/ZnS QDs for 6 and 24 h. The data represent mean ± SD of three independent experiments. Asterisk denotes statistically significant difference (*p<0.05, **p< 0.01 and ***p<0.001).

4.6. IN VITRO TOXICITY STUDIES USING HEK293 CELL LINE

4.6.1 MTT ASSAY

The result of the study summarised in figure 4.35 and found that the mitochondrial activity decreases in dose dependent manner, both in 6 h exposure (12.5 µg/ml: 90.13 ±0.05, 25 µg/ml: 85.46 ± 0.10, 50 µg/ml: 81.63 ±0.07, and 100 µg/ml: 67.33±0.03) and 24 h exposure (12.5 µg/ml: 91.31 ±0.05, 25 µg/ml: 81.66 ± 0.02, 50 µg/ml: 80.86 ±0.02 and 100 µg/ml: 61.30±0.065).

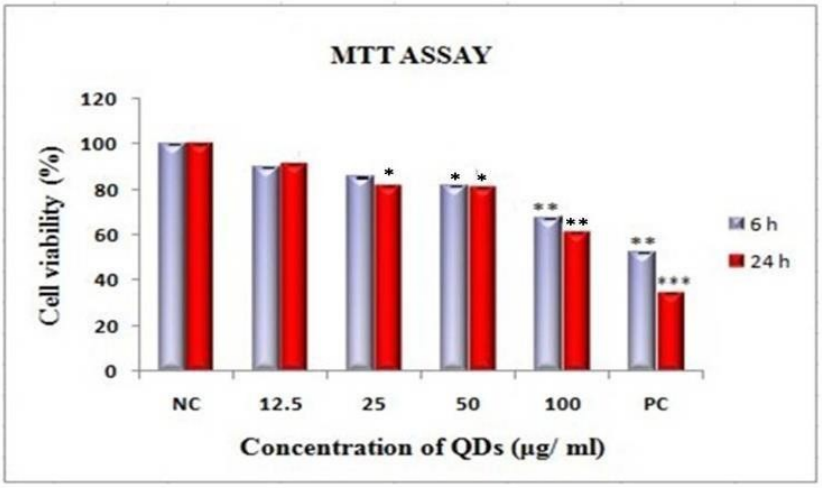

Figure 4.35. MTT assay on HEK cells exposed to ZnSe/ZnS QDs at 6 and 24h. The values are expressed in percentage with respect to control. Phenol is used as positive control. The data represent mean ± SD of three independent experiments. Asterisk denotes statistically significant difference (*p<0.05, **p< 0.01 and ***p<0.001).

4.6.2 PARTICLE DISSOLUTION AND RELATED TOXICITY

No change in mitochondrial activity observed in HEK cells exposed to the extract of ZnSe/ZnS QDs (figure 4.36). When compared with the control, a statistically significant decrease in mitochondrial activity was observed in HEK cells, directly exposed to ZnSe/ZnS QDs. The percentage mitochondrial activity observed in the extract of 100 µg/ml ZnSe/ZnS QDs is 80±0.003 whereas direct exposure of QDs is 61.30±0.065.

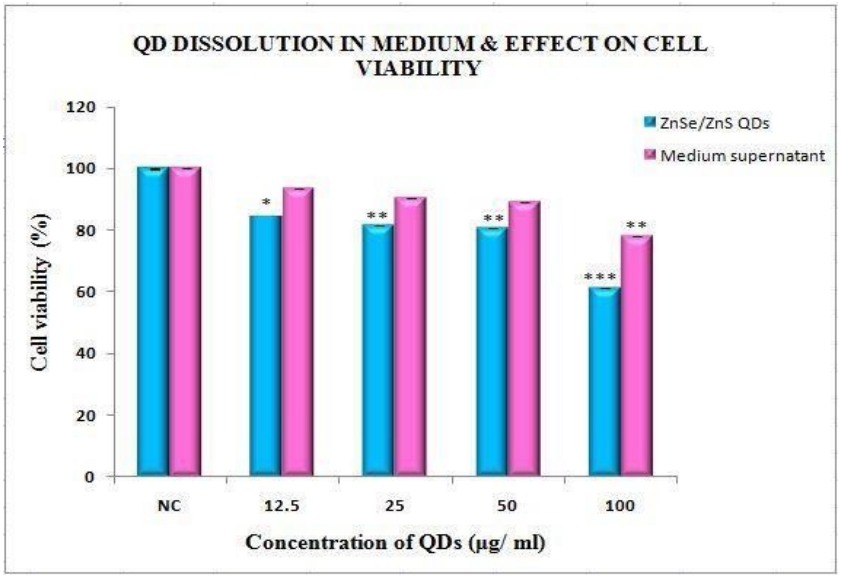

Figure 4.36 Percentage mitochondrial activity of ZnSe/ZnS QDs and its extract. The data represent mean ± SD of three independent experiments. Asterisk denotes statistically significant difference (*p<0.05, **p < 0.01, ***p<0.001).

4.6.3 NEUTRAL RED UPTAKE (NRU) ASSAY

Statically significant reduction in lysosomal activity was found at 25 µg/ml (86.13±0.02), 50 µg/ml (85.92 ±0.144) and 100 µg/ml (78.08 ±0.01) concentration of

QDs at 24 h, when compared to the control. At 6 h, there is a gradual decrease in lysosomal activity with increased concentration of ZnSe/ZnS QDs.

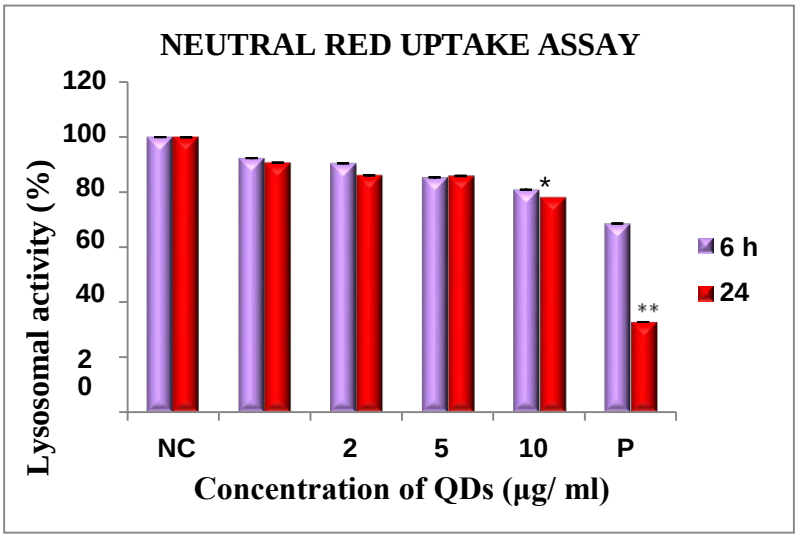

Figure 4.37. Neutral red uptake on HEK cells exposed to ZnSe/ZnS QDs at 6 and 24 h. The values were expressed in percentage with respect to control. The data represent mean ± SD of three independent experiments. Asterisk denotes statistically significant difference (*p<0.05 and **p< 0.01).

4.6.4 TRYPAN BLUE EXCLUSION ASSAY

Cytotoxicity of ZnSe/ZnS QDs with HEK is confirmed by trypan blue exclusion assay. 6h exposure of QDs of concentrations of 12.5,25, 50 and 100 µg/ml resulted in 99.1, 97.69, 92.46, 89.34, 80.98 % live cells and 0.9, 2.31, 7.54, 10.66, and 19.02 % dead cells. Upon 24 h exposure of 12.5,25,50 and 100 µg/ml QDs induced 2.28, 13.27, 14.9 and 33.66 % of cell death.

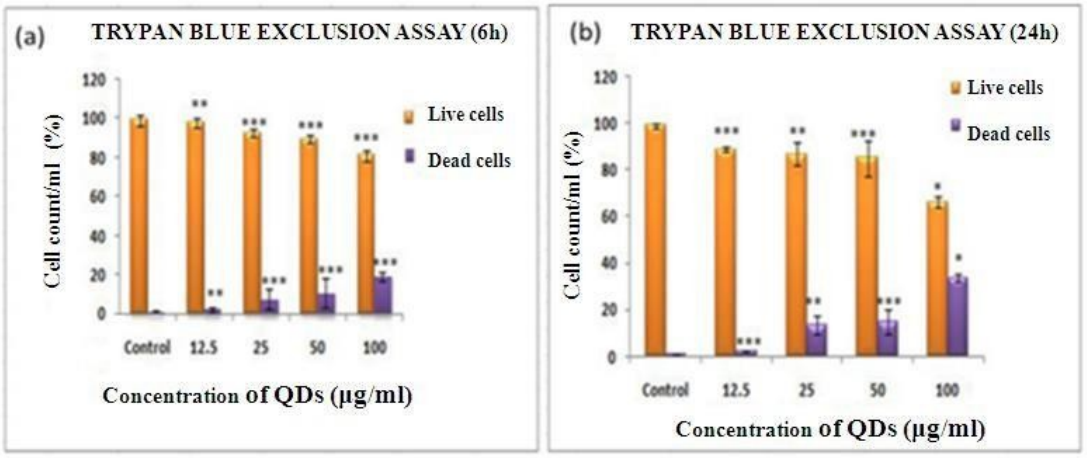

Figure 4.38a, b: Trypan blue exclusion assay on HEK cells exposed to ZnSe/ZnS QDs for 6 and 24 h. The data represent mean ± SD of three independent experiments. Asterisk denotes statistically significant when compared to the control group (*p<0.05, **p<0.01 and ***p<0.001).

4.6.5 PARTICLE UPTAKE BY CONFOCAL MICROSCOPY

Confocal microscopic image of HEK cells treated with ZnSe/ZnS QDs showed the presence of QDs the inside the cells (4 h). Blue fluorescent particles represent the QDs and are distributed inside the cells. Rhodamine-phalloidine stained F-actin filaments (red) inside the cell and nucleus stained by acridine orange (green) in fixed cells. This gave good contrast for the intracellular uptake of QDs (Figure 4.39).

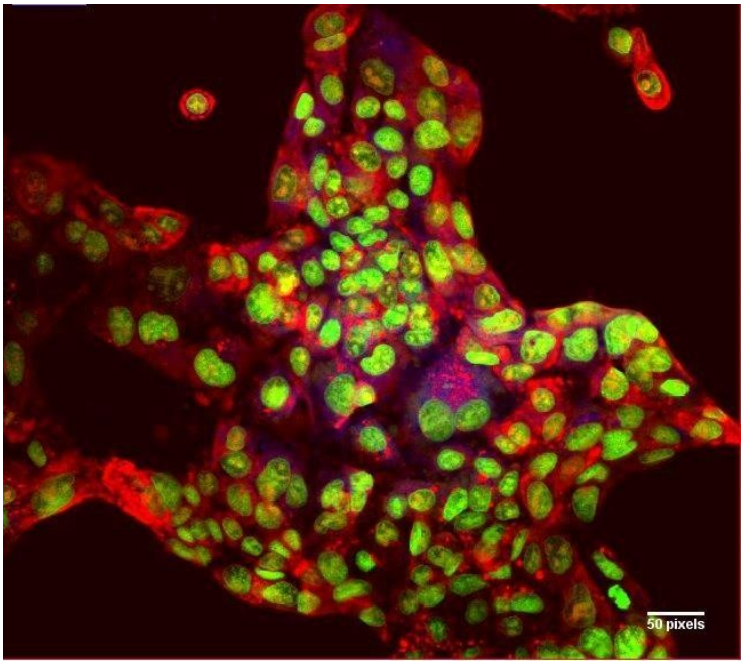

Figure 4.39. Confocal microscopic image of HEK cells. Cells stained with ZnSe/ZnS QDs, Rhodamine phalloidine and acridine orange. Green, red and blue indicates fluorescence from the nucleus, F-actin, and ZnSe/ZnS QDs respectively. Scale bar represents 50 pixels.

4.6.6 PARTICLE UPTAKE (ZnSe/ZnS QDs) IN HEK CELLS BY FLOW CYTOMETRY

Flow cytometry analysis was carried out to assess the QDs uptake (ZnSe/ZnS) in HEK cell. Figure 4.40, suggested a concentration dependent increase in SSC parameters. On the other hand, there was no corresponding change in FSC parameters (Figure 4.40).

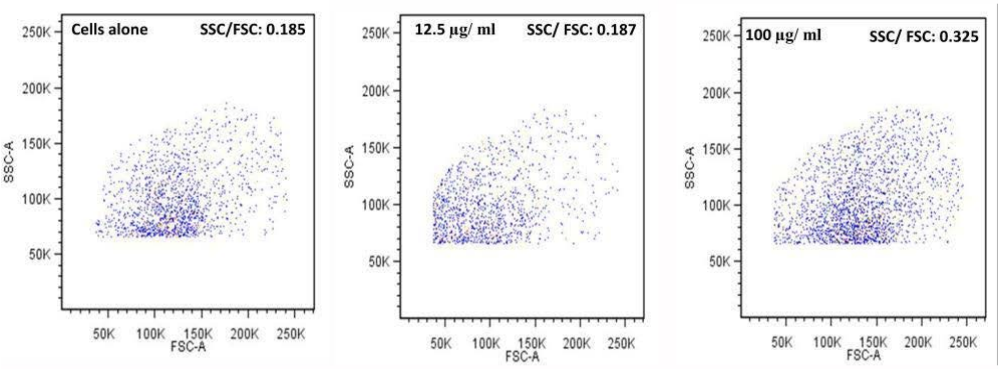

Figure 4.40: Determination of cellular uptake by flow cytometry analysis. The SSC changes indicated particle uptake by the cells. SSC: side scatter, FSC: forward scatter.

4.6.7 UPTAKE INHIBITION BY CYTOCHALASIN B

It was observed that there was no change in lysosomal activity of Cyt. B pre-treated cells (12.5 µg/ ml: 96.87± 0.06, 25 µg/ml: 94.67± 0.01, 50 µg/ ml: 93.39±0.01, 100 µg/ ml: 91.83 ±0.03) when compared to the control. While significant decrease in lysosomal activity (86.13 ± 0.06, 85.92 ± 0.14, 78.08 ±0.01, when exposed 25, 50, 100 µg/ml QDs respectively) was found when QDs directly exposed to HEK cells, without Cyt.B pre-treatment (Figure 4.41).

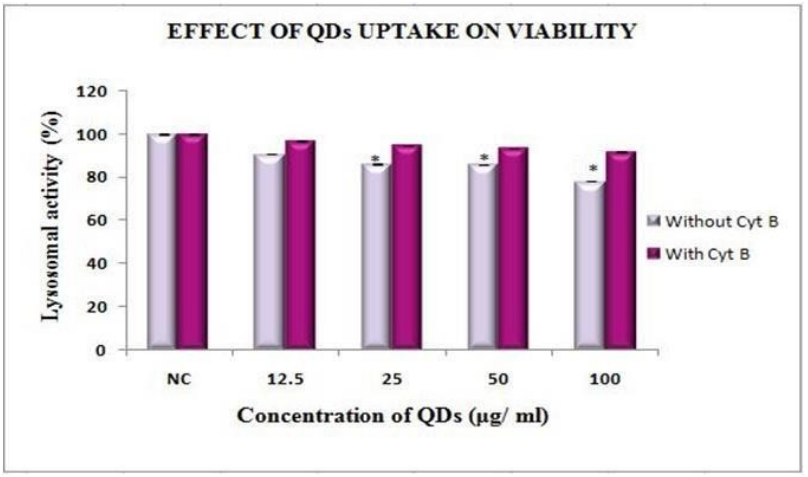

Figure 4.41. Particle uptake in presence of inhibitor cytochalasin B. The values are expressed in percentage with respect to control. The data represent mean ± SD of three independent experiments. Asterisk denotes statistically significant difference (*p<0.05)

4.6.8 LDH ASSAY

Figure 4.41 indicated that 100 µg/ml of ZnSe/ZnS QDs induced significant amount of LDH in HEK cells (143.2 ±0.04) at 6 h. Similarly, the amount of LDH release (140.64± 0.03 at 50 µg/ml and 169.08 ±0.05 at 100 µg/ ml) was significantly increased at 24 h (Figure 4.42).

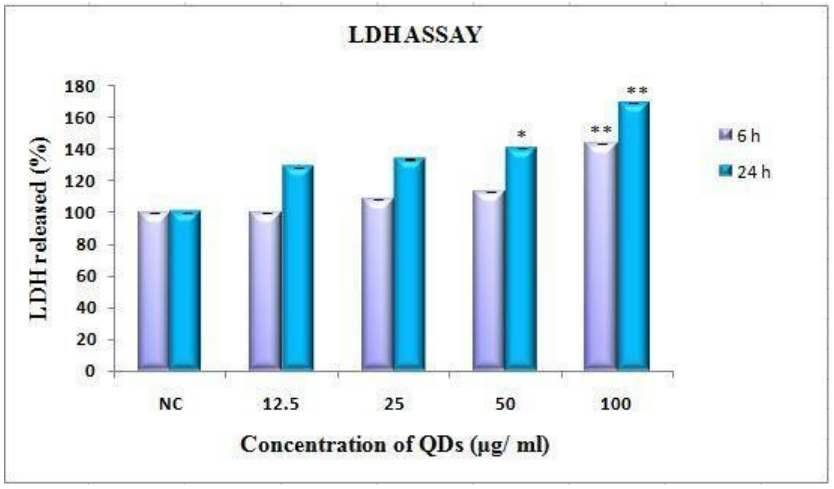

Figure 4.42: LDH release on HEK cells exposed to ZnSe/ZnS QDs at 6 and 24 h. The values are expressed in percentage with respect to control. The data represent mean ± SD of three independent experiments. Asterisk denotes statistically significant difference (*p<0.05, **p< 0.01 and ***p<0.001).

4.6.9 PHENOTYPIC OBSERVATION BY PHASE CONTRAST MICROSCOPY

Morphological change in HEK cells were observed upon treatment with ZnSe/ZnS QDs by direct imaging using phase contrast microscope. Figure 4.43 showed visible morphological changes. Cells become round shape in 100 µg/ml QDs treated cells. It was also found that the cell density was severely affected in 50 and 100 µg/ml QDs treated cells at 24 h.

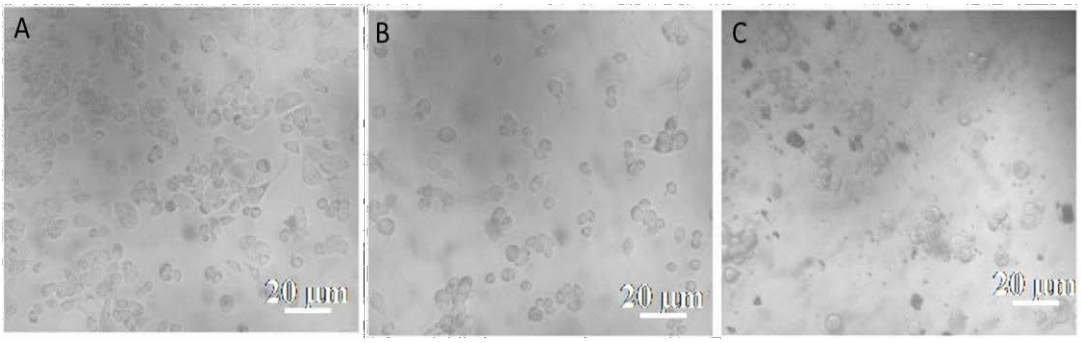

Figure 4.43. Morphology of HEK cells treated with ZnSe/ZnS QDs. A. control, B. 12.5 µg/ml, C. 100µg/ml. n=3. Magnification 20X. Scale bar represents 20 µm.

4.6.10 COOMASSIE BRILLIANT BLUE STAINING FOR MORPHOLOGY ANALYSIS

Morphological changes to the HEK cells upon treatment with ZnSe/ZnS QDs at different concentrations (Figure 4.44) were analysed by Coomassie brilliant blue staining. Evident morphological changes were observed only at 100 µg/ml concentration when compared to control, where cells become round in shape.

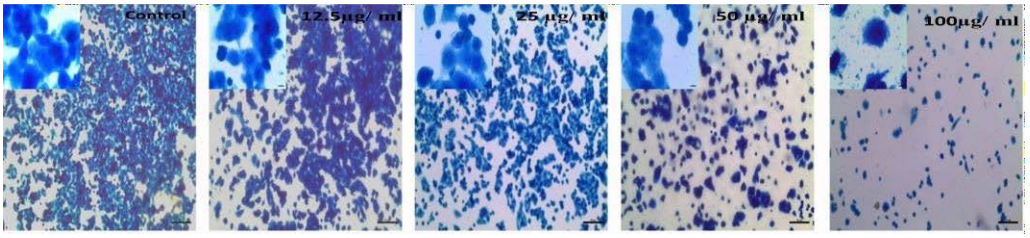

Figure 4.44. Morphology of HEK cells treated with ZnSe/ZnS QDs using Coomassie brilliant blue staining. n=3. Magnifications 10X. Scale bar represents 50 µm.

4.6.11 MMP BY JC-1

MMP was assessed by JC-1 probe. The control cells exhibited highest level of red fluorescence which indicates healthy and active mitochondria. As concentration of QDs increases, the red fluorescence decreases which indicate loss of MMP (Figure 4.45).

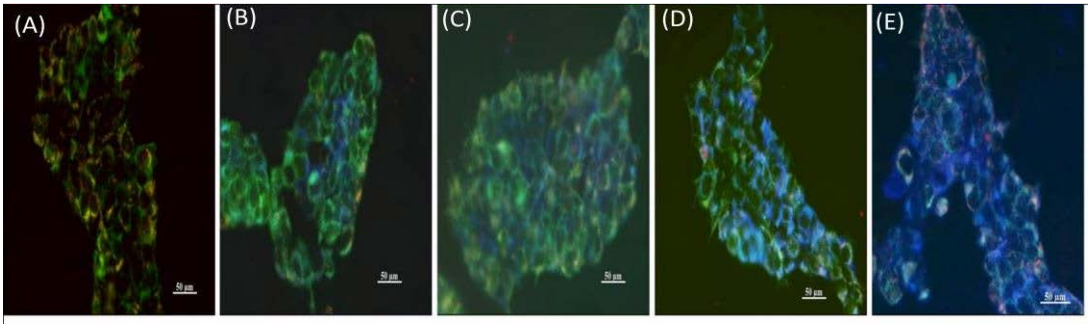

Figure 4.45. Mitochondrial membrane potential of HEK cells exposed to ZnSe/ZnS QDs for 24 h (A. control, B. 12.5 µg/ml, C. 25 µg/ ml, D. 50 µg/ ml, E. 100 µg/ ml). Untreated cells are used as control. The red signal represents JC-1 aggregates in active mitochondria and green signal represents the diffused monomers in the cytoplasm. Scale bar represents 50µm. Magnification 20X.

4.6.12 LYSOSOMAL INTEGRITY BY AO STAINING

The results (Figure 4.46) indicated that the lysosomal integrity was affected only at 100 µg/ml ZnSe/ZnS QDs exposure. There was no change in lysosomal integrity in all other treated groups and is comparable with control cells. µg/ml at 24 h. Scale bar: 20 µm, Magnification 20X.

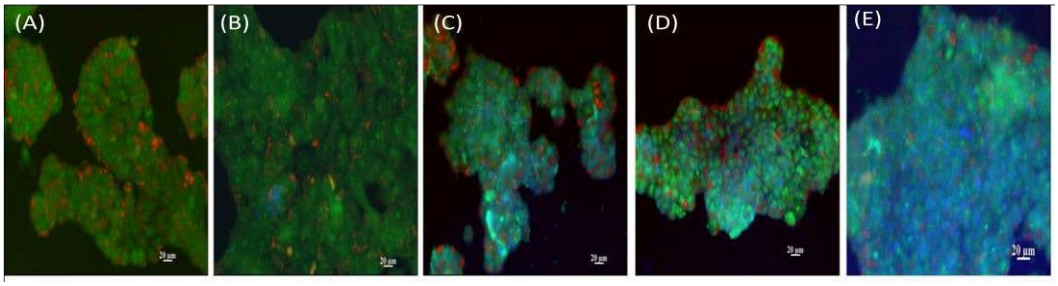

Figure 4.46 Fluorescence images of acid vesicle formation induced by ZnSe/ZnS QDs in HEK cells. (A). Acridine orange stained control cells after 24 h, (B) cells treated with ZnSe/ZnS QDs at a concentration of 12.5 µg/ml, (C) 25 µg/ml, (D) 50 µg/ml, (E) 100

4.6.13 FREE RADICAL FORMATION

4.6.13.1 DETECTION OF ROS PRODUCTION

ROS produced as a result of QDs exposure in HEK cells was detected by DCFHDA. HEK cells exhibited significant increase (25%) in DCF fluorescence only at 100 µg/ml concentration at 6 h. ROS production was comparable with the control cells in all other groups (Figure 4.47).

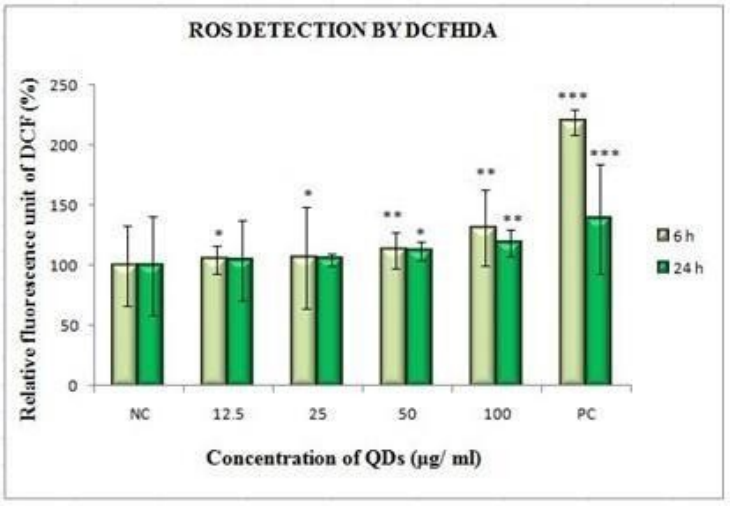

Figure 4.47. ROS production in HEK cells exposed to ZnSe/ZnS QDs at 6 and 24 h using DCFH-DA. H_2O_2 treated cells are used as positive control. The values are expressed in percentage fluorescence with respect to control. The data represent mean ± SD of three independent experiments. Asterisk denotes statistically significant difference (*p<0.05, **p< 0.01 and ***p<0.001).

4.6.13.2 INFLUENCE OF CATALASE ON ROS PRODUCTION

Catalase enzyme is an important enzyme in protecting the cells from oxidative damage by ROS. HEK cells exhibited more or less same level of ROS production compared to control cells when pre-treated with catalase inhibitor (NaN_3) at 6 and 24 h (Figure 4.48).

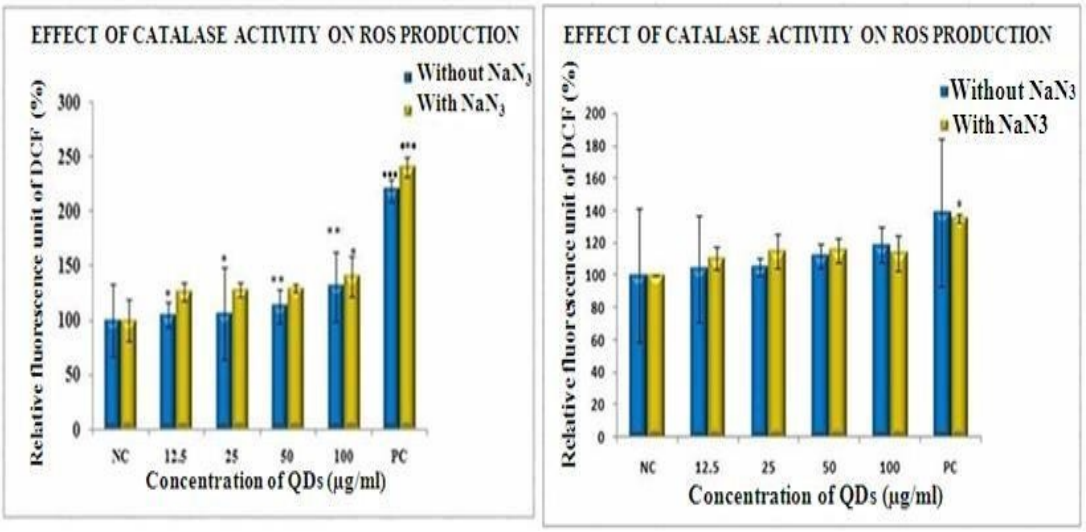

Figure 4.48. Effect of catalase activity on ROS production in HEK cells exposed to ZnSe/ZnS QDs at 6 and 24 h. The values are expressed in percentage fluorescence with respect to control. The data represent mean ± SD of three independent experiments. Asterisk denotes statistically significant difference (*p<0.05, **p< 0.01 and ***p<0.001).

4.6.13.3 NITRIC OXIDE PRODUCTION BY GRIESS REAGENT

Potential of ZnSe/ZnS QDs to induce RNS production in HEK was elucidated by grass reagent. There was no increase in RNS production in both 6 and 24 h exposure. The results are depicted in figure 4.49.

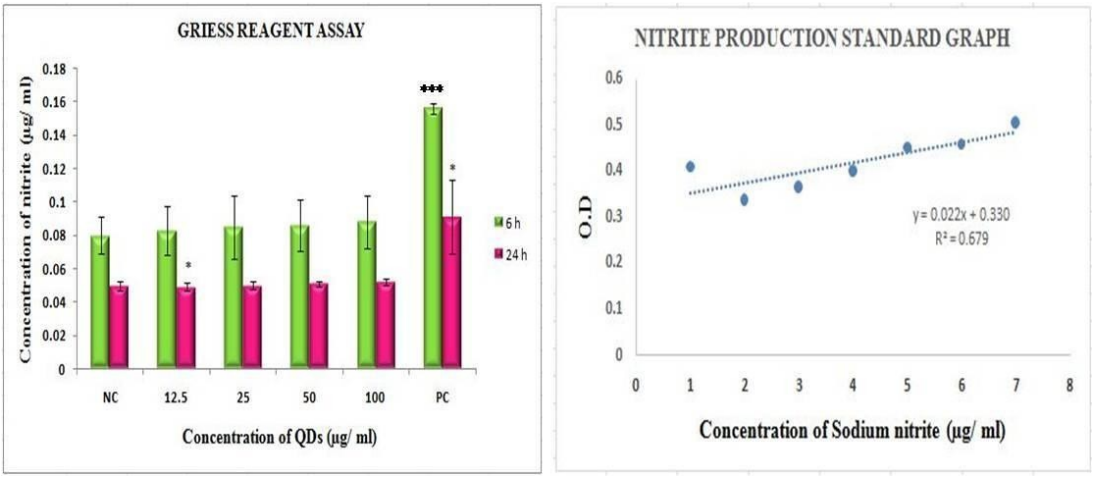

Figure 4.49. RNS production by Griess reagent assay showing RNS production in HEK cells exposed to ZnSe/ZnS QDs at 6 and 24 h. LPS treated samples were used as positive control. The data represent mean ± SD of three independent experiments. Asterisk denotes statistically

significant difference (*p<0.05 and ***P<0.001).

4.6.14 ASSESSMENT OF OXIDATIVE STRESS

4.6.14.1 PROTEIN ESTIMATION

Protein concentration in HEK cells upon treatment with QDs of different concentrations 12.5, 25, 50 and 100 µg/ml was estimated and found to be 0.586±0.015, 0.551±.008, 0.535±0.006, 0.523±0.011 respectively when compared to c o n t r o l (0.620±0.002)

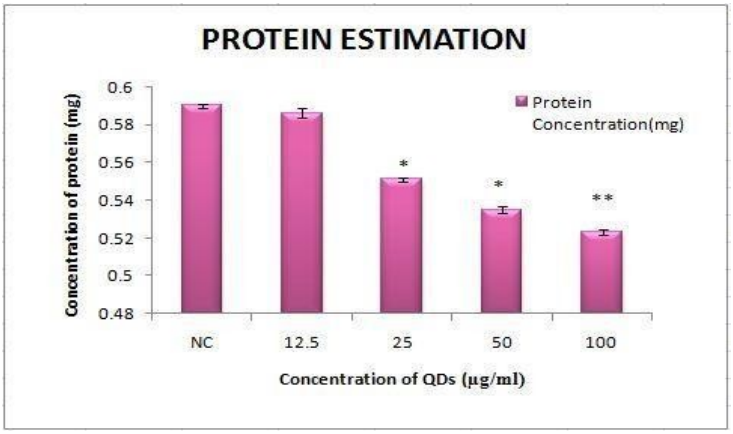

Figure 4.50. Protein estimation in HEK cells upon QDs exposure at 24 h (**P<0.01).

4.6.14.2 ESTIMATION OF GSH CONTENT

GSH level in HEK cells was significantly increased as concentration of QDs increased. The level of GSH was 1.847 ± 0.20, 2.09±0.21, 2.113± 0.218, 1.014± 0.225 at 12.5, 25, 50, 100 µg/ml respectively (Figure 4.51).

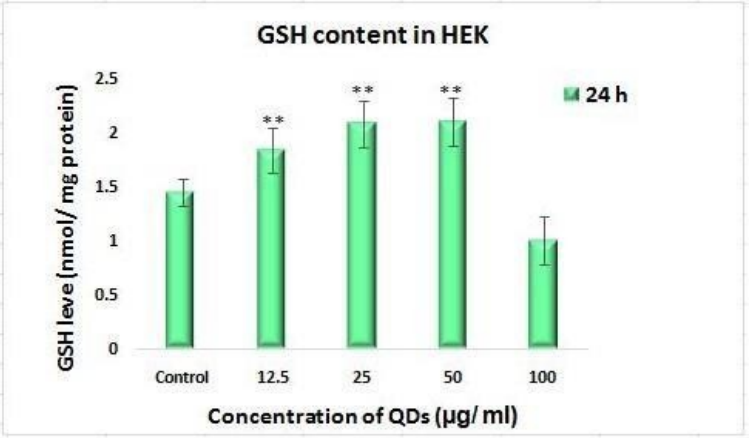

Figure 4.51. GSH level in HEK cells upon QDs exposure at 24 h (**P<0.01).

4.6.15 DNA LADDER ASSAY

Both control and treated cells showed a thick band of unfragmented DNA of more than 10,000bp size with no ladder (Figure 4.52). There was no DNA ladder or formation of smear pattern observed in the treated group.

Figure 4.52. DNA ladder assay. Lane 1. Marker DNA, lane 2. Control, Lane 3. 12.5 µg/ml, Lane 4. 25 µg/ml, Lane 5. 50 µg/ml, Lane 6. 100 µg/ml of ZnSe/ZnS QDs. Base pairs (bp) of DNA markers are indicated on the left side of the figure.

4.6.16 LIVE DEAD ASSAY BY CALCEIN AM-PI

The results of the live dead assay were shown in figure 4.53 and figure 4.54. The results suggest that 0.28, 3.27, 3.90, 13.66 % live cells and 9.08, 24.93, 28.57, 41.32 % dead cells were found when exposed to different concentrations (12.5, 25, 50 and 100 µg/ml) of ZnSe/ZnS QDs on HEK cells. Figures 4.53f and 4.54f shows graphical representation of flow cytometric analysis.

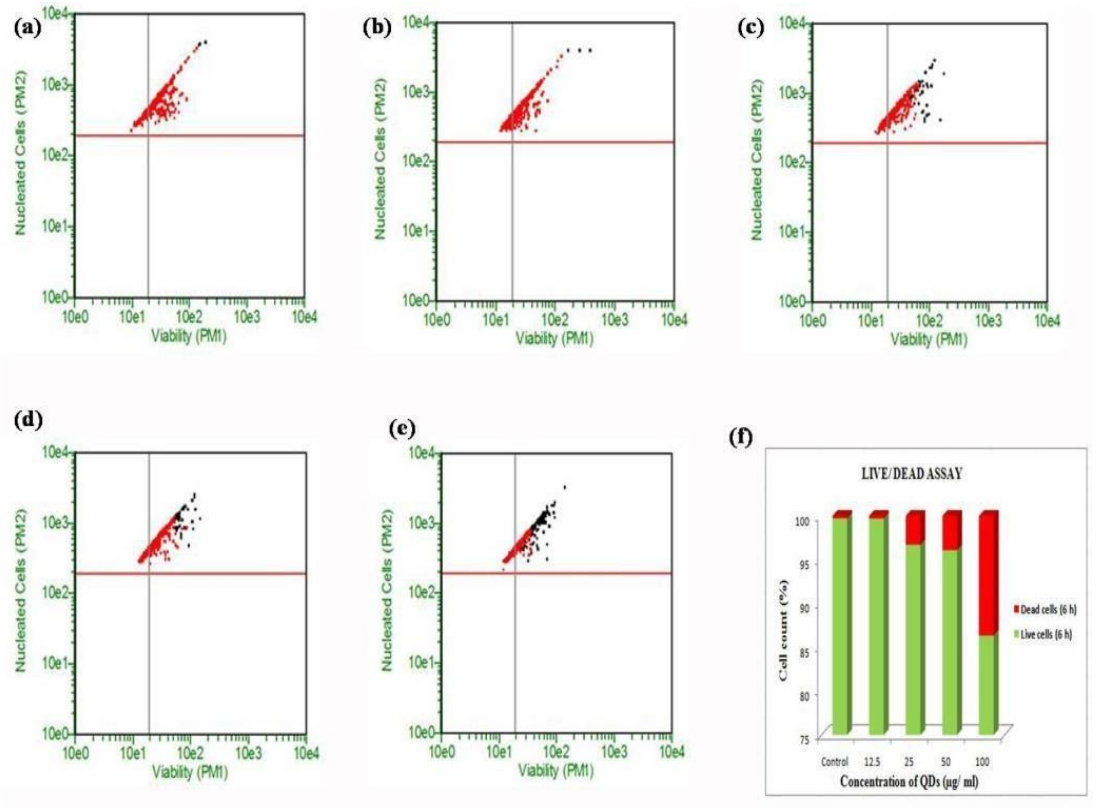

Figure 4.53. ZnSe/ZnS QDs induced death in HEK cells: A-C Flow cytometric analysis of Calcein AM stained cells. Black dots represent apoptotic cells and red dots represent viable cells. (a) untreated cells, (b) 12.5 µg/ ml (c) 25 µg/ ml (d) 50 µg/ml (e) 100 µg/ml ZnSe/ZnS QDs treated cells. (f) Graph representing percentage of viable and dead cells at different concentrations of ZnSe/ZnS QDs (5, 25, 50 and 100 µg/ml) after 6 h.

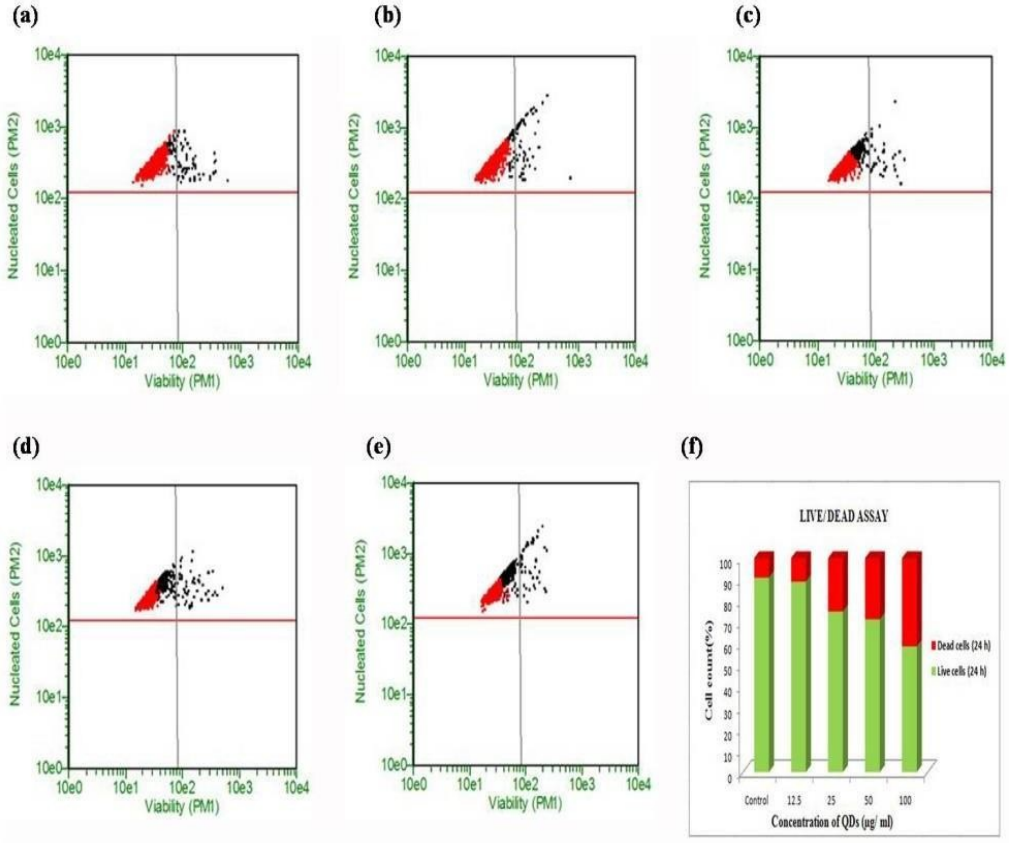

Figure 4.54. ZnSe/ZnS QDs induced death in HEK cells. a-c Flow cytometric analysis of Calcein AM stained cells. Black dots represent apoptotic cells and red dots represent viable cells. (a) untreated cells, (b) 12.5 µg/ml, (c) 25 µg/ml, (d) 50 µg/ml, (e) 100 µg/ml ZnSe/ZnS QDs treated cells. (f) Graph representing percentage of viable and dead cells at different concentrations of ZnSe/ZnS QDs (5, 25, 50 and 100µg/ml) after 24

4.6.17 APOPTOSIS BY ANNEXIN-PI FACS

Apoptosis in HEK cells was studied by Annexin V/PI staining. Gating of the population was done by appropriate controls. There was a dose dependent increase in PI positive cells and annexin V/PI double positive cells. Graphical representation of cell death mechanism of 12.5, 25, 50 and 100 µg/ml QDs treated cells with respect to control was given in the Figure 4.55.

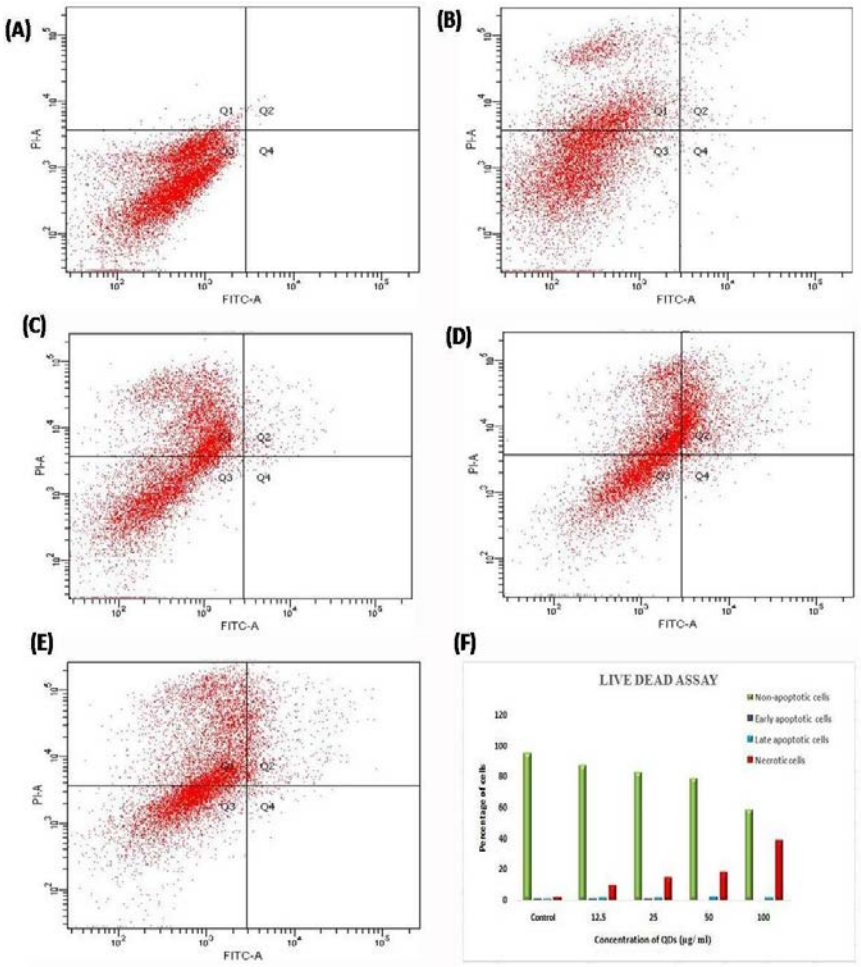

Figure 4.55. ZnSe/ZnS QDs induced death in HEK cells. A-C Flow cytometric analysis of Annexin-PI stained cells, Q_1. necrotic cells, Q_2. Late apoptotic cells, Q_3. Viable cells, Q_4. Early apoptosis (A) untreated cells, (B) 12.5 µg/ml, (C) 25µg/ml, (D) 50 µg/ml (E) 100 µg/ml ZnSe/ZnS QDs treated cells. (F) Graph representing percentage of viable and dead cells at different concentrations of ZnSe/ZnS QDs (5, 25, 50 and 100 µg/ml) after 24 h.

4.6.18 CASPASE 3/7 ACTIVATION ASSAY

It was noted that ZnSe/ZnS QDs did not exhibited a Caspase activity when compared to control cells both at 6 and 24 h. The results were normalised with total protein content (Figure 4.56).

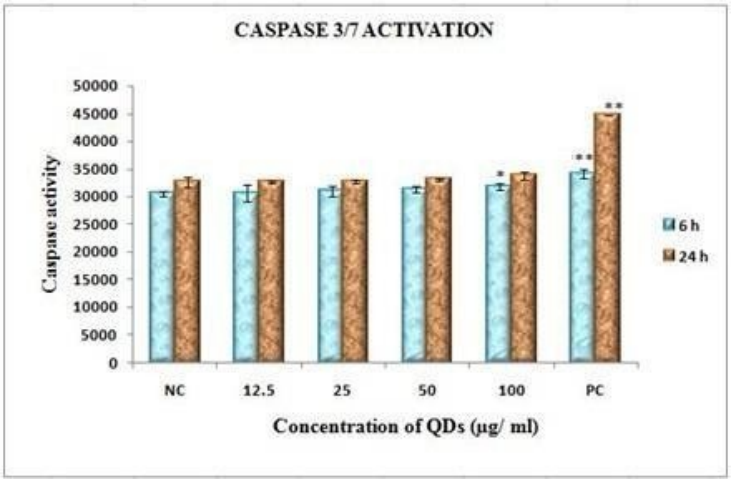

Figure 4.56. Comparison of caspase 3/7 activation in HEK cells exposed to ZnSe/ZnS QDs at 6 and 24 h. The data represent mean ± SD of three independent experiments. Asterisk denotes statistically significant difference (*$p<0.05$, and **$p<0.01$).

OBJECTIVE 3

PART I: ACUTE TOXICITY, IMMUNOTOXICITY, HAEMATOLOGICAL, CLINICAL BIOCHEMISTRY OXIDATIVE STRESS AND HISTOPATHOLOGICAL STUDIES.

4.7 CLINICAL SIGNS OF EXPERIMENTAL ANIMALS

Single exposure of ZnSe/ZnS QDs (10 mg/kg body weight) was intravenously (i.v) and intraperitoneally (i.p) administered to Swiss Albino mice. The body weight range was between 17-23 g. Animals were observed up to 14 days. A set of clinical signs associated with behavioural activities were monitored. None of the experimental animals showed any signs of clinical/behavioural changes or any adverse toxic symptoms or death during the observation periods (Table 4.3).

Clinical signs	Parameters observed	Control	ZnSe/ZnS QDs	
			i.v	i.p
General appearance	Hunched posture, piloerection, responsiveness to the surroundings, dehydration, weight loss, Swelling, clonic and tonic movements, presence of ring tail	Normal	Normal	Normal
Skin and fur	Skin elasticity, contraction of skin around the nose, discoloration, redness, ruffled fur	Normal	Normal	Normal
Eyes	Orbital tightening, keratitis, retro bulbar abscess.	Normal	Normal	Normal
Nose, mouth, ear	Whisker change, nose and cheek bulge, contraction of skin around the nose, ear position, nasal discharge, salivation	Normal	Normal	Normal
Respiratory	Sneezing	Normal	Normal	Normal
Excretion	Discoloration of urine and faeces, presence of blood in urine and faeces.	Normal	Normal	Normal
Behavioural	Eating, drinking, grooming, lack of movement.	Normal	Normal	Normal

Table 4.3. Clinical signs of experimental animals exposed to ZnSe/ZnS QDs. n=3

4.8 BODY WEIGHT GAIN OF ANIMALS

Body weights of the mice were observed throughout the experimental period. There was a slight increase in body weight gain in treated mice was observed when compared to that of control animals (Figure 4.57).

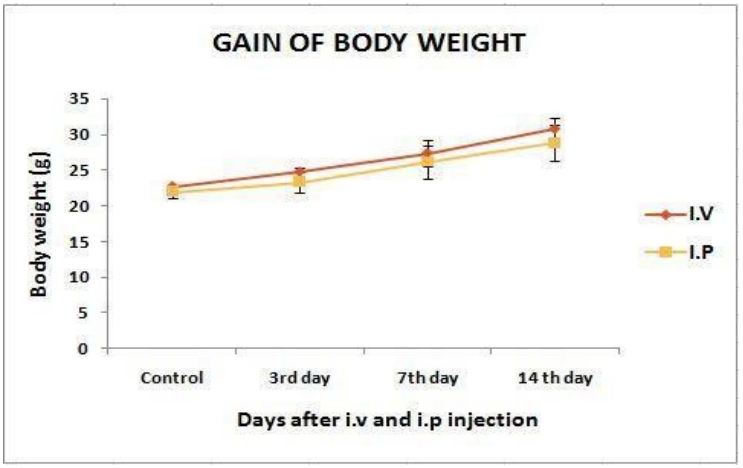

Figure4.57**:** Body weight gain of mice exposed to ZnSe/ZnS QDs (i.v. and i.p.).

4.9 URINE ANALYSIS

Kidney function was also assessed by urine analysis. The urine was collected at 3, 7 and 14 days after administration of ZnSe/ZnS QDs. The results of the study were shown in Table 4.4. The results of the study pointed out that leukocytes, nitrites, urobilinogen, proteins, blood, ketone, bilirubin and glucose were comparable in both control and treated animals. pH and specific gravity were also detected and no change was observed. This showed that there was no noticeable treatment related alternations in the kidneys.

Parameters	Control	i.v injection			i.p injection		
		3rd day	7th day	14th day	3rd day	7th day	14th day
Colour	Clear	Slightly yellow	Clear	Clear	Clear	Slightly yellow	Clear
Leukocyte	-ve	-ve	-ve	-ve	-ve	-ve	-ve
Nitrite	+ve	+ve	+ve	+ve	+ve	+ve	+ve
Urobilinogen (mg/dl)	0.1	0.1	0.1	0.1	0.1	0.1	0.1
Protein (mg/dl)	-ve	-ve	-ve	-ve	-ve	-ve	-ve
pH	5.0	5.5	5.5	5.0	5.5	5.0	5.0
Blood	-ve	-ve	-ve	-ve	-ve	-ve	-ve
Specific gravity	1.025	1.025	1.030	1.025	1.025	1.025	1.025
Ketones (mg/dl)	160	160	160	160	160	160	160
Bilirubin	Small	Small	Small	Moderate	Moderate	Small	Small
Glucose (mg/dl)	-ve	-ve	-ve	-ve	-ve	-ve	-ve

Table 4.4: Urine analysis of mice treated with ZnSe/ZnS QDs. n=3. The data represent mean ± SD.

4.10 HAEMATOLOGY ANALYSIS

Blood from the treated mice was collected at 3rd, 7th and 14thday of observation and subjected to haematological analysis. The results of the study indicated that WBC, RBC and platelets count (i.v) was slightly increased in treated mice when compared to control, but all the values are under the normal range. HCT value at 7th and 14th day of i.p treated mice was found to be slightly greater than the normal range. Haemoglobin content, MCV, MCH, MCHC remained within the normal range and was comparable to control (Figure 4.58).

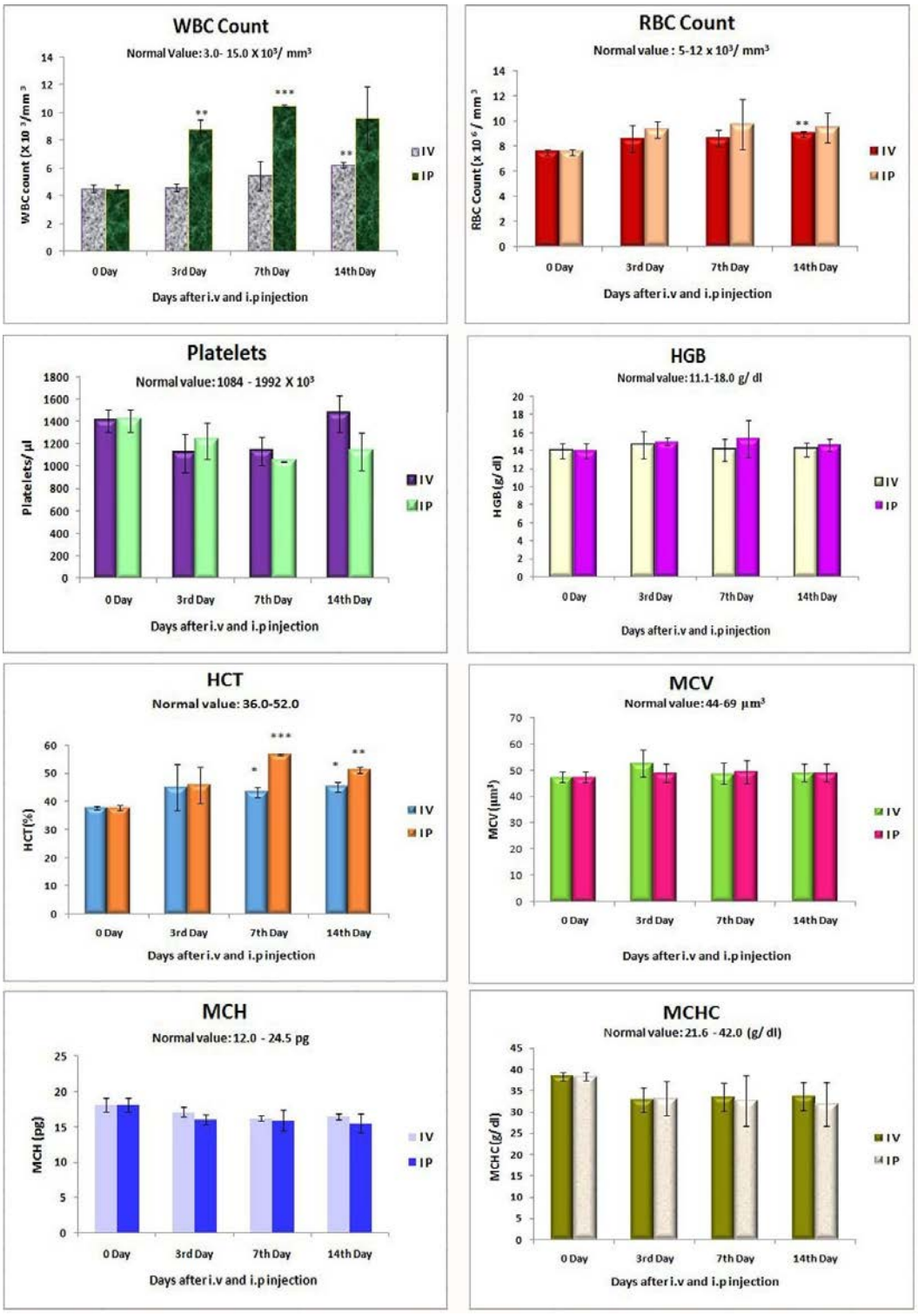

Figure 4.58: Haematological parameters of Swiss Albino mice exposed to ZnSe/ZnS QDs. WBC: white blood corpuscles, RBC: red blood corpuscles, Platelets, HGB: haemoglobin, HCT: haematocrit, MCV: Mean corpuscular volume, MCH: Mean corpuscular haemoglobin, MCHC: mean corpuscular haemoglobin concentration.

4.11 CLINICAL BIOCHEMISTRY

Liver function was assessed from the serum biochemistry of mice exposed to ZnSe/ZnS QDs. Albumin level was increased in i.p treated mice when compared to control. Total protein present in liver was slightly increased up to 7^{th} day and normalised on 14^{th} day. In both i.v and i.p treated mice, bilirubin level got decreased initially and become normal at the end of experimental period. There was a slight increase in cholesterol and ALT level in the treated animals but all the values are under the normal rage. AST level initially increased and gradually normalised to the control level in case of i.v injected mice. On the other hand, there was markedly increased level of AST in i.p injected animals when compared to that of the control. ALP level initially decreased on the 3^{rd} day and increased thereafter at 7 and 14 days when compared to that of the control (Figure 4.59).

Result of the kidney function study indicated that the level of urea and creatinine level fluctuated upon treatment with ZnSe/ZnS QDs but all the values were found to be under normal range (Figure 4.60).

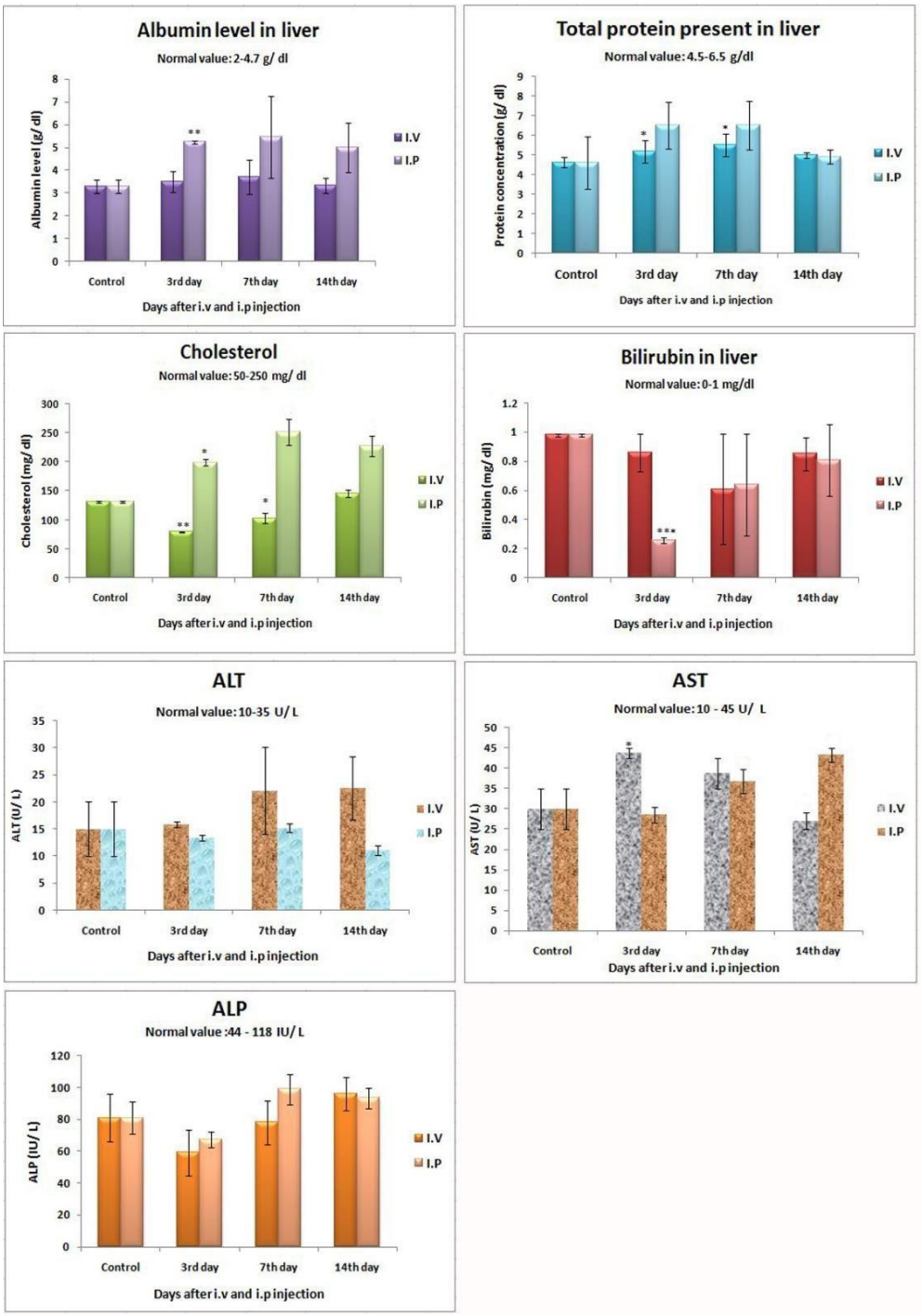

Figure 4.59. Clinical biochemistry analysis of Swiss Albino mice exposed to ZnSe/ZnS QDs, n=3. The data represents mean ± SD. Asterisk denotes statistically significant difference (*p<0.05, **p< 0.01 and ***p<0.001).

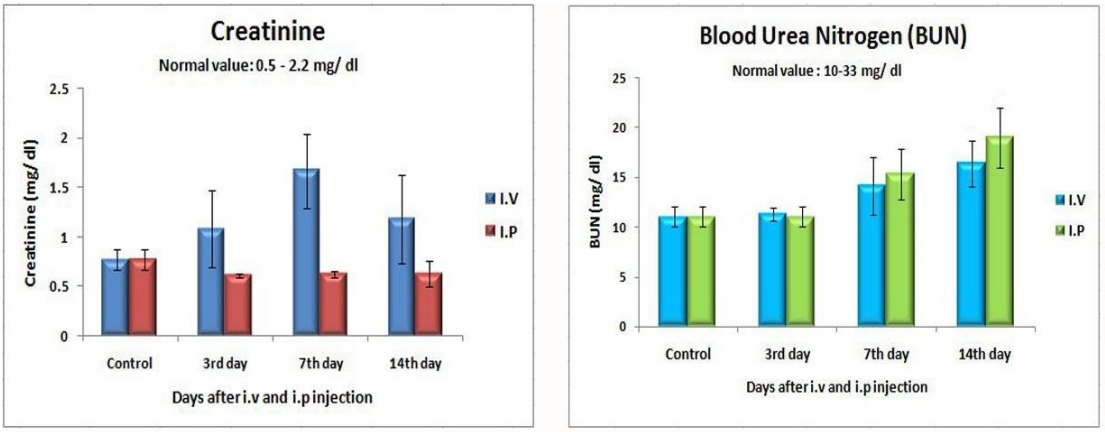

Figure 4.60 a, b. Clinical biochemistry analysis of Swiss Albino mice exposed to ZnSe/ZnS QDs, n=3. The data represents mean ± SD.

4.12 GROSS PATHOLOGY

Gross pathology of mice treated with ZnSe/ZnS QDs was similar to that of control (Figure 4.61). Gross examination did not disclose any noticeable pathological changes in i.v. and i.p treated mice.

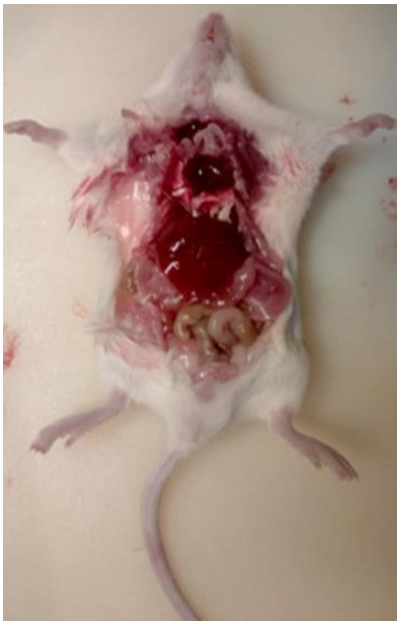

Figure 4.61: Gross pathology of mice treated with ZnSe/ZnS QDs.

4.13 ORGAN WEIGHT

Table 4.5 indicated that an increased organ weight was observed in treated mice when compared to control. Organ weight expressed in absolute wet weight.

	Groups	Organ weight (kg)			
		Liver	Kidney	Spleen	Brain
Intravenous	Control	2.649 ± 0.091	0.531± 0.048	0.116±0.016	0.306±0.005
	3rd Day	0.98±0.034**	0.315± 0.016*	0.065±0.005*	0.455±0.004*
	7th Day	1.796± 0.145	0.466± 0.045	0.123±0.005	0.43±0.02**
	14th Day	2.566±0.122***	0.56±0.055	0.115±0.01*	0.383±0.030*
Intraperitoneal	Control	2.349±0.091	0.531±0.048	0.116±0.016	0.306±0.005
	3rd Day	1.856±0.634	0.52±0.043	0.093±0.001*	0.446±0.030*
	7th Day	2.163±0.297	0.646±0.015*	0.1±0.01	0.413±0.015**
	14th Day	2.292± 0.611	0.628±0.078	0.116±0.030	0.46±0.01**

Table 4.5. Organ weight from ZnSe/ZnS QDs treated animals. All the values were expressed in mean ± SD, n=3. *, **, *** Statistically significant, $p < 0.05$, $p < 0.01$, $p < 0.001$ respectively.

4.14 HISTOPATHOLOGY

In control and 3rd day group, the central vein appeared normal, also the hepatocytes around the central vein showed granular cytoplasm with normal nucleus. Mononuclear cells were seen in the sinusoidal space. Histopathological examination showed atrophic lesions in liver on 7th and 14th days (i.v) of observation (Figure 4.62). On the whole, spleen histology of treated mice was similar to that of control. Mice exhibited normal spleen architecture comprising of white pulp, red pulp and marginal zone. Red pulp contained megakaryocytes. Spleen in all groups was found to devoid of macrophage infiltrations and lesions (Figure 4.63). Brain histology of treated animals was observed to be comparable to that of control. No changes or abnormalities were detected at the cerebral cortex in brain. Normal neurons, blood vessels and hippocampus were found in all groups. Kidney histology of 3rd and 7th day treated group was observed to be comparable with control group. The kidney showed normal cortex and Bowman's capsule. The deeper regions of the cortex exhibited normal proximal and distal convoluted tubules without any fibrillation or tubular dilations. Considering the 14th day treated mice, the glomerulus was slightly congested in the cortex region and interstitial congestion was also noted in multifocal areas.

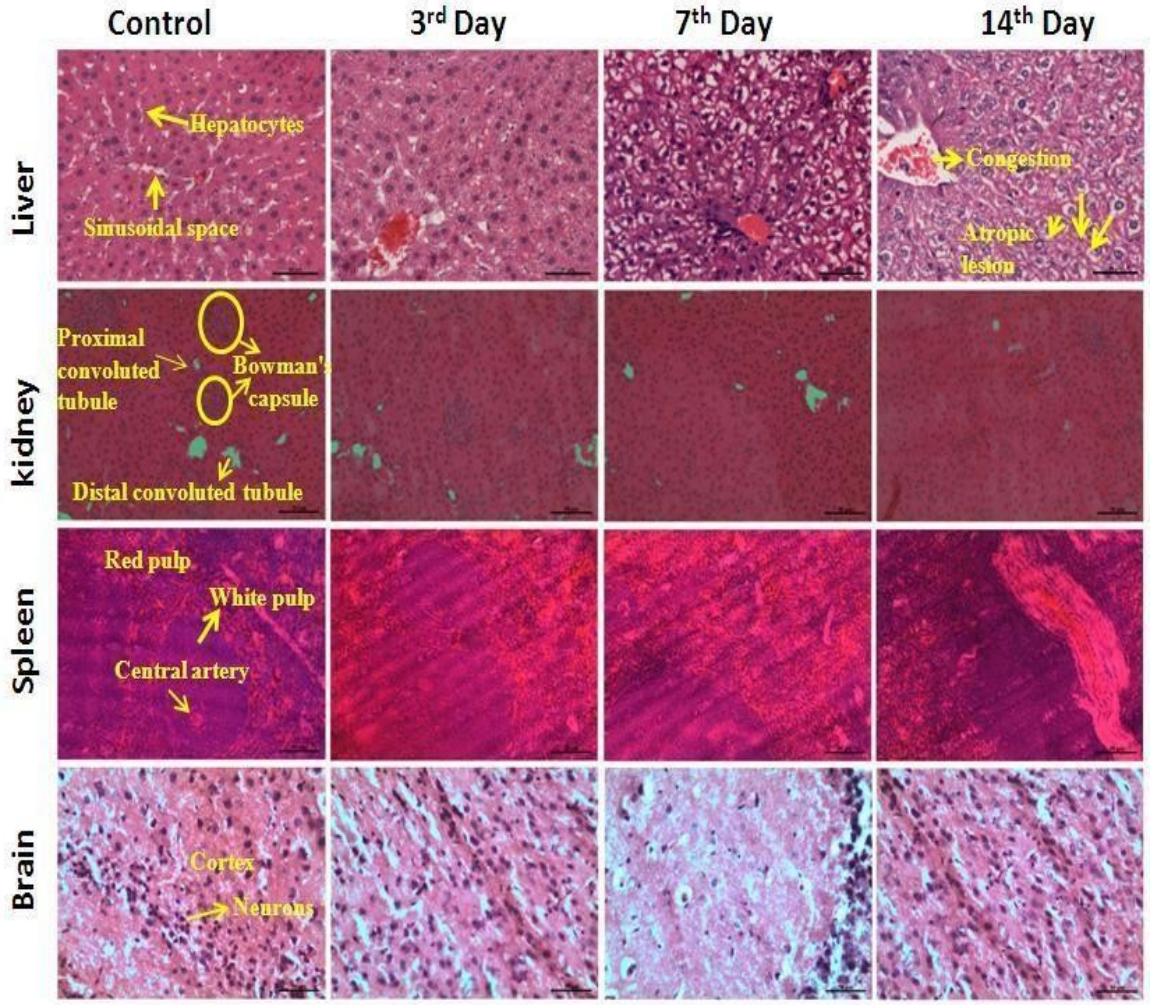

Figure 4.62: Histology section processed with H& E staining showing tissue architecture of Liver, kidney, spleen and brain of mice exposed (i.v) to ZnSe/ZnS QDs. Magnifications 40X. Scale bar represent 50µm.

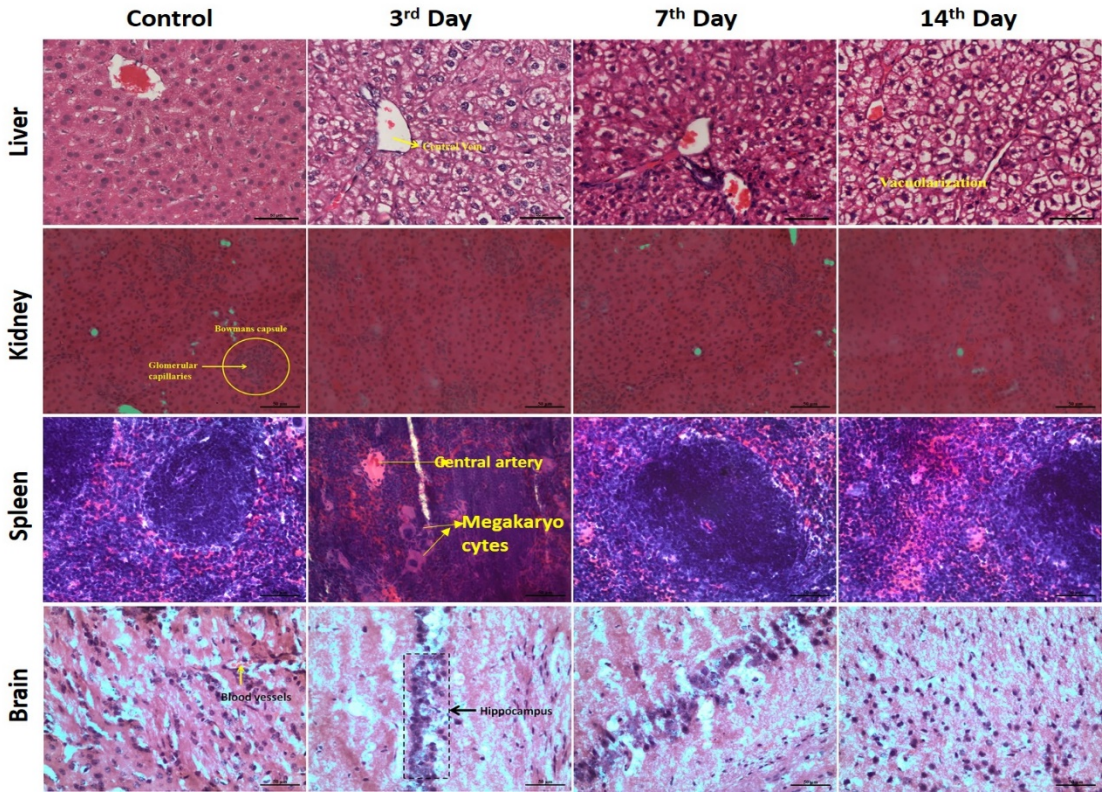

Figure 4.63: Histology section processed with H& E staining showing tissue architecture of Liver, kidney, spleen and brain of mice exposed (i.p) to ZnSe/ZnS QDs. Magnifications 40X. Scale bar represent 50 µm.

4.15 ANTIOXIDANT ASSAY

Liver and brain tissues were collected from mice injected (both i.v and i.p) with ZnSe/ZnS QDs. All the assays were carried out in 10% liver and brain homogenate. The lipid peroxidation, GSH, GR, GPx and SODs were analysed for antioxidant assays.

4.15.1 LIPID PEROXIDATION (LPO)

Lipid peroxidation is estimated by the amount of malondialdehyde formed. Statistically significant increase in malondialdehyde (MDA) was observed in the liver of ZnSe/ZnS QDs exposed mice. The results are demonstrated in Figure 4.64.

Similarly, MDA production in brain was increased significantly on 3rd and 7th day of treatment and normalised on 14th day. The results are demonstrated in figure 4.64.

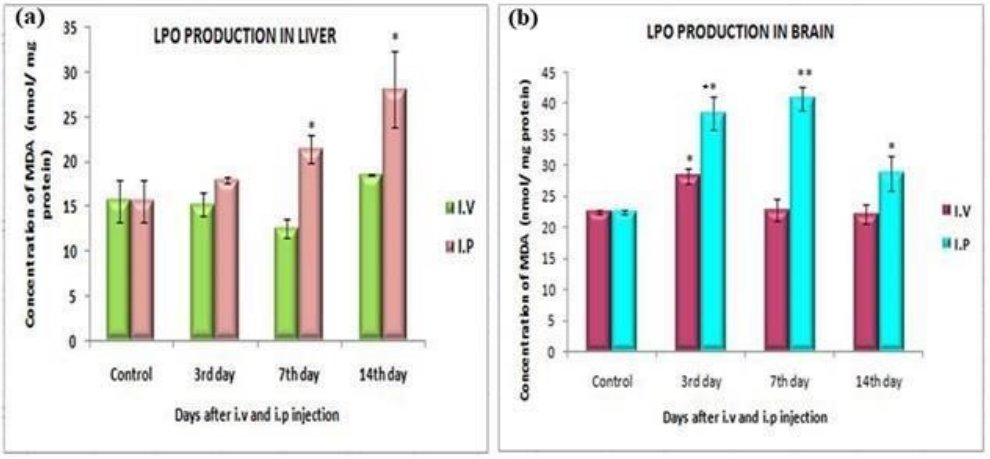

Figure 4.64: LPO production in a) liver b) brain of mice exposed to ZnSe/ZnS QDs. n=3. The data represent mean ± SD. Asterisk denotes statistically significant difference (*p<0.05, **p< 0.01).

4.15.2 REDUCED GLUTATHIONE (GSH)

The level of GSH was altered in treated animals when compared to control. A statistically significant reduction in GSH levels of liver was observed at 3rd, 7th and 14th day of observation period. In brain the GSH level was found to decreased on 3rd, 7th and 14th day when compared to control in both i.v and i.p treated mice (figure 4.65).

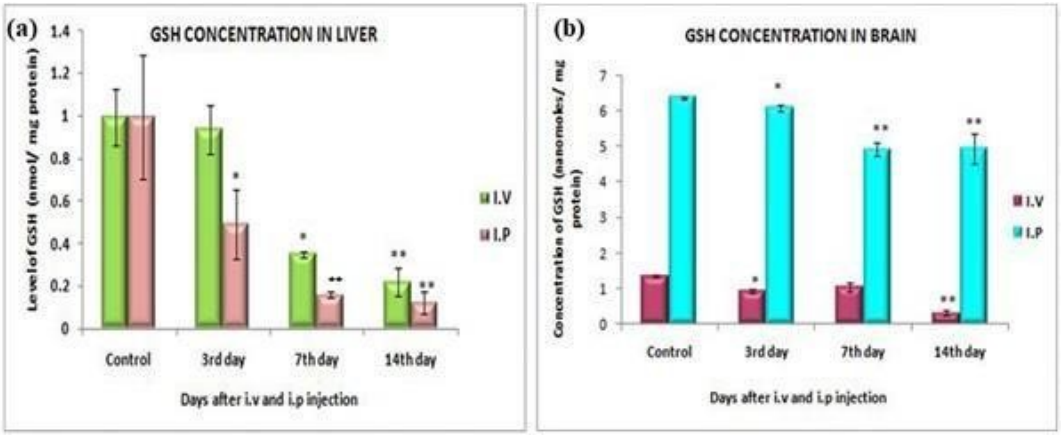

Figure 4.65: GSH level in a) liver, b) brain of mice exposed to ZnSe/ZnS QDs. n=3. The data represent mean ± SD. Asterisk denotes statistically significant difference (*p<0.05 and **p< 0.01).

4.15.3 GLUTATHIONE PEROXIDASE (GPX)

Figure 4.66 shows a statistically significant increase in GPx activity in liver on 7thday post exposure. This increase in activity was normalised on 14thday of observation period. It was observed that an increase in GPx level in brain was found at the end of 3rd day (i.v:0.052±0.006, i.p: 0.106± 0.009) and 7th Day (i.v: 0.014 ± 0.004, i.p: 0.106±0.04). The increased level of GPx was found to be normal at the end of 14 days (i.v: 0.053±0.01, i.p: 0.08±0.059). The increase was not statistically significant.

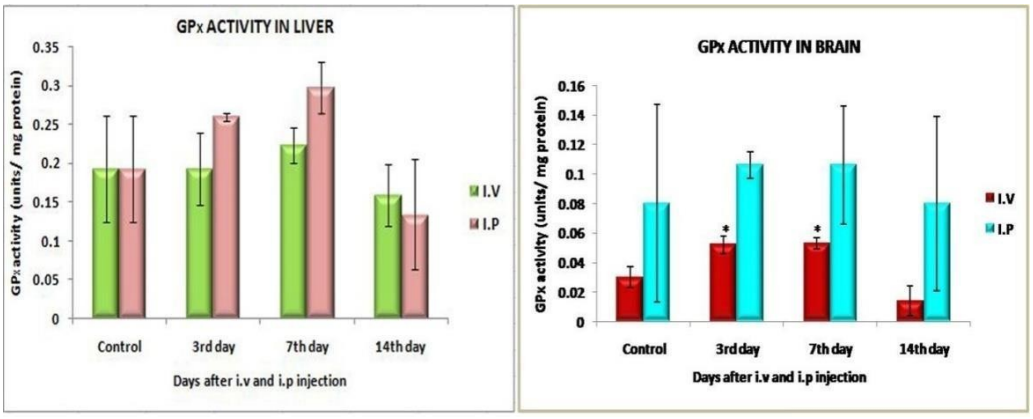

Figure 4.66 GPx activity in a) liver, b) brain of mice exposed to ZnSe/ZnS QDs. n=3. The data represent mean ± SD. Asterisk denotes statistically significant difference (*p<0.05).

4.15.4 GLUTATHIONE REDUCTASE (GR)

GR activity in liver (i.v) was reduced when compared to the control animals. A statistically significant increase in GR activity was observed in liver of treated animals on 3rd day and gradually decreased on 7th and 14th days of observation of i.p treated mice. A statistically significant increase in the GR activity was observed in the brain of ZnSe/ZnS QDs exposed mice on 3rd (i.v: 1.263±0.522, i.p: 0.941±0.0821), 7th (i.v: 0.971±0.103, i.p: 0.89±0.016) and 14th day (i.v: 1.062±0.061, i.p: 0.857±0.015) of observation (Figure 4.67).

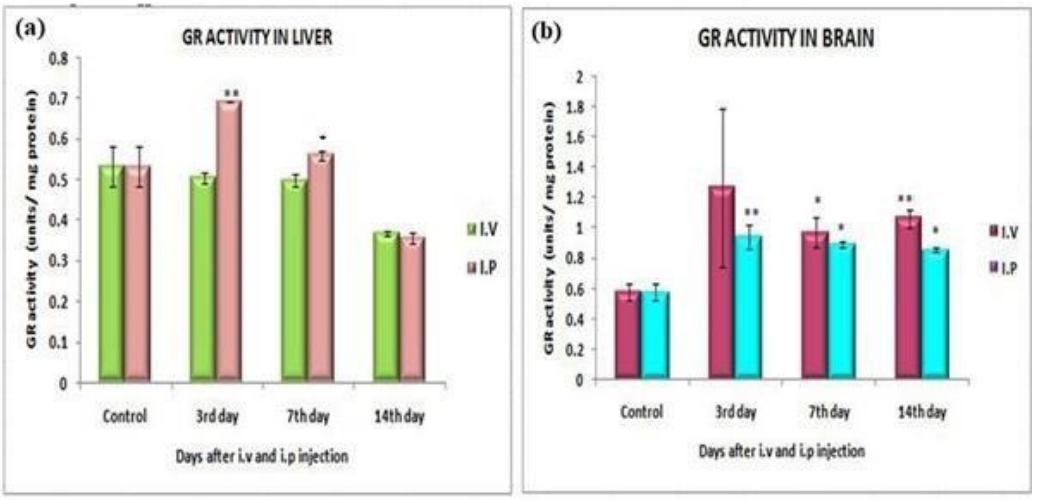

Figure 4.67. GR activity in a) liver, b) brain of mice exposed to ZnSe/ZnS QDs. n=3. The data represent mean ± SD. Asterisk denotes statistically significant difference (*p<0.05 and **p< 0.01).

4.15.5 SUPEROXIDE DISMUTASE (SOD)

A statistically significant reduction in SOD activity was observed in liver of both i.v and i.p treated animals when compared to control. An increased SOD activity was found in the brain of ZnSe/ZnS QDs exposed mice on 3rd day (i.v: 0.181 ±0.002, i.p: 0.259±0.001) and 7th day (i.v: 0.224 ± 0.002, i.p: 0.228 ±0.003). SOD level decreased on 14th day (i.v: 0.053± 0.01, i.p: 0.358 ±0.136) when compared with control mice (0.0172± 0.007). The decrease in SOD level was not statistically significant (Figure 4.68).

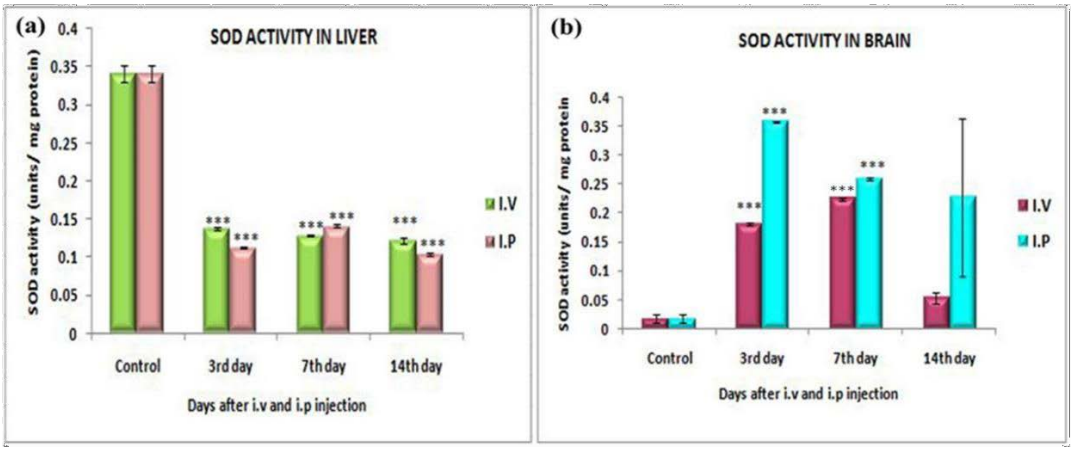

Figure 4.68. SOD activity in a) liver, b) brain of mice exposed to ZnSe/ZnS QDs.n=3. The data represent mean ± SD. Asterisk denotes statistically significant difference (***p<0.001).

4.16 IMMUNOTOXICITY BY SPLENOCYTE PROLIFERATION ASSAY

Splenocytes proliferation assay was carried out in spleen isolated from the treated mice using tritiated thymidine. Result of the study suggests that splenocytes proliferation rate is increased on 3rd day and decreased on subsequent days and become normal at the end of 14 days (Figure 4.69).

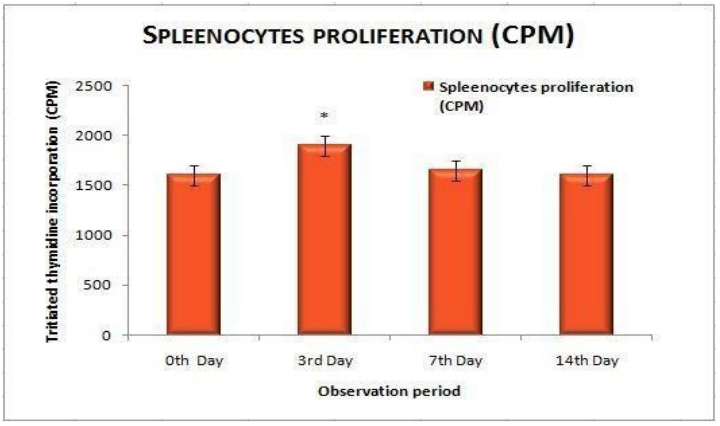

Figure 4.69. Splenocytes proliferation in mice exposed to ZnSe/ZnS QDs. n=3. Data represents mean± SD. Asterisk denotes statistically significant difference (*p<0.05).

4.17 BLOOD BRAIN BARRIER (BBB) INTEGRITY

Figure 4.70 shows the change in brain volume of mice injected with ZnSe/ZnS QDs in i.v. and i.p. administration. There was no evidence of brain volume observed in i.v or i.p injected animals.

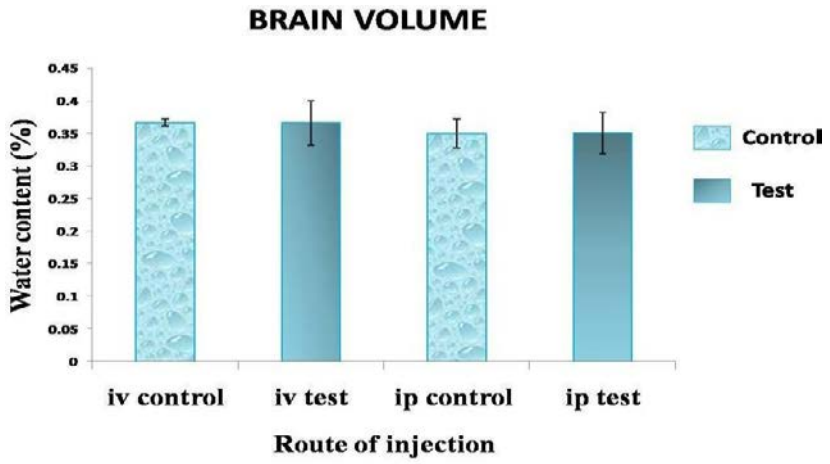

Figure 4.70: Brain volume of mice exposed to ZnSe/ZnS QDs (i.v. and i.p.). n=3.
The data represents mean ± SD.

PART 2: ELEMENTAL ANALYSIS, BIO DISTRIBUTION AND ADME & T (ABSORPTION, DISTRIBUTION, METABOLISM, EXCRETION AND TOXICITY) PROFILING STUDIES.

4.18 BIO DISTRIBUTION BY ELEMENTAL ANALYSIS

4.18.1 LIVER

Elemental analysis by ICP-OES showed alteration of metal ions content in liver. There was an increase in zinc content observed at 3rd day in i.v (40.437±9.65 ppm) and i.p (33.937±10 ppm) injected animals when compared to control (5.93±1.013 ppm). On 7th day Zn content was found to decrease by 13.77±0.95 ppm. (i.v) and 11.305±1.2 ppm (i.p). The Zn content remained same at the end of 14th day in i.v treated animals, whereas Zn content largely decreased in i.p treated animals. Se

distribution in liver was more or less similar to that of Zn in all groups. Sulphur content decreased in i.v exposed animals on 3rdday (3.78±0.17x10^3 ppm) and 7th day (2.873±0.1x10^3 ppm). Similarly, the Sulphur content in i.p exposed animals on 3rd day was 3.873± 1x10^3 ppm and 7th day 4.12±1.05x10^3 ppm.

4.18.2 KIDNEY

The zinc content in kidneys gradually increased to 32.721 ±0.608 ppm on 3rd day of i.p treatment when compared to control (26.486 ± 0.13 ppm). Zn content of i.p treated animals on 7th day and 14th day was 20.727±1 ppm and 11.328±0.965 ppm respectively. The Zn content in i.v treated animals was found to be 30.45± 0.057 ppm (3rd day), 20.30 ±0.11 (7th day) and 14.35±0.55 ppm (14th day). Se content suddenly increased on 3rd day to 1.835 ± 0.2 ppm and subsequently normalized to 0.985 ± 0.1 ppm on 7th day and 0.779 ±0.1 ppm on 14th day in i.v QDs exposed group. However, in case of i.p treatment, Se content increased on 3rd day (1.64± 0.987 ppm) and then gradually decreased on 7th day (0.895 ± 0.1 ppm) and normalized on 14th day (0.786 ± 0.097). Sulphur content decreased on 3rd day to 1.898 ±1.104x10^3 ppm, 7th day to 4.388±0.145x10^3 ppm and normalized on 14th day to 5.942±1.43x10^3 ppm when compared to control (6.792 ± 1.32x10^3 ppm) in i.v treated group. The same trend was observed in i.p treated group (3rd day: 3.326 ± 0.978x10^3 ppm, 7th day: 7.233±0.98x10^3 ppm and 14th day: 9.827±0.957x10^3 ppm).

4.18.3 SPLEEN

On 3rd day the Zn level in i.v treated mice was 117.727 ±0.1 ppm when compared to that of control (25.64±0.001 ppm), whereas the Zn level decreased to

51.985±0.92on 7th day and 22.52 ±0.946 ppm on 14th day. There was a slight increase in Zn content observed in i.p treated animals on 3rd day (57.742± 0.01ppm) and slightly decrease on 7th and 14th day to (36.95 ± 0.1) and (4.901 ±2.0 ppm) respectively. Se level was increased on 3rd day of i.v (0.485 ±0.1) and i.p (0.726 ± 0.1) treated animals. But on 7th and 14th days, it remained same as control. Sulphur content was decreased on 3rd day and gradually increased on 7th day and normalized on 14th $_{day}$ in both i.v and i.p.

4.18.4 BRAIN

In i.v treated mice the level of Zn was increased on 3rd day (22.302±2.067 ppm) and decreased on 7th day (11.04 ±1.069 ppm) and 14th day (9.018 ± 1.27 ppm) in comparison with control (25.33±1.153 ppm). On 3rd day the level of Zn was found to be 24.08 ±2.005 ppm and the level was slightly decreased to 12.183 ± 2.024 ppm on 7th day and 8.107±0.1ppm on 14th day of i.p treated animals. Se level on 3rd day was 0.196 ±0.006 ppm in i.v treated animals and this level was normalized at the end of 7th and 14th day. Similar trend was observed in i.p treated mice. Sulphur content was decreased on 3rd day to 1.256 ± 0.1x10^{3}ppm and gradually increased on 7th day to 3.4 ± 1.03x10^{3}ppm and normalized on 14th day to 6.24 ±0.x10^3 ppm of both i.v and i.p treatment group (Figure 4.71).

4.18.5 BLOOD

Figure 4.72 shows the distribution of Zn in blood. The amount of Zn was increased on 3rd, 7th and 14thday in both i.v and i.p injected animal's blood. Se level in blood was same as control in i.p treated mice. whereas Se level was increased on 3rd and 7th day (i.v) and declined at the end of 14th day. Sulphur level was decreased on 3rd day and gradually increased on 7th and 14th day when compared to control. In the case of i.p injected animals, sulphur level in blood was normalized on 14th day.

4.18.6 FAECES

Zn and S in faeces gradually increased on 3rd, 7th and 14th days when compared to control in both i.v and i.p injected animals. Se gradually decreased on 3rd and 7th day and increased on 14th day in both i.v and i.p (figure 4.72).

4.18.7 URINE

In urine, Zn content was decreased on 3rd day and gradually increased on 7th and normalized on 14th day in i.v injected animals; whereas in i.p the level of Zn was significantly increased on 7th and 14th day. Se in urine was increased gradually on 3rd, 7thand 14th day in the i.v injected animals. However, in i.p injected mice, Se remained same as that of the control throughout the observation period. Sulphur distribution in urine was found to be comparable with the control on 3rd day of both i.v and i.p treated

animals. In the case of i.v injected animals, the level of sulphur increased on 7th day. In the case of i.p injected animals, sulphur level was increased on 7thand 14th day (figure 4.71).

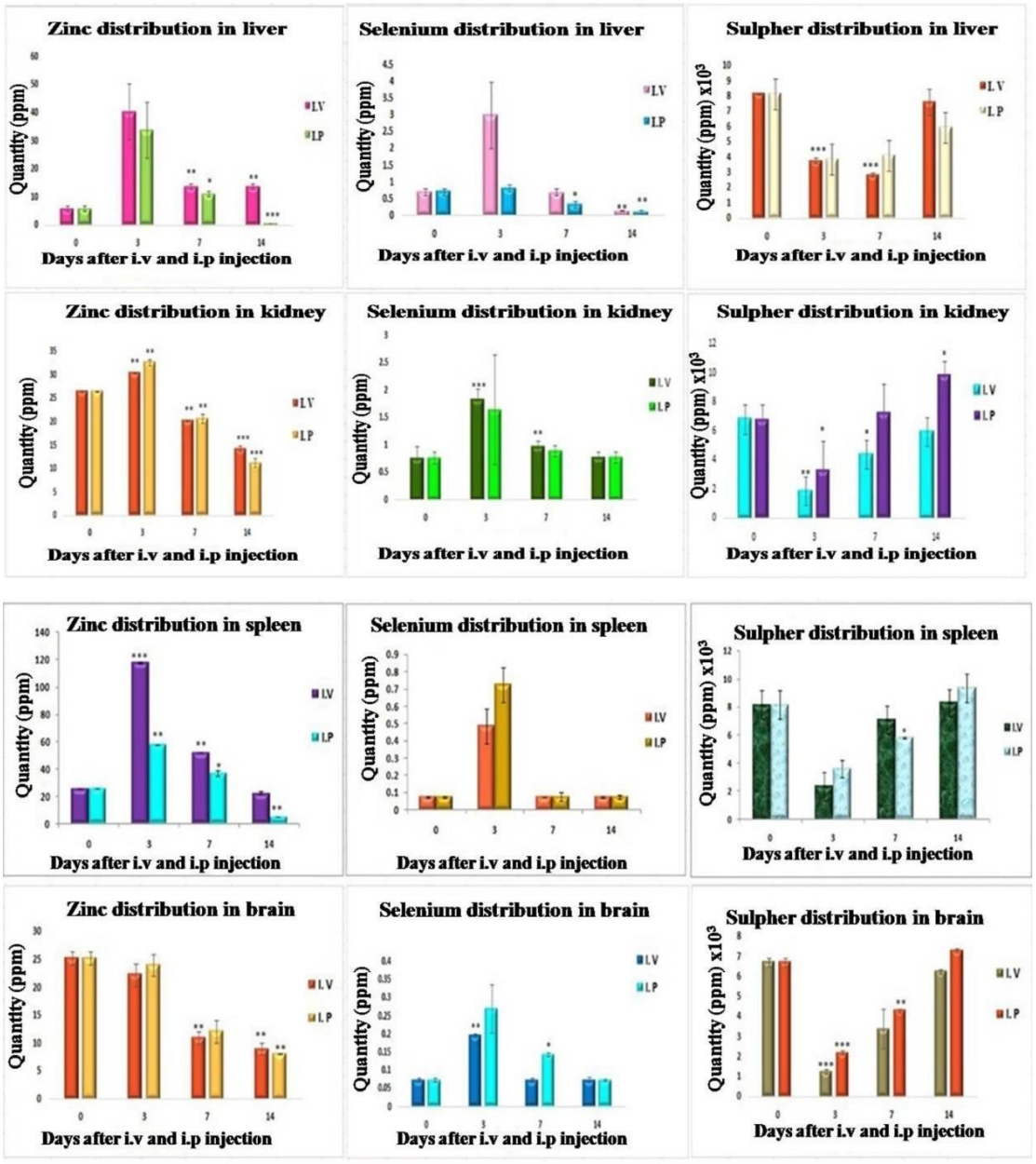

Figure 4.71: Elemental analysis of liver, kidney, spleen and brain of mice exposed to ZnSe/ ZnS QDs via i.v and i.p injection. N=3. The data represent mean ± SD. *, **, *** Statistically significant, $p<0.05$, $p<0.01$, $p<0.001$ respectively.

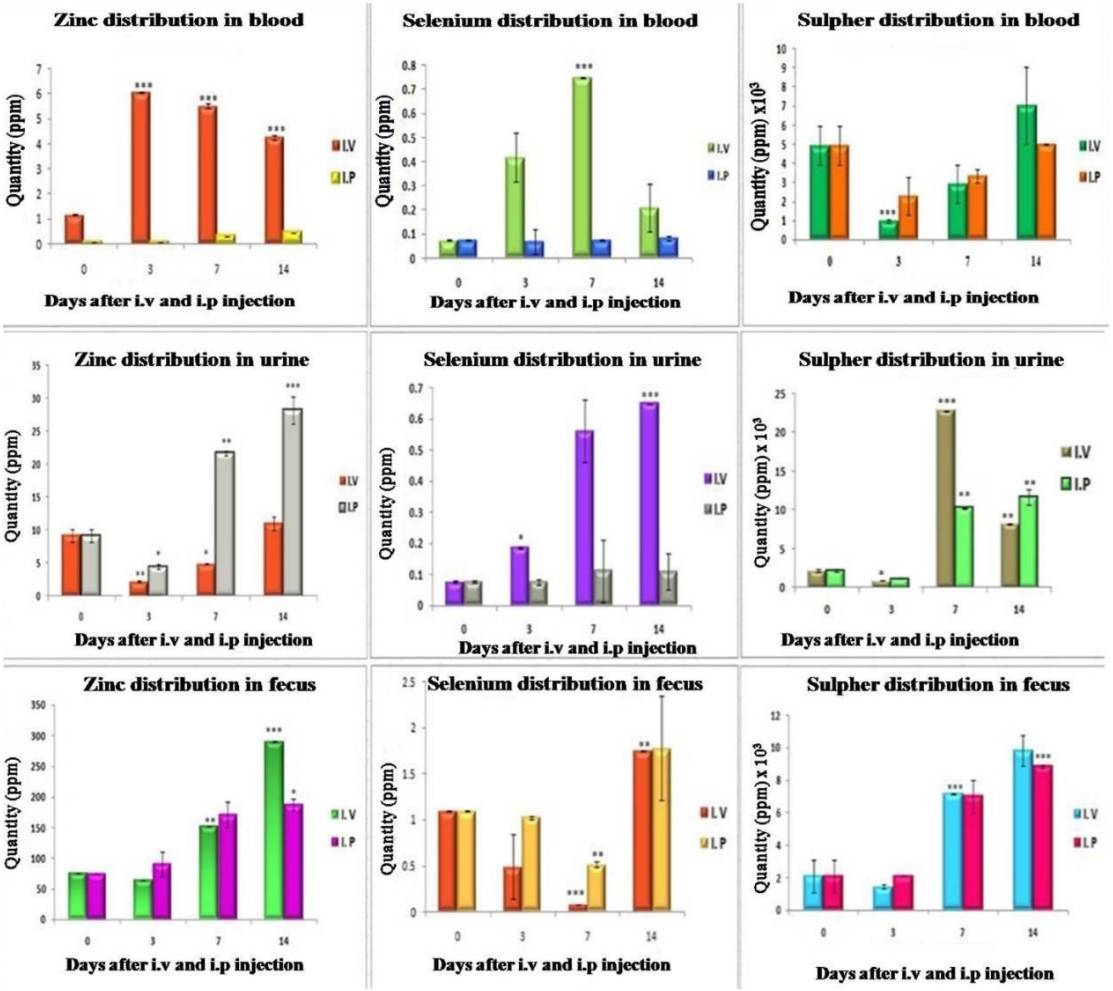

Figure 4.72: Elemental analysis of blood, urine and faeces of mice exposed to ZnSe/ZnS QDs via i.v and i.p injection. N=3. The data represent mean ± SD. *, **, *** statistically significant, p <0.05, p <0.01, p <0.001 respectively.

Sample	Total amount in mg/kg							
	Zn							
	Control		3rd Day		7th Day		14th Day	
	i.v	i.p	i.v	i.p	i.v	i.p	i.v	i.p
Liver	5.93± 1.013	5.93± 1.013	40.437 ±9.65	33.937 ±10	13.77± 0.95**	11.305 ±1.2*	13.861± 0.97**	0.9± 0.001***
Kidney	26.486 ±0.093	26.486 ±0.13	30.45± 0.05**	32.72± 0.6**	20.30± 0.11**	20.727 ±1.4**	14.353± 0.55***	11.328±0 .965***
Spleen	25.646 ±0.001	25.646 ±0.001	117.7± 0.1***	57.74± 0.01**	51.98± 0.92**	36.952 ±0.1*	22.524± 0.946	4.901±2* *
Brain	25.33± 1.153	25.33± 1.153	22.302 ±2.067	24.08± 2.005	11.04± 1.06**	12.183 ±2.024	9.018± 1.27**	8.107±0. 10**

Faeces	76.102 ±0.002	76.102 ±0.002	64.495 ±0.005	91.057 ±20	152.61 ±0.1**	171.33 5±20	290.24± 0.2***	187.259± 10

	Total amount in mg/L							
Urine	9.184± 1.3	9.184± 0.99	2.2± 0.2**	4.433± 0.4*	4.914± 0.98*	21.672 ±0.3**	11.007± 1.1	28.233±2 ***
Blood	1.175± 0.01	1.175± 0.01	6.07±0 .01***	0.0725 ±0.001	5.516± 0.1***	0.298± 0.01	4.26± 0.1***	0.457±0. 004
	Total amount in mg/kg							
	Se							
	control		3rd Day		7th Day		14th Day	
	i.v	i.p	i.v	i.p	i.v	i.p	i.v	i.p
Liver	0.71± 0.1	0.71±0 .1	3.0151 ±0.97	0.816± 0.1	0.699±0. 1	0.33± 0.1*	0.14±0.0 1**	0.108± 0.058**
Kidney	0.774± 0.1	0.774± 0.1	1.835± 0.2***	1.646± 0.987	0.985±0. 1**	0.895 ± 0.1	0.779±0. 1	0.786± 0.097
Spleen	0.075± 0.005	0.075± 0.005	0.485± 0.1	0.726± 0.1	0.075±0. 001	0.075 ±0.02 5	0.075±0. 005	0.075± 0.01
Brain	0.075± 0.005	0.075± 0.005	0.196± 0.006* *	0.27±0 .002	0.075±0. 005	0.145 ±0.06 *	0.075±0. 006	0.075± 0.005
Faeces	1.095± 0.005	1.095± 0.005	0.494± 0.351	1.028± 0.018	0.075±0. 001***	0.515 ±0.03 2**	1.752± 0.01**	1.777± 0.0568
	Total amount in mg/L							
Urine	0.075± 0.004	0.075 ±0.004	0.186± 0.003*	0.075± 0.01	0.56± 0.1	0.112 ± 0.1	0.647± 0.001***	0.108± 0.057
Blood	0.075± 0.002	0.075± 0.002	0.42± 0.1	0.068± 0.05	0.75± 0.10***	0.075 ±0.02	0.21± 0.1	0.0816± 0.1
	Total amount in mg/kg							
	S (x10$^{3)}$							
	Control		3rd Day		7th Day		14th Day	
	i.v	i.p	i.v	i.p	i.v	i.p	i.v	i.p
Liver	8.147± 0.02	8.147± 0.02	3.78 ± 0.17** *	3.873± 1.0	2.87 ± 0.09** *	4.121± 1.05	7.634± 0.857	5.957± 1.12
Kidney	6.792± 1.32	6.792± 0.98	1.89±1 .10**	3.326± 0.978*	4.388± 0.145*	7.233± 0.98	5.942± 1.43	9.827± 0.957*
Spleen	8.17±1 .5	8.17± 0.89	2.338± 0.92	3.608± 0.60	7.097± 1.19	5.827± 0.063*	8.303± 0.95	9.351± 1.08

Brain	6.713± 0.2	6.713± 0.2	1.256± 0.1***	2.207± 0.092***	3.4± 1.03	4.309± 0.1**	6.246± 0.1	7.304± 0.1
Faeces	2.106± 1.4	2.106± 0.9	1.456± 0.135***	2.136± 0.015	7.148± 0.009	7.013± 1.102	9.813± 0.950	8.87± 0.118***
	Total amount in mg/L							
Urine	2.247± 0.2	2.247± 0.2	0.90± 0.002	1.155± 0.01	22.764 ±0.1	10.192 ±0.1	8.21± 0.112	11.643± 1.21
Blood	4.944± 1.12	4.944± 0.78	0.987 ±0.19***	2.86±1.02	2.924± 0.93	3.348± 0.34	7.044± 2	5.005± 0.005

Table4.6: Table for elemental analysis.

4.19 ABSORPTION, DISTRIBUTION, METABOLISM, EXCRETION AND TOXICITY (ADME &T) PROFILING.

4.19.1 ABSORPTION

10 mg/kg body weight of ZnSe/ZnS QDs was exposed (single) to mice by intraperitoneal and intravenous injection. The absorption of ZnSe/ZnS QDs was evidenced in the organs as observed in the ICP-OES data. The quantity of ZnSe/ZnS QDs was estimated in organs such as liver, kidney, spleen and brain by ICP-OES (Table 4.6).

4.19.2 DISTRIBUTION

The distribution of ZnSe/ZnS QDs in organs was evaluated with ICP-OES at 3, 7 and 14 days post exposure. It was found that the ZnSe/ZnS QDs was distributed in blood, liver, kidney, spleen and brain (ICP-OES).

4.19.3 METABOLISM

ZnSe/ZnS QDs was administered to Swiss Albino mice by i.v. and i.p injection. ICP-OES data indicated the presence of QDs in blood. Subsequently blood was collected and subjected to clinical biochemistry evaluation. There was a slight alternation in few of the clinical biochemistry parameters (Figure 4.60).

4.19.4 EXCRETION

Urine and faeces samples were collected at 3, 7 and 14days post exposure (in both intravenous and intraperitoneal administration of ZnSe/ZnS QDs in mice. The presence of ZnSe/ZnS QDs indicated the excretion of QDs through urine and faeces and was evidenced in the ICP-OES data (Figure 4.72).

4.19.5 TOXICITY

10mg/kg body weight of ZnSe/ZnS QDs exposed animals were observed for the evidence of any toxicity. The results suggest that the material was absorbed, distributed, metabolized and partially excreted as evidenced from the ICP-OES data. It was observed that none of the animals treated with ZnSe/ZnS QDs showed any adverse symptoms however slight histopathological lesions observed in the liver of i.v exposed animals on 14^{th} day. There was a transitional changes observed in the liver histology.

CHAPTER 5: DISCUSSION

5. DISCUSSION

OBJECTIVE 1

SYNTHESIS AND CHARACTERIZATION OF QDs

5.1 SYNTHESIS OF ZnSe/ZnS QDs

ZnSe/ZnS QDs were prepared by a green method based on bottom-up aqueous colloidal synthetic (ACS) route. This 'green' synthetic process involves;

- nontoxic reaction precursors ($Zn(OAc)_2.2H_2O$, GSH, Se powder, $NaBH_4$, MPA),
- nontoxic reaction media (deionized water),
- Usage of mild reaction conditions (T: 100 ºC, pH: 10.5 and 9.5).

The novelty of this process lies in the ability to achieve the highest yield of QDs with minimum wastage and without using any harmful chemicals. A basic version of aqueous colloidal synthesis was first contributed by Gao *et al.,* in 2005. In aqueous colloidal synthesis (ACS) method, the source of the metal precursor is easily dissolved in water and coordinated by the hydrophilic agents. Examples for hydrophilic agents are glutathione (GSH), thioglycolic acid (TGA), mercapto propionic acid (MPA) and L-Cysteine (L- Cys). GSH is highly recommended among these stabilizers due to its excellent water solubility and low-cost. GSH is a tripeptide composed of glutamic acid, cysteine and glycine. It exists in almost every cell of the body (Ding *et al*., 2013). Chalcogen precursor is to be freshly prepared in aqueous medium just before its usage. NaHSe is produced from the chemical reduction of selenium (Se) in the presence of sodium borohydride ($NaBH_4$). This solution is used as the common sources of Se in QDs synthesis by ACS.

Nitrogen gas is used for providing an inert atmosphere. It will also increase the stability of chemicals involved in synthesis (Wang *et al*., 2014). The crude reaction is refluxed (100 °C) after precursor injection to advance QDs growth. Mild reaction conditions and low operating temperatures make the ACS method favourable over organometallic colloidal synthetic (OCS) methods. OCS methods require high temperature (~300 °C) for the reaction. On the other hand, some of the scientific report's emphasis that ACS of QDs is possible even at room or freezing temperature (Sun *et al*., 2012). The stabilizing agents GSH and MPA contain –SH, -COOH and – NH_2 functional groups. They possess a lone pair of electrons that can influence the nucleation, growth and stabilization of QDs. Thiol-type stabilizing agents (GSH and MPA) attach their functional group –SH to the QDs surface during the synthesis process. This leaves the hydrophilic groups available for subsequent bio conjugation processes (Smith *et al*., 2008) and also increases the solubility of QDs. They prevent growth by imposing a kinetic barrier due to the coulombic repulsion. Direct thermal energy is used in this case. pH plays an important role in increasing the solubility of QDs because deprotonation occurs at high pH. GSH was adopted in the synthesis of ZnSe core QDs (Yang *et al.,* 2005). Zheng *et al*., 2007 demonstrated the synthesis of ZnSe QDs with GSH as a stabilizer. The QYs increased from 2% to 22% by this method. GSH molecules are deprotonated to form Zn $(GSH)^{2+}$ complexes. Deprotonation occurs due to the higher affinity of S towards Zn at high pH [Zn^{2+}+GSH→ Zn $(GSH)^{2+}$]. N atom of the amide bond further participates in the coordination after deprotonation at pH above 10.3. Se powders are reduced to NaHSe by $NaBH_4$ solution. Se is reduced to Se^{2-} during this process. Se^{2-} and GSH intensely compete for Zn^{2+}. Stability of complex mainly depends on the concentration of respective reagents. ZnSe has higher stability than the Zn $(GSH)^{2+}$complex. Nucleation of GSH- capped ZnSe occurs by the addition of Se^{2-}. This happens by substituting Se^{2-} for GSH. Se^{2-}energetically favours incorporation into Zn$(GSH)^{2+}$ complexes rather than continuing to displace GSH. As a result, reacted Zn$(GSH)^{2+}$ complexes form larger particles [Zn $(GSH)^{2+}$ + HSe^{-}+OH^{-}→ ZnSe (GSH)+H_2O]. GSH plays a crucial role in the growth and nucleation of QDs. GSH prevents aggregation as well as Ostwald ripening and thereby controls the reaction kinetics. GSH can easily release S^{2-} when heated because of its weaker thermostability. nZnSe (GSH) → ZnSe (GSH)n. Fluorescence intensity of ZnSe core was enhanced by surface passivation using ZnS

shell. The ZnS shell on the core of ZnSe is formed by the thermal decomposition of MPA ligand. This occurs by releasing S^{2-} which will react with zinc source. The possible occurrence of fresh ZnS nucleation is prevented by adding an excess of MPA (Sun *et al*., 2015).

5.2 CHARACTERIZATION OF ZnSe/ZnS QDs

5.2.1 OPTICAL CHARACTERIZATION

The optical characteristics of QDs were explored by UV-visible and fluorescence spectroscopy. It can be seen that the QDs have broad absorption in the UV region and the absorption peak appears at 340 nm. The emission spectrum illustrates a relatively narrow peak at 416nm which is due to the band edge emission.

5.2.1.1 OBSERVATION UNDER U.V LIGHT

Water-soluble ZnSe/ZnS QDs showed greenish-blue fluorescence under ultraviolet light.

5.2.1.2 OBSERVATION UNDER FLUORESCENCE MICROSCOPE

QDs emit blue light upon light excitation in the UV range under DAPI filter. QDs do not emit any light under FITC (green) and RHOD (red) filter.

5.2.2 PHYSICOCHEMICAL CHARACTERIZATION

5.2.2.1 TRANSMISSION ELECTRON MICROSCOPY (TEM)

TEM image showed that the majority of ZnSe/ZnS nanoparticles have a size of 5-6 nm. Hydrodynamic radius and size distribution measurements of these QDs were carried out by the dynamic light scattering method (figure 4.5).

5.2.2.2 DYNAMIC LIGHT SCATTERING (DLS)

The DLS analysis indicates that the majority of particles have a size of 33 nm for ZnSe/ZnS. This can be explained by the fact that the dynamic light scattering determines the size of hydrated and also aggregated quantum dots which are mostly clusters. This includes a stabilizing layer and a solvation sphere formed by the molecules of the dispersion medium.

5.2.2.3 ZETA POTENTIAL

High surface charge produces stable monodispersions in the aqueous phase. The repulsive forces exceed the attractive forces when the zeta potential of an emulsion is high. This result in relatively stable system. Whereas particles between −10 and +10 mV are considered approximately neutral (Clogston and Patri, 2011). High positive or negative zeta potentials greater than 30 mV leads to monodispersity. On the other hand, low values, smaller than 5 mV, can lead to agglomeration. Zeta potential is affected not only by the properties of nanoparticles but also the nature of the solution such as pH and ionic strength (Gumustas *et al*., 2017).

5.2.2.4 FOURIER TRANSFORM INFRARED SPECTROSCOPY (FTIR)

IR spectra of ZnSe/ZnS QDs confirmed L-Glutathione and 3- mercaptopropionic acid (MPA) as mixture stabilizer. Functional groups of these stabilizers could be easily conjugated with various biomolecules. This is directly correlated with the growth mechanism of ZnSe/ZnS QDs. It is clear that the characteristic peak of –SH at the position 2523 cm^{-1} for GSH not present in the ZnSe spectra. This confirming the coordination between Zn atom and thiol (-SH) group. The peak at 2580 cm^{-1} not found in ZnSe/ZnS QDs. This peak is present in MPA arises from the stretching vibration of thiol group. This observation suggests that covalent bond formed between metal atoms of QD and –SH group of MPA.

5.2.2.5 RAMAN SPECTRA

In the case of nanomaterials, confinement of optical phonons can produce obvious changes in their vibrational spectra compared to those of bulk crystals. The broadening of the spectra, the asymmetry of the line shape and the shift of peak. towards lower frequency may be attributed to optical phonon confinement (Prabhu *et al.*, 2008). Characteristics Raman spectra was clearly observed in ZnSe/ZnS QDs (Algamdi *et al*., 2017). The idea about crystallinity and concentration of the substance is obtained from the width and the height of the peak in Raman spectra.

5.2.2.6 INDUCTIVELY COUPLED PLASMA OPTICAL EMISSION SPECTROMETRY (ICP-OES)

Elemental composition of ZnSe/ZnS QDs was quantified by ICP-OES. It was found that ZnSe/ZnS QDs contained Zn (50.03 %) and S (49.86 %) in large quantity. Amount of Se was very less and estimated to be about 0.10 %.

5.2.2.7 X-RAY POWDER DIFFRACTION (XRD)

The crystallographic signature of QDs was determined from their XRD profiles. XRD pattern normally broadens in case of finite nano crystallite size. ZnSe/ZnS QDs have two types of crystalline structures, wurtzite and zinc blende. Wurtzite has a hexagonal structure, while zinc blende is cubic. Zinc blende structure is a "diamond-type network" and the wurtzite structure has hexagonal type symmetry. The structure varies depending on the temperature. The zinc blende structure is structurally and thermodynamically more stable. In the present work, ZnSe/ZnS nanocrystals shift to higher diffraction angles located between the cubic ZnSe and ZnS XRD patterns (JCPDS File No: 32-0483). Moreover, from the XRD pattern, it was demonstrated that ZnS shells epitaxially grew on the surface of the ZnSe core rather than as a simple combination. The lattice parameter of ZnSe/ZnS QDs is found to be a= 5.701. The crystalline structure of ZnSe/ZnS QDs was estimated by using Debye Scherrer equation $D=0.9\lambda/(\beta \cos \theta)$, where D= size of crystallite, λ= wavelength of X- ray (0.1541 nm), β= Full width at half maxima, θ= diffraction angle. Meanwhile, the actual crystallite size of ZnSe QDs according to the Debye Scherrer equation was found to be about 6.56 nm.

5.2.2.8 THERMAL ANALYSIS

5.2.2.8.1 THERMOGRAVIMETRIC ANALYSIS (TGA)

TG is one of the basic methods in thermal analysis. TG provides an idea about the thermal stability of the sample and also about the composition of the initial sample, the intermediate products and the composition of solid residue if any. It is a technique in which the mass of a substance is measured as a function of temperature while a substance is subjected to a controlled temperature program. This measurement provides information about physical phenomena, such as phase transitions, absorption and desorption; as well as chemical phenomena including chemisorptions, thermal

decomposition and solid-gas reactions (e.g., oxidation or reduction) (Shriver *et al*., 2006). 12.92 % weight loss is probably credited to the volatilization of surface adsorbed water and crystal water with a corresponding endothermic peak in the DTA curve. Evident weight loss of about 16.65 % occurs which is perhaps due to the multi- stage thermal decomposition of stabilizers (MPA and GSH). The weight loss starts between 600 °C and 700 °C with a slightly endothermic process. Between 700ºC-1000 ºC, an endothermic peak appearing with a slight weight loss is probably due to further decomposition and gasification of the remaining organic materials.

5.2.2.8.2 DIFFERENTIAL THERMAL ANALYSIS (DTA):

DTA is the oldest thermo analytical method. This is a technique in which the temperature difference between a substance and a thermally inert reference material is measured as a function of the temperature (T). The substance and reference material are subjected to a controlled temperature program in this method. The material under study & an inert reference is made to undergo identical thermal cycles, (i.e., same cooling or heating program) while recording any temperature difference between sample and reference. This differential temperature is then plotted against time or against temperature (DTA curve, or thermogram). Changes in the sample either exothermic or endothermic can be detected relative to the inert reference. Thus, a DTA curve provides data on the transformations that have occurred such as glass transitions, crystallization, melting and sublimation. Melting of ZnSe/ZnS QDs occurs which is an exothermic reaction. The area under a DTA peak corresponds to enthalpy change and is not affected by the heat capacity of the sample (Anthony *et al*., 2014).

5.2.2.8.3 DERIVATIVE THERMOGRAVIMETRY (DTG):

A reliable qualitative and quantitative evaluation of the TG curve is only possible with the DTG curve. The DTG peak height at any temperature gives the rate of mass loss (µg/min). It gives an idea about maximum decomposition temperatures. Here it is 300 ºC at the rate of 167.417 µg/min.

OBJECTIVE 2

IN VITRO EVALUATION OF ZNSE/ZNS QDS WITH HEPG2 AND HEK CELL LINES.

5.3 *IN VITRO* TOXICITY STUDIES USING HEPG2 CELL LINE.

5.3.1 ASSESSMENT OF CELL VIABILITY BY MTT ASSAY

Viability and dose response in HepG2 cells were explored by MTT assay. Mitochondrial activity decreases as concentration and time of exposure increases. Mitochondria are the centres of apoptosis, complicated biological entities and are very sensitive to a multitude of chemical toxins. A progressive time and dose- dependent decline in mitochondrial and lysosomal activity were evident from the results of 24 h exposure. The 6h treatment did not show a visible change compared to the control cells. The results of the study clearly indicated that ZnSe/ZnS QDs severely altered the cellular metabolism at the highest concentration (100 µg/ml) for 24 h treatment. GSH is one of the main stabilizing agents in the ZnSe/ZnS QDs synthesis. It is a key cytosolic peptide that acts as a cofactor for a number of antioxidant and detoxifying enzymes. They are synthesized wholly in the cytosol and have specific carriers to import GSH to the mitochondria to defend against oxidative stress. It is reasonable that these carriers facilitated sequestration of GSH-QDs into mitochondria but without disrupting the respiratory chain or causing cytotoxicity only at high concentration (100 µg/ml) of long exposure (24 h) (Zheng *et al*., 2017). Also, Shu *et al* (2013) treated SCG7901 cancer cells with different concentrations of ZnSe/ZnS QDs for 24 h to determine the effect the nanoparticles. No significant cell death was seen in cells after incubation with low concentrations of ZnSe/ZnS QDs and 40 % cell viability was observed at 100 x 10^{-6}mol/L concentration.

5.3.2 INTERFERENCE OF PARTICLE WITH MTT

Ong *et al.,* (2014) demonstrated that NPs can directly interfere with MTT and would give false results. In the present study, no particles interference was observed.

5.3.3 CYTOTOXICITY ASSOCIATED WITH PARTICLE DISSOLUTION

This toxicity is due to the direct effect of QDs internalization because this study showed that particle dissolution does not occur outside the cell. In 2014, Soenen *et al.*, reported the effect of ZnSe/ZnS QDs on various cell lines: primary human umbilical vein endothelial cells (HUVEC), murine neural progenitor cells (C17.2) and rat pheochromocytoma cells (PC12).

5.3.4 ASSESSMENT OF LYSOSOMAL ACTIVITY BY NRU ASSAY

Cytotoxic effect of ZnSe/ZnS QDs was further established by NRU. Results showed that lysosomal integrity decreases as concentration and time of exposure increases. Neutral red is a cationic dye that can penetrate the cell membrane and accumulates in lysosomes. Viable cells incorporate neutral red inside their lysosomes whereas dead cells will not succeed to uptake neutral red.

5.3.5 PARTICLE UPTAKE BY CONFOCAL MICROSCOPY

ZnSe/ZnS QDs were efficiently taken up by HepG2 cells. It was found that the QDs were distributed throughout the cytoplasm and perinuclear region. The interaction of ZnSe/ZnS QDs does not affect the integrity of the hepatocytes (50 µg/ml). None of the QDs were seen inside the nucleus.

5.3.6 PARTICLE UPTAKE IN PRESENCE OF INHIBITOR

Cytochalasin B is a cell permeable mycotoxin which acts as an actin polymerization inhibitor. Cyto-B treated cells showed similar viability as that of control cells. No cellular uptake of QDs was observed in Cyto-B treated cells. Results showed that cytotoxicity is mainly due to the cellular uptake of QDs. Anionic QDs showed clathrin dependent, independent and also caveolae-independent endocytic pathway in non-phagocytic cells (Frohlich *et al*., 2012).

5.3.7 CELL COUNT BY TRYPAN BLUE EXCLUSION ASSAY

Trypan blue exclusion assay was one of the most common and earliest methods used for cell viability measurement. This was also carried out for the confirmation of the effect of ZnSe/ZnS QDs on HepG2 cells viability. Results showed the same trend as that of MTT and NRU assays.

5.3.8 ASSESSMENT OF CYTOPLASMIC ENZYME RELEASE BY LDH ASSAY

LDH assay investigates the membrane integrity and it is used as a complementary assay for the metabolic activity assay (MTT). Direct contact of cells with nanomaterials causes mechanical disruption of the cell membrane and results in LDH leakage into the culture medium. On the other hand, the formation of reactive oxygen species (ROS) induced by peroxidation of membrane lipids may lead to the loss of membrane flexibility. Also results in an abnormally high release of lactate dehydrogenase inevitably resulting in cell death (Kumar *et al*., 2018). Overall, a significant increase in LDH release from HepG2 cells at concentrations above 12.5 µg/ml occurred. The increased LDH release suggests mechanical damage to the cells.

5.3.9 CELLULAR PHENOTYPE BY PHASE CONTRAST MICROSCOPY

The cytoplasmic extensions of attached cells retract to form a round shape when attached cells are exposed to toxic substances (materials, chemicals and extracts).

5.3.10 MORPHOLOGY ANALYSIS BY GIEMSA STAINING

Morphology changes are an indication of toxicity imparted by ZnSe/ZnS QDs in HepG2 cells. Giemsa staining indicated morphological alterations in HepG2 cells only at the highest concentration (100µg/ ml).

5.3.11 ASSESSMENT OF CHANGES TO CYTOSKELETAL INTEGRITY AND NUCLEAR STRUCTURE

Cooper and Spitzer (2015) demonstrated that a number of NPs are accomplished of disrupting the cytoskeletal arrangement of the cells at sublethal concentrations leading to altered morphology and detachment of cell from the substratum. The changes in the morphology of the cells may be due to the selective disruption of cytoskeletal structure imparted by the particles. In this study, the effect of ZnSe/ZnS QDs on cytoskeletal arrangement and nucleus was analysed by Rhodamine phalloidin and acridine orange staining. The same result as that of Giemsa staining can be seen in rhodamine phalloidine-AO stained cells. Under physiological pH, the actin filaments are usually negative in charge (Li *et al*., 2014). So, negatively charged QDs do not come in interaction with actin filaments. In fixed cells, Acridine Orange (AO) is a metachromatic dye which intercalates into dsDNA and emits green fluorescence

upon excitation at 480-490 nm. Chromatin condensation and nuclear fragmentation are the typical characteristics of apoptosis.

5.3.12 MITOCHONDRIAL MEMBRANE POTENTIAL (MMP) BY JC1

MMP is a key indicator of cellular health condition. Tremendous accumulation of ROS inside the cell causes the collapse of MMP. Loss of MMP is a preliminary step in the activation of intrinsic apoptosis pathway (De Jong and Vandebriel., 2012; Heinicke *et al.* 2016) and it causes cytochrome c explosion from mitochondria to the cytosol leading to apoptosis signalling. The results of MMP showed a minor change in MMP of cells exposed to a high concentration of ZnSe/ZnS QDs as evident from increased green fluorescence of JC-1 probe.

5.3.13 ASSESSMENT OF LYSOSOMAL INTEGRITY BY ACRIDINE ORANGE (AO) STAINING

Acridine orange shows red fluorescence when present inside the lysosomes and green when present in the cytoplasm. Proton pump-driven lysosomal acidity generates a significant pH gradient resulting in the efficient concentration of AO within the lysosome organelles. The destabilization of the lysosomal membrane occurs as a result of QDs inside the lysosome because endocytosis is the main mechanism of QDs uptake by the cells. During this process, the endosomes fuse with the lysosomes to form a phagolysosome. Degradation of QDs occurs at this acidic compartment. A slight decrease in lysosomal integrity observed only at high concentration (100µg/ ml) at 24 h exposure.

5.3.14 FREE RADICALFORMATION

5.3.14.1 ASSESSMENT OF REACTIVE OXYGEN SPECIES FORMATION BY DCFHDA

Too much production of ROS is one of the common mechanisms of the toxic effects of nanomaterials. They can react with macromolecules such as lipids, proteins, DNA, *etc*., which affects the structure and function of macromolecules, and then causes oxidative cellular damage (Cho *et al*., 2007; Juzenas *et al*., 2008; L. Liu *et al*., 2015; Migita *et al*., 2014; Skalickova *et al*., 2013; Tsay & Michalet, 2005; Wang, Gao, & Su, 2010; Wang & Tang, 2018). The result of the study showed an increase in ROS

production as evident from DCFHDA assay only at 24 h exposure of QDs.

5.3.14.2 INFLUENCE OF CATALASE ACTIVITY ON ROS PRODUCTION

Catalase is a ubiquitous antioxidant enzyme that degrades hydrogen peroxide into water and oxygen. They are known as scavengers of ROS. Cytosolic-enzyme catalase (CAT) protects the cells from the damaging effects of reactive oxygen species (ROS). Catalase activity is very high in liver cells (Sani *et al.*, 2006). Influence of catalase on the ROS production was studied by using a catalase inhibitor sodium azide (2 μM). Sodium azide treated samples showed high ROS production. It was noted that catalase activity in the cells can resist the ROS production induced by ZnSe/ZnS QDs in a time and dose-dependent manner.

5.3.14.3 ASSESSMENT OF NITRILE RADICALS FORMATION BY GRIESS REAGENT

Nitric oxide (NO) is a pluripotent gaseous free radical that has been recognized as an important signalling molecule in virtually every tissue in the body. As in the case of other organs, NO has many actions and cellular sources in the liver (Clemens *et al*., 1999). Under inflammatory and stress conditions, hepatocytes are able to convey repeated inducible NO synthase (iNOS) expression. This iNOS expression regulates a number of cell viability as well as cellular functions. Hepatocytes contain mainly two pools of iNOS: a soluble pool composed of both active dimer/monomer and a peroxisomal pool of monomeric iNOS. In long-lived cells such as hepatocytes, iNOS is localized in peroxisomes as a defensive mechanism to remove incompetent enzyme. Nitric oxide (NO) has significant signalling functions within cells but can also bring about cell dysfunction or toxicity (Loughran *et al*., 2005). In the present study, cellular levels of NO produced in HepG2 cells triggered by ZnSe/ZnS QDs or lipopolysaccharide (LPS) (i.e., a pro-inflammatory marker) was examined. It was found that a significantly greater amount of NO was produced when cells were treated with LPS. However, the treatment of ZnSe/ZnS QDs at the concentrations up to 100 μg/ml caused no difference in the amount of NO.

5.3.15 ASSESSMENT OF OXIDATIVE STRESS INDUCED BY QDs

5.3.15.1 PROTEIN ESTIMATION

Protein is the vital biochemical constituent which is present in all biological systems. It is essential for the synthesis of major enzymes crucial for maintaining stable metabolic pathways. No significant changes were observed in proteir concentrations of the ZnSe/ZnS QDs treated HepG2 cells except 100 µg/ml wher compared with control.

5.3.15.2 GLUTATHIONE LEVELS

GSH is a ubiquitous and abundant cellular non-enzymatic antioxidant tripeptide, was found to be sensitive in response to NP treatment (Akhtar *et al.*,2012). The liver is the organ which contains the highest levels of GSH because it involves in GSH synthesis and metabolism. GSH can promote the metabolism of fat, sugar, and protein, and maintain normal cell metabolism and cell membrane integrity. It can bind toxic substances, such as electrophilic radicals and oxygen free radicals, and has extensive antioxidative effects (Chen *et al.,* 2008). Under physiological conditions, the liver can resist oxidative stress through GSH synthesis in hepatocytes. In the present study, GSH can resist oxidative stress by serving as a substrate for antioxidative enzymes including GSH-Px which converts hydroperoxide into less harmful fatty acids, water and GSH disulphide (Day *et al*., 2009). Therefore, GSH can resist ZnSe/ZnS QDs induced oxidative stress.

5.3.16 CELL CYCLE ANALYSIS BY FLOW CYTOMETRY

DNA content is the most often measured cellular constituent. Its quantification serves to assess cell position in the cell cycle, DNA ploidy level and may reveal the presence of apoptotic cells that are characterized by fractional DNA content. Distribution of cells within the major phases of the cell cycle is based on differences in DNA content between the pre-replicative phase cells ($G_{0/1}$) versus the cells that actually replicate DNA (S phase) versus the post-replicative plus mitotic (G_2+ M) cells. Extensive DNA fragmentation is the hallmark of apoptosis. The low molecular weight DNA fragments are extracted during cell preparation and staining. Such cells can be identified as the apoptotic cells with fractional DNA content. They are often defined as ‘sub-diploid’ or ‘sub-G_1’ cell population (Darzynkiewicz *et al*., 2010). G1,

S and G2/M represent percentages of cells in the normal phases of the cell cycle and sub-G1 represents cells that underwent apoptosis/ necrosis (Wahab R *et al*., 2014). HepG2 cells treated with ZnSe/ZnS QDs at different concentrations (except for 100 µg/ ml) do not exhibit induction of apoptosis. This is evident from the appearance of a significant increase in the number of cells in the sub G1 phase compared to that of control. A slight change in sub G1 level was observed at 100 µg/ ml concentration alone but not that much significant.

5.3.17 DNA LADDER ASSAY

DNA ladder assay is a simply available method and seems to be very useful for quick screening of apoptotic changes in cell populations. This method allows for working with cell lysates. DNA ladder assay makes the obvious hallmark of apoptosis – mono and oligonucleosomal DNA fragments (Rahbar *et al*., 2015)**.** In the present work, the ladder pattern of DNA cleavage was not exhibited in any of the treated DNA samples. This may be due to the size that prevents them from entering the nucleus or because of the surface charge carried by QDs. The negative charge of the QDs repelled with negatively charged DNA. Negatively charged NPs have no effect on the cell cycle (Liu *et al*., 2015).

5.3.18 LIVE /DEAD ASSAY BY CALCEIN AM-PI

An intact plasma membrane and ubiquitous intracellular esterase activity are distinguishing characteristics of live cells. Calcein is permeable to live cells and staining with green-fluorescent calcein-AM to indicate intracellular esterase activity and red fluorescent PI to indicate loss of plasma membrane integrity. It is adaptable to most eukaryotic cells where cytotoxic conditions produce these cellular effects. In the present study, the cells treated with ZnSe/ZnS QDs showed dose and time-dependent cell death.

5.3.19 CASPASE 3/7 ACTIVATION ASSAY

Caspase is a family of intracellular cysteine endopeptidases that are activated during the apoptotic cell death. It is an important biochemical feature of apoptotic cell death. Caspases are synthesized as inactive proenzymes which are transformed into active heterodimers by proteolytic cleavage and are accountable for the purposeful disassembly of cells into apoptotic bodies. The initiator caspases 8 and 9 and the

executioner caspase 3 are positioned at central junctions in the apoptotic pathways. The activation of the initiator caspases in response to extracellular cytotoxic agents like QDs activates the executioner caspase 3. This activation results in a series of events that lead eventually to cell lysis and disruption of normal cell processes (Payne *et al*., 2013). The present study showed a dose and time-dependent slight increase in the level of caspase enzyme indicating that cell death occurs at 100 µg/ ml of ZnSe/ZnS QDs at 24 h of exposure. This could be due to cellular apoptosis by other mechanisms like necrosis, pyroptosis *etc*.

5.4 IN VITRO TOXICITY STUDIES USING HEK293 CELL LINES.

5.4.1 MTT ASSAY

The capability of mitochondrial dehydrogenase enzyme of live cells to convert yellow tetrazolium to purple formazan was assessed. A dose-dependent slight decrease in cell viability was observed in ZnSe/ZnS QDs exposed HEK after 24h. These results substantiate with the findings from HepG2cells treated with ZnSe/ZnS QDs.

It can be seen that the cell viability of the HEK was almost similar to the result demonstrated by C Shu *et al* (2013). They established that no significant cell death was seen in mouse mononuclear macrophage cell line RAW264.7 after 24h incubation with ZnSe/ZnS QDs. Significant cytotoxic effect of ZnSe/ZnS QDs is drastically increased only at the highest concentration (100 µg/ ml) of 24h exposure. In all other cases, ZnSe/ZnS QDs was non cytotoxic. This reduction in toxic effect of ZnSe/ZnS QDs may be because the elements Zn as well as Se may be used as a source of energy and metabolism by cells and therefore support growth and division of the cells. It becomes toxic to cells only at high concentration and upon prolonged exposure.

5.4.2 PARTICLE DISSOLUTION AND RELATED TOXICITY

Correlation between dissolution behaviour and nanoparticle toxicity was studied in many of the experiments. For example, Lee *et al.,* (2018) demonstrated rapid dissolution of Ag^{+} ion from AgNPs resulted in the toxicity of zebrafish embryos. Potential toxicity and bioavailability of QDs influenced by their dissolution. Earlier studies revealed that the toxicity of cadmium based QDs is mainly because of the release of cadmium ions (King *et al*., 2009; Wiecinski *et al*., 2013). It is disputed

whether the toxicity is due to particle dissolution inside cellular compartments or in the cell culture medium. In the present study, medium supernatant of ZnSe/ZnS QDs do not induce toxic effect when compared to direct effect. Results demonstrate that ZnS shell protects core ZnSe from dissolution.

5.4.3 NEUTRAL RED UPTAKE ASSAY (NRU) ASSAY

Viable cells actively uptake neutral red into the lysosomes on contrary to non-viable ones. In the present study, HEK cells showed a dose-dependent increase in cell death when exposed to ZnSe/ZnS QDs for 24 h. The toxic effect induced by ZnSe/ZnS QDs is not because of the dissolution in the medium.

5.4.4 TRYPAN BLUE EXCLUSION ASSAY

Trypan blue exclusion assay was carried out for the confirmation of the effect of ZnSe/ZnS QDs on HEK cells viability. Results showed the same trend as that of MTT and NRU assays.

5.4.5 PARTICLE UPTAKE BY CONFOCAL MICROSCOPY

The confocal microscopic image clearly showed the cellular uptake of blue fluorescent ZnSe/ZnS QDs and that it does not affect the integrity of HEK cells. It was found that the ZnSe/ZnS QDs were distributed throughout the cytoplasm and perinuclear region. These particles have no interaction with the nucleus.

5.4.6 PARTICLE UPTAKE (ZnSe/ZnS QDs) IN HEK CELLS BY FLOW CYTOMETRY

Uptake of ZnSe/ZnS QDs by HEK was assessed using flow cytometry. Flow cytometry analysis is a popular technique employed for the nanoparticle uptake studies based on the side scattering (SSC) pattern change corresponds to the granularity of cells (Suzuki *et al.* 2007). Uptake of carbon dots by macrophages was analysed using flow cytometry by Thoo *et al* in 2017. The flow cytometry analysis revealed a concentration-dependent increase in SSC pattern in cells treated with ZnSe/ZnS QDs.

5.4.7 UPTAKE INHIBITION BY CYTOCHALASIN B

Uptake of the QDs by HEK cells was inhibited by cytochalasin B. Cyto. B is a chemical derived from a mold which prevents endocytosis by disrupting F actin

filaments and also by inhibiting the actin polymerization. i.e. actin filament-filament interactions which normally contribute to network formation (MacLean Fletcher *et al*, 1980). Result of the study indicates that endocytosis is the mechanism of QD uptake by HEK. Cyto B treated cells showed similar viability as that of control cells demonstrated that cellular uptake of QDs was not observed in Cyto-B treated cells. This result implies that cytotoxicity is mainly due to the cellular uptake of QDs.

5.4.8 LDH ASSAY

LDH release due to mechanical damage caused by ZnSe/ZnS QDs in HEK was assessed after 6 and 24 h of treatment. There was no marked increase in LDH levels in ZnSe/ZnS QDs exposed cells except at 100 µg/ml denoting that these QDs did not cause membrane damage.

5.4.9 PHENOTYPIC OBSERVATION BY PHASE CONTRAST MICROSCOPY

The cell morphology analysis is a simple and more reliable indicator of cytotoxicity. The morphological observations lend a hand in better understanding of cell viability data. It was observed from the results of Phase images that there was no noticeable change in cell morphology upon ZnSe/ZnS QDs exposure.

5.4.10 COOMASSIE BRILLIANT BLUE STAINING FOR MORPHOLOGY ANALYSIS

Coomassie G-250 has meticulous properties that enable it to be used to produce a rapid and convenient staining procedure. In the staining reaction, the Coomassie dye binds to proteins through ionic interactions between sulfonic acid groups and positive protein amine groups through Van der Waals attractions (Tal *et al.,* 1985). Morphological alterations were visible on cells treated with a higher concentration (100 µg/ml) of QDs.

5.4.11 MMP BY JC-1

Loss of MMP is the indication of apoptosis. Loss of MMP is presumed to be due to the opening of mitochondrial permeability transition pore (MPTP). This leads to the release of cytochrome c and triggers apoptosis. Exposure of HEK cells to ZnSe/ZnS QDs induced a dose and time-dependent loss of MMP similar to the effect seen in the HepG2.

5.4.12 LYSOSOMAL INTEGRITY BY AO STAINING

Stability of lysosomes in living HEK cells was assessed by using the dye Acridine Orange (AO). It is a lipophilic amine that readily diffuses into the cells. Inside the cell, AO gets protonated by the acidic pH of lysosome and emits red colour. Upon QD induced loss of lysosomal pH gradient and consequent leakage of AO into the cytosol, red emission will shift to green. In the present study, lysosomal integrity was lost very slightly as the concentration of ZnSe/ZnS QDs increased and quantitatively measured as 'loss of red dots' with slight gain of green fluorescence. Slight loss of red dots was showed by the 100 µg/ml QD treated cells when compared with control cells. Stability of ZnSe/ZnS QDs in acidic pH was established by Soensen *et al.,* (2014). Results of their study showed that fluorescence intensity does not reduce in acidic pH over for several days which implies their chemical stability. They do not get degraded by acid etching. So, no release of component ions to the surrounding environment and do not induce toxicity. This result supports the data of present work.

5.4.13 FREE RADICAL FORMATION

Induction of oxidative stress is known to be closely related to the use of zinc-containing NPs. If this oxidative stress persists over longer time periods or reaches higher levels, the cell system produces reactive oxygen species (ROS) such as superoxide, hydroxyl radical, hydrogen peroxide and reactive nitrogen species (RNS) like nitric oxide and peroxynitrite can result in cell death (Soenen *et al.*, 2014). The ability of ZnSe/ZnS QDs to induce ROS and RNS in HEK was investigated since oxidative stress is a major mechanism of nanomaterial toxicity.

5.4.13.1 DETECTION OF ROS PRODUCTION

A clear generation of reactive oxygen species (ROS) is established by the Soenen *et al.,*2014 and reaching significant levels at 30 nM for ZnSe QDs. The higher level of oxidative stress for the ZnSe QDs suggests the important role of ROS in QD cytotoxicity. ZnSe/ZnS QDs were incubated with HEK for 6h and 24 h. As observed in HepG2 cells, QDs were unable to evoke ROS generation at 24h. This effect may be either because of aggregation of QDs or because of ROS scavenging property of glutathione. The quantitative analysis of ROS can often be caught up by the intracellular presence of high levels of thiol or Sulfhydryl radicals formed by glutathione along with other agents can produce the scavenging of ROS (Cossarizza *et al., 2009).*

However, 6 h exposure to a high concentration of ZnSe/ZnS QDs led to an increased ROS generation in HEK. Catalase inhibitor sodium azide (0.2 μM) was used to study the influence of catalase on the production of ROS in HEK cells. This exposure resulted in a slight increase in ROS in sodium azide treated samples.

5.4.13.2 INFLUENCE OF CATALASE ON ROS PRODUCTION

Catalase plays a central role in ROS detoxification (Sani *et al.*, 2006). Influence of catalase on the ROS production in HEK cells were studied by using a catalase inhibitor sodium azide (2 μM). Sodium azide treated samples showed high ROS production when compared with sodium azide untreated cells. It was noted that catalase activity in the HEK cells can resist the ROS production induced by ZnSe/ZnS QDs in a time and dose-dependent manner.

5.4.13.3 NITRIC OXIDE PRODUCTION BY GRIESS REAGENT

Endothelium-derived NO is synthesized within the kidney and it plays a decisive role in the regulation of renal hemodynamics and excretory function (Bachmann *et al.*, 1994). In the present study a negligible increase in NOS production was observed in HEK cells when compared to control.

5.4.14 ASSESSMENT OF OXIDATIVE STRESS

5.4.14.1 PROTEIN ESTIMATION

Protein estimation in HEK cells followed by treatment with ZnSe/ZnS QDs confirmed that a substantial decline of protein concentration was observed in a dose dependent manner. Protein synthesis is one of the fundamental functions of cells which control all the metabolic activities take place inside the cells. Variation in protein synthesis is not perfectly related to a single biochemical system. Changes can also occur due to interactions of QDs with subcellular organelles such as the nucleus, ribosomes, endoplasmic reticulum, cytoplasm and cytoskeleton.

5.4.14.2 ESTIMATION OF GSH CONTENT

In most cells the GSH concentration is about 1-2 mM in the cytosol. Glutathione plays major roles in the different cellular compartments. In mitochondria it plays a key role in regulating apoptosis versus necrosis. GSH may be used as a marker of oxidative stress because it is considered to be one of the most important

scavengers of ROS. Results obtained for the particular study points out that, GSH level got decreased with increasing the concentration of NPs. This finding could be a sign of oxidative stress as the main toxicity mechanism. It is known that GSH is an obligatory component for preservation of thiol groups which protects mitochondria against permeability transition or opening of MPT pores and oxidative stress. The inverse linear relationship between the ROS level and the GSH level indicated that free radical species were generated by exposure to the ZnSe/ZnS QDs with decreased mitochondrial and cellular antioxidant levels.

5.4.15 DNA LADDER ASSAY

The DNA laddering technique is used to visualize the endonuclease cleavage products of apoptosis. One of the most characteristic features exhibited by cells undergoing apoptosis is the fragmentation of DNA into oligonucleosomal fragments, which can be observed as DNA laddering when genomic DNA is subjected to agarose gel electrophoresis (Barry *et al.*, 2000). Here in this study, no DNA laddering was observed in any one of the treated groups which indicated that QDs do not interact with DNA due to their negative charge.

5.4.16 LIVE DEAD ASSAY BY CALCEIN AM-PI

Calcein AM is able to penetrate viable cell membranes, producing an intense uniform green fluorescence in viable cells. PI is only capable of entering damaged membranes and gives red fluorescence upon binding to nucleic acids, thereby producing a bright red fluorescence in dead cells. Flow cytometric data showed dose and time dependent effect on cell viability.

5.4.17 APOPTOSIS BY ANNEXIN-PI FACS

Oxidative stress provoked in cells as a result of NPs exposure in turn activates apoptosis (Manke *et al*., 2013). The results of the DCFHDA assay showed slightly increased ROS generation in cells only after ZnSe/ZnS QDs exposure. Hence the effect of ZnSe/ZnS QDs to induce apoptosis in HEK cells was investigated using Annexin V/PI staining. The cells treated with ZnSe/ZnS QDs showed cell death in which few apoptotic cells and more necrotic cells were observed.

5.4.18 CASPASE 3/7 ACTIVATION ASSAY

Activation of caspase enzymes is one of the distinctive features of the early stages of apoptosis, which play a part in the cleavage of protein substrates and in the consequent disassembly of the cell (Guo *et al*., 2002). Activity of major executioner caspases (caspase 3 and caspase 7) were studied in HEK cells following ZnSe/ZnS QDs treatment for 6 and 24h. The results of the study revealed that no significant increase in caspase activity was monitored in cells exposed to ZnSe/ZnS QDs compared to control cells.

OBJECTIVES 3

PART I: ACUTE TOXICITY, IMMUNOTOXICITY, HAEMATOLOGICAL, CLINICAL BIOCHEMISTRY, OXIDATIVE STRESS AND HISTOPATHOLOGICAL STUDIES.

Possible acute toxic effect of ZnSe/ZnS QDs of dose 10mg/kg body weight was studied by administration to mice intravenously and intraperitoneally. Acute toxicity is intended to verify the adverse effects within a short period of time. This determines the dose-response relationship and lethal dose. Toxicity is mainly influenced by dose of nanomaterials. ZnSe/ZnS QDs lack a definite 'No Observed Adverse Effect Level' (NOAEL). 10 mg/kg body weight dose is selected in this study which is commonly used for clinical application. For ZnSe/ZnS QDs, 10 mg/ kg body weight is the maximum feasible dosage in aqueous solution to obtain fully soluble solution in saline. Mice are the preeminent model and were selected for this study due to their resemblance to humans in physiological, anatomical, cellular, biochemical, molecular and metabolic pathways. Also, the mouse shares with human's brain functions, such as hunger, anxiety, circadian rhythm, memory, aggression, sexual behaviour and other emotional responses. Therefore, human behavioural responses under physiological and pathological conditions are approximated with mice models for toxicological screenings. They are also small in size, have short generation time, and ease of breeding within the laboratory which further makes them ideal *in vivo* models (Van meer *et al*., 2005).

5.5 CLINICAL SIGNS OF EXPERIMENTAL ANIMALS

Cage side observation of various clinical symptoms in mice post ZnSe/ZnS QDs injection showed that it was well tolerated. Mice did not show any signs of morbidity or mortality after ZnSe/ZnS QDs injection. Eating, drinking, grooming, movement, hunched posture, piloerection, responsiveness to the surroundings, skin elasticity, facial expression of pain like orbital tightening, nose and cheek bulge, contraction of skin around the nose, ear position, whisker change and urination of the treated mice were normal throughout the observation period and well comparable with control animals. The CdSe/ZnS-treated mice died within a short time after i.p injection and even in some cases mice died almost instantly after the injection (Valipoor *et al*., 2015). In the current study single i.v. and i.p. administration of ZnSe/ZnS QDs at a dose of 10 mg/kg body weight did not induce any of clinical or behavioural response in mice.

5.6 BODY WEIGHT GAIN OF ANIMALS

The fluctuation of body weight, a useful indicator for qualitative assessing *in vivo* toxicity of NPs, was recorded every day of the entire experiment. Weight loss is a direct effect of a nanoparticle exposure because of particle interference with general physiology of animals. In the present study there was no weight loss in the organs was noted when exposed (i.v. and i.p.) to ZnSe/ZnS QDs at a dose of 10 mg/kg body weight. The body weight of the control group and the three experimental groups of mice exhibited comparable increasing trends over the observation period of post- injection. This further suggests that QDs did not interfere with the growth rate of the animals. Toxicological studies notify that it is useless to express the organ weights inrelative terms (organ to body weight ratio) because it increases the error rate and leads to misinterpretation of treatment effect (Hayes and Kruger *et al*., 2014).

5.7 URINE ANALYSIS

Urine parameters are not altered as a result of ZnSe/ZnS QDs treatment. Urine analysis did not show any trace of blood or protein. The various parameters like ketones, nitrite, leukocytes, *etc.* in the urine of treated mice were

normal. Present study confirms that single exposure of 10mg/kg ZnSe/ZnS QDs do not alter the kidney structure and function. Choi *et al.,* reported that glomerular filtration preferred by the particles larger than 10 nm (2007).

5.8 HAEMATOLOGY ANALYSIS

Haematology is the study of blood and usually refers to the study of its cellular components, including erythrocytes or red blood cells (RBCs), leukocytes or white blood cells (WBCs), and platelets. QDs can have adverse effects on haematological markers, and thus haematological parameters are an important part of assessment for the clinical applications of QDs (Dobrovolskaia *et al*., 2007). The slight increase in WBC is possibly in response to events in the liver at the time-point post injection. Slight increase of RBC and platelets occur when oxygen is deficient and inflammation occurs. Increase in RBC is also correlated with increased level of HCT value. HCT increases when dehydration occurs and may lead to decline in levels of fluid in blood. As a result, RBCs per volume of fluid falsely rises. With adequate fluid intake, the hematocrit returns to normal level. Other hematological markers like Haemoglobin content, MCV, MCH, MCHC in the QD injected groups remained statistically indistinguishable compared to control group at all-time points and injected doses.

5.9 CLINICAL BIOCHEMISTRY

Toxicity in liver cannot be ignored since it is the major accumulating and metabolizing organ for QDs. ALT (SGOT) and AST (SGPT) are the two aminotransferases located in the liver and muscles. ALT distributes in the cytoplasm mainly while that of AST in the cytoplasm and mitochondria (Yang *et al*., 2014). Loss of cellular integrity of theses tissues leads to enzymes release into the blood. By measuring a variety of factors in the serum, it is possible to assess liver function, liver cell injury, and liver obstruction (Dufour *et al*., 2006). Alanine aminotransferase (ALT) is specific for cellular damage in the liver (Tapper *et al*., 2012). Aspartate aminotransferase (AST) is also valuable but not specific. Reduction in liver function can be assessed by substances produced by the liver including albumin, globulin, total protein, alkaline phosphatase (ALP), and heme catabolism cholestasis by total bilirubin. For factors like ALT and AST, fold changes are indications of toxicity. Change of 20% can result from a

high body mass index, exercise or hemolysis prior to separation of blood cell fraction (Dufour *et al*., 2000). In this study, a minor increase in plasma levels of liver enzymes (ALT, AST and ALP), in association with increased WBC at 10 mg/kg was observed after injection which is consistent with a low grade, sub-lethal disturbance of hepatocytes.

Creatinine and blood urea nitrogen (BUN) are the indicators of kidney function. Creatinine is the most commonly used endogenous marker for assessment of glomerular function. Creatinine is the by-product of creatine phosphate in muscle, and it is produced at a constant rate by body. Creatinine is cleared from the blood completely by the kidney. Increased creatinine level in blood is as a result of decreased clearance by kidney. BUN is a nitrogen-containing compound produced in the liver as the final product of protein metabolism and urea cycle. About 85% of urea is eliminated through kidneys; the balance is excreted by means of the gastrointestinal (GI) tract. Serum urea is increased in conditions where renal clearance decreased and also conditions not linked to renal diseases such as upper GI bleeding, dehydration, catabolic states, and high protein diets. Urea may be decreased in low-protein diet, starvation, and severe liver disease. Serum creatinine is a more perfect assessment of renal function than urea. But in renal diseases, urea is increased earlier (George *et al*., 2019). Results did not indicate significant toxicity compared to control animals and reflected normal variation present in populations of mice.

5.10 ORGAN WEIGHT

Liver, kidney and brain showed no significant differences in mass in comparison with the control. However, weights of spleen in ZnSe/ZnS QDs treated groups were significantly lower than controls at 3rd day post injection. Injected ZnSe/ZnS QDs accumulated in the spleen which could due to uptake by the resident phagocytes in the spleen i.e. macrophages and B cells that are part of the MPS indicating possible translocation of ZnSe/ZnS QDs *in vivo*. Visible changes were not seen in spleen weight on the other observation days (7th and 14th day) implies that QDs were cleared on subsequent days. A relatively small amount of ZnSe/ZnS QDs were accumulated in the liver, kidney and brain.

5.11 HISTOPATHOLOGY

Histology provides qualitative macroscopic and visual evidence of toxicity. QDs exposure led to atrophic lesions in liver on 7^{th} and 14^{th}day of observation. No other histopathological variations were observed other than a slight congestion upon long term exposure (14^{th} day). Megakaryocytes were observed in histological image of spleen. Megakaryocytes are precursors of platelets. In the neonate animals, spleen is the site of hematopoiesis. Megakaryocytes presence indicates that animal is young. Spleen and brain did not show any pathological abnormalities associated with QDs treatment. Necrosis was not found in any of the histological samples analysed. Histological examination did not show any severe symptoms of toxicity but moderate pathological changes were observed only in the liver on 7^{th} and 14^{th} days of QDs exposure.

5.12 ANTIOXIDANT ASSAY

Induction of oxidative stress is one of the main mechanisms involved in the QD toxicity. Oxidative stress status of liver and brain was analysed by stress markers like LPO, GSH, GR, GPx and GR activity. In living organisms, lipid peroxidation is a well established index of cellular injury and is used as an indicator of oxidative stress in cells and tissues. These lipid peroxides are not stable and decompose to form a complex series of compounds such as reactive carbonyl compounds. MDA is one of the byproducts of LPO. Measurement of MDA has been used as an indicator of lipid peroxidation. In the current study, the level of MDA in the liver significantly increased in a dose dependent manner. This indicates the lowest values of the free radical clearance rate of the liver. The time course study showed that the levels of MDA reached their peak values at 7 days (i.p.) in case of brain tissue. These results are also in accordance with the report by wang *et al.,* (2006) that $\cdot$OH generation reached a peak value at 7^{th} day. Both the oxidative stress and the increased anti-oxidative enzyme levels induced by 10 mg/kg ZnSe/ZnS QDs indicate the elevated antioxidant capability of hepatocytes and neurons.

GSH plays an important role in the endogenous antioxidant system. A high concentration of GSH is found in the liver and brain hence it is known to have a key function in the protection process. ZnSe/ZnS QDs decreased the

hepatic and brain GSH contents, indicating that the ZnSe/ZnS QD-induced antioxidant capacity reduction in the liver and brain is associated with GSH depletion. It was believed that activity of GR may be the major determinant that regulates GSH/GSSG (Hazelton, 1985). Glutathione peroxidase and SOD are the major antioxidative enzymes in cells that can look after polyunsaturated fatty acid (PUFA) from lipid peroxidation by reducing H_2O_2 and superoxide radical (Wang *et al*., 2017). SOD quenches the free radical superoxide by converting it to peroxide, which can then be inactivated by reactions catalysed by GPx. GPx is the most important H_2O_2 scavenging enzyme, closely associated with the maintenance of reduced glutathione (Brunetti *et al*., 2013).

5.13 IMMUNOTOXICITY BY SPLENOCYTE PROLIFERATION ASSAY

Immunotoxicity of ZnSe/ZnS QDs was studied by splenocytes proliferation assay. Spleen is the major immune organ consisting of B-lymphocytes and accessory cells including macrophages. Systemic immune response induced upon exposure to ZnSe/ZnS QDs was analysed by this method. In the current study slight change in splenocytes proliferation was observed only on 3rd day, whereas no changes were seen on subsequent days. This results suggest that single exposure of ZnSe/ZnS QDs at a concentration (10 mg/Kg) induce inflammatory responses in mice only on 3rd day and eliminate by means of phagocytosis, without such effects in subsequent days.

5.14 BLOOD BRAIN BARRIER (BBB) INTEGRITY

The brain volume changes in response to injuries, inflammation and disruption of BBB. However, in the present study there was no ZnSe/ZnS QDs mediated volume changes in treated mice demonstrating that ZnSe/ZnS QDs exposure at the given concentration does not cause mechanical damage and oedema. Ou *et al*., reported that positive charged nanoparticles alter the BBB integrity and permeability when compared to negatively charged or neutral nanoparticles (2018). ZnSe/ZnS QDs and external membrane of endothelial cell have negative charge repel with each other.

PART 2: ELEMENTAL ANALYSIS, BIO DISTRIBUTION AND ADME & T (ABSORPTION, DISTRIBUTION, METABOLISM, EXCRETION AND TOXICITY) PROFILING STUDIES.

5.15 BIO DISTRIBUTION BY ELEMENTAL ANALYSIS

Pharmacokinetics of nanoparticles has to be fully explored by studying the process of absorption, distribution, metabolism, excretion (ADME), undesired toxicities and side effects caused by them (Choi and Frangioni, 2010). Various methods to measure QDs in tissues were explored. The use of fluorescence to quantify QDs distribution in tissues was judged to be challenging, owing to the elevated and erratic background fluorescence from blood and tissues. In addition, the fluorescence of the QDs is found to be liable to environmental factors inside the body. Quantum yield has been established to change drastically with surface chemistry, solvent effects, and photo enhanced oxidization (Fischer *et al*, 2006).

Any of these factors would bring large error deviations in fluorescence measurements. Radio labelling has been regularly employed to track injected species in pharmacokinetic studies. However, in present study, the synthesized QDs cannot be applied for radiolabelling procedures since the synthesis protocol opted for QDs here is not suitable for the mentioned purpose. On account of these limitations, concentration of elements like zinc, selenium and Sulphur determined by inductively coupled plasma optical emission spectroscopy (ICP-OES) was considered as the total QDs present in the system.

ADME studies are vital to determine the fate of NPs in biological system. Absorption refers to movement of particle from site of administration to blood stream. Further movement of NPs from blood stream to different body loci is referred to as distribution. Here also the rate of blood clearance of QDs was determined, followed by examined the uptake of QDs into the various organs (liver, kidney, spleen and brain) after leaving the blood stream. Faeces and urine were collected and analysed to determine if the QDs were cleared via the bile, intestinal lumen or kidney. There are two major excretion pathways available to metal- containing particles: through the kidneys into urine or by way of the liver's biliary system into faeces. It was evident from ICP-OES results that ZnSe/ZnS QDs was distributed in all the major organs such as liver, kidney, spleen and brain. Presence

of ZnSe/ZnS QDs was obvious in all organs throughout the experimental period and the percentage of distribution and kinetics varied with time.

Many reports claim that *in vivo* translocation and bio distribution of NPs are greatly influenced by the route of administration. Intravenously injected NPs come in interaction with circulatory system and translocate to organs such as liver, spleen, lymph nodes, small intestine, lungs, brain and kidneys. Following i.p administration, the NPs first translocate to liver through portal circulation and endure biotransformation or excrete into bile (Zhang *et al*., 2018).

The intensity of ZnSe/ZnS QDs in blood was increased with time and the lowest concentration (but more than control) of ZnSe/ZnS QDs was observed at the end of 14^{th} day (i.p. and i.v.). This confirms that these QDs are not likely to get cleared from the blood and if once achieve, they would then distribute to various organs from the systemic circulation. After intravenous administration, ZnSe/ZnS QDs was rapidly absorbed from systemic circulation and distributed to liver and kidney after 3 days of exposure. Maximum amount of ZnSe/ZnS QDs was seen in liver and kidney after 3 days of post exposure followed by spleen and brain. The percentage of ZnSe/ZnS QDs was decreased in subsequent days. In both type of exposure routes, those QDs accumulated in liver and kidneys were excreted through faeces and urine respectively on 14^{th} day of post exposure. Majority of QDs were bound to protein and then aggregated into larger particles. These were metabolized in the liver and excreted via faeces. Smaller QDs possessing a size of <5.5 nm was found to effectively cleared through urine and bile. Similar observation was previously being reported by Choi *et al*. (2007) in which Cysteine coated CdSe/ZnS QDs of 5.5 nm size and a zwitter ionic charge was effectively cleared from the body through urine and bile. In the present study, hydrodynamic diameter of ZnSe/ZnS QDs was found to be 33.31 nm which is obviously above the threshold for direct renal clearance. Only minor quantities of Zinc and Selenium were detected in the kidney initially. Subsequently, this level showed a slight hike during 14^{th} day of post exposure. This observation points out that ZnSe/ZnS QDs tends to undergo intracellular degradation and subsequently release the products (Zn and Se ions) through renal route. It was observed that maximum uptake of ZnSe/ZnS QDs was in spleen at the end of 3^{rd} day and its presence decreased in subsequent 7^{th} and 14^{th} days of both i.v and i.p cases. Kennel *et al*., (2008) has proposed that clearance

of QDs which have migrated to spleen occurs primarily by phagocytic cells of the reticuloendothelial (RE) system. This suggests that QDs internalized by phagocytic cells in spleen represent those QDs which are prone to get eliminated. Presence of ZnSe/ZnS QDs was evident in brain (i.p. and i.v.) suggesting that ZnSe/ZnS QDs has the potential to cross blood brain barrier and accumulate in brain. In 2019, Javidi et al., demonstrated that pharmacokinetics and bio distribution of Ag2S QDs were strongly dependent on dose, particle size and surface charge. They suggest that QDs having a small size (around 5 nm), positive surface charge and administering at a relatively low dose cleared quickly while large sized negatively charged ones do not get easily excreted if they are injected in high dose. In nutshell, present study confirms the fact that ZnSe/ZnS QDs can be used as a drug carrier conjugate, because of their larger hydrodynamic size (around 33 nm) and negative surface charge, which show longer biological half-life at 10 mg/kg dose. This can also be used for labelling and/or imaging applications because of their tendency for excretion and may get completely excrete if exposure time is more than 14 days.

CHAPTER 6: SUMMARY AND CONCLUSION

6 SUMMARY AND CONCLUSION

6.1 SUMMARY

ZnSe/ZnS QDs are type II-VI semiconductor nanocrystals with various optoelectronic, chemical and biomedical applications. They are widely used in the Photovoltaic devices, solar cells and light emitting devices. Nowadays, heavy metal "Cadmium" is the common component in most of the widely used QDs. Cadmium is a proven carcinogen with LD50 of 100-300 mg/kg. Hence Cd-QDs applications are currently restricted in both industrial and biomedical applications due to their uncertain biological fate and potential toxicity. ZnSe/ZnS QDs are considered as environment friendly broadband gap nanoparticles, which are investigated for their suitability in cadmium free blue-green light emitting applications and highly sensitive cellular imaging and drug delivery. However, data on toxicological aspect of ZnSe/ZnS QDs is largely lacking. Present study evaluated cytotoxicity of ZnSe/ZnS QDs in human liver *in vitro* model HepG2 and HEK cells. Liver is the key organ for detoxification of xenobiotics by metabolism and biliary excretion. The kidneys are responsible for eliminating waste products from the blood via urine. Therefore, understanding the toxicity mechanism of QDs in the liver and kidney is critical. Further its associated toxicity at molecular level was evaluated in Swiss Albino mice. In the present study, strong blue emitting water dispersible QDs was effectively synthesized by aqueous phase route using 3-mercaptopropaonic acid (MPA) and L- Glutathione (GSH) were used as mixture stabilizers. Here ZnSe/ZnS QDs synthesised via green synthetic method by employing nontoxic reaction precursors and reaction media (water); use of mild reaction conditions and achieving maximum yield of product with minimum waste production. Synthesised QDs were further subjected to various optical and physicochemical characterizations. Absorption and emission spectra of ZnSe/ZnS QDs was analysed. ZnSe/ZnS QDs observed under UV lamp and blue filter of fluorescent microscope showed greenish blue and blue fluorescence respectively. ZnSe/ZnS QDs were physico-chemically characterized by TEM, DLS, zeta potential analysis, FTIR, Raman spectra, ICP- OES, XRD, Thermal analysis by TGA, DTA and DTG.

In vitro bio nano interaction was studied by using HepG2 and HEK cells.

Cellular uptake, cell viability, cell number, morphological changes, cytoskeletal arrangement, ROS production, NOS production, MMP, lysosomal stability, oxidative stress, mechanism of cellular death were investigated by various cytotoxicity assays.

In vivo acute bio-nano interactions of ZnSe/ZnS QDs were carried out in mice at a dose of 10mg/kg body weight by means of i.v. and i.p. injections. All the animals exposed to ZnSe/ZnS QDs were examined for behavioural and clinical changes of toxicity, stress, and body weight changes throughout the observation period. All the animals were euthanized at the end of 3rd, 7th, and 14th day of observation period and organs were collected for further experiments. The blood samples were subjected to haematology and clinical chemistry analyses. Brain, liver, spleen and kidney were collected for histopathology analysis. Spleen was subjected to immunotoxicity and antioxidant assay was carried out on liver and brain. Along with the isolated tissues, blood, urine and faeces were used to study bio distribution and toxic kinetics by ICP- OES.

6.2 METHODOLOGY ADAPTED FOR THE STUDY

- ZnSe/ZnS QDs were prepared by 'green' aqueous colloidal synthetic (ACS) method.
- Sodium borohydride ($NaBH_4$) is the reducing agent; GSH and MPA are the stabilizing agents in the synthesis of ZnSe/ZnS QDs.
- pH is adjusted to 10.5 and 9.5 in the first and second step of synthesis and temperature was maintained at 100 ºC.
- Optical characterization was done by absorption and emission spectra analysis and fluorescence was observed under U.V light and fluorescent microscope.
- Physicochemical characterization was performed by TEM, DLS, Zeta potential analysis, FTIR, Raman spectra, ICP- OES, XRD and Thermal analysis by TGA, DTA and DTG.
- HepG2 cells were cultured in DMEM with 10% FBS.
- Cytotoxicity and cell viability of ZnSe/ZnS QD exposed HepG2 by MTT and Neutral red assay.
- Evaluated the QDs interference with the MTT.
- Estimated cytotoxicity associated QDs dissolution.

- Cytotoxic potential of ZnSe/ZnS QDs confirmed by trypan blue exclusion assay, LDH assay.
- Monitored cellular phenotype by phase contrast microscopy.
- Evaluated the cellular uptake of ZnSe/ZnS QDs by confocal microscope and also in the presence of Cyt B inhibitor.
- Examined the effect of ZnSe/ZnS QDs on morphology, cytoskeletal arrangement and cell adhesion by giemsa and actin staining. Nuclear condensation by AO staining was also evaluated.
- Examined the changes in mitochondrial membrane potential as a result of ZnSe/ZnS QD treatment by using JC1 dye.
- Studied the effect of ZnSe/ZnS QDs on lysosomal destabilization by AO staining.
- Measurement of ROS formation in HepG2 after exposure to ZnSe/ZnS QDs by DCFHDA assay. Also studied influence of catalase activity on ROS production.
- Assessment of nitrile radical formation by Griess reagent.
- Assessment of QDs induced oxidative stress by GSH level analysis.
- Cell death mechanism analysed by flow cytometry analysis of sub G1 population.
- Measurement of cell death induced after exposure to ZnSe/ZnS QDs by Calcein AM-PI live dead assay.
- Studied the potential of ZnSe/ZnS QDs to induce DNA fragmentation by Apoptotic DNA ladder assay.
- Estimation of caspase activation in HepG2 cells after ZnSe/ZnS QDs by Caspase 3/7 assay.
- HEK cells were cultured in DMEM with 10% FBS. Cellular uptake (confocal microscopy, flow cytometry), cell viability (MTT, NRU, LDH), Cell morphology (Coomassie brilliant blue staining, actin staining), MMP (JC1), lysosomal integrity (AO), ROS (DCFH-DA) and catalase activity, NOS (griess reagent), Oxidative stress by glutathione level, cell death analysis by FACS (Calcein AM-PI), cell death mechanism (Annexin V/PI kit –FACs, DNA ladder assay, Caspase activity) were analysed.
- *In vivo* bio-nano interaction was studied by exposing Swiss Albino mice to ZnSe/ZnS QDs via i.v. and i.p. injection. Three animals injected with saline

served as control. The animals were observed for up to 14 days of post exposure.

- Animals were monitored for weight changes, behavioural and clinical signs of stress throughout the observation period.
- At the end of each observation period (3, 7 and 14 days) blood, urine and faecal samples were collected and animals were euthanized for organ (Liver, kidney, spleen and brain) collection.
- The blood, urine, faeces and organ samples were subjected to toxicokinetics and bio distribution studies by ICP-OES analysis.
- Blood samples were subjected to haematology and clinical chemistry analysis to study the systemic toxicity in liver and kidney function.
- Collected organs were subjected to histopathology analysis.

- Antioxidant assays were carried out in brain and liver homogenates to study the oxidative stress.
- Splenocytes proliferation assay was carried to study the immunotoxicity response.

6.3 MAJOR FINDINGS OF THE STUDY

- Blue fluorescent coloured ZnSe/ZnS QDs with the size of 5-6 nm was successfully synthesized via green route with absorption at 340 nm and emission at 416 nm.
- ZnSe/ZnS QDs were characterized by TEM, DLS, XRD, FTIR, Raman, TGA, ICP- OES and thermal analysis by TGA, DTA and DTG.
- ZnSe/ZnS QDs were effectively internalized by both HepG2 and HEK cells and were found to distribute throughout the cytoplasm. No ZnSe/ZnS QDs were seen in nucleus.
- HepG2 cells remain intact without any morphological distortion. However, HEK cells underwent slight morphological changes at higher concentrations. Also cell density of both cell types was decreased at high concentration.
- *In vitro* exposure of ZnSe/ZnS QDs in HepG2 cells caused cytotoxicity, mechanical damage, cytoskeletal rearrangement and ROS mediated apoptosis

with slight effect in loss of MMP, lysosomal destabilization and increase in caspase 3/7 activation at higher concentration (100µg/ ml) during 24h exposure.

- ZnSe/ZnS QDs do not cause DNA laddering.
- HepG2 cells underwent apoptotic cell death.
- ZnSe/ZnS QDs exposed to kidney cells resulted in mitochondrial hypo polarization, lysosomal destabilization, and ROS generation only at 100 µg/ ml of 24h exposure. No DNA laddering observed in HEK cells.
- Cell death mechanism of HEK cells found to be due to necrosis.

- Acute toxicity (10 mg/kg body weight) of ZnSe/ZnS QDs was studied in Swiss Albino mice with single exposure via both intraperitoneal and intravenous injection.
- No clinical or behavioural changes were observed on acute exposure of ZnSe/ZnS QDs.
- Single exposure of 10 mg/kg ZnSe/ZnS QDs did not induce any loss of body and organ weight.
- No changes in haematological and clinical chemistry parameters were noted after acute exposure of ZnSe/ZnS QDs.
- ZnSe/ZnS QDs induced oxidative stress in liver but not in brain.
- Histological examination did not show any severe symptoms of toxicity in kidney, spleen and brain, but moderate pathological changes were observed in the liver.
- Exposure to ZnSe/ZnS QDs initiates immune response by increasing the splenocytes proliferation at 3rd day of post exposure which becomes normal at the end of 14th day.
- Bio distribution study by ICP-OES showed ZnSe/ZnS QDs distributed in liver, kidney, spleen and brain.
- ZnSe/ZnS QDs was not fully cleared from blood at the end of observation period (14th day).
- ADME indicated that the major route of excretion of ZnSe/ZnS QDs is by both faecal matter and urine.

6.4 CONCLUSION

ZnSe/ZnS QDs were successfully synthesized by green aqueous colloidal synthetic method and characterized by optical and physico-chemical methods. QD absorbance was found to be at 340 nm and fluorescence emission at 416 nm. Synthesized ZnSe/ZnS QDs have fluorescence stability for four months. ZnSe/ZnS QDs were characterized for size (TEM), hydrodynamic diameter (DLS) and surface charge (zeta potential analysis), functional groups (FTIR), crystal structure and purity (XRD), chemical composition (ICP-OES), structural and electrical properties (Raman spectra) and thermal stability (TGA, DTA, DTG). The results of the *in vitro* studies clearly confirmed that the ZnSe/ZnS QDs failed to induce any toxic effects in both HepG2 and HEK cells except at 100 µg/ml during 24 h exposure. The preliminary toxicity screening using HepG2 and HEK cells as *in vitro* models suggest that ZnSe/ZnS QDs can be used in biomedical applications at a concentration less than 100 µg/ ml. Further, this study promises the use of HepG2 and HEK cells as an *in vitro* model for predictive toxicity analysis. In *vivo* toxicity studies in mice showed that ZnSe/ZnS QDs slightly affect the integrity of the liver and not in others (kidney, spleen and brain). ZnSe/ZnS QDs do not induce any acute toxicity in haematological and clinical chemistry parameters. However, they induce oxidative stress and moderate pathological changes in liver. Immunotoxicity evaluation showed slight alteration and the same was recovered to the normal range. ZnSe/ZnS QDs was not fully cleared from blood at the end of observation period (14^{th} day) and cleared QDs got distributed in liver, kidney, spleen and brain. Most of them are excreted through faeces and a minor part via urine. Further long term toxicity studies are required to declare ZnSe/ZnS QDs as validated safe nanoparticles for clinical application scenarios.

6.5 FUTURE PERSPECTIVES

- Functional changes in HepG2 and HEK cells exposed to ZnSe/ZnS QDs after prolonged (more than 24 h) exposure.
- Effect of repeated exposure of ZnSe/ZnS QDs.
- Role of Protein corona in regulating the interaction of ZnSe/ZnS QDs inside the biological system.
- Chronic toxicokinetic studies
- Biotransformation of ZnSe/ZnS QDs.

REFERENCES

Adam-Vizi, V., Chinopoulos, C (2006) Bioenergetics and the formation of mitochondrial reactive oxygen species. *Trends Pharmacological Sciences* 27: 639–645.

Alghamdi, Y (2017) Composition and Band Gap Controlled AACVD of ZnSe and ZnSxSe1-x Thin Films Using Novel Single Source Precursors. *Materials Sciences and Applications 8*(10): 726-737.

Akhtar, M.J., Ahamed, M., Kumar, S., Khan, M.M., Ahmad, J. and Alrokayan, S.A. (2012) Zinc oxide nanoparticles selectively induce apoptosis in human cancer cells through reactive oxygen species. *International journal of nanomedicine 7*: 845.

Alivisatos, A.P (1996) Semiconductor clusters, nanocrystals, and Quantum Dots. *Science* 271: 933–937.

Almeer, R.S., Ali, D., Alarifi, S., Alkahtani, S. and Almansour, M (2018) Green platinum nanoparticles interaction with HEK293 cells: cellular toxicity, apoptosis, and genetic damage. *Dose-Response* 16(4), 1559325818807382.

Amirav, L., Amirav, A., Lifshitz, E (2005) A Spray-based method for the production of semiconductor nanocrystals. *The Journal of Physical Chemistry B* 109: 9857-9860.

Andreescu, S., Ornatska, M., Erlichman, J.S., Estevez, A., Leiter, J.C (2012) Biomedical applications of metal oxide nanoparticles, In Fine Particles in Medicine and Pharmacy. Springer US, Boston, MA, 57-100.

Anthony R. West (2001) Basic solid state chemistry, 2nd edition, wiley, London, 203.

Atkins, P.W., Overton, T., Rourke, J., Weller, M. and Armstrong, F.A (2006) *Shriver & Atkins Information Retrieval*. Oxford University Press.

Bachmann, S., Mundel, P (1994) Nitric oxide in the kidney: synthesis, localization, and function. *American Journal of Kidney Diseases.24*(1): 112-129.

Bailey, R.E., Smith, A.M. and Nie, S (2004) Quantum dots in biology and medicine. *Physica E: Low-Dimensional Systems and Nanostructures* 25: 1-12.

Ballou, B., Lagerholm, B.C., Ernst, L.A., Bruchez, M.P. and Waggoner, A.S (2004) Noninvasive imaging of quantum dots in mice. *Bioconjugate Chemistry*.15: 79-86.

Barry, M., Heibein, J., Pinkoski, M. and Bleackley, R.C (2000) Quantitative measurement of apoptosis induced by cytotoxic T lymphocytes. *Methods in enzymology 322*: 40-46.

Bastiaans, G (2014) Quantum Dot Surface Coatings. NanoOptical Materials. Available: http://nomcorp.com/quantum-dot-surface-coatings/ [accessed 1.29.19]

Bera, D., Qian, L., Tseng, T.-K., Holloway, P.H (2010) Quantum Dots and Their Multimodal Applications: A Review. *Materials* 3: 2260–2345.

Bonilla, C.A.M., Kouznetsov, V.V (2016) "Green" Quantum Dots: Basics, Green Synthesis, and Nanotechnological Applications. *Green Nanotechnology - Overview and Further Prospects*. 174-192.

Bonilla, J.C., Bozkurt, F., Ansari, S., Sozer, N., Kokini, J.L (2016) Applications of quantum dots in Food Science and biology. *Trends in Food Science & Technology* 53: 75–89.

Borenfreund E and Puerner JA (1985) Toxicity determined in vitro by morphological alterations and neutral red absorption. *Toxicology letters* 24: 119-124.

Boyce, M., Degterev, A. and Yuan, J (2004) Caspases: an ancient cellular sword of Damocles. *Cell death and differentiation* 11(1): 29-37.

Bruchez, M., Moronne, M., Gin, P., Weiss, S., Alivisatos, A.P (1998) Semiconductor nanocrystals as fluorescent biological labels. *Science* 281: 2013–2016.

Brunetti, V., Chibli, H., Fiammengo, R., Galeone, A., Malvindi, M.A., Vecchio, G., Cingolani, R., Nadeau, J.L. and Pompa, P.P (2013) InP/ZnS as a safer alternative to CdSe/ZnS core/shell quantum dots: in vitro and *in vivo* toxicity

assessment. *Nanoscale* 5(1): 307-317.

Burda, C., Chen, X., Narayanan, R., El-Sayed, M.A (2005) Chemistry and properties of nanocrystals of different shapes. *Chemical Reviews* 105: 1025–1102.

Buzea, C., Pacheco, I.I. and Robbie, K. (2007) Nanomaterials and nanoparticles: sources and toxicity. *Biointerphases* 2(4): MR17-MR71.

C Thomas, S., Kumar Mishra, P. and Talegaonkar, S (2015) Ceramic nanoparticles: fabrication methods and applications in drug delivery. *Current pharmaceutical design* 21(42): 6165-6188.

Cao, Y.C. and Wang, J (2004) One-pot synthesis of high-quality zinc-blende CdS nanocrystals. *Journal of the American Chemical Society* 126(44): 14336- 14337.

Cha, C., Shin, S.R., Annabi, N., Dokmeci, M.R. and Khademhosseini, A (2013) Carbon-based nanomaterials: multifunctional materials for biomedical engineering. *ACS nano* 7(4): 2891-2897.

Champion, J.A. and Mitragotri, S (2006) Role of target geometry in phagocytosis. *Proceedings of the National Academy of Sciences* 103(13): 4930-4934.

Chan, W.C. and Nie, S (1998) Quantum dot bioconjugates for ultrasensitive nonisotopic detection. *Science* 281(5385): 2016-2018.

Chan, W.H., Shiao, N.H. and Lu, P.Z (2006) CdSe quantum dots induce apoptosis in human neuroblastoma cells via mitochondrial-dependent pathways and inhibition of survival signals. *Toxicology letters* 167(3): 191-200.

Chen, J.F., Wang, Y.H., Guo, F., Wang, X.M. and Zheng, C (2000) Synthesis of nanoparticles with novel technology: high-gravity reactive precipitation. *Industrial & engineering chemistry research* 39(4): 948-954.

Chen, Z., Li, G., Zhang, L., Jiang, J., Li, Z., Peng, Z. and Deng, L (2008) A new method for the detection of ATP using a quantum-dot-tagged aptamer. *Analytical and bioanalytical chemistry* 392(6): 1185-1188.

Cheng, S., Rhee, E.P., Larson, M.G., Lewis, G.D., McCabe, E.L., Shen, D., Palma,

M.J., Roberts, L.D., Dejam, A., Souza, A.L., Deik, A.A., Magnusson, M., Fox, C.S., O'Donnell, C.J., Vasan, R.S., Melander, O., Clish, C.B., Gerszten, R.E., Wang, T.J (2012) Metabolite profiling identifies pathways associated with metabolic risk in humans. *Circulation* 125: 2222–2231.

Cho, S. J., Maysinger, D., Jain, M., Roder, B., Hackbarth, S., & Winnik, F. M. (2007). Long‐term exposure to CdTe quantum dots causes functional impairments in live cells. *Langmuir*, 23, 1974–1980.

Choi, A.O., Cho, S.J., Desbarats, J., Lovrić, J. and Maysinger, D (2007) Quantum dot-induced cell death involves Fas upregulation and lipid peroxidation in human neuroblastoma cells. *Journal of nanobiotechnology* 5(1): 1-13.

Choi, H.S. and Frangioni, J.V (2010) Nanoparticles for biomedical imaging: fundamentals of clinical translation. *Molecular imaging* 9(6): 7290-2010.

Choi, H.S., Liu, W., Misra, P., Tanaka, E., Zimmer, J.P., Ipe, B.I., Bawendi, M.G. and Frangioni, J.V (2007) Renal clearance of nanoparticles. *Nature biotechnology* 25(10): 1165-1170.

Cingarapu, S., Yang, Z., Sorensen, C.M. and Klabunde, K.J (2012) Synthesis of CdSe/ZnS and CdTe/ZnS quantum dots: refined digestive ripening. *Journal of Nanomaterials* 2012: 7-19.

Clemens, M.G (1999) Nitric oxide in liver injury. *Hepatology* 30(1): 1-5.

Clogston, J.D. and Patri, A.K. (2011) Zeta potential measurement. *In Characterization of nanoparticles intended for drug delivery* Humana Press, 63-70.

Cooper RJ and Spitzer N (2015) Silver nanoparticles at sub lethal concentrations disrupt cytoskeleton and neurite dynamics in cultured adult neural stem cells. *Neurotoxicology* 48: 231-238.

Corr, S.A (2012) Metal oxide nanoparticles. *Nanoscience*, 1: 180-207.

Cossarizza, A., Ferraresi, R., Troiano, L., Roat, E., Gibellini, L., Bertoncelli, L., Nasi, M. and Pinti, M (2009) Simultaneous analysis of reactive oxygen species and reduced glutathione content in living cells by polychromatic flow cytometry. *Nature protocols* 4(12): 1790-1797.

Crawford, E.D. and Wells, J.A (2011) Caspase substrates and cellular remodelling. *Annual review of biochemistry* 80: 1055-1087.

Darzynkiewicz, Z (2010) Critical aspects in analysis of cellular DNA content. *Current protocols in cytometry* 52(1): 7-2.

Day, B.J (2009) Catalase and glutathione peroxidase mimics. *Biochemical pharmacology* 77(3): 285-296.

Demir, H.V., Nizamoglu, S., Erdem, T., Mutlugun, E., Gaponik, N., Eychmüller, A (2011) Quantum dot integrated LEDs using photonic and excitonic color conversion. *Nano Today* 6: 632–647.

Derfus, A.M., Chan, W.C.W., Bhatia, S.N (2004) Probing the Cytotoxicity of Semiconductor Quantum Dots. *Nano Letters* 4:11–18.

Ding, L., Zhou, P.J., Zhan, H.J., Chen, C., Hu, W., Zhou, T.F. and Lin, C.W (2013) Microwave-assisted synthesis of l-glutathione capped ZnSe QDs and its interaction with BSA by spectroscopy. *Journal of Luminescence* 142: 167-172.

Dobrovolskaia, M.A. and McNeil, S.E (2007) Immunological properties of engineered nanomaterials. *Nature nanotechnology* 2(8): 469-478.

Drbohlavova, J., Adam, V., Kizek, R., Hubalek, J (2009) Quantum Dots — Characterization, Preparation and Usage in Biological Systems. *International Journal of Molecular Sciences* 10: 656–673.

Du, C.-F., You, T., Jiang, L., Yang, S.-Q., Zou, K., Han, K.-L., Deng, W.-Q (2014) Controllable synthesis of ultrasmall CuInSe quantum dots for photovoltaic application. *RSC Advances* 4: 33855–33860.

Dufour, D.R., Lott, J.A., Nolte, F.S., Gretch, D.R., Koff, R.S. and Seeff, L.B (2000) Diagnosis and monitoring of hepatic injury. I. Performance characteristics of laboratory tests. *Clinical chemistry* 46(12): 2027-2049.

Ealias, A.M. and Saravanakumar, M.P (2017) A review on the classification, characterisation, synthesis of nanoparticles and their application. Material Science and Engineering 263: 032019 .

Efros, A.L. and Efros, A.L (1982) Interband absorption of light in a semiconductor sphere. *Soviet Physics Semiconductors-Ussr* 16(7): 772-775.

Ekimov, A.I., Onushchenko, A.A. and Tzehomskii, V.A (1980) Eksitonnoye pogloshcheniye kristallami CuCl v stekloobraznoy matritse. Fizika i khimiya stekla 6(4): 511-512.

Falcaro, P., Ricco, R., Yazdi, A., Imaz, I., Furukawa, S., Maspoch, D., Ameloot, R., Evans, J.D. and Doonan, C.J (2016) Application of metal and metal oxide nanoparticles@ MOFs. *Coordination chemistry reviews* 307: 237-254.

Fan, J., Wang, S., Zhang, X., Chen, W., Li, Y., Yang, P., Cao, Z., Wang, Y., Lu, W. and Ju, D., (2018) Quantum dots elicit hepatotoxicity through lysosome- dependent autophagy activation and reactive oxygen species production. *ACS Biomaterials Science & Engineering* 4(4):1418-1427.

Ferancova, A. and Labuda, J (2008) DNA biosensors based on nanostructured materials. *Nanostructured Materials in Electrochemistry*, 409-434.

Fernie, A.R., Trethewey, R.N., Krotzky, A.J. and Willmitzer, L (2004) Metabolite profiling: from diagnostics to systems biology. *Nature reviews molecular cell biology* 5(9): 763-769.

Fischer, H.C., Liu, L., Pang, K.S. and Chan, W.C (2006) Pharmacokinetics of nanoscale quantum dots: in vivo distribution, sequestration, and clearance in the rat. *Advanced Functional Materials* 16(10): 1299-1305.

Frasco, M.F., Chaniotakis, N (2010) Bioconjugated quantum dots as fluorescent probes for bioanalytical applications. *Analytical and Bioanalytical Chemistry* 396: 229–240.

Frohlich E (2012) The role of surface charge in cellular uptake and cytotoxicity of medical nanoparticles. *International Journal of Nanomedicine* 7: 5577-5591.

Gaan, S., He, G., Feenstra, R.M., Walker, J. and Towe, E (2010) Size, shape, composition, and electronic properties of InAs/GaAs quantum dots by scanning tunneling microscopy and spectroscopy. *Journal of Applied Physics* 108(11): 114315.

Gaharwar, A.K., Peppas, N.A., Khademhosseini, A (2014) Nanocomposite hydrogels for biomedical applications. *Biotechnology and Bioengineering* 111: 441–453.

Gao, X., Yang, L., Petros, J.A., Marshall, F.F., Simons, J.W., Nie, S (2005) In vivo molecular and cellular imaging with quantum dots. *Current opinion in biotechnology* 16: 63–72.

George, J.A. and Gounden, V., 2019. Novel glomerular filtration markers. *In Advances in clinical chemistry* 88: 91-119.

Gerets, H.H.J., Hanon, E., Cornet, M., Dhalluin, S., Depelchin, O., Canning, M. and Atienzar, F.A (2009) Selection of cytotoxicity markers for the screening of new chemical entities in a pharmaceutical context: a preliminary study using a multiplexing approach. *Toxicology in Vitro* 23(2): 319-332.

Ghasemi, Y., Peymani, P. and Afifi, S (2009) Quantum dot: magic nanoparticle for imaging, detection and targeting. *Acta Bio Medica Atenei Parmensis* 80(2): 156-165

Goenka, S., Sant, V. and Sant, S (2014) Graphene-based nanomaterials for drug delivery and tissue engineering. Journal of Controlled Release 173: 75-88.

Green, M (2010) The nature of quantum dot capping ligands. *Journal of Materials Chemistry*, 20(28): 5797-5809.

Guguen-Guillouzo, C., Corlu, A. and Guillouzo, A (2010) Stem cell-derived hepatocytes and their use in toxicology. *Toxicology* 270(1): 3-9.

Gumustas, M., Sengel-Turk, C.T., Gumustas, A., Ozkan, S.A. and Uslu, B (2017) Effect of Polymer-Based Nanoparticles on the Assay of Antimicrobial Drug Delivery Systems. *In Multifunctional Systems for Combined Delivery, Biosensing and Diagnostics* 67-108.

Guo, Y., Srinivasula, S.M., Druilhe, A., Fernandes-Alnemri, T. and Alnemri, E.S (2002) Caspase-2 induces apoptosis by releasing proapoptotic proteins from mitochondria. *Journal of Biological Chemistry* 277(16): 13430-13437.

Gwinn, M.R. and Vallyathan, V (2006) Nanoparticles: health effects—pros and cons. *Environmental health perspectives* 114(12): 1818-1825.

Hagens, W.I., Oomen, A.G., de Jong, W.H., Cassee, F.R. and Sips, A.J (2007) What do we (need to) know about the kinetic properties of nanoparticles in the body? *Regulatory toxicology and pharmacology* 49(3): 217-229.

Hanaki, K.I., Momo, A., Oku, T., Komoto, A., Maenosono, S., Yamaguchi, Y. and Yamamoto, K (2003) Semiconductor quantum dot/albumin complex is a long-life and highly photostable endosome marker. *Biochemical and biophysical research communications*, 302(3): 496-501.

Haque, M.M., Im, H.Y., Seo, J.E., Hasan, M., Woo, K. and Kwon, O.S (2013) Acute toxicity and tissue distribution of CdSe/CdS-MPA quantum dots after repeated intraperitoneal injection to mice. *Journal of Applied Toxicology* 33(9): 940- 950.

Harries, H.M., Fletcher, S.T., Duggan, C.M. and Baker, V.A (2001) The use of genomics technology to investigate gene expression changes in cultured human liver cells. *Toxicology in vitro* 15(4-5): 399-405.

Hartlieb, K.J., Raston, C.L. and Saunders, M (2007) Controlled scalable synthesis of ZnO nanoparticles. *Chemistry of Materials* 19(23): 5453-5459.

Hayes, A.W (2007) Principles and methods of toxicology. Wallace Hayes, Claire L. Kruger (Eds) Crc Press.

Hazelton, G.A. and Lang, C.A (1985) Glutathione peroxidase and reductase activities in the aging mouse. *Mechanisms of ageing and development* 29(1): 71-81.

He, X. and Ma, N (2014) An overview of recent advances in quantum dots for biomedical applications. *Colloids and Surfaces B: Biointerfaces* 124: 118-131.

Heera, P. and Shanmugam, S (2015) Nanoparticle characterization and application: an overview. International Journal of Current Microbiology and Applied Sciences4 (8): 379-386.

Heinicke U, Kupka J, Fichter I and Fulda S (2016) Critical role of mitochondria-mediated apoptosis for JNJ-26481585-induced antitumor activity in rhabdomyosarcoma. *Oncogene* 35: 3729-3741.

Hett, A (2004) *Nanotechnology: Small matter, many unknowns*. M. C Rocco and W.S Bainbridge (Eds) Swiss Reinsurance Company. Zurich.

Hines, M.A. and Guyot-Sionnest, P (1998) Bright UV-blue luminescent colloidal ZnSe nanocrystals. *The Journal of Physical Chemistry B* 102(19): 3655-3657.

Hoshino, A., Fujioka, K., Oku, T., Suga, M., Sasaki, Y.F., Ohta, T., Yasuhara, M., Suzuki, K. and Yamamoto, K (2004) Physicochemical properties and cellular toxicity of nanocrystal quantum dots depend on their surface modification. *Nano Letters* 4(11): 2163-2169.

Hsieh, J.M., Ho, M.L., Wu, P.W., Chou, P.T., Tsai, T.T. and Chi, Y (2006) Iridium-complex modified CdSe/ZnS quantum dots; a conceptual design for bifunctionality toward imaging and photosensitization. *Chemical Communications* (6): 615-617.

Hussain, T., Shukla, G.S. and Chandra, S.V (1987) Effects of cadmium on superoxide dismutase and lipid peroxidation in liver and kidney of growing rats: in vivo and in vitro studies. *Pharmacology & toxicology* 60(5): 355-358.

Husseini, G.A. and Pitt, W.G (2008) Micelles and nanoparticles for ultrasonic drug and gene delivery. *Advanced drug delivery reviews* 60(10): 1137-1152.

Iikawa, F., Godoy, M.P.F.D., Nakaema, M.K.K., Brasil, M.J.S.P., Maialle, M.Z., Degani, M.A., Ribeiro, E., Medeiros-Ribeiro, G., Carvalho Jr, W. and Brum, J.A (2004) Optical properties of type-I and II quantum dots. *Brazilian journal of physics* 34(2B): 555-559.

Imamoglu, A (2003) Are quantum dots useful for quantum computation?.Physica E: Low-dimensional Systems and Nanostructures, 16(1): 47-50.

Iurlaro, R. and Muñoz‐Pinedo, C (2016) Cell death induced by endoplasmic reticulum stress. The FEBS journal, 283(14): 2640-2652.

Jamieson, T., Bakhshi, R., Petrova, D., Pocock, R., Imani, M. and Seifalian, A.M

(2007) Biological applications of quantum dots. *Biomaterials*, 28(31): 4717-4732.

Javidi, J., Haeri, A., Nowroozi, F. and Dadashzadeh, S (2019) Pharmacokinetics,

Tissue Distribution and Excretion of Ag_2S Quantum Dots in Mice and Rats: the Effects of Injection Dose, Particle Size and Surface Charge. *Pharmaceutical research* 36(3): 46.

Jeevanandam, J., Barhoum, A., Chan, Y.S., Dufresne, A., Danquah, M.K (2018) Review on nanoparticles and nanostructured materials: history, sources, toxicity and regulations. *Beilstein Journal of Nanotechnology* 9: 1050–1074.

Jennen, D.G., Magkoufopoulou, C., Ketelslegers, H.B., van Herwijnen, M.H., Kleinjans, J.C. and van Delft, J.H (2010) Comparison of HepG2 and HepaRG by whole-genome gene expression analysis for the purpose of chemical hazard identification. *Toxicological sciences* 115(1): 66-79.

Ji, X., Peng, F., Zhong, Y., Su, Y., He, Y (2014) Fluorescent quantum dots: Synthesis, biomedical optical imaging, and biosafety assessment. *Colloids and Surfaces B: Biointerfaces, Biointerfaces: Global Perspectives* 124: 132–139.

Jiao, Y., Gao, X., Lu, J., Chen, Y., Zhou, J. and Li, X (2012) A novel method for PbS quantum dot synthesis. *Materials letters* 72: 116-118.

Jin, T., Fujii, F., Komai, Y., Seki, J., Seiyama, A. and Yoshioka, Y (2008) Preparation and characterization of highly fluorescent, glutathione-coated near infrared quantum dots for in vivo fluorescence imaging. *International journal of molecular sciences*, 9(10): 2044-2061.

Juzenas, P., Generalov, R., Juzeniene, A., & Moan, J. (2008). Generation of nitrogen oxide and oxygen radicals by quantum dots. *Journal of Biomedical Nanotechnology* 4: 450–456.

Karanikolos, G.N., Alexandridis, P., Itskos, G., Petrou, A. and Mountziaris, T.J (2004) Synthesis and Size Control of Luminescent ZnSe Nanocrystals by a Microemulsion− Gas Contacting Technique. *Langmuir*, 20(3): 550-553.

Karmakar, R (2015) Quantum Dots and it method of preparations-revisited. *Prajnan O Sadhona–A Science Annual* 116-142.

Kennel, S.J., Woodward, J.D., Rondinone, A.J., Wall, J., Huang, Y. and Mirzadeh, S (2008) The fate of MAb-targeted Cd125mTe/ZnS nanoparticles in vivo.

Nuclear medicine and biology 35(4): 501-514.

Khalid, A. and Kontis, K (2008) Thermographic phosphors for high temperature measurements: principles, current state of the art and recent applications. *Sensors* 8(9): 5673-5744.

Kim, D., Kim, J., Park, Y.I., Lee, N., Hyeon, T (2018) Recent Development of Inorganic Nanoparticles for Biomedical Imaging. *ACS Central Science* 4: 324– 336.

Kim, J.-H., Kim, C.-S., Ignacio, R.M.C., Kim, D.-H., Sajo, M.E.J., Maeng, E.H., Qi, X.-F., Park, S.-E., Kim, Y.-R., Kim, M.-K., Lee, K.-J., Kim, S.-K (2014) Immunotoxicity of silicon dioxide nanoparticles with different sizes and electrostatic charge. *International Journal of Nanomedicine* 9: 183–193.

Kim, S., Lim, Y.T., Soltesz, E.G., De Grand, A.M., Lee, J., Nakayama, A., Parker, J.A., Mihaljevic, T., Laurence, R.G., Dor, D.M. and Cohn, L.H (2004) Near- infrared fluorescent type II quantum dots for sentinel lymph node mapping. *Nature biotechnology* 22(1): 93.

King-Heiden, T.C., Wiecinski, P.N., Mangham, A.N., Metz, K.M., Nesbit, D., Pedersen, J.A., Hamers, R.J., Heideman, W. and Peterson, R.E (2009) Quantum dot nanotoxicity assessment using the zebrafish embryo. *Environmental science & technology* 43(5): 1605-1611.

Kirchner, C., Liedl, T., Kudera, S., Pellegrino, T., Munoz Javier, A., Gaub, H.E., Stolzle, S., Fertig, N. and Parak, W.J (2005) Cytotoxicity of colloidal CdSe and CdSe/ZnS nanoparticles. *Nano letters*, 5(2): 331-338.

Klaassen, C.D., Liu, J. and Diwan, B.A (2009) Metallothionein protection of cadmium toxicity. *Toxicology and applied pharmacology* 238(3): 215-220.

Klayman, D.L., Griffin, T.Scott (1973) Reaction of selenium with sodium borohydride in protic solvents. A Facile Method for the introduction of selenium into organic molecules. *Journal of the American Chemical Society* 95: 197–199.

Konstantatos, G., Sargent, E.H (2010) Nanostructured materials for photon detection. *Nature Nanotechnology* 5: 391–400.

Kumar, P., Nagarajan, A. and Uchil, P.D (2018) Analysis of cell viability by the lactate dehydrogenase assay. *Cold Spring Harbor Protocols*, 2018(6): pdb- prot095497.

Lai, G.-J., Shalumon, K.T., Chen, J.-P (2015) Response of human mesenchymal stem cells to intrafibrillar nanohydroxyapatite content and extrafibrillar nanohydroxyapatite in biomimetic chitosan/silk fibroin/nanohydroxyapatite nanofibrous membrane scaffolds. *International Journal of Nanomedicine* 10:567–584.

LaMer, V.K. and Dinegar, R.H(1950) Theory, production and mechanism of formation of monodispersed hydrosols. *Journal of the American Chemical Society* 72(11): 4847-4854.

Laurent, S., Forge, D., Port, M., Roch, A., Robic, C., Vander Elst, L., Muller, R.N(2008) Magnetic iron oxide nanoparticles: synthesis, stabilization, vectorization, physicochemical characterizations, and biological applications. *Chemical Reviews* 108: 2064–2110.

Lee WS, Kim E, Cho HJ, Kang T, Kim B, Kim MY, Kim YS, Song NW, Lee JS, Jeong J (2018) The Relationship between Dissolution Behaviours and the Toxicity of Silver Nanoparticles on Zebrafish Embryos in Different Ionic Environments. *Nanomaterials* 8(9): 652-662.

Lee, J., Kang, H., Jang, H., Lee, Y., Lee, Y., Ali, B., Al-Khedhairy, A. and Kim, S (2015) Simultaneous imaging of two different cancer biomarkers using aptamer-conjugated quantum dots. *Sensors* 15(4): 8595-8604.

Li, B., Zhang, X.Y., Yang, J.Z., Zhang, Y.J., Li, W.X., Fan, C.H. and Huang, Q (2014) Influence of polyethylene glycol coating on biodistribution and toxicity of nanoscale graphene oxide in mice after intravenous injection. *International journal of nanomedicine* 9: 4697-4707.

Li, N., Than, A., Wang, X., Xu, S., Sun, L., Duan, H., Xu, C. and Chen, P (2016) Ultrasensitive profiling of metabolites using tyramine-functionalized graphene quantum dots. *ACS nano*, 10(3): 3622-3629.

Li, Y., Xu, J., Xu, Y., Huang, L., Wang, J. and Cheng, X (2015) Synthesis and

characterization of fluorescent chitosan–ZnSe/ZnS nanoparticles for potential drug carriers. *RSC Advances*, 5(49): 38810-38817.

Lignos, I., Protesescu, L., Stavrakis, S., Piveteau, L., Speirs, M.J., Loi, M.A., Kovalenko, M.V. and deMello, A.J (2014) Facile droplet-based microfluidic synthesis of monodisperse IV–VI semiconductor nanocrystals with coupled in-line NIR fluorescence detection. *Chemistry of Materials* 26(9): 2975-2982.

Lin, P. and Chen, J.W (2008) LovisW. Chang, Jui-Pin Wu, Laurel Redding and els. Computational and Ultrastructural Toxicology of a Nanoparticle, Quantum Dot 705. *Mice Environmental science & technology* 42(16): 6264-6270.

Liu, L., Tao, R., Huang, J., He, X., Qu, L., Jin, Y., Zhang, S. and Fu, Z (2015) Hepatic oxidative stress and inflammatory responses with cadmium exposure in male mice. *Environmental toxicology and pharmacology* 39(1): 229-236.

Liu, Y., Li, W., Lao, F., Liu, Y., Wang, L., Bai, R., Zhao, Y. and Chen, C (2011) Intracellular dynamics of cationic and anionic polystyrene nanoparticles without direct interaction with mitotic spindle and chromosomes. *Biomaterials* 32(32): 8291-8303.

Lopez-Terrada, D., Cheung, S.W., Finegold, M.J. and Knowles, B.B (2009) Hep G2 is a hepatoblastoma-derived cell line. *Human pathology* 40(10):1512.

Loughran, P.A., Stolz, D.B., Vodovotz, Y., Watkins, S.C., Simmons, R.L. and Billiar, T.R (2005) Monomeric inducible nitric oxide synthase localizes to peroxisomes in hepatocytes. *Proceedings of the National Academy of Sciences*, 102(39):13837-13842.

Lovrić, J., Bazzi, H.S., Cuie, Y., Fortin, G.R., Winnik, F.M. and Maysinger, D (2005) Differences in subcellular distribution and toxicity of green and red emitting CdTe quantum dots. *Journal of Molecular Medicine* 83(5): 377-385.

Lowry OH, Rosebrough NJ, Farr AL, Randall RJ (1951) Protein measurement with the Folin phenol reagent. *Journal of Biological Chemistry* 193: 265-75.

Lu, J., Tang, M. and Zhang, T (2019) Review of toxicological effect of quantum dots on the liver. *Journal of Applied Toxicology* 39(1): 72-86.

Lu, Y., Xu, S., Chen, H., He, M., Deng, Y., Cao, Z., Pi, H., Chen, C., Li, M., Ma, Q. and Gao, P., (2016) CdSe/ZnS quantum dots induce hepatocyte pyroptosis and liver inflammation via NLRP3 inflammasome activation. *Biomaterials* 90: 27-39.

MacLean-Fletcher, S. and Pollard, T.D (1980) Mechanism of action of cytochalasin B on actin. *Cell* 20(2): 329-341.

Mallouk, T.E., Webber, S.E. and White, J.M (1992) Demonstration of a shell-core structure in layered CdSe-ZnSe small particles by X-ray photoelectron and Auger spectroscopies. *Journal of Physical Chemistry* 96: 3812-3811.

Manke, A., Wang, L. and Rojanasakul, Y (2013) Mechanisms of nanoparticle-induced oxidative stress and toxicity. *BioMed research international*, 2013:1-5.

Mansoori, B., Sandoghchian Shotorbani, S., Baradaran, B (2014) RNA Interference and its Role in Cancer Therapy. *Advanced pharmaceutical bulletin,* 4:313–321.

Marczak, R., Segets, D., Voigt, M., Peukert, W (2010) Optimum between purification and colloidal stability of ZnO nanoparticles. *Advanced Powder Technology, Core-to-Core Young Researchers Meeting 2008,* 21: 41–49.

Marklund S and Marklund G (1974) Involvement of the superoxide anion radical in the autoxidation of pyrogallol and a convenient assay for superoxide dismutase. *The FEBS Journal* 47: 469-474.

Matagne, P., Destine, J., Cantraine, G. and Leburton, J.P., 2000. Modeling of the electronic properties of vertical quantum dots by the finite element method. *CMES- Computer Modeling in Engineering & Sciences*, 1(1), 1-10.

Matea, C.T., Mocan, T., Tabaran, F., Pop, T., Mosteanu, O., Puia, C., Iancu, C., Mocan, L (2017) Quantum dots in imaging, drug delivery and sensor applications. *International Journal of Nanomedicine* 12: 5421–5431.

McMillan, J., Batrakova, E., Gendelman, H.E (2011) Cell delivery of therapeutic nanoparticles. *Progress in molecular biology and translational science* 104: 563–601.

Migita, S., Moquin, A., Fujishiro, H., Himeno, S., Maysinger, D., Winnik, F. M., &

Taniguchi, A. (2014) Quantum dots induce heat shock‐related cytotoxicity at intracellular environment. In Vitro Cellular & Developmental Biology-Animal 50: 367–372

Mize CE and Langdon RG (1962) Hepatic glutathione reductase I. Purification and general kinetic properties. *Journal of Biological Chemistry* 237: 1589-1595.

Mo, D., Hu, L., Zeng, G., Chen, G., Wan, J., Yu, Z., Huang, Z., He, K., Zhang, C. and Cheng, M (2017) Cadmium-containing quantum dots: properties, applications, and toxicity. *Applied microbiology and biotechnology* 101(7): 2713-2733.

Moron MS, Depierre JW, Mannervik B (1979) Levels of glutathione, glutathione reductase and glutathione S-transferase activities in rat lung and liver. *Biochim Biophys Acta* 582: 67-78.

Mourdikoudis, S., Pallares, R.M. and Thanh, N.T (2018) Characterization techniques for nanoparticles: Comparison and complementarity upon studying nanoparticle properties. *Nanoscale* 10(27): 12871-12934.

Mu, X., Wang, J.Y., Bai, X., Xu, F., Liu, H., Yang, J., Jing, Y., Liu, L., Xue, X., Dai, H. and Liu, Q (2017) Black phosphorus quantum dot induced oxidative stress and toxicity in living cells and mice. *ACS applied materials & interfaces* 9(24): 20399-20409.

Murray, C., Norris, D.J. and Bawendi, M.G (1993) Synthesis and characterization of nearly monodisperse CdE (E= sulfur, selenium, tellurium) semiconductor nanocrystallites. *Journal of the American Chemical Society* 115(19): 8706- 8715.

Nguyen, K.C., Willmore, W.G. and Tayabali, A.F (2013) Cadmium telluride quantum dots cause oxidative stress leading to extrinsic and intrinsic apoptosis in hepatocellular carcinoma HepG2 cells. *Toxicology* 306: 114-123.

Oberdorster, G., Maynard, A., Donaldson, K., Castranova, V., Fitzpatrick, J., Ausman, K., Carter, J., Karn, B., Kreyling, W., Lai, D., Olin, S., Monteiro-Riviere, N., Warheit, D., Yang, H., ILSI Research Foundation/Risk Science Institute Nanomaterial Toxicity Screening Working Group (2005) Principles for characterizing the potential human health effects from exposure to

nanomaterials: elements of a screening strategy. *Part Fibre Toxicology* 2(1): 8.

Obrien, P.J., Irwin, W., Diaz, D., Howard-Cofield, E., Krejsa, C.M., Slaughter, M.R., Gao, B., Kaludercic, N., Angeline, A., Bernardi, P. and Brain, P (2006) High concordance of drug-induced human hepatotoxicity with in vitro cytotoxicity measured in a novel cell-based model using high content screening. *Archives of toxicology* 80(9): 580-604.

Ogawa, S., Hu, K., Fan, F.R.F. and Bard, A.J (1997) Photoelectrochemistry of films of quantum size lead sulfide particles incorporated in self-assembled monolayers on gold. *The Journal of Physical Chemistry B* 101(29): 5707-5711.

Ohkawa H, Ohishi N and Yagi K (1979) Assay for lipid peroxides in animal tissues by thiobarbituric acid reaction. *Analytical biochemistry* 95: 351-358.

Ong KJ, MacCormack TJ, Clark RJ, Ede JD, Ortega VA, Felix LC, Dang MK, Ma G, Fenniri H and Veinot JG (2014) Widespread nanoparticle-assay interference: implications for nanotoxicity testing. *PLoS One* 9: e90650.

Ou H, Cheng T, Zhang Y, Liu J, Ding Y, Zhen J, Shen W, Xu, Y, Yang W, Niu P. and Liu J (2018) Surface-adaptive zwitterionic nanoparticles for prolonged blood circulation time and enhanced cellular uptake in tumor cells. *Acta biomaterialia* 65:339-348.

Paesano, L., Perotti, A., Buschini, A., Carubbi, C., Marmiroli, M., Maestri, E., Iannotta, S. and Marmiroli, N (2016) Markers for toxicity to HepG2 exposed to cadmium sulphide quantum dots; damage to mitochondria. *Toxicology*, 374:18- 28.

Pan, Y., Li, Y.R., Zhao, Y. and Akins, D.L (2015) Synthesis and characterization of quantum dots: a case study using PbS. *Journal of Chemical Education* 92(11): 1860-1865.

Patil, M., Mehta, D.S. and Guvva, S (2008) Future impact of nanotechnology on medicine and dentistry. *Journal of Indian society of periodontology* 12(2): 34.

Payne, A.M., Zorman, J., Horton, M., Dubey, S., ter Meulen, J. and Vora, K.A (2013) Caspase activation as a versatile assay platform for detection of cytotoxic

bacterial toxins. *Journal of clinical microbiology* 51(9): 2970-2976.

Peng, L., He, M., Chen, B., Wu, Q., Zhang, Z., Pang, D., Zhu, Y. and Hu, B (2013) Cellular uptake, elimination and toxicity of CdSe/ZnS quantum dots in HepG2 cells. *Biomaterials*, 34(37):9545-9558.

Pokropivny, V.V. and Skorokhod, V.V (2007) Classification of nanostructures by dimensionality and concept of surface forms engineering in nanomaterial science. *Materials Science and Engineering: C* 27(5-8): 990-993.

Prabhu, R.R. and Khadar, M.A (2008) Study of optical phonon modes of CdS nanoparticles using Raman spectroscopy. *Bulletin of Materials Science* 31(3): 511-515.

Qiu, Y., Cai, G., Su, M., Chen, T., Zheng, X., Xu, Y., Ni, Y., Zhao, A., Xu, L.X., Cai, S. and Jia, W (2009) Serum metabolite profiling of human colorectal cancer using GC− TOFMS and UPLC− QTOFMS. *Journal of proteome research* 8(10): 4844-4850.

Radu, G.L., Truica, G.I., Penu, R., Moroeanu, V. and Litescu, S.C(2012) Use of the Fourier transform infrared spectroscopy in characterization of specific samples. *UPB Scientific Bulletin B: Chemical and Materials Science*74(4): 137-148.

Rajput, N (2015) Methods of preparation of nanoparticles-A review. *International Journal of Advances in Engineering & Technology* 7(6): 1806-1811.

Ramos, A.P., Cruz, M.A., Tovani, C.B. and Ciancaglini, P (2017) Biomedical applications of nanotechnology. *Biophysical reviews* 9(2): 79-89.

Rao, J.P. and Geckeler, K.E (2011) Polymer nanoparticles: preparation techniques and size-control parameters. *Progress in polymer science,* 36(7): 887-913.

Reed, M.A., Randall, J.N., Aggarwal, R.J., Matyi, R.J., Moore, T.M. and Wetsel, A.E (1988) Observation of discrete electronic states in a zero-dimensional semiconductor nanostructure. *Physical Review Letters* 60(6): 535-537.

Reshma, V.G., Mohanan, P.V (2019) Quantum dots: Applications and safety consequences. *Journal of Luminescence* 205: 287–298.

Richter, M., Vidovic, N., Honrath, B., Mahavadi, P., Dodel, R., Dolga, A.M. and Culmsee, C., (2016) Activation of SK2 channels preserves ER Ca^{2+} homeostasis and protects against ER stress-induced cell death. *Cell death and differentiation* 23(5): 814-827.

Rizvi, S.B., Ghaderi, S., Keshtgar, M. and Seifalian, A.M (2010) Semiconductor quantum dots as fluorescent probes for in vitro and in vivo bio-molecular and cellular imaging. *Nano reviews* 1(1): 5161-5176.

Rosenthal, S.J., Chang, J.C., Kovtun, O., McBride, J.R., Tomlinson, I.D (2011) Biocompatible Quantum Dots for Biological Applications. *Chemistry & Biology* 18: 10–24.

Rzigalinski, B.A. and Strobl, J.S (2009) Cadmium-containing nanoparticles: perspectives on pharmacology and toxicology of quantum dots. *Toxicology and applied pharmacology*, 238(3): 280-288.

Saadat, Y.R., Saeidi, N., Vahed, S.Z., Barzegari, A. and Barar, J (2015) An update to DNA ladder assay for apoptosis detection. *BioImpacts: BI* 5(1): 25.

Samia, A.C.S., Dayal, S., Burda, C (2006) Quantum dot-based energy transfer: perspectives and potential for applications in photodynamic therapy. *Photochemistry and Photobiology*. 82: 617–625.

Sandros, M.G., Behrendt, M., Maysinger, D., Tabrizian, M (2007) InGaP@ZnS-Enriched Chitosan Nanoparticles: A Versatile Fluorescent Probe for Deep-Tissue Imaging. *Advanced Functional Materials* 17: 3724–3730.

Sani, M., Sebaï, H., Gadacha, W., Boughattas, N.A., Reinberg, A. and Mossadok, B.A (2006) Catalase activity and rhythmic patterns in mouse brain, kidney and liver.*Comparative Biochemistry and Physiology Part B: Biochemistry and Molecular Biology* 145(3-4): 331-337.

Sashchiuk, A., Lifshitz, E., Reisfeld, R., Saraidarov, T., Zelner, M., Willenz, A (2002) Optical and Conductivity Properties of PbS Nanocrystals in Amorphous Zirconia Sol-Gel Films. *Journal of Sol-Gel Science and Technology* 24: 31–38.

Sassa, S., Sugita, O., Galbraith, R.A. and Kappas, A (1987) Drug metabolism by the

human hepatoma cell, Hep G2. *Biochemical and biophysical research communications* 143(1): 52-57.

Scheers, E.M., Ekwall, B. and Dierickx, P.J (2001) In vitro long-term cytotoxicity testing of 27 MEIC chemicals on Hep G2 cells and comparison with acute human toxicity data. *Toxicology in vitro* 15(2): 153-161.

Scheerschmidt, K. and Werner, P (2002) Characterization of structure and composition of quantum dots by transmission electron microscopy. *In Nano- Optoelectronics*, Springer, Berlin, Heidelberg: 67-98.

Scher, E.C., Manna, L. and Alivisatos, A.P (2002) Shape control and applications of nanocrystals. *Philosophical Transactions of the Royal Society of London. Series A: Mathematical, Physical and Engineering Sciences* 361(1803): 241- 257.

Semonin, O.E., Luther, J.M., Beard, M.C (2012) Quantum dots for next-generation photovoltaics. *Materials Today* 15: 508–515.

Shu, C., Huang, B., Chen, X., Wang, Y., Li, X., Ding, L. and Zhong, W (2013) Facile synthesis and characterization of water soluble ZnSe/ZnS quantum dots for cellar imaging. *Spectrochimica Acta Part A: Molecular and Biomolecular Spectroscopy*, 104: 143-149.

Shukla, S.K (2014) Recent developments in biomedical applications of quantum dots. *Advanced materials Review* 1(1): 2-12.

Skalickova, S., Zitka, O., Nejdl, L., Krizkova, S., Sochor, J., Janu, L., Ryvolova, M., Hynek, D., Zidkova, J., Zidek, V. and Adam, V (2013) Study of interaction between metallothionein and CdTe quantum dots. *Chromatographia*, 76(7-8): 345-353.

Smith, A.M., Duan, H., Mohs, A.M., Nie, S (2008) Bioconjugated Quantum Dots for In Vivo Molecular and Cellular Imaging. *Advanced Drug Delivery Reviews* 60: 1226–1240.

Soenen, S.J., Manshian, B.B., Aubert, T., Himmelreich, U., Demeester, J., De Smedt,

S.C., Hens, Z. and Braeckmans, K (2014) Cytotoxicity of cadmium-free quantum dots and their use in cell bioimaging. *Chemical research in toxicology* 27(6): 1050-1059.

Srivastava, S., Mishra, S., Dewangan, J., Divakar, A., Pandey, P.K. and Rath, S.K., 2018. Principles for In Vitro Toxicology. *In In Vitro Toxicology* Academic Press: 21-43.

Srivatsan, T.S (2012) Nanomaterials: Synthesis, Properties, and Applications, A. S. Edelstein and R. C. Cammarata, (Eds) institute of Physics, London, 1996: 596.

Steigerwald, M.L. and Brus, L.E (1990) Semiconductor crystallites: a class of large molecules. *Accounts of Chemical Research* 23(6): 183-188.

Steponkiene, S., Valanciunaite, J., Skripka, A., Rotomskis, R (2014) Cellular uptake and photosensitizing properties of quantum dot-chlorin e6 complex: in vitro study. *Journal of Biomedical Nanotechnology* 10: 679–686.

Stier, O., Grundmann, M. and Bimberg, D (1999) Electronic and optical properties of strained quantum dots modeled by 8-band k · p theory. *Physical Review B* 59(8): 5688-5701.

Su, Y., He, Y., Lu, H., Sai, L., Li, Q., Li, W., Wang, L., Shen, P., Huang, Q., Fan, C (2009) The cytotoxicity of cadmium based, aqueous phase - synthesized, quantum dots and its modulation by surface coating. *Biomaterials* 30: 19–25.

Suckow, M.A., Brayton, C. and Danneman, P (2012) *The laboratory mouse*. Hans Hedrich (Eds) CRC press.

Sukhanova, A., Bozrova, S., Sokolov, P., Berestovoy, M., Karaulov, A. and Nabiev, I (2018) Dependence of nanoparticle toxicity on their physical and chemical properties. *Nanoscale research letters* 13(1): 44.

Sullivan, P., Agardy, F.J. and Clark, J.J (2005) The environmental science of drinking water. Elsevier.368. ISBN: 0-7506-7876-3.

Sun, L., Gong, F., Zhou, C., Wang, H. and Yao, S (2015) Facile synthesis and optimization of ZnSe–GSH quantum dots by hydrothermal method. *Materials Express* 5(3): 219-225.

Sun, Q., Fu, S., Dong, T., Liu, S., Huang, C (2012) Aqueous Synthesis and Characterization of TGA-capped CdSe Quantum Dots at Freezing Temperature. *Molecules* 17: 8430–8438.

Suzuki H, Toyooka T and Ibuki Y (2007) Simple and easy method to evaluate uptake potential of nanoparticles in mammalian cells using a flow cytometric light scatter analysis. *Environmental Science & Technology* 41: 3018-3024.

Tagit, O., De Ruiter, M.V., Brasch, M., Ma, Y. and Cornelissen, J.J.L.M (2017) Quantum dot encapsulation in virus-like particles with tuneable structural properties and low toxicity. *RSC advances* 7(60): 38110-38118.

Tal, M., Silberstein, A. and Nusser, E (1985) Why does Coomassie Brilliant Blue R interact differently with different proteins? A partial answer. *Journal of biological chemistry* 260(18): 9976-9980.

Tang, Y., Han, S., Liu, H., Chen, X., Huang, L., Li, X. and Zhang, J (2013) The role of surface chemistry in determining in vivo biodistribution and toxicity of CdSe/ZnS core–shell quantum dots. *Biomaterials* 34(34): 8741-8755.

Tanida, I (2011) Autophagy basics. *Microbiology and immunology* 55(1): 1-11.

Tapper, E.B., Cohen, E.B., Patel, K., Bacon, B., Gordon, S., Lawitz, E., Nelson, D., Nasser, I.A., Challies, T. and Afdhal, N (2012) Levels of alanine aminotransferase confound use of transient elastography to diagnose fibrosis in patients with chronic hepatitis C virus infection. *Clinical Gastroenterology and Hepatology* 10(8): 932-937.

Tsay, J. M., & Michalet, X (2005). New light on quantum dot cytotoxicity. *Chemistry & Biology* 12: 1159–1161.

Tytus, M., Krasnyj, J., Jacak, W., Chuchmala, A., Donderowicz, W., Jacak, L (2008) Differences between photoluminescence spectra of type-I and type-II quantum dots. In *Journal of Physics: Conference Series*. 104: 012011.

Valipoor, A., Amiri, G., Parivar, K., Modaresi, M., Taheri, J., Kazemi, A., Abasi, M. and Mirzakhani, A (2015) A comparative study about toxicity of CdSe quantum dots on reproductive system development of mice and controlling this

toxicity by ZnS coverage. *Nanomedicine Journal* 2(4): 261-268.

Valizadeh, A., Mikaeili, H., Samiei, M., Farkhani, S.M., Zarghami, N., kouhi, M., Akbarzadeh, A., Davaran, S (2012) Quantum dots: synthesis, bioapplications, and toxicity. *Nanoscale Research Letters 7*: 480-494.

Van Meer, P. and Raber, J (2005) Mouse behavioural analysis in systems biology. *Biochemical Journal* 389(3): 593-610.

Vandebriel RJ and De Jong WH (2012) A review of mammalian toxicity of ZnO nanoparticles. *Nanotechnology, science and applications* 5: 61-71.

Vázquez-González, M., Carrillo-Carrion, C., 2014. Analytical strategies based on quantum dots for heavy metal ions detection. *J Biomed Opt* 19: 101503.

Wahab, R., Siddiqui, M.A., Saquib, Q., Dwivedi, S., Ahmad, J., Musarrat, J., Al-Khedhairy, A.A. and Shin, H.S (2014) ZnO nanoparticles induced oxidative stress and apoptosis in HepG2 and MCF-7 cancer cells and their antibacterial activity. *Colloids and surfaces B: Biointerfaces* 117: 267-276.

Walkey, C.D. and Chan, W.C (2014) Quantum Dots for Traceable Therapeutic Delivery. *In Cancer Theranostics*. Academic Press: 393-417.

Wang, C., Gao, X. and Su, X. (2010) In vitro and in vivo imaging with quantum dots. *Analytical and bioanalytical chemistry* 397(4): 1397-1415.

Wang, J., Chen, C., Li, B., Yu, H., Zhao, Y., Sun, J., Li, Y., Xing, G., Yuan, H., Tang, J. and Chen, Z (2006) Antioxidative function and biodistribution of [Gd@ C82 (OH) 22] n nanoparticles in tumor-bearing mice. *Biochemical pharmacology* 71(6): 872-881.

Wang, J., Sun, H., Meng, P., Wang, M., Tian, M., Xiong, Y., Zhang, X. and Huang, P (2017) Dose and time effect of CdTe quantum dots on antioxidant capacities of the liver and kidneys in mice. *International journal of nanomedicine* 12: 6425-6435.

Wang, W., Lu, Y.C., Huang, H., Feng, J.J., Chen, J.R. and Wang, A.J (2014) Facile synthesis of water-soluble and biocompatible fluorescent nitrogen-doped carbon dots for cell imaging. *Analyst* 139(7): 1692-1696.

Wang, Y., & Tang, M. (2018). Review of in vitro toxicological research of quantum dot and potentially involved mechanisms. *Science of the Total Environment* 625: 940–962.

Wang, Y., Fang, J., Leonard, S.S., Rao, K.M.K (2004) Cadmium inhibits the electron transfer chain and induces reactive oxygen species. *Free Radical Biology and Medicine* 36: 1434–1443.

Wang, Y., Wu, B., Yang, C., Liu, M., Sum, T.C. and Yong, K.T (2016) Synthesis and characterization of Mn: ZnSe/ZnS/ZnMnS sandwiched QDs for multimodal imaging and theranostic applications. *Small* 12(4): 534-546.

Wang, Y., Xia, Y (2004) Bottom-Up and Top-Down Approaches to the Synthesis of Monodispersed Spherical Colloids of Low Melting-Point Metals. *Nano Letters*. 4: 2047–2050.

Wang, Z.H., Wang, X.F., Jiang, H., Ding, J., Wang, J.D., Shi, W.B (2012) Probing Near-Infrared Quantum Dots for Imaging and Biomedical Applications. *In Advanced Materials Research* 345:3-11. Trans Tech Publications Ltd.

Want, E.J., O'Maille, G., Smith, C.A., Brandon, T.R., Uritboonthai, W., Qin, C., Trauger, S.A. and Siuzdak, G (2006) Solvent-dependent metabolite distribution, clustering, and protein extraction for serum profiling with mass spectrometry. *Analytical chemistry* 78(3): 743-752.

Wei, Y., Yan, B (2016) Nano products in daily life: to know what we do not know. *National Science Review* 3, 414–415.

Westerink, W.M. and Schoonen, W.G (2007) Cytochrome P450 enzyme levels in HepG2 cells and cryopreserved primary human hepatocytes and their induction in HepG2 cells. *Toxicology in vitro* 21(8): 1581-1591.

Whitehead, K.A., Langer, R., Anderson, D.G (2009) Knocking down barriers: advances in siRNA delivery. *Nature Reviews Drug Discovery* 8: 129–138.

Wiecinski, P.N., Metz, K.M., King Heiden, T.C., Louis, K.M., Mangham, A.N., Hamers, R.J., Heideman, W., Peterson, R.E. and Pedersen, J.A (2013) Toxicity of oxidatively degraded quantum dots to developing zebrafish (Danio rerio).

Environmental science & technology 47(16): 9132-9139.

Winnik, F.M., Maysinger, D (2013) Quantum dot cytotoxicity and ways to reduce it. *Accounts of Chemical Res*earch 46, 672–680.

Wróblewski, F. and Ladue, J.S (1955) Lactic dehydrogenase activity in blood. Proceedings *of the Society for Experimental Biology and Medicine* 90(1) 210-213.

Xu, G., Zeng, S., Zhang, B., Swihart, M.T., Yong, K.-T., Prasad, P.N (2016) New Generation Cadmium-Free Quantum Dots for Biophotonics and Nanomedicine. *Chemical Reviews* 116: 12234–12327.

Yang L, Wang F, Han H, Yang L, Zhang G, Fan Z (2015) Functionalized graphene oxide as a drug carrier for loading pirfenidone in treatment of subarachnoid hemorrhage. *Colloids Surf B Biointerfaces* 129: 21-9.

Yang, H., Santra, S., Holloway, P.H (2005) Syntheses and applications of Mn-doped II-VI semiconductor nanocrystals. *Journal of Nanoscience and Nanotechnology* 5: 1364–1375.

Yang, Y., Zhao, T., Cheng, T., Shen, J., Liu, X., Yu, B., Lv, S. and Zhang, H (2014) Hepatotoxicity induced by ZnO quantum dots in mice. *Rsc Advances* 4(11): 5642-5648.

Yang, Y.A., Wu, H., Williams, K.R. and Cao, Y.C (2005) Synthesis of CdSe and CdTe nanocrystals without precursor injection. *Angewandte Chemie International Edition*, 44(41): 6712-6715.

Yin, Y. and Alivisatos, A.P (2004) Colloidal nanocrystal synthesis and the organic–inorganic interface. *Nature*, 437(7059): 664-670.

Yu, W.W., Chang, E., Drezek, R., Colvin, V.L (2006) Water-soluble quantum dots for biomedical applications. *Biochemical and Biophysical Research Communications* 348: 781–786.

Zhang, S., Gao, H. and Bao, G (2015) Physical principles of nanoparticle cellular endocytosis. *ACS nano* 9(9): 8655-8671.

Zhang, T., Hu, Y., Tang, M., Kong, L., Ying, J., Wu, T., Xue, Y. and Pu, Y (2015) Liver toxicity of cadmium telluride quantum dots (CdTe QDs) due to oxidative stress in vitro and in vivo. *International journal of molecular sciences* 16(10): 23279-23299.

Zhang, Z., Li, H., Xu G., Yao, P (2018) Liver targeted delivery of insulin loaded nanoparticles via enterohepatic circulation of bile acids. *Drug delivery* 25(1): 1224-1233.

Zheng, H., Mortensen, L.J., Ravichandran, S., Bentley, K. and DeLouise, L.A (2017) Effect of nanoparticle surface coating on cell toxicity and mitochondria uptake. *Journal of biomedical nanotechnology* 13(2): 155-166.

Zheng, Y., Gao, S., Ying, J.Y (2007) Synthesis and Cell-Imaging Applications of Glutathione-Capped CdTe Quantum Dots. *Advanced Materials*19: 376–380.

Zhu, J., Koltypin, Y., Gedanken, A (2000) General Sonochemical Method for the Preparation of Nanophasic Selenides: Synthesis of ZnSe Nanoparticles. *Chemistry of Materials* 12: 73–78.

ANNEXURE

LIST OF PUBLICATIONS

1. **Reshma VG**, Mohanan PV (2018) Quantum dots: Applications and safety consequences. Journal of Luminescence 205, 287-298, IF 2.961

2. **Reshma VG**, Mohanan PV (2017) Cellular interactions of Zinc oxide nanoparticles with human embryonic kidney (HEK 293) cells. Colloids and Surfaces B: Biointerfaces 157: 182-190. IF 3.973

3. **Reshma VG**, Nathiya Krishnan, Mohanan P.V (2018) Medical application and safety of engineered nanoparticles. EC Pharmacology and Toxicology, 6 (3), 141-151.

4. **Reshma VG**, Syama S, Sruthi S, Reshma SC, Remya NS and Mohanan PV (2017). Engineered nanoparticles with antimicrobial activity. Curr Drug Metab. doi: 10.2174/1389200218666170-925122201. IF. 2.659

5. **Reshma VG**, Mohanan PV (2016) Induction of Cytotoxicity and Oxidative Stress of Dextran Coated Ferrite Nanoparticles (DFNPs) on A549 Cell Lines. J of Pharmacol & Clin Res .1(5): 555572. DOI:10.19080/JPCR.2016.01.555572.

6. **VG Reshma[1]**, KS Rajeev[2], K. Manoj[1], PV. Mohanan[1]Synthesis of water dispersible ZnSe/ZnS Quantum dots: Assessment of cellular integration, toxicity and bio-distribution (Submitted)

7. **Reshma VG**, Mohanan PV Biointegrity of zinc selenium /zinc sulfide (ZnSe/ ZnS) quantum dots with HEK 293 cells and mice model (Submitted)

8. **Reshma VG**, Mohanan PV Assessment of immunotoxicity, genotoxicity and oxidative stress responses of cadmium free QDs: in both *in vitro* and *in vivo* scenario (Submitted).

Online publications

9. **Reshma VG**, Mohanan PV (2018) Hidden toxicity of Zinc oxide nanoparticles. Atlas of Science, September 17, 2018

Book Chapters

10. Ashtami J, Athira SS, **Reshma VG**, Mohanan PV (2019) Black phosphorous based nanodevices. In book: Black Phosphorous: Synthesis, Properties and Applications. Springer Publication (accepted)

11. Anju S, Prajitha N, **Reshma VG**, Mohanan PV (2019) Black phosphorous quantum dots. In book: Black Phosphorous: Synthesis, Properties and Applications. Springer Publication (accepted)

CONFERENCES PARTICIPATED

1. **Reshma VG**, Mohanan PV (2019) Biointeraction of human embryonic kidney (HEK 293) cells with cadmium free zinc selennium / zinc sulfide (ZnSe/ ZnS) quantum dots. International Conference on Emerging Advancement in Science & Technology and 10th India-Japan Science &Technology Conclave, 5-6 September 2019, held at Manekshaw Centre, New Delhi, India. (Poster paper presentation).

2. **Reshma VG**, Mohanan PV (2018) Cellular interactions of cadmium free ZnSe/ZnS Quantum Dots with HepG2 Cell lines. International Conference on the Role of Toxicology in Public Health & 38th Annual Conference of Society of Toxicology, India, 12-14 December 2018 held at Sri Balaji Vidyapeeth, Puducherry. (Poster paper presentation).

3. **Reshma VG**, Mohanan PV (2018) Toxicity of Cadmium free Zinc selenium/Zinc Sulfide Quantum dots using HepG2 cells. 28th Swedeshi Science Congress, 7-9 November 2018, held at National Institute for Interdisciplinary Sciences and Technology, Trivandrum. (Oral paper presentation).

4. **Reshma VG**, Mohanan PV (2017) Biointeractions of ZnO Nanoparticles with Human Embryonic Kidney (HEK 293) Cells. Presented at the 6th Asian Biomaterial Congress, 25-27 October 2017 held at Trivandrum. (Poster paper presentation).